THE NUTRIENT-RESPONSIVE REGULATION OF CELL DIVISION AND QUIESCENCE IN *CHLAMYDOMONAS REINHARDTII*

By

Tomomi Takeuchi

A DISSERTATION

Submitted to
Michigan State University
in partial fulfillment of the requirements
for the degree of

Biochemistry and Molecular Biology—Doctor of Philosophy

2019

ABSTRACT

THE NUTRIENT-RESPONSIVE REGULATION OF CELL DIVISION AND QUIESCENCE IN *CHLAMYDOMONAS REINHARDTII*

By

Tomomi Takeuchi

Faced with adverse conditions, nearly all cells are able to cease energy-costly processes associated with the cell division cycle and enter a reversible alternative state known as quiescence (G0). In the green microalga *Chlamydomonas reinhardtii*, the entry into and exit from such a non-dividing state is mediated in response to the availability of nutrients, such as nitrogen (N). Following N starvation, a whole-sale reprogramming of intracellular processes takes place in order to maximize the chances of survival, including the repression of cell cycle-related genes, the multi-level downregulation of photosynthesis, the induction of autophagy, and the diversion of carbon (C) towards triacylglycerols (TAG).

One protein implicated in the regulation of nutrient-responsive quiescence-associated transcriptomic programs in Chlamydomonas is Compromised Hydrolysis of TAG 7 (CHT7). The CHT7 protein contains cysteine-rich motifs that are often collectively referred to as the CXC domain, which is widely known for its ability to bind DNA in a sequence-specific manner in animals. A number of CXC domain-containing proteins in both animals and plants have been identified as core constituents of transcriptional regulatory complexes termed DREAM (DP, RB, E2F and Myb-MuvB) complexes, which act to coordinate cell cycle-related gene expression in response to various signals present during quiescence, cell proliferation and differentiation, and development. Through the generation of newly introgressed cell-walled lines and the detailed examination of the *cht7* mutant at cellular levels, my dissertation work identified novel quiescence-related transcriptional defects in *cht7* during N starvation, including derepression of DNA

metabolism and cell cycle-related genes and downregulation of oxidoreductase- and nutrient transporter-encoding genes. Largely due to their inability to repress S/M (DNA synthesis/mitosis) phase-specific gene expression, the *cht7* cells were unable to properly arrest nuclear replication and cell division following N removal. The loss of viability during N starvation and the abortive divisions during N refeeding were identified as causal for the observed delay in resuming growth and the reduction in colony formation in *cht7* following N resupply.

The homolog of the retinoblastoma tumor suppressor (RB) protein in Chlamydomonas, MAT3, and CHT7 were shown to coimmunoprecipitated together during N-replete synchronized growth and following N deprivation, and several phosphorylated isoforms of CHT7 were identified under these conditions. Despite the presence of the presumed DNA-binding function of the CXC domain in CHT7, the largely disordered C-terminal half of CHT7 with predicted protein-binding domains, and not the proposed CXC DNA-binding domain, was essential for the ability of CHT7 to form stable complexes, and to restore the cellular phenotypes and transcript levels back to wild-type levels in the *cht7* mutant. Taken together, while the mechanism of CHT7 function likely differs from that of canonical CXC domain proteins, CHT7 is necessary for the establishment of an effective quiescent state and thus, the nutrient-mediated life-cycle transitions in Chlamydomonas. A better understanding of how the cell division cycle is regulated in response to nutrient scarcity may improve the prospects of biofuels and biomass production in microalgae.

ACKNOWLEDGMENTS

First of all, I would like to thank my advisor, Christoph Benning, for his unwavering support throughout my Ph.D. I appreciate all the times he gave me helpful suggestions and his patience and trust in me as I developed into a more mature scientist. Despite his incredibly busy schedule, I feel he always made time and cared for his students, and I never had to doubt that he has my best interest in mind. I am grateful for all the opportunities he has given me during my Ph.D. and especially for welcoming me into his lab with open arms. Secondly, I would like to thank Dr. Barb Sears for teaching me about the biology of Chlamydomonas and for her consistent support in numerous aspects of my Ph.D. Her words of encouragements and positive influence were much appreciated when my project was tough. She brightened many of my days in the lab, and I am indebted to her and my colleagues in the Benning lab for many fun memories, which I can look back upon with fondness. It has been a delight to work with Barb, and I feel fortunate to have had such a wonderful scientific mentor and a collaborator by my side. Both Christoph and Barb have spent many hours reading, improving, and providing critical feedback on my writing, and I believe I've become a better writer and a thinker thanks to them.

Furthermore, I would like to thank the members of the Benning lab, from past to the present, for stimulating discussions, collegial environment, and entertaining conversations. A fellow graduate student in the algae group, Yang-Tsung Lin, has been vital to our collaborative efforts. He has been a fantastic colleague, and our time course experiments would no doubt have been more grueling and difficult if it was not for his hard work and contributions. I am thankful for the help of Dr. Krzysztof and Agnieszka Zienkiewicz, who have taken the time to teach me how to prepare samples for transmission electron microscopy (TEM) and confocal microscopy. I

would also like to give thanks to the undergraduate students that I had chance to mentor and work with over the years. Nick Fekaris had helped greatly in assembling and running environmental photobioreactors (ePBRs) during the initial stages of this project. Chase Lindeboom has made a significant contribution by making various constructs to determine the functional domain of CHT7, and I am very appreciative of the hours he has spent in helping me maintain my ever-growing collection of Chlamydomonas strains. Finally, I am grateful to my husband for his continuous support, patience and understanding in countless aspects of my life. He has always been there for me, and I could not have asked for a better friend and a partner.

Last but not least, I would like to thank the members of my committee. I greatly appreciate Dr. Robert Last for mentoring me as a part of the Plant Biotechnology for Health and Sustainability program and providing me with new perspectives on different science careers. It has undoubtedly enriched my graduate training. I am thankful for the helpful suggestions made by Dr. David Arnosti and Dr. Gregg Howe on my project, and for their invaluable insights in improving the quality of my scientific work. Furthermore, I am grateful to Dr. Eva Farre, who has given me a chance to participate in research as an undergraduate student in her lab and for introducing me to the world of plant science. She has been a great mentor, a patient teacher and an excellent role model for me since the day one of my research career.

I sincerely appreciate you all.

TABLE OF CONTENTS

LIST OF TABLES

LIST OF FIGURES

KEY TO ABBREVIATIONS

AA – Amino acid

ACC1 – Acetyl-CoA carboxylase 1

ALCOdb – Algal Coexpression Database

ALY2/3 – Always Early 2/3

AMPK – AMP-activated kinase

APC/C – Anaphase-promoting complex/cyclosome

ATG – Autophagy-related protein

BF – Bright field

BN-PAGE – Blue native polyacrylamide gel electrophoresis

BP – Biological process

BS – Binding site

BUB1 – Budding Uninhibited by Benzimidazoles 1

C – Carbon

CAH4/5 – Carbonic Anhydrase 4/5

CBBP – CXC domain b1-repeat binding protein

CBLP – Chlamydomonas beta-subunit-like polypeptide

CC – Cellular component

CDC45 – Cell Division Cycle 45

CDK – Cyclin-dependent kinase

CDKN1A/B – Cyclin-dependent kinase inhibitor 1A/B

CDT1-like – Chromatin Licensing and DNA Replication Factor 1-like

ChIP – Chromatin Immunoprecipitation

Chl – Chlorophyll

CHR – Cell cycle genes homology region

CHT7 – Compromised Hydrolysis of Triacylglycerols 7

CIP – Calf intestinal phosphatase

CKIN – Chlamydomonas kinase

Co-IP – Co-immunoprecipitation

CP – Commitment point

CPP1 – Cysteine-rich polycomb-like protein 1

Ct – Cycle threshold

Cw^- – Cell-wall minus

Cw^+ – Cell-wall plus

CYC – Cyclin

CYC6 – Cytochrome c6

DAG – Diacylglycerols

DAPI – 4',6-diamidino-2-phenylindole

DGAT/DGTT – Diacylglycerol acyltransferase type 1/ type 2

DP – Dimerization partner

DREAM – DP, RB, E2F, Myb-MuvB

DYRK – Dual-specificity tyrosine phosphorylation-regulated kinase

E2F – Adenovirus early gene 2 binding factor

ePBR – Environmental photobioreactor

ER – Endoplasmic reticulum

FAMEs – Fatty acid methyl esters

FAS1/2 – Fatty acid synthase 1/ 2

FKBP12 – FK506-binding protein

FOXM1 – Forkhead box M1

FRB – FKBP12-rapamycin binding

FT – Flow through

G1/2 – Growth phase 1/2

GAS28 – Gamete-Specific Glycoprotein 28

GFP – Green Fluorescent Protein

GINS3 – GINS complex subunit 3

GO – Gene ontology

GPAT – Glycerol-3-phosphate acyltransferase

H3 – Histone 3

HA – Hemagglutinin

HFO – Histone H4

HRP – Horseradish peroxidase

HS – High salt medium

HSP70A – Heat shock protein 70A

InsP – Inositol polyphosphate

IP – Immunoprecipitation/ Immunoprecipitated

LHCA8 – Light-harvesting complex A8

LIP1 – Lipase 1

Log_2 FC – Log_2 fold change

LST8 – Lethal with SEC13 protein 8

MAT3 – Mating-type protein 3/ RB homolog

MCM2/10 – Minichromosome Maintenance 2/10

MGDG – Monogalactosyldiacylglycerols

MIND/E – Mini-cells D/E

MIP – Myb-interacting protein

MP – Molecular process

MSA – Mitosis specific activator element

Mt^- – Mating-type minus

Mt^+ – Mating-type plus

MuvB – Multi-vulva class B

MYB3R – Myb three repeats protein

N – Nitrogen

NIT1 – Nitrate reductase 1

OD – Optical density

ORC1 – Origin Recognition Complex 1

P – Phosphorus

PAGE – Polyacrylamide gel electrophoresis

PCC – Pearsons correlation coefficient

PCN1/A – Proliferating Cell Nuclear Antigen

PDAT – Phospholipid: diacylglycerol acyltransferase

PE – Phosphatidylethanolamine

PETO – Cytochrome b6f complex subunit V

PGD1 – Plastid Galactoglycerolipid Degradation 1

PL – Parental line

POLA4 – DNA polymerase alpha 4

PRI2 – DNA primase 2

RAPTOR – Regulatory-associated protein of TOR

RB – Retinoblastoma tumor suppressor protein

RBSC2 – Rubisco 2

RICTOR – Rapamycin-insensitive companion of TOR

RIR1/2 – Ribonucleoside-diphosphate Reductase 1/2

ROS – Reactive oxygen species

RPA1 – Replication Protein A1

RPKM – Reads per kilobase of transcript per million mapped reads

RT-qPCR – Real-time quantitative-PCR

S/M phase – DNA synthesis and mitosis phase

S6K – S6 kinase

SDM – Site directed mutagenesis

SMR – Siamese-related

Snf1 – Sucrose nonfermenting 1

SnRK – Sucrose nonfermenting-related kinase

SOL1/2 – Suppressor of LLP1 1/2

Sulfur – S

TAG – Triacylglycerols

TAP – Tris-acetate-phosphate

TAR1 – TAG Accumulation Regulator 1

TBARS – Thiobarbituric Reactive Substances

TCX5 – TSO1-like CXC 5

TEM–Transmission electron microscopy

TOPOII – Topoisomerase II

TOR – Target of rapamycin

TORC1/2 – Target of rapamycin complex 1/ 2

US – Upstream

UTR – Untranslated Region

YAK1 – Yet Another Kinase 1

ZT – Zeitgeber

CHAPTER 1

Introduction: Nitrogen-dependent coordination of cell cycle, quiescence and TAG accumulation in Chlamydomonas – A literature review[1]

[1]The content presented in this chapter has been modified from the manuscript submitted to the Biotechnology for Biofuels journal as a review article. I conceptualized the manuscript and prepared the first draft of all sections and figures. Christoph Benning provided the critical review and contributed to the writing and editing of all sections.

Takeuchi T. and Benning C. (2019). Nitrogen-dependent coordination of cell cycle, quiescence and TAG accumulation in Chlamydomonas. Biotechnol Biofuels. Accepted for publication.

ABSTRACT

Microalgae hold great promises as sustainable cellular factories for the production of alternative fuels, feeds, and biopharmaceuticals for human health. While the biorefinery approach for fuels along with the coproduction of high-value compounds with industrial, therapeutic, or nutraceutical applications have the potential to make algal biofuels more economically viable, a number of challenges continue to hamper algal production systems at all levels. One such hurdle includes the metabolic trade-off often observed between the increased yields of desired products, such as triacylglycerols (TAG), and the growth of an organism. Initial genetic engineering strategies to improve lipid productivity in microalgae, which focused on overproducing the enzymes involved in fatty acid and TAG biosynthesis or inactivating competing carbon (C) metabolism, have seen some successes albeit at the cost of often greatly reduced biomass. Emergent approaches that aim at modifying the dynamics of entire metabolic pathways by engineering of pertinent transcription factors or signaling networks appear to have successfully achieved a balance between growth and neutral lipid accumulation. However, the biological knowledge of key signaling networks and molecular components linking these two processes is still incomplete in photosynthetic eukaryotes, making it difficult to optimize the metabolic engineering strategies for microalgae. Here, we focus on nitrogen (N) starvation of the model green microalga, *Chlamydomonas reinhardtii*, to present the current understanding of the nutrient-dependent switch between proliferation and quiescence, and the drastic reprogramming of metabolism that results in the storage of C compounds following N starvation. We discuss the potential components mediating the transcriptional repression of cell cycle genes and the establishment of quiescence in Chlamydomonas, and highlight the importance of signaling pathways such as those governed by the target of rapamycin (TOR) and sucrose nonfermenting-related (SnRK) kinases in the coordination of metabolic status with cellular

growth. A better understanding of how the cell division cycle is regulated in response to nutrient scarcity and of the signaling pathways linking cellular growth to energy and lipid homeostasis, is essential to improve the prospects of biofuels and biomass production in microalgae.

Coordination of metabolism and the cell division cycle in algae: potential biotechnical implications

The use of algae as a potential source of renewable fuel, animal feeds in addition to nutrients and pharmaceuticals for human health has been recognized and exploited for decades. Both micro- and macro-algae constitute a diverse group of aquatic photosynthetic organisms with varying levels of complexity, and their natural biochemical compositions (e.g., high contents of oil, carbohydrates, proteins, sugars, vitamins, pigments, or minerals) make them uniquely suitable for different commercial purposes. In addition to their relevance in agriculture as fertilizers, soil conditioners and livestock feeds, algae provide many nutrients essential for human health, including vitamins, minerals, anti-oxidants, and polyunsaturated fatty acids such as docosahexaenoic acids and eicosapentaenoic acids (Pulz and Gross, 2004; Mata et al., 2010; Yen et al., 2013). Furthermore, algae-derived products are also used as gelling agents and stabilizers in various food products, cosmetics and pharmaceuticals (Pulz and Gross, 2004; Mata et al., 2010; Yen et al., 2013). Over thirty recombinant proteins have been successfully produced in microalgae to date, including hormones, enzymes, antibodies, vaccines and immunotoxins, highlighting the biotechnical utilities and potentials of these organisms (Barrera and Mayfield, 2013; Almaraz-Delgado et al., 2014; Rasala and Mayfield, 2015; Scranton et al., 2015). In the past few decades, microalgae have garnered renewed interests as alternative feedstocks for the sustainable production of biofuels, in the forms of biodiesel, bioethanol, biogas and hydrogen. Many microalgae are able to grow rapidly

to high cell densities using CO_2 or other provided carbon (C) sources, can be cultivated using nonarable land and water sources not suited for agriculture, and accumulate more triacylglycerols (TAG) per dry weight or per unit area than agricultural oil crops (Chisti, 2007; Hu et al., 2008; Li et al., 2008; Scott et al., 2010; Jones and Mayfield, 2012). Because algae maintain high productivity in nutrient-rich waters, they can be used to remove excess nutrients from waste water and mitigate fertilizer runoff from farms, while simultaneously yielding biomass and precursors for the production of biofuels (Woertz et al., 2009; Park et al., 2011; Pittman et al., 2011). In addition, the use of industrial flue gas as a source of C, the biorefinery-based approach to biofuel production, and the concurrent cultivation of high-value compounds were also proposed as a potential means to further lower the cost of algal biofuels (Chisti, 2007; Hu et al., 2008; Li et al., 2008; Wang et al., 2008; Jones and Mayfield, 2012).

Although the production of sustainable energy and economically valuable compounds from algae hold great promises, a number of hurdles persist. These include the species-dependent recalcitrance to various genetic manipulations, suboptimal utilization and conversion of light energy and CO_2 to biomass due to light saturation and or photoinhibition, limited light penetrance in the culture, undesirable contamination, and high costs ultimately associated with sustaining optimal growth and metabolic outputs, as well as high costs of extraction and processing (Chisti, 2007; Hannon et al., 2010; Radakovits et al., 2010; Scott et al., 2010; Jones and Mayfield, 2012). Another major impediment that prevents algal biofuels from becoming a competitive alternative to fossil petroleum on a commercial scale involves the inverse relationship between the yield of cellular products and the growth of the organism. A plethora of abiotic stresses such as nutrient deprivation, extreme light conditions and changes in temperature, salinity or pH is known to induce the accumulation of sought-after molecules in algae, including TAG, hydrogen, and carotenoids

like β-carotene and astaxanthin (Hu et al., 2008; Radakovits et al., 2010; Merchant et al., 2012; Sharma, 2012; Skjånes et al., 2013; Cheng and He, 2014; Gonzalez-Ballester et al., 2015; Du and Benning, 2016; Minhas et al., 2016). However, the increase in these compounds often comes at the expense of inhibited growth, resulting in the considerable reduction of biomass. A two-stage cultivation strategy, where the algal cells are subjected to stress only after a period of optimal growth and accumulation of biomass, has been proposed and tested to circumvent this problem (Rodolfi et al., 2009; Singh et al., 2011; Singh et al., 2016), but this production method is still costly due to its extended requirement for time and the inherent complexity in monitoring and optimizing the production process.

Genetic engineering strategies in algae, which aimed to alter the expression levels of genes encoding individual enzymes involved in lipid metabolism, TAG biosynthesis and catabolism, or other competing C metabolic pathways, have seen mixed outcomes in achieving the optimal balance between lipid productivity and growth (Liang and Jiang, 2013; Shahid et al., 2019). Recent approaches targeting transcription factors or signaling pathways that regulate C and growth metabolisms in algae appear to achieve more consistent successes in increasing TAG content with little or no compromise in cellular growth and proliferation by simultaneously modifying multiple components of a metabolic pathway (Zhang et al., 2014; Ngan et al., 2015; Bajhaiya et al., 2016; Ajjawi et al., 2017; Bajhaiya et al., 2017; Prioretti et al., 2017). However, the regulatory components and signaling networks coordinating the allocations of C towards storage and growth are still not well characterized in photosynthetic eukaryotes. Therefore, a better understanding of the molecular mechanisms by which metabolism and growth are regulated and coupled will likely advance the metabolic engineering efforts of algae. Here, the nutrient-dependent transitions between the cell division and quiescence cycles, the shifts in metabolism towards the synthesis of

C storage compounds following nutrient starvation, and the potential molecular components mediating the cessation of growth and entry into quiescence under stress conditions are discussed focusing on nitrogen (N) starvation in the model green microalgae, *Chlamydomonas reinhardtii*, as a reference. Our current understanding of the signaling pathways integrating the changes in metabolism and the cell division cycle in response to nutrient availability in algae is presented, followed by concluding remarks on the potential biotechnological implications of the presented concepts.

Chlamydomonas as a model to study key life-cycle transitions

At the cell biological level, many abiotic stresses will induce cells to accumulate storage compounds and exit the normal cell division cycle to enter an alternative reversible state known as quiescence, or G0 (Rittershaus et al., 2013). When the conditions are again conducive to growth, cells degrade the accumulated storage compounds, exit quiescence and reenter the cell division cycle (Gray et al., 2004). Chlamydomonas serves as a particularly excellent model system to study the coordination between metabolism, cell division cycle and quiescence in photosynthetic organisms for several reasons. Chlamydomonas can be grown rapidly under heterotrophic, photoautotrophic or mixotrophic conditions, depending on the research needs (Harris, 1989). For instance, the growth and division of Chlamydomonas cells can be synchronized with alternating light and dark cycles when they are grown photoautotrophically, enabling the facile isolation of cells at different stages of the cell cycle (Spudich and Sager, 1980) (Figure 1.1). In addition, the life-cycle transitions between cell division to quiescence and vice versa can be discretely controlled and analyzed by selective removal or resupply of nutrient(s) in the medium (Figure 1.1). Furthermore, a great number of –omics based studies has been conducted using Chlamydomonas

under different stress conditions in the past decade, and a wealth of literature on how Chlamydomonas cells reprogram their metabolism in response to nutrient shortage, such as N starvation at the levels of transcriptome, proteome and metabolome is available (Bölling and Fiehn, 2005; Miller et al., 2010; Longworth et al., 2012; Msanne et al., 2012; Blaby et al., 2013; Goodenough et al., 2014; Schmollinger et al., 2014; Valledor et al., 2014; Park et al., 2015). While Chlamydomonas is not typically considered a candidate alga for the production of biofuel feedstocks, Chlamydomonas cells still accumulate a significant amount of TAG just as other oleaginous algae do in response to nutrient starvation (Merchant et al., 2012). Combined with the availability of well-established molecular genetics and genomic tools (e.g., the annotated genome, transformation protocols, reverse genetic engineering tools, and mutant libraries (Day and Goldschmidt-Clermont, 2011; Blaby et al., 2014; Jinkerson and Jonikas, 2015; Li et al., 2016a)) and the haploid genome of Chlamydomonas during vegetative growth (Harris, 1989), there is a solid infrastructure for the further exploration of the regulatory link between metabolism and life-cycle transitions in this alga.

The intersection between the cell division and quiescence cycles in Chlamydomonas

In the presence of sufficient nutrients, Chlamydomonas and many other green algae grow and divide by a modified cell cycle involving multiple fissions, where the cells go through a prolonged growth or G1 phase followed by a rapid succession of S/M (DNA synthesis and mitosis) cycles (Coleman, 1982; Bisova and Zachleder, 2014; Cross and Umen, 2015) (Figure 1.1). The gap between the S and M phases (known as the G2 phase) is not observed in the cell cycle of Chlamydomonas (Jones, 1970). In contrast, when the nutrients are limiting, single-celled organisms exit from the active proliferative cycle and forego the anabolic, energy-consuming

metabolism that is required for growth and division in favor of energy-saving metabolism that defines quiescence (Valcourt et al., 2012). This is also the case for microalgae such as Chlamydomonas (Figure 1.1). The ability of ancestral eukaryotic cells to enter a state of quiescence, maintain viability, and subsequently resume growth when the conditions improve, was likely critical, not only for their immediate survival but the subsequent evolution of species. The molecular mechanisms by which cells transition from active cell division to quiescence cycles and vice versa in response to nutrient availability are best characterized in yeast (Gray et al., 2004). However, the capacity to orchestrate these life-cycle changes is evolutionarily conserved in many organisms. For instance, the entry into quiescence in cultured mammalian cells can be induced by serum and amino acid starvation, high cell density, and anchorage deprivation (Benecke et al., 1978; Dean et al., 1986; Pardee, 1989; Davis et al., 2001; Coller et al., 2006), although their proliferation is typically controlled by the developmental and contextual cues within the organism. Thus, some features of quiescent cells appear to be more universal. Although exceptions exist, these include the arrest of growth and cell division before the genome replicates, chromosome compaction, induction of autophagy, reduced rates of transcription and translation, and increased content of C storage molecules (Gray et al., 2004; Valcourt et al., 2012; Rittershaus et al., 2013; Dhawan and Laxman, 2015).

An increasing body of work in opisthokonts as well as in Chlamydomonas suggests that quiescence is a poised and actively maintained state, where the entry into and exit from such a state represent distinct processes governed by unique signaling and gene-regulatory networks, rather than a phase of the cell division cycle or a passive inactive state (Gray et al., 2004; Coller et al., 2006; Lemons et al., 2010; Coller, 2011; Tsai et al., 2014; Dhawan and Laxman, 2015; Tsai et al., 2018) (Figure 1.1). In the opisthokont models of quiescence, the intersection between the

cell division cycle and the so called quiescence cycle is thought to occur early in the G1 phase or during the "restrictive window" following the completion of a previous cell cycle before the cells pass their respective G1 checkpoints (Gray et al., 2004; Dhawan and Laxman, 2015). In Chlamydomonas, it is also during the G1 or the post-mitotic resting phase prior to the passage of the commitment point that the cells are faced with a decision whether to proceed with the subsequent steps of the cell division cycle or to enter an alternative quiescence cycle (Figure 1.1). After passing the commitment point, Chlamydomonas cells will undergo at least one round of division even after nutrients or light are withdrawn (Spudich and Sager, 1980; Donnan and John, 1983), likely because the completion of the cell division cycle is under the control of the intrinsic oscillation of cell cycle regulators such as cyclin-dependent kinases (CDKs) (Cross and Umen, 2015). Thus, it is only when the cyclical transcriptional waves during the cell cycle cease and the cells arrive at the pre-commitment stage that they are able to enter into the quiescence cycle.

The entry into the quiescence cycle in the early G1 phase before genome replication is likely important for the maintenance of viability during quiescence and the successful reentry into the cell division cycle in response to growth-promoting cues. Because quiescent cells cannot effectively dilute out molecules such as DNA damaged by reactive oxygen species (ROS) through growth and cell division, replace them through active synthesis, or repair them by energy-costly mechanisms, the condensation of chromosomes facilitates the preservation of genomic integrity and promotes survival (Gray et al., 2004; Valcourt et al., 2012; Rittershaus et al., 2013). Although the transcripts and protein products of most cell cycle genes are not essential for the maintenance of quiescence and survival in mammalian quiescent cells, the repression of genes that promote cell cycle progression, including genes encoding mitotic CDKs and their associated cyclins, is critical for the appropriate exit from the cell division cycle, the establishment of quiescence and the

subsequent resumption of growth (Valcourt et al., 2012; Sadasivam and DeCaprio, 2013; Fischer and Muller, 2017). In response to quiescence-inducing cues, the inhibitors of G1 CDKs become upregulated in various quiescent mammalian cell-lineages (Valcourt et al., 2012). For instance, these inhibitors act to maintain the hematopoietic stem cells in quiescence and prevent them from inappropriately or precociously entering the cell cycle (Steinman et al., 2004; Walkley et al., 2005; Valcourt et al., 2012). These functions of CDK inhibitors appear conserved also in yeast (Costanzo et al., 2004). Yeast mutant cells that have lost the ability to repress certain growth and cell cycle-related genes following glucose exhaustion also have shortened lifespan and fail to successfully exit quiescence upon glucose refeeding (Miles et al., 2013). In Chlamydomonas, the cell density of mixotrophically grown cells will approximately double using the finite reservoir of intracellular N within the first 24 h of N starvation (Blaby et al., 2014; Schmollinger et al., 2014). Following this increase in cell number, the expression of genes involved in cell cycle progression, DNA synthesis, and replication is substantially reduced (Miller et al., 2010), and by day two of N deprivation, greater than 70% of the cellular population arrests growth with 1C (one copy) chromatin content (Tsai et al., 2018). Therefore, in the face of starvation, the arrest of further growth and division prior to DNA replication during the pre-commitment phase is also likely an important factor enabling successful life-cycle transitions of Chlamydomonas.

Cellular changes that accompany N starvation and the entry into quiescence in Chlamydomonas

As the universal features of quiescence are further refined, it is becoming evident that the transition from the cell division cycle to the quiescence cycle and its reversal require the genome-wide adjustment of regulatory networks, metabolism, and intracellular structures (discussed in details

below and summarized in Figure 1.2), and where applicable, necessitate the repression of alternative non-dividing cell fates such as apoptosis, senescence and differentiation (Coller et al., 2006; Sousa-Victor et al., 2014; Dhawan and Laxman, 2015). Despite the conservation of many quiescence-associated components and processes, the generation of chemical energy from light and CO_2 imposes another layer of complexity on the maintenance of a non-replicating, viable, and reversible state in photosynthetic organisms. While many abiotic stresses trigger algal cells to enter a quiescent state and to form lipid droplets rich in TAG, the consequences of nutrient deprivation, especially that of N, is the best studied process (Rodolfi et al., 2009; Tsai et al., 2014). It has been long known that N starvation induces the transcriptional program necessary for gametogenesis, during which the cells of opposite mating types differentiate into gametes capable of mating (Martin and Goodenough, 1975). The fusion of these gametes allows for the formation of diploid zygospores, which are markedly more resilient to environmental insults than Chlamydomonas cells during vegetative growth (Cavalier-Smith, 1970; Brawley and Johnson, 1992). In more recent years, multiple –omics based approaches have been successfully applied to study the systems-level responses of this alga to N deprivation, revealing the wholesale cellular reprogramming of transcriptome, proteome and metabolome that results in the accumulation of C storage and a reversible quiescent state (Bölling and Fiehn, 2005; Miller et al., 2010; Longworth et al., 2012; Msanne et al., 2012; Blaby et al., 2013; Goodenough et al., 2014; Schmollinger et al., 2014; Tsai et al., 2014; Valledor et al., 2014; Gargouri et al., 2015; Park et al., 2015; Tsai et al., 2018) (Figure 1.2).

Although some responses of the starved cells are nutrient-specific, the underlying fundamental principles governing microbes under starvation can be summarized in three words—scavenge, conserve, and recycle (Merchant and Helmann, 2012). In general, nutrient-deprived

Chlamydomonas cells actively increase the scavenging and uptake of the limiting nutrient(s), curtail anabolic energy-consuming metabolism associated with growth and proliferation, and strategically repurpose nonessential macromolecules to maximize survival (Figure 1.2). Although ammonium is the preferred source of N, Chlamydomonas cells can also assimilate other inorganic N-containing compounds (Fernández et al., 2009). Thus, following N deprivation, the abundance of transcripts and proteins involved in the transport and the metabolism of alternative, less favorable N sources increases almost immediately (within 0.5-1 h) (Fernández et al., 2009; Schmollinger et al., 2014). The cellular-wide reprogramming of metabolism occurs at the levels of transcripts and proteins to conserve energy and minimize N consumption. The levels of both cytoplasmic and chloroplast ribosomes decrease substantially (Siersma and Chiang, 1971; Martin et al., 1976), and the total cellular contents of RNA (Plumley and Schmidt, 1989) and protein (Schmollinger et al., 2014) per cell become reduced by approximately 60% and 50%, respectively. It has been reported that the proteins whose abundance increases upon transfer of cells to N-free medium, such as those needed for N acquisition and metabolism, contain less N on average than those that decrease in abundance, highlighting the evolutionarily selected N sparing strategy to reduce the cellular demand for N when it is not readily available in the environment (Schmollinger et al., 2014). Chlamydomonas cells also utilize a similar conservation mechanism during sulfur (S) shortage, such that the abundant proteins under S-deficient conditions contain less S in their amino acid side chains (Gonzalez-Ballester et al., 2010). While the genes encoding the key enzymes of glyoxylate cycle and gluconeogenesis are downregulated (Miller et al., 2010), those involved in the biosynthesis and branching of starch peak shortly after the transfer of cells to N-free medium, followed by a steady decrease in their transcript levels until the new basal level is achieved (Blaby et al., 2013). This is in contrast to genes encoding enzymes of TAG biosynthesis,

whose transcript abundance gradually increases over the two day time course (Boyle et al., 2012; Blaby et al., 2013), consistent with the observations that starch accumulation precedes the increase in TAG (Siaut et al., 2011; Fan et al., 2012; Msanne et al., 2012). To recycle and repurpose intracellular reserves of N, the nonessential or damaged macromolecules are engulfed within a specialized double-membrane vesicle called autophagosome and are trafficked for degradation into the vacuole (Perez-Perez et al., 2010). The induction of autophagy is one of the hallmarks of quiescent cells. Although many growth-inhibiting stresses lead to the activation of autophagy in eukaryotes (Gray et al., 2004; Perez-Perez et al., 2010; Perez-Perez et al., 2012), this catabolic process is also necessary for the survival and maintenance of quiescent lymphocytes and hematopoietic stem cells in mammals (Valcourt et al., 2012). Yeast mutants defective in autophagy accumulate higher levels of ROS and rapidly lose viability during nutrient starvation due to their inability to remobilize amino acids and synthesize proteins necessary for stress adaptation (Tsukada and Ohsumi, 1993; Onodera and Ohsumi, 2005; Suzuki et al., 2011). A similar loss of viability was recently shown for autophagy-defective mutants of Chlamydomonas in response to deprivation of N, P (phosphorus) and S (Kajikawa et al., 2018), suggesting the importance of this catabolic pathway for stress acclimation and cellular homeostasis of this alga (Perez-Perez et al., 2012).

Following N deprivation, Chlamydomonas cells increasingly rely on respiratory metabolism to produce energy instead of photosynthesis (Schmollinger et al., 2014). The cessation of chlorophyll synthesis, which is regulated both transcriptionally and post-translationally, leads to a drastic decrease in cellular chlorophyll content (Blaby et al., 2013; Schmollinger et al., 2014; Juergens et al., 2015). A marked multi-level downregulation of photosynthesis takes place. The abundances of many transcripts and proteins encoding the subunits of light-harvesting complexes,

the cytochrome *b*$_6$*f* complex, photosystems I and II, and the plastid ATP synthase complex decrease with different kinetics, ultimately leading to reduced photosynthetic capacity, efficiency and flux (Plumley and Schmidt, 1989; Peltier and Schmidt, 1991; Bulte and Wollman, 1992; Majeran et al., 2000; Miller et al., 2010; Schmollinger et al., 2014; Juergens et al., 2015). After two days of N deprivation, the cellular levels of plastid membrane lipids, especially of monogalactosyldiacylglycerol (MGDG), are reduced while the TAG content increases, likely to sequester acyl groups inertly in lipid droplets as the extent of the photosynthetic membrane decreases (Fan et al., 2011; Siaut et al., 2011; Yoon et al., 2012; Juergens et al., 2015). Most transcripts and enzymes of the Calvin-Benson cycle, especially rubisco, are reduced in abundance following two days of N deprivation, resulting in the increased levels of its intermediates (Miller et al., 2010; Schmollinger et al., 2014). In agreement with these observations, the rates of carbon assimilation and consumption decrease significantly during N starvation (Juergens et al., 2016). Although the mRNA levels of mitochondrial respiratory complexes remain relatively stable during the two days of N starvation, their protein levels, along with the corresponding mitochondrial ATP synthase and cytochrome *bc1* complex components, become more abundant (Schmollinger et al., 2014). Consistently, the oxygen consumption increases on a protein basis, further corroborating the bioenergetic preference for respiration over photosynthesis during N deprivation (Schmollinger et al., 2014).

The revived interest in regulatory and metabolic pathways governing TAG accumulation in microalgae have led to the identification of key enzymes responsible for the biosynthesis of TAG in Chlamydomonas (Merchant et al., 2012). Although the expression changes of many fatty acid and lipid metabolism genes are modest, notable changes in the transcript levels of genes involved in TAG biosynthesis and a number of lipases are observed following N deprivation

(Miller et al., 2010; Boyle et al., 2012; Schmollinger et al., 2014). The Chlamydomonas genome encodes one type I (*DGAT1*) and five type II (*DGTT1*-5) diacylglycerol acyltransferases, which catalyze the transfer of an acyl-moiety from acyl-CoA to the *sn*-3 position of diacylglycerols (DAG), and one phospholipid: DAG acyltransferase (PDAT), which catalyzes the transfer of an acyl chain at the *sn*-2 position of membrane lipids to the *sn*-3 position of DAG, resulting in the synthesis of TAG (Merchant et al., 2012; Liu and Benning, 2013; Li-Beisson et al., 2015). Among them, the transcript levels of *DGAT1*, *DGTT1*, and *PDAT* show the most significant upregulation following N deprivation (Miller et al., 2010; Boyle et al., 2012; Schmollinger et al., 2014). The Chlamydomonas PDAT catalyzes the biosynthesis of TAG through its acyltransferase and acylhydrolase activities toward a broad range of acyl-lipid substrates, including galactolipids, phospholipids, cholesteryl esters and TAG (Yoon et al., 2012). The genes encoding proteins with potential roles in TAG lipolysis, such as acylglycerol lipase, *LIP1* (*Lipase 1*) with a likely role in DAG turnover (Li et al., 2012a) and those encoding the putative peroxisomal β-oxidation enzymes are concurrently downregulated (Miller et al., 2010). Chlamydomonas cells can directly funnel exogenous acetate towards the synthesis of fatty acids and TAG following N deprivation, and the presence of acetate increases the TAG yield (Miller et al., 2010; Fan et al., 2011; Goodson et al., 2011; Fan et al., 2012). Under mixotrophic conditions, over 80% of starch molecules are produced from the assimilated photosynthates or CO_2. However, under these conditions, approximately 75% of the C used for the de novo-synthesis of fatty acids and 70% of the subsequently assembled TAG or other lipid species are derived from acetate following N starvation (Juergens et al., 2016), supporting the previous 30% estimate of the contribution of membrane lipid turnover to TAG synthesis (Fan et al., 2011). Additional fatty acids are derived from the remodeling of plastid

membranes by enzymes such as PGD1 (Plastid Galactoglycerolipid Degradation 1), a lipase responsible for cleaving the acyl chains from MGDG for the synthesis of TAG (Li et al., 2012b).

Many studies have historically observed how N deprivation results in the diversion of C towards storage compounds, namely TAG and starch, at the expense of decreased growth in a number of microalgae (Spoehr and Milner, 1949; Martin and Goodenough, 1975; Shifrin and Chisholm, 1981; Granum et al., 2002; Hu et al., 2008). The tight coupling and inverse relationship between TAG accumulation and proliferation have also been demonstrated in yeast, where the inhibition of cell cycle progression leads to the increased formation of lipid droplets, regardless of whether the delay is caused by drugs or mutations in genes encoding cell cycle regulators (Madeira et al., 2019). It was also recently reported that the mRNAs encoding early fatty acid synthesis enzymes (e.g., Acetyl-CoA Carboxylase 1, ACC1 and Fatty Acid Synthase 1 and 2, FAS1 and 2) are translated in a cell cycle and nutrient dependent manner in yeast (Blank et al., 2017). However, the analogous proteins in Chlamydomonas are less abundant following N deprivation than in yeast (Schmollinger et al., 2014). Nevertheless, different hypotheses and theories were put forward to answer the question of why algae accumulate TAG in response to growth-inhibiting stresses following entry into quiescence. The potential physiological roles of lipid droplets and TAG during stress include fatty acid storage for survival and future membrane biosynthesis, a transient reservoir of acyl groups for the remodeling of the lipids in the photosynthetic membrane, a reservoir of carotenoids for photoprotection, and a sink for excess and unused photosynthetic energy and reductants to prevent photo-oxidative damage (Roessler, 1990; Murphy, 2001; Hu et al., 2008; Li et al., 2012b; Solovchenko, 2012; Klok et al., 2014; Du and Benning, 2016; Goncalves et al., 2016; Juergens et al., 2016; Zienkiewicz et al., 2016). The studies in yeast suggest that the availability of acetyl-CoA, a central carbon metabolite that is derived from the breakdown of C

storage, is a crucial factor for the cellular exit from quiescence and reentry into the cell division cycle. These studies suggest that the rapid increase in acetyl-CoA that results upon a suitable metabolic stimulation is necessary for driving the acetylation of histones at growth regulatory genes, their activation, and consequently enable cells to exit from quiescence (Cai et al., 2011; Shi and Tu, 2013). Whether these regulatory principles apply to algae remains to be explored.

The DREAM complex: A master transcriptional regulator of cell division cycle also in algae?

Despite the recent advances in understanding the impact of nutrient availability on gene expression and metabolism of Chlamydomonas, the signaling pathways and molecular components enabling the entry into, maintenance of, and exit from quiescence remain largely unknown in photosynthetic eukaryotes. One potential regulatory component that may play a role in the nutrient-dependent life-cycle transitions of Chlamydomonas is the evolutionarily conserved multi-protein transcriptional regulatory complex known as DREAM (DP, RB, E2F and Myb-MuvB) (Figure 1.3), although its presence in algae has yet to be confirmed. It is notably absent from yeast, but organisms from many evolutionary lineages including mammals (Litovchick et al., 2007; Pilkinton et al., 2007; Schmit et al., 2007), fruit flies (Korenjak et al., 2004; Lewis et al., 2004), worms (Harrison et al., 2006; Harrison et al., 2007) and plants (Kobayashi et al., 2015) utilize this structurally conserved module to coordinate the expression of the cell division cycle-dependent and development-specific genes in response to different cues present during quiescence, cell proliferation and differentiation, and organismal or sexual organ development (Sadasivam and DeCaprio, 2013; Fischer and Muller, 2017). The core components of DREAM complexes are conserved among species, which include retinoblastoma (RB) tumor suppressor proteins,

adenovirus early gene 2 binding factor (E2F) family of transcription factors and their dimerization partners (DP), and the members of the multi-vulva class B (MuvB) complexes, which were initially identified through mutations that cause synthetic multivulva phenotypes in *Caenorhabditis elegans* (Sadasivam and DeCaprio, 2013; Fischer and Muller, 2017).

One of the best characterized core constituents of the metazoan MuvB complexes are the proteins that contain two tandem cysteine-rich motifs or domains that are collectively referred hereafter as the CXC domain. These CXC domain proteins include the mammalian LIN54 (Litovchick et al., 2007; Schmit et al., 2007), Drosophila Mip120 (Beall et al., 2002; Korenjak et al., 2004), and *C. elegans* Lin-54 (Harrison et al., 2006), and their CXC domains are necessary for the sequence-specific binding of DNA (Beall et al., 2002; Schmit et al., 2009; Tabuchi et al., 2011; Marceau et al., 2016). For instance, the CXC domain of mammalian LIN54 is known to directly bind the cis-regulatory element known as the cell cycle genes homology region (CHR) (Schmit et al., 2009; Marceau et al., 2016), which is a primary promoter element involved in the regulation of G2/M phase genes (Muller and Engeland, 2010; Muller et al., 2012; Muller et al., 2014; Muller et al., 2016). Consequently, LIN54 is essential for the recruitment of both activator and repressor DREAM complexes to these sites (Fischer and Muller, 2017). The CHR consensus sequences, defined by TTYRAA where Y and R represent pyrimidine and purine bases, respectively (Marceau et al., 2016), are enriched in the promoter regions of MuvB-target genes, not only in humans (Muller et al., 2012; Muller et al., 2014; Muller et al., 2016) but also in flies (Korenjak et al., 2012) and worms (Tabuchi et al., 2011). Although a CXC domain protein, TCX5, is present in both the activator and repressor forms of Arabidopsis DREAM-like complexes, which play a crucial role in the regulation of G2/M phase-specific gene expression, its functional contributions within these

complexes remain unknown, and the CHR elements are yet to be identified in plants (Fischer and DeCaprio, 2015; Kobayashi et al., 2015; Fischer and Muller, 2017).

Other transcription factors are also known to associate with the core complexes, but their presence is less conserved among different organisms. While recruitment of the forkhead box M1 (FOXM1) transcription factor to the MuvB complex is necessary for the full activation of G2/M phase genes in mammals, no forkhead transcription factors have been found in the orthologous complexes of flies, worms, and plants (Fischer and Muller, 2017). Furthermore, Myb-type transcription factors, which function as activators of gene expression both in mammals and flies, are apparently missing from the DRM complex of *C. elegans*, and the *C. elegans* DRM is thought to act primarily as a transcriptional repressor (Harrison et al., 2006; Fischer and Muller, 2017). This is in contrast to DREAM-like complexes of Arabidopsis, where a small family of Myb3R transcription factors with three Myb-repeats with activator or repressor function(s) regulate the expression of many G2/M phase-specific genes by interacting with the promoter sequence known as the mitosis-specific activator (MSA) element (Ito et al., 1998; Ito et al., 2001; Ito, 2005; Haga et al., 2011; Kobayashi et al., 2015). Therefore, Myb3Rs play an important role in determining the direction of transcriptional regulation mediated by Arabidopsis DREAM-like complexes along with the corresponding E2Fs, and despite the seeming absence of the CHR elements in plants, the target promoter regions of Myb3R-containing DREAM-like complexes of Arabidopsis are found to be enriched in MSA and or E2F elements (Kobayashi et al., 2015).

The Chlamydomonas genome also encodes some of the conserved components of DREAM complexes (Figure 1.3), including the homologs of RB (MAT3 in Chlamydomonas) pathway proteins with known roles in the control of cell-size homeostasis, the cell division cycle, and quiescence. A single Myb3R gene is encoded within the genome of Chlamydomonas, whose

expression is upregulated when the light-dark synchronized Chlamydomonas cells go through division (Tulin and Cross, 2015). The coexpression network generated for Chlamydomonas using genome-wide transcriptomics conducted under a number of conditions, including nutrient deprivation, has also found this gene to coexpress or cluster closely with other cell cycle genes (Romero-Campero et al., 2016). Despite the intriguing observation that the five repeats of the Arabidopsis MSA elements are found within the 600 bp upstream of the translational start site of Myb3R gene itself, no obvious enrichment of this motif has been observed in the promoter regions of cell cycle genes when the entire genome was used as a reference (Tulin and Cross, 2015). Furthermore, since none of the previously identified candidate cis-regulatory elements with a potential to regulate the diurnal transcription programs in Chlamydomonas appear to resemble the MSA motif (Panchy et al., 2014; Tulin and Cross, 2015), further studies are needed to implicate Myb3R in cell cycle regulation or cell division.

In addition to the aforementioned genes, the Chlamydomonas genome encodes at least three proteins with annotated CXC domains. Although the literature on these proteins is scarce, one CXC domain protein in Chlamydomonas with characterized functions in the transcriptional regulation of quiescence-associated programs is the Compromised Hydrolysis of TAG 7 (CHT7) protein. The *cht7* mutant is impaired in its ability to remobilize TAG and shows delayed growth upon N or P resupply and rapamycin removal (following a period of N or P starvation and rapamycin treatment, respectively (Tsai et al., 2014)). Decades ago, a similar delay in the resumption of growth was also observed for the *mat3* mutant during N refeeding (Armbrust et al., 1995). Similarly to RB and related proteins, CHT7 proteins are located in the nucleus, although some are also observed in the cytosol (Tsai et al., 2014). Although no obvious defects in growth are detected in the *cht7* mutant during N-replete growth, many genes are misregulated in the mutant

under this condition. Of these genes, nearly 50%, including those involved in photosynthesis, flagellum assembly and autophagy, are expressed in *cht7* cells under N-replete conditions in a similar manner as in wild-type cells, which are subjected to N deprivation (Tsai et al., 2014). In addition, many genes involved in chloroplast-related functions, including photosynthesis, tetrapyrrole synthesis and plastid ribosomal protein synthesis, fail to reverse their expression upon N refeeding in *cht7* as would be typical for genes in the wild type (Tsai et al., 2018). Thus, CHT7 has been hypothesized as an apparent repressor, during N-replete growth and N refeeding of a subset of transcriptomic programs associated with N deprivation-induced quiescence. Furthermore, it was hypothesized that the complete exit from quiescence during N refeeding requires the repression of these programs by CHT7 (Tsai et al., 2014; Tsai et al., 2018). However, the mechanisms governing CHT7 activity and its precise functions during N-mediated life-cycle transitions remain unclear. Thus, further studies are needed to explore how CHT7 complex affects quiescence, whether the CHT7 protein plays a direct or indirect role in the transcriptional regulation of cell cycle genes, or whether or not the Chlamydomonas CHT7 complex is functionally analogous to DREAM complexes in other organisms.

Signaling networks linking the metabolic status to growth in Chlamydomonas: TOR and SnRK/CKIN pathways

Evolutionarily conserved signaling pathways with a central role in the coordination of nutrient status with metabolism and cellular growth in eukaryotes, including photosynthetic organisms, are those involving the target of rapamycin (TOR) kinases and their antagonists, AMPK/Snf1/SnRK/CKIN kinases (Figure 1.4). As suggested by their names, TOR1 and TOR2 kinases were first identified by a genetic mutant screen in yeast as targets of rapamycin (Heitman

et al., 1991), an antifungal and immunosuppressant compound isolated from the soil bacterium *Streptomyces hygroscopicus* (Sehgal et al., 1975; Vezina et al., 1975). Whereas the treatment of wild-type yeast cells leads to the arrest of the cell cycle in the G1 phase, those with a mutation in the *TOR1* or *2* are resistant to the drug (Heitman et al., 1991). Although most organisms contain only a single TOR (Wullschleger et al., 2006), the functional equivalents of two distinct multi-protein complexes discovered in yeast, TOR complex 1 (TORC1) and 2 (TORC2) (Loewith et al., 2002; Wedaman et al., 2003; Reinke et al., 2004), are present in many organisms (Soulard et al., 2009; Gonzalez and Hall, 2017; Saxton and Sabatini, 2017). Despite the identification of TOR and the conservation of TORC1 components, such as RAPTOR (regulatory-associated protein of TOR) and LST8 (lethal with SEC13 protein 8) in plants and algae (Menand et al., 2002; Anderson et al., 2005; Crespo et al., 2005; Diaz-Troya et al., 2008a; Moreau et al., 2012; Shemi et al., 2015), no obvious homologs of TORC2 components have been identified in organisms of the green-lineage, although its functional equivalent is postulated to exist (van Dam et al., 2011; Shemi et al., 2015; Dobrenel et al., 2016a; Perez-Perez et al., 2017; Shi et al., 2018). Nevertheless, the primary functions of the TOR pathways and the mechanisms of TOR inhibition by rapamycin appear conserved in nearly all groups of organisms. When nutrients are ample, TOR complexes act as positive regulators of cellular growth by promoting anabolic processes such as nucleotide synthesis, transcription, ribosome biogenesis and translation, while inhibiting the opposing catabolic processes including mRNA degradation and autophagy (Crespo and Hall, 2002; Diaz-Troya et al., 2008b; Dobrenel et al., 2016a; Gonzalez and Hall, 2017; Perez-Perez et al., 2017; Shi et al., 2018) (Figure 1.4).

Rapamycin acts to inhibit TOR by interacting with a 12-kDa proline isomerase immunophilin known as FK506-binding protein (FKBP12) (Heitman et al., 1991). The FKBP12-

rapamycin complex subsequently binds to the FRB (FKBP12-rapamycin binding) domain of TOR, leading to its inactivation by limiting the accessibility of its kinase domain to the substrate (Aylett et al., 2016). In opisthokonts, TORC1 is sensitive to rapamycin whereas TORC2 is not (Hara et al., 2002; Kim et al., 2002; Loewith et al., 2002; Wedaman et al., 2003; Jacinto et al., 2004), largely owing to the presence of RICTOR (rapamycin-insensitive companion of TOR) in TORC2 which renders the FRB domain inaccessible to the FKBP12-rapamycin (Sarbassov et al., 2004; Gaubitz et al., 2015). In addition, since the FKBP12 proteins of many plant species are unable to stably associate with rapamycin, land plants are resistant or highly tolerant to the growth-inhibitory effects of rapamycin (Xu et al., 1998; Menand et al., 2002; Sormani et al., 2007; Xiong and Sheen, 2012; Xiong et al., 2016). In contrast, growth and cell cycle progression of Chlamydomonas are sensitive to rapamycin treatment, although to a lesser extent when compared to yeast or mammals due to the lower affinity of its FKBP12 protein to rapamycin (Crespo et al., 2005). As observed for other organisms, the Chlamydomonas TOR protein exists as part of a large molecular weight complex, and its single copy LST8 co-purifies with TOR and FKB12 in the presence of rapamycin, confirming the existence of Chlamydomonas TORC1 (Diaz-Troya et al., 2008a). The Chlamydomonas LST8 plays a functionally analogous role to those of yeast and mammals, where the associations of the LST8 proteins with the kinase domains of respective TORs are necessary for their full catalytic activities (Kim et al., 2003; Wullschleger et al., 2005), and the seven WD-40 domains present within Chlamydomonas LST8 may have an additional function in facilitating the association of TORC1 with its various protein substrates (Diaz-Troya et al., 2008a). Furthermore, some fractions of both TOR and LST8 appear to be peripherally associated with membranes of the endoplasmic reticulum (ER) system, particularly near the peri-basal body

regions at the base of flagella, where the demand for protein synthesis is likely high (Rosenbaum and Witman, 2002; Diaz-Troya et al., 2008a).

In animals and yeast, the network governed by TORC1 constitutes one of the major signaling pathways linking nutrient availability to the autophagic machinery, by the phosphorylation-mediated regulation of ATG (autophagy-related) proteins that orchestrate autophagy (Noda and Ohsumi, 1998; Kamada et al., 2000; Alers et al., 2012). As discussed earlier, the activation of autophagy is a necessary cellular response to promote survival during starvation and the consequent establishment of a reversible state of quiescence. The ATG proteins are also conserved in Chlamydomonas (Diaz-Troya et al., 2008b), and the FKBP12-rapamycin mediated inhibition of TORC1 leads to an increased bleaching and vacuolization (Crespo et al., 2005). One such conserved ATG protein, ATG8 has also been demonstrated as an autophagy-specific marker in Chlamydomonas (Perez-Perez et al., 2010; Pérez-Pérez, 2017). In many organisms, the covalent attachment of phosphatidylethanolamine (PE) to ATG8 (known as lipidation) allows for the association of ATG8 proteins with the autophagosome vesicle until the fusion of the ATG8-autophagosome with the vacuole takes place (Geng and Klionsky, 2008). Because the amount of ATG8 proteins is directly related to the number and size of autophagosomes, the levels of lipidated ATG8 and their altered cellular localization can be used as markers of active autophagy (Klionsky et al., 2016), which holds true also for Chlamydomonas (Perez-Perez et al., 2010; Pérez-Pérez, 2017). The treatment of Chlamydomonas cells with rapamycin leads to the accumulation of ATG8 and its lipidated forms, followed by their relocation to large punctate structures in the cytoplasm, indicating the inhibition of TORC1 as an important step in the activation of autophagy (Perez-Perez et al., 2010). Moreover, the same ATG8-marker responses are induced upon subjecting the cells to nutrient starvation and oxidative or ER stresses, illuminating the role of the TORC1

pathway in regulating stress-induced autophagy of this alga (Perez-Perez et al., 2010; Perez-Martin et al., 2014).

In opisthokonts as well as plants, the mechanisms by which TORC1 promotes protein synthesis are known (Chung et al., 1992; De Virgilio and Loewith, 2006; Urban et al., 2007; Ma and Blenis, 2009; Dobrenel et al., 2016b). For instance, in mammals, the direct phosphorylation and activation of S6 kinase (S6K) by TORC1 leads to the S6K-dependent phosphorylation of the ribosomal protein S6, resulting in increased rates of translation initiation (Chung et al., 1992; Ma and Blenis, 2009). The TOR-S6K pathway is also conserved in plants, and the translation initiation of cytosolic S6 ribosomal protein in Arabidopsis is like-wise regulated by this pathway (Zhang et al., 1994; Xiong and Sheen, 2012; Dobrenel et al., 2016b; Schepetilnikov and Ryabova, 2018). The Arabidopsis TOR kinase also promotes plastid ribosomal biogenesis by upregulating the transcription and translation of genes and mRNAs, respectively, for nuclear encoded plastid ribosomal proteins (Dobrenel et al., 2016b). Although Chlamydomonas TOR kinase is implicated in the regulation of de novo amino acid synthesis (Jüppner et al., 2018; Mubeen et al., 2018), and rapamycin treatment is also known to inhibit protein synthesis in this alga (Diaz-Troya et al., 2011), the signaling pathways downstream of TOR controlling protein synthesis are generally less well characterized in algae. However, TOR-dependent phosphorylation sites were also recently identified in S6K and ribosomal S6 protein of Chlamydomonas through phosphoproteomic studies of cells treated with rapamycin, AZD-8055, or Torin1 (Thoreen et al., 2009; Benjamin et al., 2011; Roustan and Weckwerth, 2018; Werth et al., 2019), and TORC1-mediated phosphorylation of the ribosomal S6 protein at serine-245 was shown to be regulated by N as well as P availability in Chlamydomonas (Roustan et al., 2017; Couso et al., 2019). Furthermore, a recent study has begun to establish the regulatory link between P availability and TORC1 signaling Chlamydomonas

(Couso et al., 2019). Using the phosphorylation of ribosomal S6 protein as a marker of TORC1 activity, it was shown that TORC1 becomes inhibited following P starvation likely through a drastic reduction in the abundance of LST8 proteins, which are necessary for the activity of TOR complexes (Loewith et al., 2002; Kim et al., 2003; Wullschleger et al., 2005; Couso et al., 2019). Therefore, it is increasingly evident that the inhibition of TORC1 and the deprivation of nutrients both trigger similar cellular processes and stress responses, not only in yeast where the role of TOR pathways in the coordination of nutrient status to cellular growth is firmly established (Barbet et al., 1996; Beck and Hall, 1999; Hardwick et al., 1999; Komeili et al., 2000), but also in algae (Imamura et al., 2015; Imamura et al., 2016; Mukaida et al., 2016; Couso et al., 2017; Prioretti et al., 2017). In addition to the cessation of growth, the activation of autophagy and the reduction in protein synthesis that occur upon TORC1 inhibition and nutrient starvation, the repression of TORC1 and N shortage both induce the formation of TAG-rich lipid droplets in various species of algae (Imamura et al., 2015; Imamura et al., 2016; Mukaida et al., 2016; Prioretti et al., 2017). In Chlamydomonas and the red alga *Cyanidioschyzon merolae*, the repression of TORC1 pathways by pharmacological means (rapamycin, AZD8055, or Torin1) has been shown to result in the upregulation of key enzymes involved in TAG biosynthesis, such as glycerol-3-phosphate acyltransferase (GPAT) and DGAT (Imamura et al., 2015; Imamura et al., 2016). Consistent with these observations, the accumulation of TAG and starch is also reported for Arabidopsis seedlings with inducible repression of TOR (Caldana et al., 2013).

Although the molecular mechanisms by which TOR pathways regulate lipid metabolism or TAG accumulation are currently not well known in algae, a recent genetic screen for Chlamydomonas mutants with increased sensitivity to rapamycin has identified the *VIP1* locus, suggesting a relationship between inositol polyphosphates (InsPs), TAG accumulation, and TOR

(Couso et al., 2016). The *VIP1* gene encodes a kinase responsible for the pyrophosphorylation of $InsP_6$ to yield $InsP_7$ and $InsP_8$, which are important signaling molecules (Couso et al., 2016). The *vip1-1* mutant has decreased levels of $InsP_7$ and $InsP_8$, slower growth and increased levels of TAG during mixotrophic growth in the presence of acetate (Couso et al., 2016). A similar reduction in the $InsP_7$ and $InsP_8$ content was observed for rapamycin treated wild-type cells, further suggesting a link between InsPs, TAG, and the TOR pathway (Couso et al., 2016). In addition, the expression profiles of thousands of genes are reported to change in response to the rapamycin treatment of Chlamydomonas cells (Ramundo et al., 2014), and they appear to at least partially resemble the transcriptional program associated with nutrient starvation. Following rapamycin treatment, where genes involved in autophagy, vacuolar function, amino acid metabolism and transport tend to be upregulated, genes involved in processes that require a robust anabolic metabolism, e.g. nucleotide synthesis to sustain DNA replication and the cell cycle become downregulated (Ramundo et al., 2014). The decrease in the transcript levels of cell cycle-related genes in response to rapamycin is not only consistent with the observed inhibition of growth following TORC1 inactivation in Chlamydomonas (Crespo et al., 2005; Jüppner et al., 2018) but also with studies in Arabidopsis, where the expression of E2Fa and E2Fb targets with central roles in the regulation of cell cycle is activated by the TORC1-mediated phosphorylation and repressed upon TORC1 inhibition (Xiong et al., 2013; Li et al., 2017). Arabidopsis TORC1 was also recently shown to phosphorylate and inhibit a member of the DRYK (dual-specificity tyrosine phosphorylation-regulated kinase) family, AtYAK1 an orthologue of Yet Another Kinase 1 in yeast), which acts as a negative regulator of plant growth (Barrada et al., 2019; Forzani et al., 2019; Van Leene et al., 2019). Under conditions where TORC1 is inactive, the repression on AtYAK1 is lifted, and AtYAK1 activates plant-specific CDK inhibitors, SMR (Siamese-related) proteins, to negatively regulate cell cycle

progression (Barrada et al., 2019). Yeast YAK1 and its metazoan orthologs, mammalian DYRK1A and fly Minibrain kinases, also have known roles in inhibiting proliferation (Garrett and Broach, 1989; Jaspersen et al., 1998; Hämmerle et al., 2011; Litovchick et al., 2011; Soppa et al., 2014; Thompson et al., 2015; Shaikh et al., 2016). The mammalian DYRK1A upregulates the expression of the gene encoding CDK inhibitor, *CDKN1B* (also known as $p27_{KIP1}$) (Hämmerle et al., 2011). The DYRK1A-mediated phosphorylation of CDKN1B, in addition to cyclin D1 and D3, promotes CDKN1B stabilization, cyclin D degradation and consequently cell cycle exit (Soppa et al., 2014; Thompson et al., 2015). Furthermore, the mammalian DYRK1A also phosphorylates LIN52, a component of the MuvB core, to facilitate DREAM complex formation and to promote entry into quiescence or senescence (Litovchick et al., 2011). In these contexts, it may be worthy to note that Chlamydomonas also has an ortholog of YAK1 named TAR1 (TAG accumulation regulator 1), another green-lineage specific DRYK kinase, DYRKP, and other DRYK-related kinases (Kajikawa et al., 2015; Schulz-Raffelt et al., 2016). While both TAR1 and DYRKP have been shown to regulate the accumulation of TAG and for DYRKP, of starch during N and S deprivation (Kajikawa et al., 2015; Schulz-Raffelt et al., 2016), their potential role in the nutrient-dependent regulation of the Chlamydomonas cell cycle is not yet clear.

In animals and yeast, AMP-activated kinase (AMPK) and sucrose nonfermenting 1 (Snf1) kinase respectively, are central signaling components that are activated by nutrient limitation and other stresses, and act antagonistically to TORC1 (Hardie et al., 1998; Kimura et al., 2003; Hedbacker and Carlson, 2008; Mihaylova and Shaw, 2011; Hardie et al., 2012). The orthologs of AMPK/Snf1 are also conserved in plants and algae, and they are known as Snf-related kinases (SnRKs) in Arabidopsis and sometimes referred to as CKINs (Chlamydomonas kinases) in Chlamydomonas (Dobrenel et al., 2016a; Colina et al., 2019). In general, the activated

AMPK/Snf1/SnRK/CKIN signaling pathway promotes cellular survival and cessation of growth during stress by upregulating catabolic processes to generate more energy and downregulating growth-promoting processes to consume less energy (Baena-Gonzalez and Sheen, 2008; Hedbacker and Carlson, 2008; Hardie, 2011; Hardie et al., 2012; Hindupur et al., 2015; Dobrenel et al., 2016a; Colina et al., 2019) (Figure 1.4). In mammalian cells, AMPK is known to inactivate TORC1 in response to energy and nutrient stresses by phosphorylating one of its constituents, RAPTOR, and by the subsequent recruitment of 14-3-3 proteins (Gwinn et al., 2008). In addition to its inhibitory effect on TORC1, AMPK facilitates the arrest of the cell cycle during the G1 phase prior to the replication of DNA by upregulating and stabilizing the levels of CDK inhibitors, CDKN1A (also known as $p21_{WAF1}$) and CDKN1B (also known as $p27_{KIP1}$), respectively (Imamura et al., 2001; Jones et al., 2005; Liang et al., 2007). The AMPK also promotes the initiation of autophagy, upregulates the uptake of glucose and fatty acids, and facilitates the breakdown of these molecules by the activation of glycolysis and fatty acid oxidation, respectively (Hardie, 2011; Hardie et al., 2012). In a similarly opposing manner to TORC1, AMPK acts to inhibit the biosynthesis of nearly all macromolecules, including proteins, ribosomal RNA, lipids, and carbohydrates by the direct phosphorylation of various key components and regulatory factors of these anabolic pathways (Hardie et al., 2012).

The SnRK family of kinases in Arabidopsis is classified into three subfamilies; the SnRK1 subfamily represents the smallest group with three genes (*SnRK1α1-3*), and they have the greatest similarity to the yeast Snf1 (Hrabak et al., 2003). The SnRK1 family of genes coordinates the energy and redox homeostasis of plants in response to a plethora of growth-inhibiting stresses and regulates a broad range of metabolic pathways through the phosphorylation of the key enzymes or transcription factors to improve stress tolerance and promote survival (Polge and Thomas, 2007;

Halford and Hey, 2009; Wurzinger et al., 2017). In this context, the members of the SnRK1 family act to inhibit highly anabolic processes such as protein synthesis and proliferation, while activating stress-induced responses such as gluconeogenesis and starch synthesis in plants (Dobrenel et al., 2016a). The antagonistic activities of SnRK1α1 towards TORC1 have also been demonstrated in Arabidopsis by its ability to interact with and phosphorylate RAPTOR1B (Nukarinen et al., 2016). Although a complete knockout of *SnRK1* genes results in embryonic lethality in Arabidopsis (Nukarinen et al., 2016), similarly to the knockout mutants of *TOR* (Menand et al., 2002), inducible *amiRNA::SnRK1α2* transgenic plants in the *snrk1α1* mutant background show a hyper-phosphorylation of ribosomal protein S6, indicating their crucial role in the suppression of TORC1 and the downregulation of translation (Nukarinen et al., 2016). The SnRK2 and 3 subfamilies in Arabidopsis are also reported to function in the adaptation of plants to a wide range of abiotic stresses, including drought, flood, cold, salinity, and nutrient scarcity (Coello et al., 2011). Although the characterization of the SnRK family in algae lags behind, a number of studies in Chlamydomonas have suggested the role of SnRKs/CKINs in the cellular response to abiotic stresses, including cold (Valledor et al., 2013) and shortages of S (Davies et al., 1999; Gonzalez-Ballester et al., 2008; Gonzalez-Ballester et al., 2010) and N (Valledor et al., 2014). In Chlamydomonas SAC1 and SnRK2.2 have been implicated in the regulation of TAG synthesis during S deprivation by modulating the expression of *DGTT1-4* (Sato et al., 2014). Indeed, the biotechnical implications of this signaling pathway has recently prompted the genome-wide identification of 22 CKIN proteins in Chlamydomonas as orthologs of plant SnRKs (Colina et al., 2019). Whether the orthologous DREAM complex components in Chlamydomonas are targeted by members of a TOR or SnRK/CKIN signaling cascade to relay cellular nutrient status and to regulate the transitions between cell division and quiescence cycles, remains to be elucidated.

However, these studies are starting to shed light on the significance of signaling pathways involving TOR and SnRK/CKIN in the coordination of nutrient availability, energy metabolism, and cellular growth in photosynthetic organisms. This emerging knowledge provides an essential basis for the further exploration of these signaling networks and assessment of their bioengineering potential in microalgae.

Concluding remarks

Given the ongoing biotechnological interests in algae, increasing numbers of studies are giving rise to a systems-level understanding of how various algal species respond to nutrient starvation, and how the metabolic pathways leading to the accumulation of TAG are regulated. Although the knowledge of transcriptomic and metabolic changes accompanying nutrient shortage and the entry into quiescence in algae continues to improve and evolve, the signaling and molecular components coordinating metabolism, energy status and cell division cycle are still not well understood. The trade-offs between growth and the accumulation of economically valuable compounds thus continue to hinder the directed metabolic engineering of algae for biofuels and the commercial viability of utilizing algae as a chassis for the synthesis of high-value products. However, a better understanding of the controls of the cell division cycle in response to nutrient shortage and the signaling pathways coupling the cellular growth to energy and lipid homeostasis has the potential to improve the future metabolic engineering strategies of algae. Indeed, emerging evidence suggests that the manipulation of signaling pathways, such as TOR, represents a viable approach to increasing the lipid productivity in algae with little to no growth penalties (Prioretti et al., 2017; Prioretti et al., 2019). Thus, further studies of the signaling networks and the downstream components mediating and linking these biological processes is crucial in bridging a critical

knowledge gap, which currently prevents us from achieving the optimal balance between the production of biofuels and biomass in algae employing simple and robust culturing conditions.

Overview

The thesis work presented hereafter aims to expand the knowledge of how a photosynthetic eukaryote such as Chlamydomonas orchestrates the transition from the cell division cycle to quiescence and its reverse, with CHT7 as the focus. The results in Chapter 2 extend the functions of CHT7 to the N-responsive establishment of effective quiescence and resumption of growth. Chapter 3 examines the functional contributions of presumed its CXC domain and sheds new light on the broadly accepted mechanisms by which CXC domain-containing proteins function, especially in photosynthetic organisms. Chapter 4 gives insight into how CHT7 activity is modulated during N-replete synchronized growth and N deprivation, and in Chapter 5, concluding remarks and future perspectives are presented.

APPENDIX

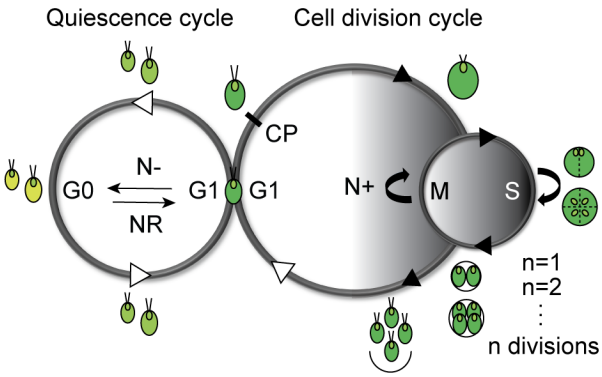

Figure 1.1. The intersection between the cell division and the quiescence cycles in Chlamydomonas.
The circles to the right represent the cell division cycle of Chlamydomonas characterized by multiple fissions, where the cells increase in volume during a prolonged growth (G1) phase during the light phase (white left half), followed by rapid rounds of S/M (DNA synthesis and mitosis) cycles during the dark phase (shaded right half) to give rise to 2^n daughter cells of equal size. The commitment point (CP) represents the size-dependent checkpoint. Upon the passage of CP, the cells commit to completing at least one round of division even when the light or nutrients are subsequently withdrawn. The left circle represents the quiescence cycle, where the cells cease further growth and division with 1C (one copy) chromatin content. The entry into and exit from the quiescence (G0) are controlled by the availability of nutrients, such as nitrogen (N), and the respective changes in chlorophyll content of Chlamydomonas cells are depicted by different shades of green. The coupling of these two opposing cycles occurs during the post-mitotic resting stage or G1 phase prior to the passage of CP. Cell cycle-dependent steps are represented by the black arrow heads, while the nutrient-dependent steps are represented by the white arrow heads. N-replete growth, N+; N deprivation, N-; N refeeding, NR.

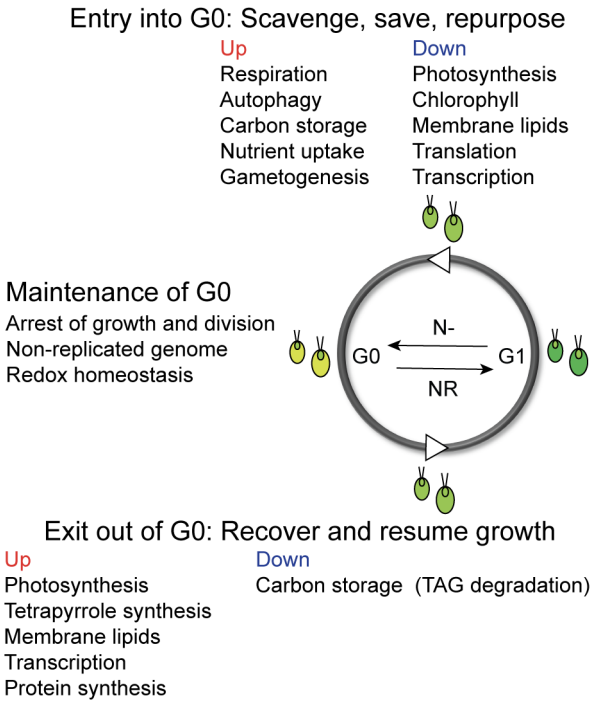

Figure 1.2. Cellular changes accompanying the entry into and exit out of quiescence in Chlamydomonas.
The quiescence cycle of Chlamydomonas cells is depicted, where the cells are colored in different shades of green according to the respective changes in chlorophyll content. The summary of characteristics that Chlamydomonas cells must acquire during the entry into (following N deprivation, N-) and exit of quiescence (G0) (following N refeeding, NR) are shown. The maintenance of a quiescent state is an active process. The repression of genes associated with cell cycle progression, DNA synthesis and replication must be maintained in order to prevent the premature entry into the cell division cycle in the absence of nutrient(s), such as N. The effective management of damaging reactive oxygen species (ROS) and the achievement of redox homeostasis are necessary to promote cellular survival during the non-dividing, energy-limited state. When N becomes available, the cells that remain viable and metabolically active are able to remobilize the accumulated carbon storage, such as triacylglycerols (TAG), remodel photosynthetic membranes, and resume the synthesis of macromolecules in order to reenter the growth (G1) phase. The white arrow heads depict the nutrient-dependent nature of these steps.

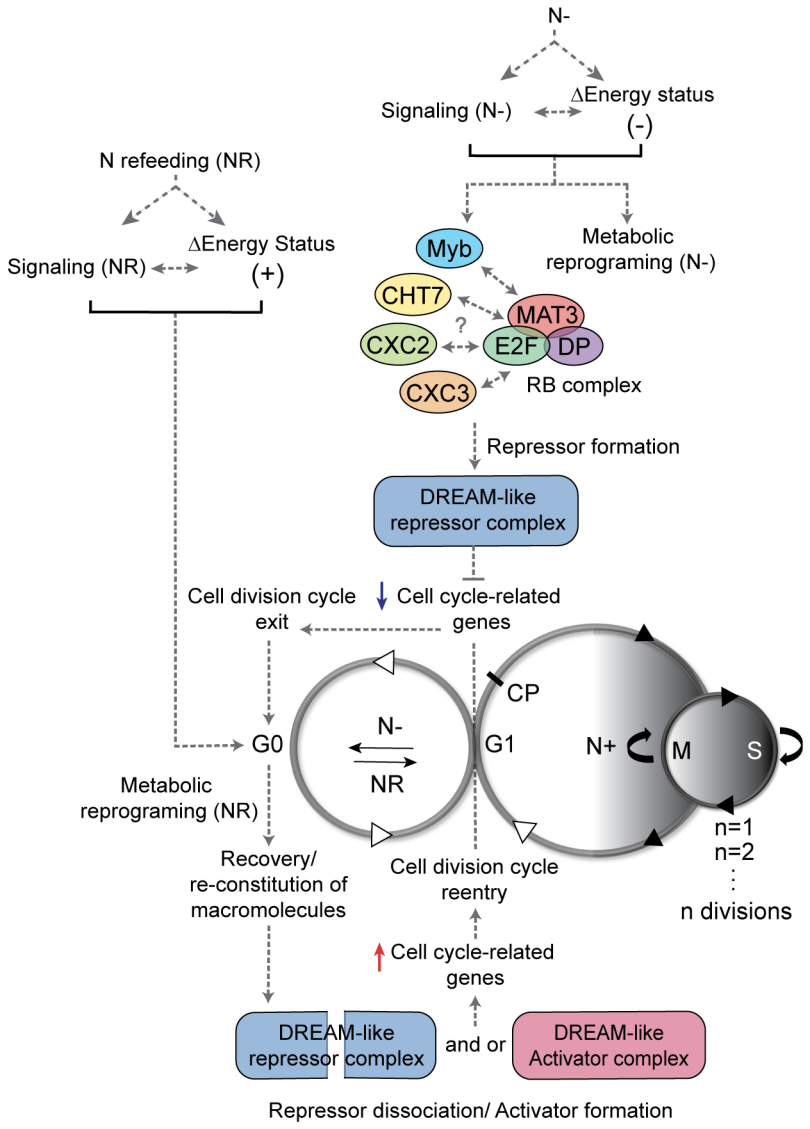

Figure 1.3. Proposed role of putative DREAM-like complexes in the nutrient-dependent life-cycle transitions of Chlamydomonas.
Although the existence of DREAM-like (DP, RB, E2F and Myb-MuvB) complexes has not been confirmed for the green lineage, the repression of genes related to the cell cycle and the cessation of growth and division with 1C (one copy) DNA content in the absence of N have been previously observed. Furthermore, some components of DREAM-like complexes are conserved in Chlamydomonas, including the RB pathway proteins (MAT3/RB, Cre06.g255450; E2F1, Cre01.g052300; DP1, Cre07.g323000), three CXC domain-containing proteins (CHT7, Cre11.g481800; CXC2, Cre08.g361400 and CXC3, Cre12.g550250; potential orthologs of mammalian LIN54, fly Mip120, worm lin-54, and Arabidopsis TCX5), and one Myb protein with three Myb-repeats (Myb3R, Cre12.g522400). The model of their hypothetical functions within the putative DREAM-like complexes in mediating the nutrient-dependent entry into and exit from quiescence (G0) is illustrated. The grey dotted lines are used to denote the hypothesized interactions. In line with the literature demonstrating their importance in the transcriptional regulation of cell cycle-dependent gene expression in other model organisms, the

Figure 1.3 (cont'd)

putative Chlamydomonas DREAM-like repressor complex is postulated to repress the genes associated with cell cycle progression during the post-mitotic or G1 phase prior to the passage of commitment point (CP) in response to N deprivation (N-), allowing the exit from active proliferation and entry into quiescence. Conversely, upon sensing the replenishment of N, the cells need to reinstate their capacity for energy capture and macromolecular synthesis. Once their metabolism is sufficiently restored to sustain further growth, the cell cycle-related genes are postulated to become activated by the dissociation of a DREAM-like repressor complex and or the formation of its activator counterpart, allowing the cells to fully exit from quiescence to reenter the cell division cycle. Although these complexes may also play a role in the progression of the cell division cycle itself, they are omitted from the model for the sake of simplicity. The plus and the minus signs next to the energy status represent energy sufficient and deficient states, respectively. Cell cycle-dependent steps are represented by black arrow heads, while the nutrient-dependent steps are represented by white arrow heads. N-replete growth, N+; N deprivation, N-; N refeeding, NR.

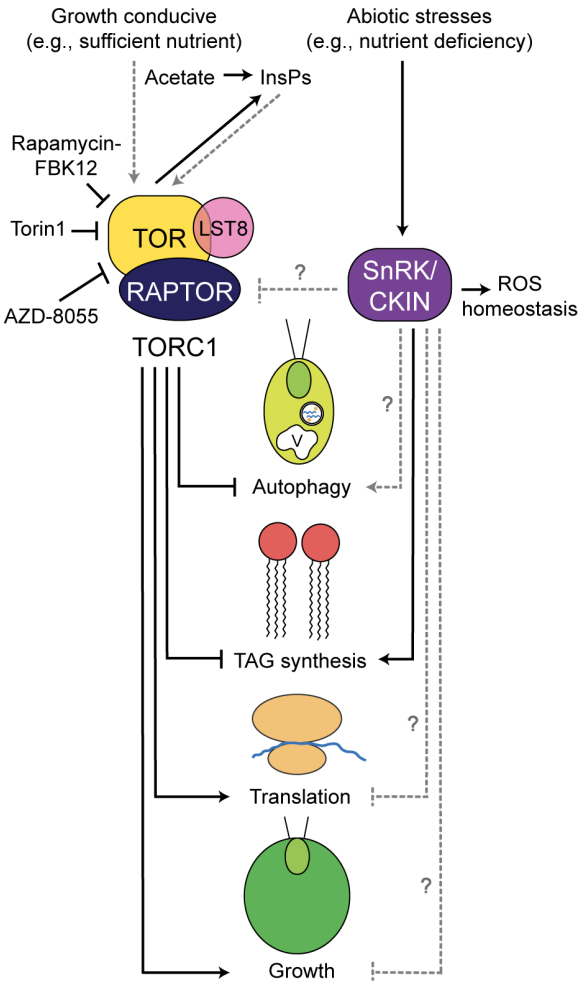

Figure 1.4. Working model of TOR and SnRK/CKIN family of kinases and their major functions in Chlamydomonas stress biology.
Chlamydomonas rapamycin-sensitive TOR complex 1 (TORC1) consists of TOR, LST8 and RAPTOR. The inhibition of TORC1 by pharmacological means (rapamycin, AZD-8055 or Torin1) has enabled the studies of TOR pathway functions in Chlamydomonas, whereas the components of TORC2 have not been identified in photosynthetic organisms. When the conditions are conducive to growth (i.e., in the absence of abiotic stresses), the TORC1 complex promotes anabolic processes such as protein synthesis and therefore growth and represses stress-induced responses such as TAG synthesis and the induction of autophagy. TORC1 has also been shown to positively regulate the levels of inositol polyphosphates (InsPs), $InsP_7$ and $InsP_8$, to promote growth and inhibit TAG accumulation. Although the members of the SnRK and CKIN family of kinases in Chlamydomonas and microalgae are not well-characterized to date, several studies have shown the functions of some members in the acclimation of cells to abiotic stresses, including the adjustment of reactive oxygen species (ROS), accumulation of TAG and sulfur (S) assimilation during sulfur deprivation. The relationships that are supported by experiments, are shown in solid black lines, whereas the dotted grey lines with question marks represent the hypothesized regulatory links based on previous findings in other model organisms that require further studies in Chlamydomonas. The positive and negative regulatory relationships are represented by arrows and T-bars, respectively.

REFERENCES

REFERENCES

Ajjawi, I., Verruto, J., Aqui, M., Soriaga, L.B., Coppersmith, J., Kwok, K., Peach, L., Orchard, E., Kalb, R., Xu, W., et al. (2017). Lipid production in *Nannochloropsis gaditana* is doubled by decreasing expression of a single transcriptional regulator. Nat Biotechnol 35: 647-652.

Alers, S., Loffler, A.S., Wesselborg, S., and Stork, B. (2012). Role of AMPK-mTOR-Ulk1/2 in the regulation of autophagy: cross talk, shortcuts, and feedbacks. Mol Cell Biol 32: 2-11.

Almaraz-Delgado, A.L., Flores-Uribe, J., Pérez-España, V.H., Salgado-Manjarrez, E., and Badillo-Corona, J.A. (2014). Production of therapeutic proteins in the chloroplast of *Chlamydomonas reinhardtii*. AMB Express 4: 57-57.

Anderson, G.H., Veit, B., and Hanson, M.R. (2005). The Arabidopsis AtRaptor genes are essential for post-embryonic plant growth. BMC Biol 3: 12.

Armbrust, E., Ibrahim, A., and Goodenough, U.W. (1995). A mating type-linked mutation that disrupts the uniparental inheritance of chloroplast DNA also disrupts cell-siz control in Chlamdomonas. Mol Biol Cell 6: 1807-1818.

Aylett, C.H., Sauer, E., Imseng, S., Boehringer, D., Hall, M.N., Ban, N., and Maier, T. (2016). Architecture of human mTOR complex 1. Science 351: 48-52.

Baena-Gonzalez, E., and Sheen, J. (2008). Convergent energy and stress signaling. Trends Plant Sci 13: 474-482.

Bajhaiya, A.K., Ziehe Moreira, J., and Pittman, J.K. (2017). Transcriptional engineering of microalgae: Prospects for high-value chemicals. Trends Biotechnol 35: 95-99.

Bajhaiya, A.K., Dean, A.P., Zeef, L.A.H., Webster, R.E., and Pittman, J.K. (2016). PSR1 is a global transcriptional regulator of phosphorus deficiency responses and carbon storage metabolism in *Chlamydomonas reinhardtii*. Plant Physiol 170: 1216-1234.

Barbet, N.C., Schneider, U., Helliwell, S.B., Stansfield, I., Tuite, M.F., and Hall, M.N. (1996). TOR controls translation initiation and early G1 progression in yeast. Mol Biol Cell 7: 25-42.

Barrera, D.J., and Mayfield, S. (2013). High-value recombinant protein production in microalgae. In Handbook of Microalgal Culture: Applied Phycology and Biotechnology, A. Richmond and Q. Hu, eds (Blackwell Publishing Ltd), pp. 532-544.

Beall, E.L., Manak, J.R., Zhou, S., Bell, M., Lipsick, J.S., and Botchan, M.R. (2002). Role for a Drosophila Myb-containing protein complex in site-specific DNA replication. Nature 420: 833-837.

Beck, T., and Hall, M.N. (1999). The TOR signalling pathway controls nuclear localization of nutrient-regulated transcription factors. Nature 402: 689-692.

Benecke, B.-J., Ben-Ze'ev, A., and Penman, S. (1978). The control of mRNA production, translation and turnover in suspended and reattached anchorage-dependent fibroblasts. Cell 14: 931-939.

Benjamin, D., Colombi, M., Moroni, C., and Hall, M.N. (2011). Rapamycin passes the torch: a new generation of mTOR inhibitors. Nat Rev Drug Discov 10: 868-880.

Bisova, K., and Zachleder, V. (2014). Cell-cycle regulation in green algae dividing by multiple fission. J Exp Bot 65: 2585-2602.

Blaby, I., Blaby-Haas, C., Tourasse, N., Hom, E., Lopez, D., Aksoy, M., Grossman, A., Umen, J., Dutcher, S., Porter, M., et al. (2014). The Chlamydomonas genome project: a decade on. Trends Plant Sci 19.

Blaby, I.K., Glaesener, A.G., Mettler, T., Fitz-Gibbon, S.T., Gallaher, S.D., Liu, B., Boyle, N.R., Kropat, J., Stitt, M., Johnson, S., et al. (2013). Systems-level analysis of nitrogen starvation-induced modifications of carbon metabolism in a *Chlamydomonas reinhardtii* starchless mutant. Plant Cell 25: 4305-4323.

Blank, H.M., Perez, R., He, C., Maitra, N., Metz, R., Hill, J., Lin, Y., Johnson, C.D., Bankaitis, V.A., Kennedy, B.K., et al. (2017). Translational control of lipogenic enzymes in the cell cycle of synchronous, growing yeast cells. EMBO J 36: 487-502.

Bölling, C., and Fiehn, O. (2005). Metabolite profiling of *Chlamydomonas reinhardtii* under nutrient deprivation. Plant Physiol 139: 1995-2005.

Boyle, N.R., Page, M.D., Liu, B., Blaby, I.K., Casero, D., Kropat, J., Cokus, S.J., Hong-Hermesdorf, A., Shaw, J., Karpowicz, S.J., et al. (2012). Three acyltransferases and nitrogen-responsive regulator are implicated in nitrogen starvation-induced triacylglycerol accumulation in Chlamydomonas. J Biol Chem 287: 15811-15825.

Brawley, S.H., and Johnson, L.E. (1992). Gametogenesis, gametes and zygotes: An ecological perspective on sexual reproduction in the algae. Br Phycol J 27: 233-252.

Brzeska, K., Brzeski, J., Smith, J., and Chandler, V.L. (2010). Transgenic expression of CBBP, a CXC domain protein, establishes paramutation in maize. Proc Natl Acad Sci U S A 107: 5516-5521.

Bulte, L., and Wollman, F.A. (1992). Evidence for a selective destabilization of an integral membrane protein, the cytochrome b6/f complex, during gametogenesis in *Chlamydomonas reinhardtii*. Eur J Biochem 204: 327-336.

Cai, L., Sutter, B.M., Li, B., and Tu, B.P. (2011). Acetyl-CoA induces cell growth and proliferation by promoting the acetylation of histones at growth genes. Mol Cell 42: 426-437.

Caldana, C., Li, Y., Leisse, A., Zhang, Y., Bartholomaeus, L., Fernie, A.R., Willmitzer, L., and Giavalisco, P. (2013). Systemic analysis of inducible target of rapamycin mutants reveal a general metabolic switch controlling growth in *Arabidopsis thaliana*. Plant J 73: 897-909.

Cavalier-Smith, T. (1970). Electron microscopic evidence for chloroplast fusion in zygotes of *Chlamydomonos reinhardii*. Nature 228: 333-335.

Cheng, D., and He, Q. (2014). Assessment of environmental stresses for enhanced microalgal biofuel production – An overview. Front Energy Res 2.

Chisti, Y. (2007). Biodiesel from microalgae. Biotechnol Adv 25: 294-306.

Chung, J., Kuo, C.J., Crabtree, G.R., and Blenis, J. (1992). Rapamycin-FKBP specifically blocks growth-dependent activation of and signaling by the 70 kd S6 protein kinases. Cell 69: 1227-1236.

Coello, P., Hey, S.J., and Halford, N.G. (2011). The sucrose non-fermenting-1-related (SnRK) family of protein kinases: potential for manipulation to improve stress tolerance and increase yield. J Exp Bot 62: 883-893.

Coleman, A.W. (1982). The nuclear cell cycle in Chlamydomonas (Chlorophyceae). J Phycol 18: 192-195.

Colina, F., Amaral, J., Carbo, M., Pinto, G., Soares, A., Canal, M.J., and Valledor, L. (2019). Genome-wide identification and characterization of CKIN/SnRK gene family in *Chlamydomonas reinhardtii*. Sci Rep 9: 350.

Coller, H.A. (2011). Cell biology. The essence of quiescence. Science 334: 1074-1075.

Coller, H.A., Sang, L., and Roberts, J.M. (2006). A new description of cellular quiescence. PLoS Biol 4: 7.

Costanzo, M., Nishikawa, J.L., Tang, X., Millman, J.S., Schub, O., Breitkreuz, K., Dewar, D., Rupes, I., Andrews, B., and Tyers, M. (2004). CDK activity antagonizes Whi5, an inhibitor of G1/S transcription in yeast. Cell 117: 899-913.

Couso, I., Pérez-Pérez, M.E., Martínez-Force, E., Kim, H.-S., He, Y., Umen, J.G., and Crespo, J.L. (2017). Autophagic flux is required for the synthesis of triacylglycerols and ribosomal protein turnover in Chlamydomonas. J Exp Bot 69: 1355-1367.

Couso, I., Evans, B., Li, J., Liu, Y., Ma, F., Diamond, S., Allen, D.K., and Umen, J.G. (2016). Synergism between inositol polyphosphates and TOR kinase signaling in nutrient sensing, growth control and lipid metabolism in Chlamydomonas. Plant Cell 6: 00351.

Craigie, R.A., and Cavalier-Smith, T. (1982). Cell volume and the control of the Chlamydomonas cell cycle. J Cell Sci 54: 173-191.

Crespo, J.L., and Hall, M.N. (2002). Elucidating TOR signaling and rapamycin action: lessons from *Saccharomyces cerevisiae*. Microbiol Mol Biol Rev 66: 579-591.

Crespo, J.L., Diaz-Troya, S., and Florencio, F.J. (2005). Inhibition of target of rapamycin signaling by rapamycin in the unicellular green alga *Chlamydomonas reinhardtii*. Plant Physiol 139: 1736-1749.

Cross, F.R., and Umen, J.G. (2015). The Chlamydomonas cell cycle. Plant J 82: 370-392.

Cvitanich, C., Pallisgaard, N., Nielsen, K.A., Hansen, A.C., Larsen, K., Pihakaski-Maunsbach, K., Marcker, K.A., and Jensen, E.O. (2000). CPP1, a DNA-binding protein involved in the expression of a soybean leghemoglobin c3 gene. Proc Natl Acad Sci 97: 8163-8168.

Davies, J.P., Yildiz, F.H., and Grossman, A.R. (1999). Sac3, an Snf1-like serine/threonine kinase that positively and negatively regulates the responses of Chlamydomonas to sulfur limitation. Plant Cell 11: 1179-1190.

Davis, P.K., Ho, A., and Dowdy, S.F. (2001). Biological methods for cell-cycle synchronization of mammalian cells. BioTechniques 30: 1322-1326, 1328, 1330-1321.

Day, A., and Goldschmidt-Clermont, M. (2011). The chloroplast transformation toolbox: selectable markers and marker removal. Plant Biotechnol J 9: 540-553.

De Virgilio, C., and Loewith, R. (2006). Cell growth control: little eukaryotes make big contributions. Oncogene 25: 6392-6415.

Dean, M., Levine, R.A., Ran, W., Kindy, M.S., Sonenshein, G.E., and Campisi, J. (1986). Regulation of c-myc transcription and mRNA abundance by serum growth factors and cell contact. J Biol Chem 261: 9161-9166.

Dhawan, J., and Laxman, S. (2015). Decoding the stem cell quiescence cycle – lessons from yeast for regenerative biology. J Cell Sci 128: 4467-4474.

Diaz-Troya, S., Florencio, F.J., and Crespo, J.L. (2008a). Target of rapamycin and LST8 proteins associate with membranes from the endoplasmic reticulum in the unicellular green alga *Chlamydomonas reinhardtii*. Eukaryot Cell 7: 212-222.

Diaz-Troya, S., Perez-Perez, M.E., Florencio, F.J., and Crespo, J.L. (2008b). The role of TOR in autophagy regulation from yeast to plants and mammals. Autophagy 4: 851-865.

Diaz-Troya, S., Perez-Perez, M.E., Perez-Martin, M., Moes, S., Jeno, P., Florencio, F.J., and Crespo, J.L. (2011). Inhibition of protein synthesis by TOR inactivation revealed a conserved regulatory mechanism of the BiP chaperone in Chlamydomonas. Plant Physiol 157: 730-741.

Dobrenel, T., Caldana, C., Hanson, J., Robaglia, C., Vincentz, M., Veit, B., and Meyer, C. (2016a). TOR signaling and nutrient sensing. Annu Rev Plant Biol 67: 261-285.

Dobrenel, T., Mancera-Martinez, E., Forzani, C., Azzopardi, M., Davanture, M., Moreau, M., Schepetilnikov, M., Chicher, J., Langella, O., Zivy, M., et al. (2016b). The Arabidopsis TOR kinase specifically regulates the expression of nuclear genes coding for plastidic ribosomal proteins and the phosphorylation of the cytosolic ribosomal protein S6. Front Plant Sci 7: 1611.

Donnan, L., and John, P.C.L. (1983). Cell cycle control by timer and sizer in Chlamydomonas. Nature 304: 630-633.

Du, Z.Y., and Benning, C. (2016). Triacylglycerol accumulation in photosynthetic cells in plants and algae. Subcell Biochem 86: 179-205.

Fan, J., Andre, C., and Xu, C. (2011). A chloroplast pathway for the de novo biosynthesis of triacylglycerol in *Chlamydomonas reinhardtii*. FEBS Lett 585: 1985-1991.

Fan, J., Yan, C., Andre, C., Shanklin, J., Schwender, J., and Xu, C. (2012). Oil accumulation is controlled by carbon precursor supply for fatty acid synthesis in *Chlamydomonas reinhardtii*. Plant Cell Physiol 53: 1380-1390.

Fang, S.C., de los Reyes, C., and Umen, J.G. (2006). Cell size checkpoint control by the retinoblastoma tumor suppressor pathway. PLoS Genet 2: e167.

Fernández, E., Llamas, Á., and Galván, A. (2009). Chapter 3 - Nitrogen Assimilation and its Regulation. In The Chlamydomonas Sourcebook (Second Edition), E.H. Harris, D.B. Stern, and G.B. Witman, eds (London: Academic Press), pp. 69-113.

Fischer, M., and DeCaprio, J.A. (2015). Does *Arabidopsis thaliana* DREAM of cell cycle control? EMBO J 34: 1987-1989.

Fischer, M., and Muller, G.A. (2017). Cell cycle transcription control: DREAM/MuvB and RB-E2F complexes. Crit Rev Biochem Mol Biol 52: 638-662.

Gargouri, M., Park, J.-J., Holguin, F.O., Kim, M.-J., Wang, H., Deshpande, R.R., Shachar-Hill, Y., Hicks, L.M., and Gang, D.R. (2015). Identification of regulatory network hubs that control lipid metabolism in *Chlamydomonas reinhardtii*. J Exp Bot 66: 4551-4566.

Gaubitz, C., Oliveira, T.M., Prouteau, M., Leitner, A., Karuppasamy, M., Konstantinidou, G., Rispal, D., Eltschinger, S., Robinson, G.C., Thore, S., et al. (2015). Molecular basis of the rapamycin insensitivity of target Of rapamycin complex 2. Mol Cell 58: 977-988.

Geng, J., and Klionsky, D.J. (2008). The Atg8 and Atg12 ubiquitin-like conjugation systems in macroautophagy. 'Protein modifications: beyond the usual suspects' review series. EMBO Rep 9: 859-864.

Goncalves, E.C., Wilkie, A.C., Kirst, M., and Rathinasabapathi, B. (2016). Metabolic regulation of triacylglycerol accumulation in the green algae: identification of potential targets for engineering to improve oil yield. Plant Biotechnol J 14: 1649-1660.

Gonzalez-Ballester, D., Jurado-Oller, J.L., and Fernandez, E. (2015). Relevance of nutrient media composition for hydrogen production in Chlamydomonas. Photosynth Res 125: 395-406.

Gonzalez-Ballester, D., Pollock, S.V., Pootakham, W., and Grossman, A.R. (2008). The central role of a SNRK2 kinase in sulfur deprivation responses. Plant Physiol 147: 216-227.

Gonzalez-Ballester, D., Casero, D., Cokus, S., Pellegrini, M., Merchant, S.S., and Grossman, A.R. (2010). RNA-seq analysis of sulfur-deprived Chlamydomonas cells reveals aspects of acclimation critical for cell survival. Plant Cell 22: 2058-2084.

Gonzalez, A., and Hall, M.N. (2017). Nutrient sensing and TOR signaling in yeast and mammals. EMBO J 36: 397-408.

Goodenough, U., Blaby, I., Casero, D., Gallaher, S.D., Goodson, C., Johnson, S., Lee, J.-H., Merchant, S.S., Pellegrini, M., Roth, R., et al. (2014). The path to triacylglyceride obesity in the *sta6* strain of *Chlamydomonas reinhardtii*. Eukaryot Cell 13: 591-613.

Goodson, C., Roth, R., Wang, Z.T., and Goodenough, U. (2011). Structural correlates of cytoplasmic and chloroplast lipid body synthesis in *Chlamydomonas reinhardtii* and stimulation of lipid body production with acetate boost. Eukaryot Cell 10: 1592-1606.

Granum, E., Kirkvold, S., and Myklestad, S., M. . (2002). Cellular and extracellular production of carbohydrates and amino acids by the marine diatom *Skeletonema costatum*: diel variations and effects of N depletion. Mar Ecol Prog Ser 242: 83-94.

Gray, J.V., Petsko, G.A., Johnston, G.C., Ringe, D., Singer, R.A., and Werner-Washburne, M. (2004). "Sleeping beauty": Quiescence in *Saccharomyces cerevisiae*. Microbiol Mol Biol Rev 68: 187-206.

Gwinn, D.M., Shackelford, D.B., Egan, D.F., Mihaylova, M.M., Mery, A., Vasquez, D.S., Turk, B.E., and Shaw, R.J. (2008). AMPK phosphorylation of raptor mediates a metabolic checkpoint. Mol Cell 30: 214-226.

Haga, N., Kobayashi, K., Suzuki, T., Maeo, K., Kubo, M., Ohtani, M., Mitsuda, N., Demura, T., Nakamura, K., Jürgens, G., et al. (2011). Mutations in MYB3R1 and MYB3R4 cause pleiotropic developmental defects and preferential down-regulation of multiple G2/M-specific genes in Arabidopsis. Plant Physiol 157: 706-717.

Halford, N.G., and Hey, S.J. (2009). Snf1-related protein kinases (SnRKs) act within an intricate network that links metabolic and stress signalling in plants. Biochem J 419: 247-259.

Hannon, M., Gimpel, J., Tran, M., Rasala, B., and Mayfield, S. (2010). Biofuels from algae: challenges and potential. Biofuels 1: 763-784.

Hara, K., Maruki, Y., Long, X., Yoshino, K., Oshiro, N., Hidayat, S., Tokunaga, C., Avruch, J., and Yonezawa, K. (2002). Raptor, a binding partner of target of rapamycin (TOR), mediates TOR action. Cell 110: 177-189.

Hardie, D.G. (2011). AMPK and autophagy get connected. EMBO J 30: 634-635.

Hardie, D.G., Carling, D., and Carlson, M. (1998). The AMP-activated/SNF1 protein kinase subfamily: metabolic sensors of the eukaryotic cell? Annu Rev Biochem 67: 821-855.

Hardie, D.G., Ross, F.A., and Hawley, S.A. (2012). AMPK: a nutrient and energy sensor that maintains energy homeostasis. Nat Rev Mol Cell Biol 13: 251-262.

Hardwick, J.S., Kuruvilla, F.G., Tong, J.K., Shamji, A.F., and Schreiber, S.L. (1999). Rapamycin-modulated transcription defines the subset of nutrient-sensitive signaling pathways directly controlled by the Tor proteins. Proc Natl Acad Sci U S A 96: 14866-14870.

Harris, E.H. (1989). Chlamydomonas Sourcebook. (New York: Academic Press).

Harrison, M.M., Lu, X., and Horvitz, H.R. (2007). LIN-61, one of two *Caenorhabditis elegans* malignant-brain-tumor-repeat-containing proteins, acts with the DRM and NuRD-like protein complexes in vulval development but not in certain other biological processes. Genetics 176: 255-271.

Harrison, M.M., Ceol, C.J., Lu, X., and Horvitz, H.R. (2006). Some *C. elegans* class B synthetic multivulva proteins encode a conserved LIN-35 Rb-containing complex distinct from a NuRD-like complex. Proc Natl Acad Sci 103: 16782-16787.

Hauser, B.A., Villanueva, J.M., and Gasser, C.S. (1998). Arabidopsis *TSO1* regulates directional processes in cells during floral organogenesis. Genetics 150: 411-423.

Hauser, B.A., He, J.Q., Park, S.O., and Gasser, C.S. (2000). TSO1 is a novel protein that modulates cytokinesis and cell expansion in Arabidopsis. Development 127: 2219-2226.

Hedbacker, K., and Carlson, M. (2008). SNF1/AMPK pathways in yeast. Front Biosci 13: 2408-2420.

Heitman, J., Movva, N.R., and Hall, M.N. (1991). Targets for cell cycle arrest by the immunosuppressant rapamycin in yeast. Science 253: 905-909.

Hindupur, S.K., Gonzalez, A., and Hall, M.N. (2015). The opposing actions of target of rapamycin and AMP-activated protein kinase in cell growth control. Cold Spring Harb Perspect Biol 7: a019141.

Hrabak, E.M., Chan, C.W., Gribskov, M., Harper, J.F., Choi, J.H., Halford, N., Kudla, J., Luan, S., Nimmo, H.G., Sussman, M.R., et al. (2003). The Arabidopsis CDPK-SnRK superfamily of protein kinases. Plant Physiol 132: 666-680.

Hu, Q., Sommerfeld, M., Jarvis, E., Ghirardi, M., Posewitz, M., Seibert, M., and Darzins, A. (2008). Microalgal triacylglycerols as feedstocks for biofuel production: perspectives and advances. Plant J 54: 621-639.

Imamura, K., Ogura, T., Kishimoto, A., Kaminishi, M., and Esumi, H. (2001). Cell cycle regulation via p53 phosphorylation by a 5'-AMP activated protein kinase activator, 5-aminoimidazole- 4-carboxamide-1-beta-D-ribofuranoside, in a human hepatocellular carcinoma cell line. Biochem Biophys Res Commun 287: 562-567.

Imamura, S., Kawase, Y., Kobayashi, I., Shimojima, M., Ohta, H., and Tanaka, K. (2016). TOR (target of rapamycin) is a key regulator of triacylglycerol accumulation in microalgae. Plant Signal Behav 11: e1149285.

Imamura, S., Kawase, Y., Kobayashi, I., Sone, T., Era, A., Miyagishima, S.-y., Shimojima, M., Ohta, H., and Tanaka, K. (2015). Target of rapamycin (TOR) plays a critical role in triacylglycerol accumulation in microalgae. Plant Mol Biol 89: 309-318.

Ito, M. (2005). Conservation and diversification of three-repeat Myb transcription factors in plants. J Plant Res 118: 61-69.

Ito, M., Iwase, M., Kodama, H., Lavisse, P., Komamine, A., Nishihama, R., Machida, Y., and Watanabe, A. (1998). A novel cis-acting element in promoters of plant B-type cyclin genes activates M phase-specific transcription. Plant Cell 10: 331-341.

Ito, M., Araki, S., Matsunaga, S., Itoh, T., Nishihama, R., Machida, Y., Doonan, J., and Watanabe, A. (2001). G2/M-phase-specific transcription during the plant cell cycle is mediated by c-Myb-like transcription factors. Plant Cell 13.

Jacinto, E., Loewith, R., Schmidt, A., Lin, S., Ruegg, M.A., Hall, A., and Hall, M.N. (2004). Mammalian TOR complex 2 controls the actin cytoskeleton and is rapamycin insensitive. Nat Cell Biol 6: 1122-1128.

Jinkerson, R.E., and Jonikas, M.C. (2015). Molecular techniques to interrogate and edit the Chlamydomonas nuclear genome. Plant J 82: 393-412.

Jones, C.S., and Mayfield, S.P. (2012). Algae biofuels: versatility for the future of bioenergy. Curr Opin Biotechnol 23: 346-351.

Jones, R.F. (1970). Physiological and biochemical aspects of growth and gametogenesis in *Chlamydomonas reinhardtii*. Ann N Y Acad Sci 175: 648-659.

Jones, R.G., Plas, D.R., Kubek, S., Buzzai, M., Mu, J., Xu, Y., Birnbaum, M.J., and Thompson, C.B. (2005). AMP-activated protein kinase induces a p53-dependent metabolic checkpoint. Mol Cell 18: 283-293.

Juergens, M.T., Disbrow, B., and Shachar-Hill, Y. (2016). The relationship of triacylglycerol and starch accumulation to carbon and energy flows during nutrient deprivation in *Chlamydomonas reinhardtii*. Plant Physiol 171: 2445-2457.

Juergens, M.T., Deshpande, R.R., Lucker, B.F., Park, J.-J., Wang, H., Gargouri, M., Holguin, F.O., Disbrow, B., Schaub, T., Skepper, J.N., et al. (2015). The regulation of photosynthetic structure and function during nitrogen deprivation in *Chlamydomonas reinhardtii*. Plant Physiol 167: 558-573.

Jüppner, J., Mubeen, U., Leisse, A., Caldana, C., Wiszniewski, A., Steinhauser, D., and Giavalisco, P. (2018). The target of rapamycin kinase affects biomass accumulation and cell cycle progression by altering carbon/nitrogen balance in synchronized *Chlamydomonas reinhardtii* cells. Plant J 93: 355-376.

Kajikawa, M., Yamauchi, M., Shinkawa, H., Tanaka, M., Hatano, K., Nishimura, Y., Kato, M., and Fukuzawa, H. (2018). Isolation and characterization of Chlamydomonas autophagy-related mutants in nutrient-deficient conditions. Plant Cell Physiol 60: 126-138.

Kamada, Y., Funakoshi, T., Shintani, T., Nagano, K., Ohsumi, M., and Ohsumi, Y. (2000). Tor-mediated induction of autophagy via an Apg1 protein kinase complex. J Cell Biol 150: 1507-1513.

Kim, D.H., Sarbassov, D.D., Ali, S.M., King, J.E., Latek, R.R., Erdjument-Bromage, H., Tempst, P., and Sabatini, D.M. (2002). mTOR interacts with raptor to form a nutrient-sensitive complex that signals to the cell growth machinery. Cell 110: 163-175.

Kim, D.H., Sarbassov, D.D., Ali, S.M., Latek, R.R., Guntur, K.V., Erdjument-Bromage, H., Tempst, P., and Sabatini, D.M. (2003). GbetaL, a positive regulator of the rapamycin-

sensitive pathway required for the nutrient-sensitive interaction between raptor and mTOR. Mol Cell 11: 895-904.

Kimura, N., Tokunaga, C., Dalal, S., Richardson, C., Yoshino, K.-i., Hara, K., Kemp, B.E., Witters, L.A., Mimura, O., and Yonezawa, K. (2003). A possible linkage between AMP-activated protein kinase (AMPK) and mammalian target of rapamycin (mTOR) signalling pathway. Genes Cells 8: 65-79.

Klionsky, D.J., Abdelmohsen, K., Abe, A., Abedin, M.J., Abeliovich, H., Acevedo Arozena, A., Adachi, H., Adams, C.M., Adams, P.D., Adeli, K., et al. (2016). Guidelines for the use and interpretation of assays for monitoring autophagy (3rd edition). Autophagy 12: 1-222.

Klok, A.J., Lamers, P.P., Martens, D.E., Draaisma, R.B., and Wijffels, R.H. (2014). Edible oils from microalgae: insights in TAG accumulation. Trends Biotechnol 32: 521-528.

Kobayashi, K., Suzuki, T., Iwata, E., Nakamichi, N., Chen, P., Ohtani, M., Ishida, T., Hosoya, H., Muller, S., Leviczky, T., et al. (2015). Transcriptional repression by MYB3R proteins regulates plant organ growth. EMBO J 34: 1992-2007.

Komeili, A., Wedaman, K.P., O'Shea, E.K., and Powers, T. (2000). Mechanism of metabolic control. Target of rapamycin signaling links nitrogen quality to the activity of the Rtg1 and Rtg3 transcription factors. J Cell Biol 151: 863-878.

Korenjak, M., Anderssen, E., Ramaswamy, S., Whetstine, J.R., and Dyson, N.J. (2012). RBF binding to both canonical E2F targets and noncanonical targets depends on functional dE2F/dDP complexes. Mol Cell Biol 32: 4375-4387.

Korenjak, M., Taylor-Harding, B., Binne, U.K., Satterlee, J.S., Stevaux, O., Aasland, R., White-Cooper, H., Dyson, N., and Brehm, A. (2004). Native E2F/RBF complexes contain Myb-interacting proteins and repress transcription of developmentally controlled E2F target genes. Cell 119: 181-193.

Lemons, J.M.S., Feng, X.-J., Bennett, B.D., Legesse-Miller, A., Johnson, E.L., Raitman, I., Pollina, E.A., Rabitz, H.A., Rabinowitz, J.D., and Coller, H.A. (2010). Quiescent fibroblasts exhibit high metabolic activity. PLoS Biol 8: e1000514.

Lewis, P.W., Beall, E.L., Fleischer, T.C., Georlette, D., Link, A.J., and Botchan, M.R. (2004). Identification of a Drosophila Myb-E2F2/RBF transcriptional repressor complex. Genes Dev 18: 2929-2940.

Li-Beisson, Y., Beisson, F., and Riekhof, W. (2015). Metabolism of acyl-lipids in *Chlamydomonas reinhardtii*. Plant J 82: 504-522.

Li, X., Benning, C., and Kuo, M.H. (2012a). Rapid triacylglycerol turnover in *Chlamydomonas reinhardtii* requires a lipase with broad substrate specificity. Eukaryot Cell 11: 1451-1462.

Li, X., Moellering, E.R., Liu, B., Johnny, C., Fedewa, M., Sears, B.B., Kuo, M.H., and Benning, C. (2012b). A galactoglycerolipid lipase is required for triacylglycerol accumulation and survival following nitrogen deprivation in *Chlamydomonas reinhardtii*. Plant Cell 24: 4670-4686.

Li, X., Zhang, R., Patena, W., Gang, S.S., Blum, S.R., Ivanova, N., Yue, R., Robertson, J.M., Lefebvre, P.A., Fitz-Gibbon, S.T., et al. (2016a). An indexed, mapped mutant library enables reverse genetics studies of biological processes in *Chlamydomonas reinhardtii*. Plant Cell 28: 367-387.

Li, Y., Horsman, M., Wu, N., Lan, C.Q., and Dubois-Calero, N. (2008). Biofuels from Microalgae. Biotechnol Prog 24: 815-820.

Li, Y., Liu, D., Lopez-Paz, C., Olson, B.J., and Umen, J.G. (2016b). A new class of cyclin dependent kinase in Chlamydomonas is required for coupling cell size to cell division. Elife 5: e10767.

Liang, J., Shao, S.H., Xu, Z.X., Hennessy, B., Ding, Z., Larrea, M., Kondo, S., Dumont, D.J., Gutterman, J.U., Walker, C.L., et al. (2007). The energy sensing LKB1-AMPK pathway regulates p27(kip1) phosphorylation mediating the decision to enter autophagy or apoptosis. Nat Cell Biol 9: 218-224.

Liang, M.-H., and Jiang, J.-G. (2013). Advancing oleaginous microorganisms to produce lipid via metabolic engineering technology. Prog Lpid Res 52: 395-408.

Litovchick, L., Sadasivam, S., Florens, L., Zhu, X., Swanson, S.K., Velmurugan, S., Chen, R., Washburn, M.P., Liu, X.S., and DeCaprio, J.A. (2007). Evolutionarily conserved multisubunit RBL2/p130 and E2F4 protein complex represses human cell cycle-dependent genes in quiescence. Mol Cell 26: 539-551.

Liu, B., and Benning, C. (2013). Lipid metabolism in microalgae distinguishes itself. Curr Opin Biotechnol 24: 300-309.

Liu, Z., Running, M.P., and Meyerowitz, E.M. (1997). TSO1 functions in cell division during Arabidopsis flower development. Development 124: 665-672.

Loewith, R., Jacinto, E., Wullschleger, S., Lorberg, A., Crespo, J.L., Bonenfant, D., Oppliger, W., Jenoe, P., and Hall, M.N. (2002). Two TOR complexes, only one of which is rapamycin sensitive, have distinct roles in cell growth control. Mol Cell 10: 457-468.

Longworth, J., Noirel, J., Pandhal, J., Wright, P.C., and Vaidyanathan, S. (2012). HILIC- and SCX-based quantitative proteomics of *Chlamydomonas reinhardtii* during nitrogen starvation induced lipid and carbohydrate accumulation. J Proteome Res 11: 5959-5971.

Ma, X.M., and Blenis, J. (2009). Molecular mechanisms of mTOR-mediated translational control. Nat Rev Mol Cell Biol 10: 307-318.

Madeira, J.B., Matos, G.S., Messias, L.S., Bozaquel-Morais, B.L., Masuda, C.A., and Montero-Lomeli, M. (2019). Induction of triacylglycerol synthesis in yeast by cell cycle arrest. FEMS Yeast Res 19.

Majeran, W., Wollman, F.A., and Vallon, O. (2000). Evidence for a role of ClpP in the degradation of the chloroplast cytochrome b(6)f complex. Plant Cell 12: 137-150.

Marceau, A.H., Felthousen, J.G., Goetsch, P.D., Iness, A.N., Lee, H.W., Tripathi, S.M., Strome, S., Litovchick, L., and Rubin, S.M. (2016). Structural basis for LIN54 recognition of CHR elements in cell cycle-regulated promoters. Nat Commun 7: 12301.

Martin, N.C., and Goodenough, U.W. (1975). Gametic differentiation in *Chlamydomonas reinhardtii*. I. Production of gametes and their fine structure. J Cell Biol 67: 587-605.

Martin, N.C., Chiang, K.S., and Goodenough, U.W. (1976). Turnover of chloroplast and cytoplasmic ribosomes during gametogenesis in *Chlamydomonas reinhardi*. Dev Biol 51: 190-201.

Mata, T.M., Martins, A.A., and Caetano, N.S. (2010). Microalgae for biodiesel production and other applications: a review. Renew Sustain Energy Rev 14: 217-232.

Menand, B., Desnos, T., Nussaume, L., Berger, F., Bouchez, D., Meyer, C., and Robaglia, C. (2002). Expression and disruption of the Arabidopsis TOR (target of rapamycin) gene. Proc Natl Acad Sci U S A 99: 6422-6427.

Merchant, S.S., and Helmann, J.D. (2012). Elemental economy: microbial strategies for optimizing growth in the face of nutrient limitation. Adv Microb Physiol 60: 91-210.

Merchant, S.S., Kropat, J., Liu, B., Shaw, J., and Warakanont, J. (2012). TAG, you're it! Chlamydomonas as a reference organism for understanding algal triacylglycerol accumulation. Curr Opin Biotechnol 23: 352-363.

Mihaylova, M.M., and Shaw, R.J. (2011). The AMPK signalling pathway coordinates cell growth, autophagy and metabolism. Nat Cell Biol 13: 1016-1023.

Miles, S., Li, L., Davison, J., and Breeden, L.L. (2013). Xbp1 directs global repression of budding yeast transcription during the transition to quiescence and is important for the longevity and reversibility of the quiescent state. PLoS Genet 9: e1003854.

Miller, R., Wu, G., Deshpande, R.R., Vieler, A., Gartner, K., Li, X., Moellering, E.R., Zauner, S., Cornish, A.J., Liu, B., et al. (2010). Changes in transcript abundance in *Chlamydomonas reinhardtii* following nitrogen deprivation predict diversion of metabolism. Plant Physiol 154: 1737-1752.

Minhas, A.K., Hodgson, P., Barrow, C.J., and Adholeya, A. (2016). A review on the assessment of stress conditions for simultaneous production of microalgal lipids and carotenoids. Front Microbiol 7: 546.

Moreau, M., Azzopardi, M., Clement, G., Dobrenel, T., Marchive, C., Renne, C., Martin-Magniette, M.L., Taconnat, L., Renou, J.P., Robaglia, C., et al. (2012). Mutations in the Arabidopsis homolog of LST8/GbetaL, a partner of the target of Rapamycin kinase, impair plant growth, flowering, and metabolic adaptation to long days. Plant Cell 24: 463-481.

Msanne, J., Xu, D., Konda, A.R., Casas-Mollano, J.A., Awada, T., Cahoon, E.B., and Cerutti, H. (2012). Metabolic and gene expression changes triggered by nitrogen deprivation in the photoautotrophically grown microalgae *Chlamydomonas reinhardtii* and *Coccomyxa sp. C-169*. Phytochemistry 75: 50-59.

Mukaida, S., Ogawa, T., Ohishi, K., Tanizawa, Y., Ohta, D., and Arita, M. (2016). The effect of rapamycin on biodiesel-producing protist Euglena gracilis. Biosci Biotechnol Biochem 80: 1223-1229.

Muller, G.A., and Engeland, K. (2010). The central role of CDE/CHR promoter elements in the regulation of cell cycle-dependent gene transcription. FEBS J 277: 877-893.

Muller, G.A., Stangner, K., Schmitt, T., Wintsche, A., and Engeland, K. (2016). Timing of transcription during the cell cycle: protein complexes binding to E2F, E2F/CLE, CDE/CHR, or CHR promoter elements define early and late cell cycle gene expression. Oncotarget 8: 97736-97748.

Muller, G.A., Wintsche, A., Stangner, K., Prohaska, S.J., Stadler, P.F., and Engeland, K. (2014). The CHR site: definition and genome-wide identification of a cell cycle transcriptional element. Nucleic Acids Res 42: 10331-10350.

Muller, G.A., Quaas, M., Schumann, M., Krause, E., Padi, M., Fischer, M., Litovchick, L., DeCaprio, J.A., and Engeland, K. (2012). The CHR promoter element controls cell cycle-dependent gene transcription and binds the DREAM and MMB complexes. Nucleic Acids Res 40: 1561-1578.

Murphy, D.J. (2001). The biogenesis and functions of lipid bodies in animals, plants and microorganisms. Prog Lipid Res 40: 325-438.

Ngan, C.Y., Wong, C.-H., Choi, C., Yoshinaga, Y., Louie, K., Jia, J., Chen, C., Bowen, B., Cheng, H., Leonelli, L., et al. (2015). Lineage-specific chromatin signatures reveal a regulator of lipid metabolism in microalgae. Nat Plants 1: 15107.

Noda, T., and Ohsumi, Y. (1998). Tor, a phosphatidylinositol kinase homologue, controls autophagy in yeast. J Biol Chem 273: 3963-3966.

Nukarinen, E., Nägele, T., Pedrotti, L., Wurzinger, B., Mair, A., Landgraf, R., Börnke, F., Hanson, J., Teige, M., Baena-Gonzalez, E., et al. (2016). Quantitative phosphoproteomics reveals the role of the AMPK plant ortholog SnRK1 as a metabolic master regulator under energy deprivation. Sci Rep 6: 31697.

Olson, B.J., Oberholzer, M., Li, Y., Zones, J.M., Kohli, H.S., Bisova, K., Fang, S.C., Meisenhelder, J., Hunter, T., and Umen, J.G. (2010). Regulation of the Chlamydomonas cell cycle by a stable, chromatin-associated retinoblastoma tumor suppressor complex. Plant Cell 22: 3331-3347.

Onodera, J., and Ohsumi, Y. (2005). Autophagy is required for maintenance of amino acid levels and protein synthesis under nitrogen starvation. J Biol Chem 280: 31582-31586.

Panchy, N., Wu, G., Newton, L., Tsai, C.H., Chen, J., Benning, C., Farre, E.M., and Shiu, S.H. (2014). Prevalence, evolution, and cis-regulation of diel transcription in *Chlamydomonas reinhardtii*. G3 4: 2461-2471.

Pardee, A.B. (1989). G1 events and regulation of cell proliferation. Science 246: 603-608.

Park, J.B.K., Craggs, R.J., and Shilton, A.N. (2011). Wastewater treatment high rate algal ponds for biofuel production. Bioresour Technol 102: 35-42.

Park, J.J., Wang, H., Gargouri, M., Deshpande, R.R., Skepper, J.N., Holguin, F.O., Juergens, M.T., Shachar-Hill, Y., Hicks, L.M., and Gang, D.R. (2015). The response of *Chlamydomonas reinhardtii* to nitrogen deprivation: a systems biology analysis. Plant J 81: 611-624.

Peltier, G., and Schmidt, G.W. (1991). Chlororespiration: an adaptation to nitrogen deficiency in *Chlamydomonas reinhardtii*. Proc Natl Acad Sci U S A 88: 4791-4795.

Perez-Martin, M., Perez-Perez, M.E., Lemaire, S.D., and Crespo, J.L. (2014). Oxidative stress contributes to autophagy induction in response to endoplasmic reticulum stress in *Chlamydomonas reinhardtii*. Plant Physiol 166: 997-1008.

Perez-Perez, M., Florencio, F., and Crespo, J. (2010). Inhibition of TOR signaling and stress activate autophagy in *Chlamydomonas reinhardtii*. Plant Physiol 152.

Perez-Perez, M.E., Lemaire, S.D., and Crespo, J.L. (2012). Reactive oxygen species and autophagy in plants and algae. Plant Physiol 160: 156-164.

Perez-Perez, M.E., Couso, I., and Crespo, J.L. (2017). The TOR signaling network in the model unicellular green alga *Chlamydomonas reinhardtii*. Biomolecules 7.

Pérez-Pérez, M.E.C., I.; Heredia-Martínez, L.G.; Crespo, J.L. (2017). Monitoring autophagy in the model green microalga *Chlamydomonas reinhardtii*. Cells 6: 36.

Pilkinton, M., Sandoval, R., and Colamonici, O.R. (2007). Mammalian Mip/LIN-9 interacts with either the p107, p130/E2F4 repressor complex or B-Myb in a cell cycle-phase-dependent context distinct from the Drosophila dREAM complex. Oncogene 26: 7535-7543.

Pittman, J.K., Dean, A.P., and Osundeko, O. (2011). The potential of sustainable algal biofuel production using wastewater resources. Bioresour Technol 102: 17-25.

Plumley, F.G., and Schmidt, G.W. (1989). Nitrogen-dependent regulation of photosynthetic gene expression. Proc Natl Acad Sci U S A 86: 2678-2682.

Polge, C., and Thomas, M. (2007). SNF1/AMPK/SnRK1 kinases, global regulators at the heart of energy control? Trends Plant Sci 12: 20-28.

Prioretti, L., Carriere, F., Field, B., Avilan, L., Montané, M.-H., Menand, B., and Gontero, B. (2019). Targeting TOR signaling for enhanced lipid productivity in algae. Biochimie.

Prioretti, L., Avilan, L., Carrière, F., Montané, M.-H., Field, B., Grégori, G., Menand, B., and Gontero, B. (2017). The inhibition of TOR in the model diatom *Phaeodactylum tricornutum* promotes a get-fat growth regime. Algal Res 26: 265-274.

Pulz, O., and Gross, W. (2004). Valuable products from biotechnology of microalgae. Appl Microbiol Biotechnol 65: 635-648.

Radakovits, R., Jinkerson, R.E., Darzins, A., and Posewitz, M.C. (2010). Genetic engineering of algae for enhanced biofuel production. Eukaryot Cell 9: 486-501.

Ramundo, S., Casero, D., Muhlhaus, T., Hemme, D., Sommer, F., Crevecoeur, M., Rahire, M., Schroda, M., Rusch, J., Goodenough, U., et al. (2014). Conditional depletion of the Chlamydomonas chloroplast ClpP protease activates nuclear genes involved in autophagy and plastid protein quality control. Plant Cell 26: 2201-2222.

Rasala, B.A., and Mayfield, S.P. (2015). Photosynthetic biomanufacturing in green algae: production of recombinant proteins for industrial, nutritional, and medical uses. Photosynth Res 123: 227-239.

Reinke, A., Anderson, S., McCaffery, J.M., Yates, J., 3rd, Aronova, S., Chu, S., Fairclough, S., Iverson, C., Wedaman, K.P., and Powers, T. (2004). TOR complex 1 includes a novel component, Tco89p (YPL180w), and cooperates with Ssd1p to maintain cellular integrity in *Saccharomyces cerevisiae*. J Biol Chem 279: 14752-14762.

Rittershaus, E.S., Baek, S.H., and Sassetti, C.M. (2013). The normalcy of dormancy: Common themes in microbial quiescence. Cell Host Microbe 13: 643-651.

Rodolfi, L., Chini Zittelli, G., Bassi, N., Padovani, G., Biondi, N., Bonini, G., and Tredici, M.R. (2009). Microalgae for oil: strain selection, induction of lipid synthesis and outdoor mass cultivation in a low-cost photobioreactor. Biotechnol Bioeng 102: 100-112.

Roessler, P.G. (1990). Environmental control of glycerolipid metabolism in microalgae: commercial implications and future research directions. J Phycol 26: 393-399.

Romero-Campero, F.J., Perez-Hurtado, I., Lucas-Reina, E., Romero, J.M., and Valverde, F. (2016). ChlamyNET: a Chlamydomonas gene co-expression network reveals global properties of the transcriptome and the early setup of key co-expression patterns in the green lineage. BMC Genomics 17: 227.

Rosenbaum, J.L., and Witman, G.B. (2002). Intraflagellar transport. Nat Rev Mol Cell Biol 3: 813-825.

Roustan, V., and Weckwerth, W. (2018). Quantitative phosphoproteomic and system-level analysis of TOR inhibition unravel distinct organellar acclimation in *Chlamydomonas reinhardtii*. Front Plant Sci 9: 1590.

Sadasivam, S., and DeCaprio, J.A. (2013). The DREAM complex: master coordinator of cell cycle-dependent gene expression. Nat Rev Cancer 13: 585-595.

Sarbassov, D.D., Ali, S.M., Kim, D.H., Guertin, D.A., Latek, R.R., Erdjument-Bromage, H., Tempst, P., and Sabatini, D.M. (2004). Rictor, a novel binding partner of mTOR, defines a rapamycin-insensitive and raptor-independent pathway that regulates the cytoskeleton. Curr Biol 14: 1296-1302.

Sato, A., Matsumura, R., Hoshino, N., Tsuzuki, M., and Sato, N. (2014). Responsibility of regulatory gene expression and repressed protein synthesis for triacylglycerol accumulation on sulfur-starvation in *Chlamydomonas reinhardtii*. Front Plant Sci 5: 444-444.

Saxton, R.A., and Sabatini, D.M. (2017). mTOR signaling in growth, metabolism, and disease. Cell 168: 960-976.

Schepetilnikov, M., and Ryabova, L.A. (2018). Recent discoveries on the role of TOR (target of rapamycin) signaling in translation in plants. Plant Physiol 176: 1095-1105.

Schmit, F., Cremer, S., and Gaubatz, S. (2009). LIN54 is an essential core subunit of the DREAM/LINC complex that binds to the cdc2 promoter in a sequence-specific manner. FEBS J 276: 5703-5716.

Schmit, F., Korenjak, M., Mannefeld, M., Schmitt, K., Franke, C., von Eyss, B., Gagrica, S., Hanel, F., Brehm, A., and Gaubatz, S. (2007). LINC, a human complex that is related to pRB-containing complexes in invertebrates regulates the expression of G2/M genes. Cell Cycle 6: 1903-1913.

Schmollinger, S., Muhlhaus, T., Boyle, N.R., Blaby, I.K., Casero, D., Mettler, T., Moseley, J.L., Kropat, J., Sommer, F., Strenkert, D., et al. (2014). Nitrogen-sparing mechanisms in Chlamydomonas affect the transcriptome, the proteome, and photosynthetic metabolism. Plant Cell 26: 1410-1435.

Scott, S.A., Davey, M.P., Dennis, J.S., Horst, I., Howe, C.J., Lea-Smith, D.J., and Smith, A.G. (2010). Biodiesel from algae: challenges and prospects. Curr Opin Biotechnol 21: 277-286.

Scranton, M.A., Ostrand, J.T., Fields, F.J., and Mayfield, S.P. (2015). Chlamydomonas as a model for biofuels and bio-products production. Plant J 82: 523-531.

Sehgal, S.N., Baker, H., and Vezina, C. (1975). Rapamycin (AY-22,989), a new antifungal antibiotic. II. Fermentation, isolation and characterization. J Antibiot (Tokyo) 28: 727-732.

Shahid, A., Rehman, A.U., Usman, M., Ashraf, M.U.F., Javed, M.R., Khan, A.Z., Gill, S.S., and Mehmood, M.A. (2019). Engineering the metabolic pathways of lipid biosynthesis to develop robust microalgal strains for biodiesel production. Biotechnol Appl Biochem pre-print (ePub): doi: 10.1002/bab.1812.

Sharma, K.K.S., H.; Schenk, P.M. (2012). High lipid induction in microalgae for biodiesel production. Energies 5: 1532-1553.

Shemi, A., Ben-Dor, S., and Vardi, A. (2015). Elucidating the composition and conservation of the autophagy pathway in photosynthetic eukaryotes. Autophagy 11: 701-715.

Shi, L., and Tu, B.P. (2013). Acetyl-CoA induces transcription of the key G1 cyclin *CLN3* to promote entry into the cell division cycle in *Saccharomyces cerevisiae*. Proc Natl Acad Sci U S A 110: 7318-7323.

Shi, L., Wu, Y., and Sheen, J. (2018). TOR signaling in plants: conservation and innovation. Development 145: 160887.

Shifrin, N.S., and Chisholm, S.W. (1981). Phytoplankton lipids: interspecific differences and effects of nitrate, silicate and light-dark cycles. J Phycol 17: 374-384.

Siaut, M., Cuine, S., Cagnon, C., Fessler, B., Nguyen, M., Carrier, P., Beyly, A., Beisson, F., Triantaphylides, C., Li-Beisson, Y., et al. (2011). Oil accumulation in the model green alga *Chlamydomonas reinhardtii*: characterization, variability between common laboratory strains and relationship with starch reserves. BMC Biotechnol 11: 1472-6750.

Siersma, P.W., and Chiang, K.S. (1971). Conservation and degradation of cytoplasmic and chloroplast ribosomes in *Chlamydomonas reinhardtii*. J Mol Biol 58: 167-185.

Sijacic, P., Wang, W., and Liu, Z. (2011). Recessive antimorphic alleles overcome functionally redundant loci to reveal TSO1 function in Arabidopsis flowers and meristems. PLoS Genet 7: e1002352.

Simmons, A.R., Davies, K.A., Wang, W., Liu, Z., and Bergmann, D.C. (2019). SOL1 and SOL2 regulate fate transition and cell divisions in the Arabidopsis stomatal lineage. Development 146: dev171066.

Singh, A., Nigam, P.S., and Murphy, J.D. (2011). Mechanism and challenges in commercialisation of algal biofuels. Bioresour Technol 102: 26-34.

Singh, P., Kumari, S., Guldhe, A., Misra, R., Rawat, I., and Bux, F. (2016). Trends and novel strategies for enhancing lipid accumulation and quality in microalgae. Renew Sustain Energy Rev 55: 1-16.

Skjånes, K., Rebours, C., and Lindblad, P. (2013). Potential for green microalgae to produce hydrogen, pharmaceuticals and other high value products in a combined process. Crit Rev Biotechnol 33: 172-215.

Solovchenko, A.E. (2012). Physiological role of neutral lipid accumulation in eukaryotic microalgae under stresses. Russ J Plant Physiol 59: 167-176.

Song, J.Y., Leung, T., Ehler, L.K., Wang, C., and Liu, Z. (2000). Regulation of meristem organization and cell division by TSO1, an Arabidopsis gene with cysteine-rich repeats. Development 127: 2207-2217.

Sormani, R., Yao, L., Menand, B., Ennar, N., Lecampion, C., Meyer, C., and Robaglia, C. (2007). *Saccharomyces cerevisiae* FKBP12 binds *Arabidopsis thaliana* TOR and its expression in plants leads to rapamycin susceptibility. BMC Plant Biol 7: 26.

Soulard, A., Cohen, A., and Hall, M.N. (2009). TOR signaling in invertebrates. Curr Opin Cell Biol 21: 825-836.

Sousa-Victor, P., Gutarra, S., García-Prat, L., Rodriguez-Ubreva, J., Ortet, L., Ruiz-Bonilla, V., Jardí, M., Ballestar, E., González, S., Serrano, A.L., et al. (2014). Geriatric muscle stem cells switch reversible quiescence into senescence. Nature 506: 316.

Spoehr, H.A., and Milner, H.W. (1949). The chemical composition of Chlorella: effect of environmental conditions. Plant Physiol 24: 120-149.

Spudich, J.L., and Sager, R. (1980). Regulation of the Chlamydomonas cell cycle by light and dark. J Cell Biol 85: 136-145.

Steinman, R., Yaroslavskiy, B., Goff, J.P., Alber, S.M., and Watkins, S.C. (2004). Cdk-inhibitors and exit from quiescence in primitive haematopoietic cell subsets. Br J Haematol 124: 358-365.

Suzuki, S.W., Onodera, J., and Ohsumi, Y. (2011). Starvation induced cell death in autophagy-defective yeast mutants is caused by mitochondria dysfunction. PLoS One 6: e17412.

Tabuchi, T.M., Deplancke, B., Osato, N., Zhu, L.J., Barrasa, M.I., Harrison, M.M., Horvitz, H.R., Walhout, A.J., and Hagstrom, K.A. (2011). Chromosome-biased binding and gene regulation by the *Caenorhabditis elegans* DRM complex. PLoS Genet 7: e1002074.

Thoreen, C.C., Kang, S.A., Chang, J.W., Liu, Q., Zhang, J., Gao, Y., Reichling, L.J., Sim, T., Sabatini, D.M., and Gray, N.S. (2009). An ATP-competitive mammalian target of rapamycin inhibitor reveals rapamycin-resistant functions of mTORC1. J Biol Chem 284: 8023-8032.

Tsai, C.H., Uygun, S., Roston, R., Shiu, S.H., and Benning, C. (2018). Recovery from N deprivation is a transcriptionally and functionally distinct state in Chlamydomonas. Plant Physiol 176: 2007-2023.

Tsai, C.H., Warakanont, J., Takeuchi, T., Sears, B.B., Moellering, E.R., and Benning, C. (2014). The protein Compromised Hydrolysis of Triacylglycerols 7 (CHT7) acts as a repressor of cellular quiescence in Chlamydomonas. Proc Natl Acad Sci U S A 111: 15833-15838.

Tsukada, M., and Ohsumi, Y. (1993). Isolation and characterization of autophagy-defective mutants of *Saccharomyces cerevisiae*. FEBS Lett 333: 169-174.

Tulin, F., and Cross, F.R. (2015). Cyclin-dependent kinase regulation of diurnal transcription in Chlamydomonas. Plant Cell 27: 2727-2742.

Umen, J.G., and Goodenough, U.W. (2001). Control of cell division by a retinoblastoma protein homolog in Chlamydomonas. Genes Dev 15: 1652-1661.

Urban, J., Soulard, A., Huber, A., Lippman, S., Mukhopadhyay, D., Deloche, O., Wanke, V., Anrather, D., Ammerer, G., Riezman, H., et al. (2007). Sch9 is a major target of TORC1 in *Saccharomyces cerevisiae*. Mol Cell 26: 663-674.

Valcourt, J.R., Lemons, J.M., Haley, E.M., Kojima, M., Demuren, O.O., and Coller, H.A. (2012). Staying alive: metabolic adaptations to quiescence. Cell Cycle 11: 1680-1696.

Valledor, L., Furuhashi, T., Hanak, A.M., and Weckwerth, W. (2013). Systemic cold stress adaptation of *Chlamydomonas reinhardtii*. Mol Cell Proteomics 12: 2032-2047.

Valledor, L., Furuhashi, T., Recuenco-Munoz, L., Wienkoop, S., and Weckwerth, W. (2014). System-level network analysis of nitrogen starvation and recovery in *Chlamydomonas reinhardtii* reveals potential new targets for increased lipid accumulation. Biotechnol Biofuels 7: 171.

van Dam, T.J., Zwartkruis, F.J., Bos, J.L., and Snel, B. (2011). Evolution of the TOR pathway. J Mol Evol 73: 209-220.

Vezina, C., Kudelski, A., and Sehgal, S.N. (1975). Rapamycin (AY-22,989), a new antifungal antibiotic. I. Taxonomy of the producing streptomycete and isolation of the active principle. J Antibiot (Tokyo) 28: 721-726.

Walkley, C.R., Fero, M.L., Chien, W.M., Purton, L.E., and McArthur, G.A. (2005). Negative cell-cycle regulators cooperatively control self-renewal and differentiation of haematopoietic stem cells. Nat Cell Biol 7: 172-178.

Wang, B., Li, Y., Wu, N., and Lan, C.Q. (2008). CO_2 bio-mitigation using microalgae. Appl Microbiol Biotechnol 79: 707-718.

Wang, W., Sijacic, P., Xu, P., Lian, H., and Liu, Z. (2018). Arabidopsis TSO1 and MYB3R1 form a regulatory module to coordinate cell proliferation with differentiation in shoot and root. Proc Natl Acad Sci U S A 115: E3045-E3054.

Wedaman, K.P., Reinke, A., Anderson, S., Yates, J., 3rd, McCaffery, J.M., and Powers, T. (2003). Tor kinases are in distinct membrane-associated protein complexes in *Saccharomyces cerevisiae*. Mol Biol Cell 14: 1204-1220.

Werth, E.G., McConnell, E.W., Couso Lianez, I., Perrine, Z., Crespo, J.L., Umen, J.G., and Hicks, L.M. (2019). Investigating the effect of target of rapamycin kinase inhibition on the *Chlamydomonas reinhardtii* phosphoproteome: from known homologs to new targets. New Phytol 221: 247-260.

Woertz, I., Feffer, A., Lundquist, T., and Nelson, Y. (2009). Algae grown on dairy and municipal wastewater for simultaneous nutrient removal and lipid production for biofuel feedstock. J Environ Eng 135: 1115-1122.

Wullschleger, S., Loewith, R., and Hall, M.N. (2006). TOR signaling in growth and metabolism. Cell 124: 471-484.

Wullschleger, S., Loewith, R., Oppliger, W., and Hall, M.N. (2005). Molecular organization of target of rapamycin complex 2. J Biol Chem 280: 30697-30704.

Wurzinger, B., Mair, A., Fischer-Schrader, K., Nukarinen, E., Roustan, V., Weckwerth, W., and Teige, M. (2017). Redox state-dependent modulation of plant SnRK1 kinase activity differs from AMPK regulation in animals. FEBS Lett 591: 3625-3636.

Xiong, F., Dong, P., Liu, M., Xie, G., Wang, K., Zhuo, F., Feng, L., Yang, L., Li, Z., and Ren, M. (2016). Tomato FK506 binding protein 12KD (FKBP12) mediates the interaction between rapamycin and target of rapamycin (TOR). Front Plant Sci 7: 1746.

Xiong, Y., and Sheen, J. (2012). Rapamycin and glucose-target of rapamycin (TOR) protein signaling in plants. J Biol Chem 287: 2836-2842.

Xiong, Y., McCormack, M., Li, L., Hall, Q., Xiang, C., and Sheen, J. (2013). Glucose-TOR signalling reprograms the transcriptome and activates meristems. Nature 496: 181-186.

Xu, Q., Liang, S., Kudla, J., and Luan, S. (1998). Molecular characterization of a plant FKBP12 that does not mediate action of FK506 and rapamycin. Plant J 15: 511-519.

Yen, H.-W., Hu, I.C., Chen, C.-Y., Ho, S.-H., Lee, D.-J., and Chang, J.-S. (2013). Microalgae-based biorefinery – From biofuels to natural products. Bioresour Technol 135: 166-174.

Yoon, K., Han, D., Li, Y., Sommerfeld, M., and Hu, Q. (2012). Phospholipid:diacylglycerol acyltransferase is a multifunctional enzyme involved in membrane lipid turnover and degradation while synthesizing triacylglycerol in the unicellular green microalga *Chlamydomonas reinhardtii*. Plant Cell 24: 3708-3724.

Zhang, J., Hao, Q., Bai, L., Xu, J., Yin, W., Song, L., Xu, L., Guo, X., Fan, C., Chen, Y., et al. (2014). Overexpression of the soybean transcription factor GmDof4 significantly enhances the lipid content of *Chlorella ellipsoidea*. Biotechnol Biofuels 7: 128.

Zhang, S.H., Lawton, M.A., Hunter, T., and Lamb, C.J. (1994). atpk1, a novel ribosomal protein kinase gene from Arabidopsis. I. Isolation, characterization, and expression. J Biol Chem 269: 17586-17592.

Zienkiewicz, K., Du, Z.Y., Ma, W., Vollheyde, K., and Benning, C. (2016). Stress-induced neutral lipid biosynthesis in microalgae-molecular, cellular and physiological insights. Biochim Biophys Acta 1861: 1269-1281.

Zones, J.M., Blaby, I.K., Merchant, S.S., and Umen, J.G. (2015). High-resolution profiling of a synchronized diurnal transcriptome from *Chlamydomonas reinhardtii* reveals continuous cell and metabolic differentiation. Plant Cell 27: 2743-2769.

CHAPTER 2

Chlamydomonas CHT7 is required for an effective quiescent state by regulating nutrient-responsive cell cycle gene expression[1]

[1]The work presented in this chapter has been reviewed, and the revised manuscript has been submitted to the Plant Cell journal.

Takeuchi T., Sears B.B., Lindeboom C., Lin YT., Fekaris N., Zienkiewicz K., Zienkiewicz, A., Poliner E., Benning C. (2019). Chlamydomonas CHT7 is required for an effective quiescent state by regulating nutrient-responsive cell cycle gene expression. Plant Cell. Revision submitted.

ABSTRACT

COMPROMISED HYDROLYSIS OF TRIACYLGLYCEROLS 7 (CHT7) in *Chlamydomonas reinhardtii* was previously shown to affect the transcription of a subset of genes during nitrogen (N)-replete growth and following N refeeding. Here, we show that an extensive derepression of genes involved in DNA metabolism and cell cycle-related processes, as well as downregulation of genes encoding oxidoreductases and nutrient transporters occurs in the *cht7* mutant during N deprivation. Cellular mutant phenotypes are consistent with the observed transcriptome misregulation as *cht7* cells fail to properly arrest growth, nuclear replication and cell division following N deprivation. Reduction in *cht7* colony formation following N refeeding is explained by its compromised viability during N deprivation and by the occurrence of abortive divisions during N refeeding. These results highlight that CHT7 is necessary for the nutrient-responsive regulation of cell cycle genes and the orderly establishment of a quiescence state, in addition to the coordinated resumption of growth following N refeeding in Chlamydomonas.

INTRODUCTION

Through the course of evolution, unicellular organisms have adapted strategies to persist in constantly changing and often nutrient-scarce environments that are suboptimal for growth. When the basic nutrient requirements for growth are not met, one strategy for survival is exiting the normal cell division cycle to enter a reversible state called G0 or quiescence (Rittershaus et al., 2013). Upon sensing the scarcity of nutrients, the majority of the cell population slows or arrests growth in a non-replicating but viable state, and the anabolic metabolism characteristic of growth is curtailed in favor of a catabolic, energy-conserving metabolism characteristic of quiescence (Valcourt et al., 2012). When nutrients become available again, the cells that remain metabolically

responsive are able to transition out of quiescence, re-enter the cell division cycle and resume growth. Therefore, the ability of microorganisms to successfully reprogram and tailor their metabolism and growth in response to the availability of nutrients is crucial in conferring organismal fitness. However, contrary to heterotrophs, the coordination between the metabolic status of the cell and the cell division cycle is not well known in photosynthetic eukaryotes, whose metabolism and growth are uniquely linked to photosynthesis.

One protein in Chlamydomonas with a proposed role in the control of quiescence-related gene expression programs is COMPROMISED HYDROLYSIS OF TRIACYLGLYCEROLS 7 (CHT7) (Tsai et al., 2014; Tsai et al., 2018). The *cht7* mutant was originally isolated in a forward genetic screen for mutants delayed in degradation of TAG and resumption of growth during N refeeding following a period of N starvation (Tsai et al., 2014). The initial mutagenesis was performed by random insertion of a selectable Hygromycin B marker gene, *aph7*, using a cell wall-compromised strain (dw15; cw^{-}) as the parental line (PL). The *cht7* mutant was subsequently found to carry an 18,087-bp deletion affecting four genes; however, complementation studies showed that the presence of the *CHT7* gene alone was sufficient to rescue the defects in TAG degradation and to overcome the delay in regrowth after N refeeding (Tsai et al., 2014). The initial phenotypic characterization of the cell wall-deficient *cht7* mutant revealed no obvious physiological defects in the mutant during N-replete growth and following N deprivation. The growth of the *cht7* mutant was comparable to that of the PL under N-replete conditions, and no reduction in apparent cell viability was observed for the mutant or PL during five days of N starvation using the SYTOX Green stain (Tsai et al., 2014). At the population level, the cw^{-} *cht7* mutant cells showed signs of normal metabolic activity in response to N deprivation. The mutant cells accumulated TAG, had similar levels of RNA and protein as the PL, and remained competent for gametogenesis and

mating during N deprivation (Tsai et al., 2014). The *cht7* cells also appeared capable of modulating the RNA and protein content in accordance to the availability of N, ruling out a more specific N sensing defect. However, when the *cht7* mutant was grown in liquid culture, starved for N, and then plated on N-replete TAP (tris-acetate-phosphate) agar, only 20% of the cells produced colonies, and many of them were smaller in diameter than those of the PL (Tsai et al., 2014). Based on these results, it was concluded that the *cht7* mutant is viable and metabolically active during N starvation, but failed to resume cell growth and division once the N is resupplied (Tsai et al., 2014).

In addition to the general phenotypic characterization, global transcriptomic analyses of the cell wall-deficient *cht7* mutant and the PL were previously performed under N-replete growth, following N deprivation (N- 48 h) and subsequent N refeeding (NR 6 and 12 h) (Tsai et al., 2014; Tsai et al., 2018). In the *cht7* mutant, a substantial number of genes (~50%) that are misregulated under N-replete conditions (N+ *cht7*/ N+ PL comparison) are differentially expressed in the PL during N deprivation (N- PL/ N+ PL comparison), suggesting that the transcriptomic programs of *cht7* under N-replete conditions partially resemble those associated with N starvation in the PL (Tsai et al., 2014). A subsequent study described the functional enrichment of genes that fail to reverse their expression or turn on in the *cht7* mutant during N resupply following N deprivation (Tsai et al., 2018). Based on these results, CHT7 was proposed to act as a repressor of a subset of genes associated with N deprivation-induced quiescence during N-replete growth and N refeeding, and it was concluded that while CHT7 did not appear to affect the establishment of a quiescent state during N deprivation, its presence was necessary to mediate the orderly and timely repression of quiescence-associated programs and therefore the resumption of cell growth and division upon N resupply (Tsai et al., 2014; Tsai et al., 2018).

In this study, the previously obtained transcriptomic data of cell wall-deficient *cht7* and its PL were re-examined with a new focus on the N deprivation dataset in order to better define the function of CHT7 following N deprivation. To accurately assess the physiological consequences of the misregulated *cht7* transcriptome following N starvation, the *cht7* mutant locus was introgressed into a cell-walled (cw^+) near wild-type background to circumvent any effects of the cell wall mutation (cw^-), which is reported to affect cell size (Fan et al., 2017), cause an excess secretion of cell wall matrix glycoproteins into the medium (Zhang and Robinson, 1990), and which we found here to affect the outcomes of viability staining assays. Detailed phenotypic characterization of the cw^+ *cht7* mutant cells showed a reduction in cell viability contrary to what was previously observed for the original cw^- *cht7* mutant and revealed the inability of the mutant cells to properly exit from the cell division cycle following N deprivation. Furthermore, the growth and division of *cht7* cells were often impaired during N refeeding even when they survived N starvation. Taken together, these results indicate that CHT7 is necessary for the proper transitions into and out of quiescence in response to changing N availability.

RESULTS

Coexpression analysis of misregulated genes in the original cw^- *cht7* mutant following N deprivation

Global gene expression analyses of the original cw^- *cht7* mutant and the corresponding PL, dw15, were performed previously on cells grown in N-replete medium, following 48 h of N deprivation (Tsai et al., 2014), and after 6 and 12 h of N refeeding (Tsai et al., 2018). Focusing specifically on the function of CHT7 following N starvation, we performed a coexpression analysis of the *cht7* transcriptomic datasets. A two-fold expression change and an adjusted p-value (or false discovery

rate, q) of less than 0.05 were used to define a significant differential expression. For facile comparisons during N deprivation in the context of GO functional enrichment and existing co-expression relationships, differentially regulated genes from two comparisons, N-starved PL versus N-replete PL (N- PL/ N+ PL) and N-starved *cht7* versus N-starved PL (N- *cht7*/ N- PL), were visualized as nodes on the global coexpression network of Chlamydomonas (ChlamyNET) generated by Romero-Campero et al. (2016). ChlamyNET consists of nine functionally-annotated clusters containing 9171 nodes corresponding to genes and 139019 edges representing significant co-expression relationships, as defined by an absolute Pearsons correlation coefficient (PCC) of greater than 0.90, across diverse physiological conditions including nutrient deprivation (Romero-Campero et al., 2016).

Highly coexpressed genes across a number of conditions often participate in functionally related-biological processes (Hughes et al., 2000), which holds true for plants (Aoki et al., 2007; Usadel et al., 2009; Bassel et al., 2011; Cai et al., 2014) and algae, including Chlamydomonas (Aoki et al., 2016; Lauersen et al., 2016; Romero-Campero et al., 2016; Colina et al., 2019). Highly coexpressed genes form hubs (Wang and Chen, 2003), or highly connected nodes on the coexpression network. In ChlamyNET, the most authoritative hub genes that connect key biological processes and likely control the dynamics of the transcriptome are located in the center of the network (Romero-Campero et al., 2016). In this context, the coexpression networks generated from differentially regulated genes in the N- PL/ N+ PL comparison showed the dynamics of highly coordinated transcriptional changes that occur during the establishment of a quiescent state in the PL following N deprivation (Figures 2.1A-B and 2.2A-B). The downregulation of centrally located genes involved in photosynthesis and light-related responses (cluster 8; turquoise) appeared to be coordinated with the downregulation of other key biological

processes such as protein assembly (part of cluster 7; green), translation (part of cluster 4; purple), ribosome biogenesis (part of cluster 3; red) and cell division (cluster 2; brown) (Figure 2.1A). This was accompanied by the concurrent upregulation of genes involved in carbon (C) and nitrogen (N) metabolism (part of cluster 9; blue), transmembrane transport (part of cluster 9; blue), autophagy (cluster 1; orange), membrane lipid turnover (part of cluster 4; purple) and TAG biosynthesis (part of cluster 3; red) (Figure 2.1B). These observations were consistent with the findings by others (Miller et al., 2010; Msanne et al., 2012; Schmollinger et al., 2014; Valledor et al., 2014; Park et al., 2015) and the results of independent Fisher's Exact enrichment analyses performed using the GO-slim terms (GO-Consortium, 2004) and differentially expressed genes, where the whole Chlamydomonas genome served as a reference (Figure 2.3A and B). When the coexpression networks were generated using differentially expressed genes in the N- *cht7*/ N- PL comparison, the differences in the transcriptome of *cht7* and that of PL following N deprivation became apparent (Figure 2.1C-D). Although the number and extent of misregulation observed for the downregulated genes in *cht7* as compared to PL during N deprivation were smaller than those observed for upregulated genes (Figure 2.2C and D), a cluster of centrally located genes involved in transmembrane transport was more downregulated in *cht7* as compared to PL following N deprivation (Figure 2.1C). A wide range of genes encoding the transporters of macro- and micronutrients such as nitrite, nitrate, ammonium, urea, sulfate, molybdate, potassium, magnesium, zinc and formate ions were downregulated to different extents in *cht7* following N starvation (Figure 2.2E). Genes that encode previously characterized mitochondrial carbonic anhydrases, *CAH4* and *CAH5* (Eriksson et al., 1996; Giordano et al., 2003), predicted oxidoreductases such as mitochondrial rubredoxin and NADP adrenodoxin-like ferredoxin, and several low CO_2 inducible proteins were also found among the significantly downregulated genes

in N-deprived *cht7* (Figure 2.2E). The enriched molecular function GO-slim terms among the 968 significantly downregulated genes in *cht7* as compared to PL following N deprivation as determined by the Fisher's Exact Test included oxidoreductases, membrane transporters, and lyases (Figure 2.1E). Gene model IDs and $\log_2$ fold change (FC) expression values of the genes mentioned, in addition to the GO identifiers, p- and q-values of the enriched GO-slim terms are found in Table 2.2.

The coexpression network of significantly upregulated genes in *cht7* as compared to PL following N deprivation revealed the extensive derepression of genes or nodes within the brown (2) cluster and to a much lesser extent within the red (3) and other clusters (Figures 2.1D and 2.2D). During the establishment of an N deprivation-induced quiescent state in PL, nearly all genes within the brown (2) cluster involved in DNA replication, chromosome organization and cell cycle regulation were tightly repressed (Figures 2.1A and 2.2A). In stark contrast, these genes were not repressed in the *cht7* mutant following N deprivation (Figure 2.1D). Since a large number of derepressed genes in *cht7* were found within the brown cluster, representative genes involved in DNA metabolism and cell cycle-related processes were analyzed further as discussed below. However, it is worth noting that some of the most derepressed genes in *cht7* within the red (3) and other clusters included not only those involved in signaling (i.e., phosphorylation) but also a large number of pherophorins, extracellular matrix glycoproteins in Volvocales that share sequence similarities with sex-inducing pheromones (Godl et al., 1995), a related hydroxyproline-rich gamete-specific glycoprotein, GAS28 (Rodriguez et al., 1999; Hoffmann and Beck, 2005), and some gametolysin-like matrix metalloproteinases (Figure 2.2F). Among the 2753 significantly upregulated genes in *cht7* following N deprivation, the enriched GO-slim terms as determined by Fisher's Exact Test consisted of DNA-binding, DNA metabolism, chromosome organization,

ATPase activity, cytoskeleton organization, cell division, cilium, mitotic cell cycle, chromosome segregation, and microtubule organizing center (Figure 2.1F; Table 2.2B). Furthermore, although *CHT7* was not included in the published ChlamyNET (Romero-Campero et al., 2016), the most enriched GO-term among the top 100 genes that are coexpressed with *CHT7* was cell cycle (GO:0007049) with a p-value of $2.357e10^{-3}$ using the algal coexpression database, ALCOdb (Aoki et al., 2016).

A total of 3721 genes were significantly misregulated in *cht7* when compared to PL following N deprivation using a two-fold expression cut-off and an adjusted p-value of 0.05. Almost 74% (2753/ 3721) of these genes consisted of derepressed or upregulated genes while the other 26% (968) consisted of downregulated genes, suggesting that CHT7 acts primarily as a repressor following N deprivation. Almost 60% of the upregulated genes (1649/ 2753) and 51% of the downregulated genes (498/ 968) in the N- *cht*7/ N- PL comparison were expressed in the opposite manner in the N- PL/ N+ PL comparison (purple overlaps, Figure 2.3C and D). Out of the 14 GO-slim terms (at $p < 0.05$) that were enriched among the significantly derepressed or upregulated genes in the N- *cht7*/ N- PL comparison, six were found among the significantly downregulated genes in the N- PL/ N+ PL comparison (Figures 2.1F and 2.3A). When the same set of analyses were applied to the differentially expressed genes identified in *cht7* during N-replete growth (N+ *cht7*/ N+ PL comparison), the genes within the brown (2) cluster were again found to be derepressed in *cht7*, although to a lesser degree in both number and fold expression change in comparison to those observed following N deprivation (Figure 2.4A-D). The results of Fisher's Exact Test performed on down- (1491) and upregulated (1477) genes in *cht7* during N-replete growth suggested that at least some of the downregulation of genes involved in transmembrane transporter activity and the derepression of those involved in DNA-, chromosome- and cell cycle-

related processes are constitutive in *cht7* regardless of N availability (Figure 2.4E and F). While the PL was able to appropriately upregulate genes involved in nutrient uptake and transport and repress those involved in growth-oriented energy-consuming processes in response to N starvation, the *cht7* mutant could not.

Misexpression of genes involved in DNA metabolism and cell cycle-related processes in *cht7* across different N conditions

The coexpression analysis above clearly identified a group of misregulated genes in the *cht7* mutant, with various functions in DNA replication, chromosome organization and cell division cycle (Figure 2.1D). Therefore, the expression changes of a representative set of 108 curated genes in Chlamydomonas that affect different aspects of DNA replication, chromosome organization and segregation, cell size, cell cycle and chloroplast division (Zones et al., 2015) were visualized through a heat-map for different *cht7* to PL comparisons across varying N conditions (Figure 2.5; columns 1, 4, 5 and 6). During the light-dark synchronized N-replete growth in Chlamydomonas, this set of genes is strongly induced as cells enter the S/M (DNA synthesis/mitosis) phase of the cell division cycle (Bisova et al., 2005; Panchy et al., 2014; Tulin and Cross, 2015; Zones et al., 2015; Atkins and Cross, 2018). A comparison of the differential expression of N-starved PL compared to N-replete PL is provided in Figure 2.5, column 2 to show that many of these genes are strongly downregulated in the PL following N deprivation. An additional comparison between N-starved *cht7* and N-replete *cht7* is shown in Figure 2.5, column 3 to directly examine whether the mutant lacks the ability to repress these genes following N deprivation. In line with the global meta-analysis described above, DNA metabolism and cell cycle-related genes were already slightly derepressed in *cht7* compared to PL during N-replete growth (Figure 2.5; column 1).

However, derepression of many of these genes became more apparent in the *cht7* mutant following N deprivation as the PL exited the cell division cycle and established a state of quiescence (Figure 2.5; comparison of columns 2 and 4). Moreover, the expression levels of nearly all S/M phase-related genes remained similar in both N-deprived and N-replete *cht7* cells (Figure 2.5; column 3), further demonstrating the inability of the *cht7* mutant to repress these genes. In general, the extent of derepression observed for these genes in N-deprived *cht7* corresponded to the degree to which they were repressed in the N-starved PL (Figure 2.5; comparison of columns 2 and 4). The relative derepression of these genes in *cht7* progressively became less pronounced at 6 and 12 h after N resupply, likely due to their increased transcription in PL cells as they resume the cell division cycle (Figure 2.5; columns 5 and 6), further supporting the notion that CHT7 is acting in a repressor function. Although it is impossible to deduce the dynamics of cell cycle regulation from transcript levels alone, our data point to the role of CHT7 as a transcriptional repressor of S/M phase genes and suggest that CHT7 is necessary for the transcriptional establishment of quiescence following N deprivation.

Phenotypes of cell-walled *cht7* lines and CHT7-dependent derepression of genes related to DNA metabolism and the cell cycle

Based on our own observations and aforementioned findings by others on the impact of the cw^- mutation of Chlamydomonas cells on cell size (Fan et al., 2017) and physiological functions (Zhang and Robinson, 1990), we were concerned that the presence of the cw^- mutation in the original *cht7* mutant would interfere with the identification of bona-fide *cht7* phenotypes caused solely by the loss of CHT7. Therefore, the *cht7* mutation was introduced into a cw^+ wild-type background by a series of crosses to produce 9^{th} generation cw^+ *cht7* lines, hereafter simply

referred to as *cht7* (1-3) (Figure 2.6A). The corresponding complemented lines, *CHT7:cht7* (1-3), were generated through the transformation of *cht7* (1-3) lines with a construct containing the Paromomycin resistance marker *aphv8* and a genomic *CHT7* gene, including 1,000 bps upstream and downstream of the coding sequence (Figure 2.6A). The identities of the *cht7* (1-3) as well as complemented lines were verified by PCR-based genotyping for the Hygromycin resistance marker *aphv7* and *CHT7* sequences and by immunoblotting to visualize the CHT7 protein (Figure 2.6C-D). During N-replete mixotrophic growth, the phenotypes of two wild types (21gr, mt^+ and 6145c, mt^-), three cell-walled *cht7* (1-3) mutant lines and three *CHT7:cht7* (1-3) complemented lines were essentially indistinguishable in terms of growth rate, cell and organelle ultrastructure, nuclear and cell morphologies, and colony formation (Figure 2.7A-D). When the same set of lines described above were N-deprived for 48 h and N was resupplied, the *cht7* (1-3) mutants showed a strong delay in regrowth (Figure 2.8A). This was also visibly apparent in the coloration of the cultures, with the *cht7* mutant cultures being less green 24 h following N refeeding (Figure 2.8B). All lines accumulated TAG to equal levels after 48 h of N deprivation; however, while TAG was mostly degraded after 24 h of N refeeding in the wild-type and complemented lines, TAG degradation in *cht7* (1-3) lines lagged behind (Figure 2.8C). These observations were consistent with the previously reported phenotypes of cell wall-deficient *cht7* lines (Tsai et al., 2014).

To test that the derepression of DNA and cell cycle-related genes observed among the RNA-Seq datasets of cw^- *cht7* recapitulates in the cw^+ *cht7* line and is solely caused by the absence of CHT7, the transcript levels of a representative set of genes involved in DNA metabolism and replication, chromosomal organization, cell cycle progression and chloroplast division were analyzed in the new cw^+ *cht7* (1) mutant, its complemented line, *CHT7:cht7* (1), and two wild types using quantitative PCR (qPCR) (Figures 2.8D-F and 2.9A-E). Following N deprivation for

48 h and N resupply for 6 and 12 h, derepressed genes identified in the transcriptomics of cell wall-deficient *cht7* were also derepressed in the newly introgressed cell-walled *cht7* (1) mutant line as determined by qPCR, with the target expression normalized to *CBLP* as the reference gene (Schloss, 1990). The elevated transcript levels of genes pertinent to DNA synthesis and initiation of DNA replication during the S phase, such as *RIR1* and *RIR2* (*Ribonucleoside-diphosphate Reductase 1*, *2*), *CDT1-like* (*Chromatin Licensing and DNA Replication Factor 1-like*), *ORC1* (*Origin Recognition Complex 1*), *MCM2* and *10* (*Minichromosome Maintenance 2, 10*), *CDC45* (*Cell Division Cycle 45*), and *GINS3* (*GINS complex subunit 3*) were observed in *cht7* (1) (Figures 2.8D and 2.9A-B). Genes that encode the small catalytic and probable large subunits of DNA primase (*POLA4* and *PRI2*), *Proliferating Cell Nuclear Antigen* (*PCN1/PCNA*) that acts as a DNA clamp to confer processivity to DNA polymerase δ, *Replication Protein A1* (*RPA1*) which binds and stabilizes single stranded DNA intermediate along with other RPA proteins, *topoisomerase II* (*TOPOII*) and *histone H4* (*HFO*) were also derepressed in *cht7* (1) (Figures 2.8E and 2.9B) (Yao and O'Donnell, 2010). Genes involved in the progression of the mitotic cell cycle, such as *Cyclin-dependent kinases*, *CDKA1* and *CDKB1*, and their corresponding *Cyclins*, *CYCA1, CYCB1* and *CYCAB1 (Atkins and Cross, 2018)*, in addition to *WEE1* (Featherstone and Russell, 1991) and *BUB1* (Bernard et al., 1998; Tang et al., 2004) kinases, where the former acts as a negative regulator of mitosis by phosphorylation and inactivation of CDK1-Cyclin B1 complex and the latter is essential for the initiation of spindle-assembly checkpoint and inhibition of APC/C in opisthokonts, all showed elevated expression in *cht7* (1) following N deprivation and during N refeeding (Figures 2.8F and 2.9D). Homologs of plant chloroplast division site determinants, *MIND1* and *MINE1*, and two other CXC domain protein encoding genes in Chlamydomonas, *Cre12.g550250* and *Cre08.g361400*, were also derepressed in *cht7* (1) following N deprivation for

48 h and N resupply for 6 and 12 h (Figure 2.9C and E). Since the Ct (cycle threshold) values observed for the *CBLP* gene used for normalization were similar across all lines and conditions, transcripts of the aforementioned genes were indeed more abundant in the *cht7* (1) mutant as compared to the two wild types and the complemented *CHT7:cht7* (1) line following N deprivation. In addition, the transcript levels of the tested genes not only remained consistently higher in *cht7* (1) than the rest of the lines even 12 h into N refeeding, many of them increased even further in *cht7* (1) following N resupply. On the contrary, reintroduction of *CHT7* into *cht7* (1) in the complemented line completely restored the expression levels of these genes back to those observed for the two wild types, indicating that the absence of CHT7 is responsible for the derepression of these genes observed in *cht7* (1) following N deprivation and during N resupply.

CHT7 is needed for the proper arrest of cell cycle-associated processes following N deprivation and the orderly resumption of the cell division cycle after N refeeding

To explore the physiological consequences of the misregulated DNA metabolism and cell cycle-related genes in *cht7* following N starvation and N resupply, cells from two wild types, *cht7* (1-3) and the respective complemented lines were stained with DAPI to observe their nuclear and cellular morphology by confocal microscopy after 48 h of N deprivation or after 24 h of N resupply following 48 h of N deprivation (Figure 2.10A and C, respectively; representative images from *cht7* (1) are shown). Within 24 h of shifting the Chlamydomonas cells to N-free medium, those that presumably passed the cell size checkpoint called Commitment (Spudich and Sager, 1980; Donnan and John, 1983) will divide at least once before ceasing further division, and the cell numbers approximately double during this time (Blaby et al., 2013; Schmollinger et al., 2014). Since this division occurs at the expense of intracellular reserves of N even in the absence of

externally available N, the arrest of division at a proper cell cycle stage during N deprivation is likely crucial for cellular survival, the proper establishment of a quiescent state and the subsequent resumption of growth when N becomes available again. In support of this notion, the transcriptional repression of growth and cell cycle-related genes have been previously shown as important for the prolonged lifespan and the reversibility of the quiescent state in yeast cells following glucose exhaustion and refeeding (Miles et al., 2013). While greater than 95% of the cells of two wild types and the complemented line had arrested nuclear and cell division with one condensed nuclear structure per cell following 48 h of N starvation, approximately 11 $\pm$ 3.8% of *cht7* (1-3) cells (average and standard deviation of three independent lines) became increasingly enlarged, misshapen or absent in chlorophyll signals, and 27 $\pm$ 10.3% (average and standard deviation of three independent lines) was observed to have multiple nuclei (Figure 2.10A and B). This result indicates that some *cht7* cells continued to grow but did not initiate or complete division while some failed to arrest division at a non-replicating state, suggesting that the cellular growth, karyokinesis and cytokinesis are not properly coordinated in the mutant following N deprivation. In addition, *cht7* cells did not resume growth and division in a manner that were observed for the two wild types and the complemented lines following N refeeding. The dividing wild-type and the complemented cells showed a symmetrical plane of division, producing daughter cells that were approximately equal in size and organelle content following 24 h of N resupply (Figure 2.10C). In contrast, even after 24 h of N refeeding, some *cht7* cells remained at a large size or grew in volume without completing division while those that initiated division produced multiple daughter cells that were largely disorganized and unequal in size (Figure 2.10C). To objectively estimate the fraction of abnormally dividing *cht7* cells during N refeeding, the percentages of dividing mother cells with daughter cell(s) that showed terminated division (Figure 2.10C; white arrow heads) were

assessed (Figure 2.10D). Whereas the vast majority (> 90%) of both non-dividing and dividing wild-type and the complemented population appeared normal, over half of the *cht7* (1-3) population did not, where most of them existed as dividing mother cells with one or more visibly aborted daughter cell(s) (Figure 2.10D). Taken together, we conclude that the presence of CHT7 is needed for cells to arrest growth, nuclear replication and cell division at an appropriate stage of cell cycle following N deprivation and to properly re-enter the cell division cycle when N is resupplied.

The *cht7* mutation affects mitotic but not meiotic divisions following N refeeding

During N deprivation, the haploid Chlamydomonas cells gain competency in mating (Martin and Goodenough, 1975), and the sexually competent gametes of opposing mating types fuse to create a diploid zygospore, which undergoes meiotic divisions upon N resupply. In constructing the cell-walled *cht7* (1-3) lines, we observed that about half of the progeny from every generation of crosses yielded zygospores that produced meiotic progeny that did not divide further and produce colonies. Such meiotic inviability was observed for the ninth generation *cht7* (1-3) lines when they were crossed with CC-110, one of the mt^+ parents used in the backcrossing scheme (Table 2.1A; Figure 2.6A). However, the same results were also observed when the wild-type mt^- backcross parent, 6145c and the *CHT7:cht7* (1-3) complemented lines were crossed to CC-110 (Table 2.1A). Furthermore, when the same set of lines were crossed to 21gr, another wild-type mt^+ backcross parent, no severe decline in meiotic viability was observed for any of the crosses regardless of the mt^- partner (Table 2.1B). These results suggested that the incompatible genetic backgrounds and not the *cht7* mutation was causal for the observed meiotic inviability. Nevertheless, additional ninth generation mt^+ and mt^- *cht7* lines, *cht7* (4) and *cht7* (5) respectively, were selected to test the

impacts of homozygous null *cht7* mutations on the ability of diploid zygospores to successfully undergo meiotic division and produce colonies. The new *cht7* (4) mt^+ line appeared to have the same incompatibility as did CC-110 when crossed with control 6145c or *cht7* (1). However, good meiotic viability (> 50% of tetrads) was observed when it was crossed with the new mt^- *cht7* (5) line (Table 2.1C). Hence, we conclude that the apparent meiotic inviability observed was a result of the incompatible genetic backgrounds of the two backcross strains, CC-110 and 6145c, and was not caused by the *cht7* mutation.

CHT7 promotes cellular survival during N deprivation and N refeeding

Because the transcriptome and cell division-related phenotypes of the *cht7* mutant following N deprivation suggested highly misregulated physiological processes, viability of *cht7* (1-3) mutants was examined by two different methods. First, we assessed the ability of N-deprived *cht7* (1-3) cells to form colonies following a shift to N-replete medium. For this purpose, wild-type, *cht7* (1-3) and *CHT7:cht7* (1-3) complemented cells were transferred during N-replete mid-log growth to N-free medium for different lengths of time, and the percentage of cells that would form colonies on N-replete TAP plates was assessed (Figure 2.11A). While approximately 60-80% of cells of wild-type and complemented lines were consistently able to form colonies during five days of N deprivation, *cht7* (1-3) cells rapidly lost that ability, with only about 20% of the mutant cells giving rise to colonies after 48 h of N deprivation (Figure 2.11A). The progressive decline in the ability to form colonies after N resupply following N deprivation was also previously observed for the cell wall-deficient *cht7* mutant (Tsai et al., 2014). To determine the fraction of *cht7* (1-3) cells that remained viable at the time of plating, we used SYTOX Green nucleic acid stain, which is excluded from live cells but not from the dead cells. Using this approach, we observed that the apparent

viability of cells from wild-type and complemented lines remained above 80% even after 120 h of N deprivation (Figure 2.11B). For the wild-type and complemented cells, the percentages of viable cells as assessed by SYTOX stain were similar to those capable of colony formation, suggesting most of these cells that remained viable during N deprivation as observed by SYTOX stain go on to form colonies when they are transferred to N-replete agar plates. In contrast, the viability of *cht7* (1-3) cells declined to about 60-70% after 48 h of N deprivation and continued to decline at subsequent time points before stabilizing at 40-50% after 96 h (Figure 2.11B). This result was notable for two reasons. First, using the same SYTOX assay and conditions, no apparent loss of viability was observed for the original cw$^-$ *cht7* mutant line, suggesting that the presence or absence of the cell wall affected the outcome of the SYTOX-based viability staining during N deprivation. However, the progressive loss of viability in *cht7* (1-3) during N deprivation was also supported by the concurrent accumulation of malondialdehyde (Figure 2.12A), a byproduct of lipid oxidation by reactive oxygen species (ROS), and by the severe degradation of thylakoids and ghost cells observed in the mutant following N deprivation by transmission electron microscopy (TEM) (Figure 2.12B). Second, the percentage of *cht7* (1-3) cells that remained viable during N deprivation according to the SYTOX stain (Figure 2.11B) was much greater than the percentage of cells capable of forming colonies when plated on N-replete agar medium (Figure 2.11A). For instance, although 60-70% of *cht7* (1) cells remained viable according to the SYTOX assay at N deprivation of 48 h (Figure 2.11B), only 20-30% of *cht7* (1) cells N-starved for the same time formed colonies after seven days of growth on N-replete TAP plates (Figure 2.11A), suggesting almost 40% of *cht7* (1) cells that remained viable at the time of N deprivation subsequently fail to divide and produce colonies after N is resupplied.

To gain further insight into the reduced ability of *cht7* (1-3) to form colonies following N deprivation, we tracked individual cells of *cht7* (1) for six days by microscopy after plating cells that were N-deprived for 48 h on N-replete agar medium (Figures 2.13 and 2.14) and classified the cells based on their appearance and ability to divide and form colonies on day two of N resupply (Figure 2.13B). After only two days of growth on N-replete plates, the differences in colony sizes were visibly apparent (Figure 2.13A). Most N-deprived wild-type (~70%) and complemented cells (~80%) divided into normal colonies (defined as class 1, containing 64 cells or more) after two days on N-replete plates, and only a small number of cells with the *CHT7* allele (wild-type or complemented lines) lagged in their division, producing colonies with fewer than 32 cells (class 2), or remained non-responsive to N (class 4) at the same time point (Figure 2.13B). In contrast, almost all *cht7 (*1) mutant cells showed an aberrant response to resupply of N, and only a very small fraction of *cht7 (*1) cells (< 3%; class 1) readily entered the cell division cycle to form normal colonies after two days on N-replete agar medium (Figure 2.13B). Specifically, most of the mutant cells either did not respond to N (class 4; ~50%), increased in volume but failed to divide into colonies (class 3; ~35%), or were slow to divide (~15%; class 2), forming colonies much smaller than 32 cells by the same time (Figure 2.13B). Hence, about 50% of *cht7* (1) cells (class 1, 2, and 3) remained metabolically active after 48 h of N depletion in that they exhibited a response to N resupply by growing in volume, while the other 50% showed no response. Out of those that remained responsive to N, approximately 20% of N-deprived *cht7* (1) cells were able to form colonies (class 1 and 2) while the other 35% showed signs of metabolism by growing in size or attempting to divide but eventually displaying abortive division without colony formation (Figure 2.13B), explaining the observed differences between the results of the two viability assessments (Figure 2.11A and B). Examples of the *cht7* (1) cells that were completely non-responsive to N

resupply (cells 1-4; class 4) and those that enlarged and attempted to divide (cells 5-8; class 3) are shown in Figure 2.13C and D. It is also noteworthy that some *cht7* (1) cells already showed signs of improper cell division arrest following 48 h of N deprivation (Figure 2.13D; day 0 images of cells 2, 6, 7, 8). The *cht7* (1) cells that appeared to show signs of cell division in the presence of visible starch granules and lipid droplets were also observed by TEM following 48 h of N starvation (Figure 2.12C). These results were largely in line with the observations made by confocal microscopy (Figure 2.10A). Thus, the findings from these experiments suggested a role for CHT7 in promoting cellular survival during N deprivation, and that the establishment of a proper quiescent state during N deprivation is likely crucial in mediating the subsequent reentry into the cell division cycle.

DISCUSSION

Extending our previous studies of CHT7 function (Tsai et al., 2014; Tsai et al., 2018), the focus of this study was on the processes affected by CHT7 during N deprivation to gain deeper mechanistic insights into its role in establishing a proper quiescent state, which ultimately also affects how cells reenter the cell cycle following N refeeding. One key conclusion based on the current study is that derepressed genes in the N-deprived *cht7* mutant were enriched in genes involved in DNA metabolism and cell cycle-related processes (Figure 2.1D and F). As illustrated in Figure 2.15A and B, we are proposing that CHT7 is needed to successfully establish a state of quiescence in response to N deprivation by tightly repressing these genes at an appropriate stage of the cell division cycle until nutrients become available again (Figures 2.1A, 2.3A and 2.5, column 2). This hypothesis is largely based on our interpretation of the phenotype of the *cht*7 mutant. Although the *cht7* mutant cells appear to perceive and respond to N deprivation by adjusting their transcriptome

and metabolism to accumulate TAG (Figure 2.8C) and starch (Figure 2.12B), the repression of DNA metabolic and cell cycle-related genes does not occur in the absence of CHT7, especially following N deprivation (Figure 2.5, columns 3 and 4) (illustrated in Figure 2.15C). Furthermore, unlike the wild type, the *cht7* cells are unable to upregulate genes involved in uptake and transport of nutrients when no external N is available (Figure 2.1C and E). The observed misregulation of the transcriptome is likely preventing the full adjustments of cellular metabolism in the cw^+ *cht7* mutant, which negatively impacts viability during N deprivation, as we in fact observed (Figure 2.11). Taken together, these results highlight the importance of CHT7 in mediating the transcriptional establishment of a proper quiescent state following N deprivation, setting the stage for subsequent detailed phenotypic analyses.

As such, the physiological consequences of the altered transcriptome in the absence of CHT7 were readily reflected in the phenotypes of the newly generated cw^+ *cht7* lines following N deprivation compared to cells capable of producing CHT7. Following N deprivation, the vast majority of wild-type and *CHT7:cht7* complemented cells arrest further growth and exit from the cell division cycle during the post-mitotic, or pre-commitment phase with a single non-replicating nucleus following 48 h of N deprivation (Figure 2.10A and B; illustrated in Figure 2.15B). In contrast, a number of N-deprived *cht7* cells are unable to coordinate this arrest (Figure 2.10A and B; illustrated in Figure 2.15C). Indeed, approximately 11% of *cht7* cells continued to grow in size and became occasionally misshapen, while 27% still showed signs of nuclear division or contained divided nuclei (Figure 2.10A and B), suggesting that these cells failed to exit the cell division cycle at an appropriate stage and were unable to enter an effective quiescent state (illustrated in Figure 2.15C). The adverse impacts of a highly misregulated transcriptome of *cht7* were also apparent from the progressive loss of viability observed in cw^+ *cht7* by SYTOX staining during five days

of N deprivation (Figure 2.11B). Loss of viability of the cell population was in agreement with the concurrent accumulation of ROS-induced lipid peroxidation byproducts in *cht7* (Figure 2.12A), an extensive degradation of thylakoid membranes, and the increasing presence of cell ghosts visualized by ultrastructural analyses of the *cht7* cell population following N deprivation (Figure 2.12B). Although it is unclear why the SYTOX assay failed to indicate a reduction in viability following N deprivation in cell wall-deficient cw^- *cht7* cells (Tsai et al., 2014), the observed aberrancies in the transcriptome were inarguably present in the original cw^- *cht7* mutant (Figures 2.1 and 2.5) and the cw^+ *cht7* lines constructed here (Figure 2.8). In addition, a similar decline in the ability of N-starved *cht7* cells to form colonies was also observed for both the cw^- (Tsai et al., 2014) and cw^+ *cht7* mutant lines (Figure 2.11A) upon N refeeding by plating on N-replete TAP-agar plates.

As hypothesized above, the observed *cht7* phenotypes during N refeeding can be explained by the inability of *cht7* cells to transcriptionally establish a proper quiescent state following N deprivation. Single cell tracking of the N-deprived *cht7* cells after plating on N-replete agar revealed that their growth and division are often ultimately terminated even in metabolically responsive *cht7* cells that manage to increase in volume during N refeeding (Figure 2.13B-D, class 3). The observed phenotypes of the *cht7* mutant during N refeeding, including slow resumption of growth, delayed remobilization of TAG, and reduction in colony formation, therefore are likely explained not only by the reduction of viability in *cht7* cells following N deprivation (Figures 2.11B and 2.13B-D, a portion of class 4), but also by a heterologous population of *cht7* cells that were slow (Figure 2.13A and B, class 2) or all together unable (Figure 2.13B-D, class 3) to resume growth and cell division. Indeed, the elevated transcript levels of DNA metabolism and cell cycle-related genes in N-deprived *cht7* cells persisted, or in some cases increased even more following

N refeeding (Figures 2.8D-F and 2.9). On the other hand, the repression of DNA metabolism and cell cycle-related genes in wild-type cells during the post-mitotic or pre-commitment phase following N deprivation likely represents the appropriate expression state of these genes and thus allows for the coordinated entry back into the cell division cycle following N refeeding (Figure 2.15B). Therefore, an important finding here is that a functional CHT7 is not only necessary for promoting cellular survival during N deprivation but also for the orderly reentry of quiescent cells into the cell division cycle. These results indicate that CHT7 is necessary for the effective establishment of a quiescent state and the subsequent resumption of growth and division following N refeeding.

MATERIALS AND METHODS

Generation and Validation of Lines

The cell wall-less *Chlamydomonas reinhardtii* parental line, dw15 (cw15, *nit1*, mt^+) was obtained from A. Grossman, Department of Plant Biology, Carnegie Institution for Science, Stanford, CA. Generation of the original cell wall-less *cht7* mutant in the dw15 background was described previously (Tsai et al., 2014). Since the *cht7* mutation is linked to a Hygromycin B resistance marker *aphv7*, Hygromycin B-resistant lines were selected from meiotic progeny of four successive crosses to cw^+ CC-198 (*er-u-37*, *str-u-2-60*, cw^+, mt^-) or CC-110 (*spr-u-1-6-2*, cw^+, mt^+). The resulting 5^{th} generation cw^+ *cht7* mutant was further crossed four times to the wild types, mt^+ 21gr (Sager, 1955) or mt^- 6145c (Fernandez and Cardenas, 1982) to produce 9^{th} generation cw^+ *cht7 (1-3)* lines used in this study. CC-198 and CC-110 were obtained from the Chlamydomonas Resource Center (http://www.chlamycollection.org/), and 21gr and 6145c were obtained from J. Umen, Donald Danforth Plant Science Center, St. Louis, MO.

Generation of the CHT7 complementation construct, *pMN24 CHT7*, which carries the Chlamydomonas nitrate reductase *NIT1* gene as a selectable marker and the *CHT7* genomic fragment with 1 kb upstream and downstream of this gene, was previously described (Tsai et al., 2014). To generate the complementation construct, *pSL18 CHT7*, *pSL18* obtained from the Chlamydomonas Resource Center was digested with *Stu*I/*Psi*I, dephosphorylated, and ligated with the phosphorylated PCR product of *CHT7* amplified from *pMN24 CHT7* to form *pSL18 CHT7*. To remove the *Asc*I site from the *HSP70/Rbsc2* promoter (to make *pSL18 (-Asc*I*) CHT7*, which only contains one *Asc*I site), the *CHT7* and *HSP70* promoter were released by digestion with *Hind*III and gel extracted. A fragment of *pSL18* from the *Rbsc2* promoter to the *AmpR* gene was amplified with the primers *pSL18 Hind*III-F and *pSL18 Hind*III-R (Table 2.4), digested with *Hind*III, and ligated with the *Hind*III digested *CHT7-HSP70* fragment. Properly oriented inserts were identified through colony PCR and verified by restriction digest. For the transformation of cell-walled *cht7* mutant lines, all constructs were linearized first with *Ahd*I and introduced into the cells by electroporation as previously described (Shimogawara et al., 1998) using a Bio-Rad Gene Pulser-II and 0.4 cm slit width cuvette. The cell walls were not removed prior to electroporation, and the settings of 800 kV, 25 μF and no resistance were used. Previously published primers *APH7*-F and *APH7*-R and *CHT7*-F and *CHT7*-R (Table 2.4) (Tsai et al., 2014) were used for PCR in some cases to validate the presence of the *aphv7* insert and the *CHT7* gene, respectively. The presence of CHT7 proteins was verified by SDS-PAGE followed by immunoblotting with CHT7 antibody as previously described (Tsai et al., 2014).

Growth Conditions

Cells were cultured in Tris acetate phosphate (TAP) medium (Harris, 1989) at 22 ºC under 100-120 μmol $m^{-2}s^{-1}$ of light . To induce N deprivation, mid-log phase cells grown in TAP were harvested by centrifugation (3,000 x g, 4 ºC, 5 min), washed twice with TAP N^- (without NH_4Cl) and resuspended in TAP N^- at OD750 of 0.3 (Tsai et al., 2014). N was resupplied from a 100 x NH_4Cl solution at indicated times. The growth curves were performed by measuring OD750 at indicated times. Pre-growth and N deprivation for gametogenesis and crossing the lines were as previously described (Li et al., 2012b).

Protein Extraction and Quantification for SDS-PAGE

For the preparation of denatured total protein, the cells during mid-log growth were resuspended in 2x Laemmli sample buffer (4% SDS, 20% glycerol, 125 mM Tris-HCl, pH 6.8, 0.004% bromophenol blue) containing 1x Roche cOmplete protease inhibitor (Sigma-Aldrich), 1:100 dilutions of plant protease inhibitor cocktail (Sigma-Aldrich), phosphatase inhibitor cocktail (Halt™, Thermo Scientific) and PMSF (Sigma-Aldrich, 93482), and 5% v/v of β-mercaptoethanol. Samples were incubated for 5 min at 95 ºC, and the protein concentration was assessed using RC DC protein assay (Bio-Rad). Equal amounts of total protein were separated by SDS-PAGE and subjected to immunoblotting as described in Tsai et al. (2014).

Visualization of Coexpression Networks and GO Enrichment Analyses

The Chlamydomonas coexpression network and RNA-Seq datasets of cell wall-deficient *cht7* were previously generated by (Romero-Campero et al., 2016) and (Tsai et al., 2014; Tsai et al., 2018), respectively. The Chlamydomonas coexpression network in gml format was downloaded, and the

nodes were colored based on the GO-annotations of different clusters previously described (Romero-Campero et al., 2016) or based on the log_2 FC values from the RNA-Seq datasets in Cytoscape 3.7.1. Genes that were significantly differentially expressed (using the two-fold cut-off and adjusted p-value of < 0.05) from different comparisons were respectively selected on the co-expression network, and the corresponding nodes and associated edges were isolated and visualized in Cytoscape. GO enrichment analyses were performed using Blast2GO PRO software using Fisher's Exact Test, with the entire Chlamydomonas genome as a reference. GO-annotations from previous studies (Tsai et al., 2014; Tsai et al., 2018) were loaded onto Blast2GO PRO, and the generic GO-slim was applied to reduce the complexity of GO-terms prior to performing the enrichment analyses. The identifiers of enriched GO-slim terms with $p < 0.05$ are provided in Table 2.2.

Lipid Analysis

Total lipids were extracted with methanol: chloroform: 88% formic acid (2: 1: 0.1, v/v/v); separation of the organic phase was achieved by the addition of 0.5 volume of extraction buffer (1M KCl; 0.2M H_3PO_4) followed by centrifugation. The organic phase was dried to completion under N gas, resuspended in 125 μL of chloroform, and 25 μL of lipid extracts were separated by thin layer chromatography (TLC) on Silica Gel 60 plates (EMD chemicals) using the following solvent system for neutral lipids: petroleum ether: diethyl ether: acetic acid (80: 20: 1, v/v). The identity of TAG was confirmed based on the separation of known lipid standards. Following the visualization of lipids by brief iodine staining, fatty acid methyl esters (FAMEs) of each lipid as well as total cellular lipids were prepared in 1M methanolic HCl by heating the samples at 80 ºC for 20 min. 5 μg pentadecanoic acid was used as an internal standard. Following the phase

separation with hexane and 0.9% (w/v) NaCl, the organic phase containing FAMEs was completely dried under N gas, resuspended in 60 μL of hexane and quantified by gas chromatography with flame ionization detection (Agilent Technologies, 7890A GC system) using a temperature and run profile previously described with minor modifications (Zauner et al., 2012).

Assessment of Cell Viability by SYTOX Green and Percent Colony Formation

SYTOX Green from Molecular Probes Inc. was used to assess the viability of N-deprived cells as previously published (Tsai et al., 2014). At times indicated, SYTOX Green stain was added at a final concentration of 5 μM to a small aliquot of cell resuspension. Cells were observed by fluorescence microscopy (Leica DRMA2) with excitation at 488 nm using an FITC filter for SYTOX Green and a Texas Red filter for chlorophyll autofluorescence. Images were subsequently analyzed using ImageJ. For the assessment of colony formation, the cell densities of N-starved cells at respected time points were determined by hemocytometer, and a known number of cells were transferred to N-replete TAP agar plates. The plates were kept under approximately 80-100 μmol $m^{-2}s^{-1}$ of light (5600K; YUJILEDS® VTC Series High CRI LED 2835), and the colonies were counted on day 7 and re-assessed on day 9-10 for confirmation.

Determination of Meiotic Viability

Meiotic viability was assessed by counting colonies arising from a known number of zygospores transferred to TAP agar to induce germination, and spread with a drop of liquid TAP and a bent glass rod, followed by a 30 sec exposure to chloroform vapor to kill any contaminating unmated cells.

Microscopic Tracking of Single Cells

After 48 h N deprivation in liquid TAP N^-, a series of very small aliquots of cells were placed on N-replete TAP agar in 10 x 100 mm petri plates, and these cells were viewed and photographed with a Nikon Eclipse Ci-S microscope (Nikon Instruments Inc., NY, USA) without removing the lids. Multi-colored grids drawn onto the back of each plate and the physical marks made by the pipette tip when dispensing cells were used as landmarks to identify and return to the same exact site. The cells were subsequently tracked manually and imaged for 6-11 days. The images collected with NIS-Elements software (https://www.microscope.healthcare.nikon.com/products/software) were used to visually categorize the cells into the different phenotypic classes described. ~100 to 150 cells were analyzed per line.

Assessment of Lipid Peroxidation

Lipid peroxidation was assessed by a TBARS (Thiobarbituric Reactive Substances) assay as described (Warakanont et al., 2015). Two aliquots of 5 mL N-deprived cultures were harvested by centrifugation at 3,000 x g for 5 min at 4 ºC, and the pellets were resuspended in 1 mL of 20% trichloroacetic acid with or without 0.5% thiobarbituric acid. After heating the mixture for 15 min at 95 ºC, absorbance was measured at 440, 532 and 600 nm and the concentration of malondialdehyde was estimated as described in (Hodges et al., 1999).

Transmission Electron Microscopy

Cells were fixed with 2.5% (v/v) glutaraldehyde in sterile-filtered TAP medium overnight at 4 ºC. Then the samples were washed with TAP medium and post-fixed with 1% OsO_4 for 2 h at room temperature. Following washing with TAP medium, the samples were dehydrated in a graded

ethanol series and embedded in Spurr's epoxy resin (Electron Microscopy Sciences, Hatfield, PA, USA). Ultrathin sections (70 nm thick) were obtained with a RMC Boeckeler ultramicrotome (Tucson, Arizona, USA) and mounted on 150 mesh formvar-coated copper grids. Finally, sections were stained with 5% (v/v) uranyl acetate for 30 min at room temperature, washed with ultrapure water and stained 10 min with 1% (v/v) lead citrate. The samples were analyzed with a JEOL100 CXII transmission electron microscope (Japan Electron Optics Laboratories) at the Centre of Advanced Microscopy at Michigan State University.

Confocal Microscopy

All images were captured using an inverted Olympus FluoView1000 confocal laser scanning microscope (Olympus Corporation, USA). Cells were stained with 4', 6-Diamidino-2-Phenylindole (DAPI, 358/461) from Life Technologies with a final concentration of 0.2 μg/μL and observed using a 100x UPlanSApo oil objective (N.A. 1.4). DAPI fluorochromes were excited using a 405 nm blue diode laser, and the emission signals were filtered using the BA430-470 band pass filter. Chlorophylls were excited using an argon 488 nm laser, and the signals from autofluorescence were filtered using a BA650 far-red band pass filter. Post-imaging analyses were performed using ImageJ, obtained from nih.gov. The signals from the DAPI and chlorophyll channels were assigned the colors, blue and red, respectively. These two channels were subsequently merged to give rise to the composite images shown. For quantification, each cell or dividing mother cell was treated as one counting unit, and ~50-150 such units per line were visually assessed from the confocal images.

Real-Time Quantitative PCR (RT-qPCR)

Total RNA was extracted using an RNeasy Plant Mini Kit (Qiagen). Purified RNA was treated with TURBO DNA-free DNase (Thermo Fisher) and subjected to reverse transcription using SuperScript III reverse transcriptase (Life Technologies). The resulting cDNA was diluted three-fold with water, and qPCR was performed using SYBR-Green Master Mix (Applied Biosystems) and Eppendorf single-color real-time PCR detection system (Master Cycle Realplex2) with 1.5 μL of the diluted cDNA template and 0.25 μM of each primer. Quantification was carried out by using the cycle threshold (CT)$2^{-\Delta\Delta CT}$ method. All target gene expression was normalized against a common Chlamydomonas endogenous reference gene, *CBLP* (Schloss, 1990), which is not induced by N deprivation. Two technical replicates for each of three biological replicates per line/treatment were analyzed for all experiments. The primers used are described in Table 2.5.

APPENDIX

Table 2.1. Meiotic viability of *cht7* lines.
From each cross, 80-300 zygospores were transferred to TAP agar, counted using a dissecting microscope, and then spread to allow them to germinate and grow into individual colonies, which were counted 7 days after transfer. The percentage of zygospores that produced a colony is given as % Viability, with the number of total colonies listed in the last column. If even a single meiotic product divided and grew, a colony would have been produced.
(**A**) The ninth generation mt^- lines were crossed with the common mt^+ tester strain CC-110 used for back-crossing.
(**B**) The ninth generation mt^- lines were crossed with the recurrent mt^+ backcross parent strain 21gr.
(**C**) Two additional ninth generation *cht7* lines, mt^+ *cht7* (4) and mt^- *cht7* (5), were used to test for meiotic viability when crossed to the wild-type strains and for complementation test crosses (*cht7* x *cht7*).

A	**mt^+**	**mt^-**	**Zygospores**	**% Viability**	**Colonies**
	CC-110	*cht7* (1)	230	2%	4
	CC-110	*cht7* (2)	135	4%	5
	CC-110	*cht7* (3)	214	1%	2
	CC-110	*CHT7:cht7*(1)	207	4%	9
	CC-110	*CHT7:cht7*(2)	114	0%	0
	CC-110	*CHT7:cht7*(3)	258	1%	3
	CC-110	6145c	149	6%	9
	CC-110	CC-198	199	79%	158
B	**mt^+**	**mt^-**	**Zygospores**	**% Viability**	**Colonies**
	21gr	*cht7* (1)	137	55%	75
	21gr	*cht7* (2)	300	39%	118
	21gr	*cht7* (3)	212	47%	100
	21gr	*CHT7:cht7*(1)	153	68%	104
	21gr	*CHT7:cht7*(2)	226	77%	173
	21gr	*CHT7:cht7*(3)	93	68%	63
	21gr	CC-198	167	79%	132
	21gr	6145c	82	56%	46
C	**mt^+**	**mt^-**	**Zygospores**	**% Viability**	**Colonies**
	cht7 (4)	6145c	4	0%	0
	cht7 (4)	*cht7* (1)	249	0%	1
	cht7 (4)	*cht7* (1)	233	1%	3
	cht7 (4)	CC-198	198	58%	114
	21gr	*cht7* (5)	135	55%	74
	cht7 (4)	*cht7* (5)	169	80%	135
	cht7 (4)	*cht7* (5)	139	61%	85

Table 2.2. GO IDs, p- and q-values for the GO-slim terms enriched among different comparisons.
(**A**) GO-slim terms enriched among 968 downregulated genes from N- *cht7*/ N- PL comparison ($Log_2FC < -1$, p-adjusted < 0.05).
(**B**) GO-slim-terms enriched among 2753 upregulated genes from N- *cht7*/ N- PL comparison ($Log_2FC > 1$, p-adjusted < 0.05).
(**C**) GO-slim terms enriched among 3346 downregulated genes from N- PL/ N+ PL comparison ($Log_2FC < -1$, p-adjusted < 0.05).
(**D**) GO-slim terms enriched among 2647 upregulated genes from N- PL/ N+ PL comparison ($Log_2FC > 1$, p-adjusted < 0.05).
(**E**) GO-slim terms enriched among 1491 downregulated genes from N+ *cht7*/ N+ PL comparison ($Log_2FC < -1$, p-adjusted < 0.05).
(**F**) GO-slim terms enriched among 1477 upregulated genes from N+ *cht7*/ N+ PL comparison ($Log_2FC > 1$, p-adjusted < 0.05).

A	GO name	GO Category	GO ID	p-value	q-value
	Small molecule metabolic process	BP	GO:0044281	3.88E-02	8.30E-01
	Oxidoreductase activity	MF	GO:0016491	1.30E-04	2.94E-02
	Transmembrane transporter activity	MF	GO:0022857	4.35E-02	8.30E-01
	Cofactor metabolic process	BP	GO:0051186	4.34E-02	8.30E-01
	Lyase activity	MF	GO:0016829	2.31E-03	2.21E-01
	Ligase activity	MF	GO:0016874	1.08E-02	6.20E-01
	Transferase activity, transferring acyl groups	MF	GO:0016746	4.20E-03	3.01E-01
	Homeostatic process	BP	GO:0042592	2.93E-02	8.30E-01
	Endoplasmic reticulum	CC	GO:0005783	4.92E-02	8.30E-01
	Isomerase Activity	MF	GO:0016853	4.28E-02	8.30E-01
	DNA-binding transcription factor activity	MF	GO:0003700	2.12E-02	8.30E-01
	Cell death	BP	GO:0008219	4.19E-02	8.30E-01

Table 2.2 (cont'd)

	Nitrogen cycle metabolic process	BP	GO:0071941	4.69E-02	8.30E-01

B	GO name	GO Category	GO ID	p-value	q-value
	DNA binding	MF	GO:0003677	2.75E-03	3.28E-02
	DNA metabolic process	BP	GO:0006259	1.07E-08	2.04E-07
	Chromosome organization	BP	GO:0051276	3.82E-07	6.08E-06
	ATPase activity	MF	GO:0016887	1.59E-02	1.57E-01
	Cytoskeleton organization	BP	GO:0007010	1.91E-07	3.23E-06
	Cell division	BP	GO:0051301	3.65E-06	4.76E-05
	Cillium	CC	GO:0005929	1.23E-23	8.84E-22
	Mitotic cell cycle	BP	GO:0000278	1.04E-08	2.04E-07
	Chromosome segregation	BP	GO:0007059	1.29E-06	1.86E-05
	Microtubule organizing center	CC	GO:0005815	3.40E-09	1.18E-10
	Cell proliferation	BP	GO:0008283	3.14E-06	4.29E-05
	Nuclear chromosome	CC	GO:0000228	9.96E-07	1.50E-05
	Cell motility	BP	GO:0048870	8.85E-03	9.41E-02
	Cytoskeleton-dependent intracellular transport	BP	GO:0030705	1.57E-07	2.81E-06

C	GO name	GO Category	GO ID	p-value	q-value
	Plastid	CC	GO:0009536	1.04E-05	1.99E-04
	Generation of precursor metabolites and energy	BP	GO:0006091	8.19E-15	3.36E-13

Table 2.2 (cont'd)

Cofactor metabolic process	BP	GO:0051186	1.12E-03	1.54E-02
Thylakoid	CC	GO:0009579	1.46E-19	8.37E-18
Sulfur compound metabolic process	BP	GO:0006790	8.65E-04	1.31E-02
Photosynthesis	BP	GO:0015979	2.10E-13	7.52E-12
Isomerase activity	MF	GO:0016853	4.49E-07	9.91E-06
Cytoskeleton organization	BP	GO:0007010	1.25E-03	1.63E-02
Secondary metabolic process	BP	GO:0019748	1.84E-02	1.89E-01
Cell division	BP	GO:0051301	3.38E-03	4.04E-02
Cillium	CC	GO:0005929	1.12E-25	8.02E-24
Mitotic cell cycle	BP	GO:0000278	4.98E-04	8.92E-03
Microtubule organizing center	CC	GO:0005815	7.71E-10	1.84E-08
Peroxisome	CC	GO:0005777	9.02E-03	9.59E-02
Cell proliferation	BP	GO:0008283	6.78E-04	1.14E-02
Transferase activity, transferring alkyl or aryl (other than methyl) group	MF	GO:0016765	7.96E-04	1.27E-02
Aging	BP	GO:0007568	5.57E-03	6.39E-02
Pigmentation	BP	GO:0043473	4.95E-02	4.31E-01
Cytoskeleton-dependent intracellular transport	BP	GO:0030705	1.22E-06	2.49E-05
Extracellular matrix	CC	GO:0031012	3.21E-02	2.88E-01

D	GO name	GO Category	GO ID	p-value	q-value
	Transmembrane transporter activity	MF	GO:0022857	3.96E-04	2.29E-02

Table 2.2 (cont'd)

	Nucleoside-triphosphatase activity	MF	GO:0017111	3.83E-02	6.51E-01
	DNA-binding transcription factor activity	MF	GO:0003700	2.83E-07	4.09E-05
	Hydrolase activity, acting on glycosyl bonds	MF	GO:0016798	1.23E-02	3.54E-01
	Hydrolase activity, acting on carbon-nitrogen (but not peptide) bonds	MF	GO:0016810	1.76E-04	1.69E-02
	Nucleocytoplasmic transport	BP	GO:0006913	2.17E-02	5.23E-01
	Lipid binding	MF	GO:0008289	3.16E-02	6.51E-01
	Endosome	CC	GO:0005768	4.76E-03	2.29E-01
	Autophagy	BP	GO:0006914	7.66E-03	2.77E-01

E	**GO name**	**GO Category**	**GO ID**	**p-value**	**q-value**
	Signal transduction	BP	GO:0007165	2.78E-02	4.20E-01
	Transmembrane transporter activity	MF	GO:0022857	1.52E-03	5.45E-02
	Thylakoid	CC	GO:0009579	3.75E-04	1.79E-02
	Photosynthesis	BP	GO:0015979	3.47E-05	1.99E-03
	Extracellular region	CC	GO:0005576	4.01E-03	1.05E-01
	Cillium	CC	GO:0005929	1.61E-09	1.16E-07
	Microtubule organizing center	CC	GO:0005815	1.75E-02	3.35E-01
	Cell motility	BP	GO:0048870	4.72E-02	5.77E-01
	Cytoskeleton-dependent intracellular transport	BP	GO:0030705	3.42E-03	9.81E-02

Table 2.2 (cont'd)

F	GO name	GO Category	GO ID	p-value	q-value
	DNA binding	MF	GO:0003677	4.20E-02	6.63E-01
	DNA metabolic process	BP	GO:0006259	4.26E-05	1.22E-02
	Chromosome organization	BP	GO:0051276	9.87E-03	2.02E-01
	Cell cycle	BP	GO:0007049	2.82E-03	8.57E-02
	Helicase activity	MF	GO:0004386	8.95E-03	1.97E-01
	Chromosome segregation	BP	GO:0007059	8.02E-04	3.55E-02
	Nuclear chromosome	CC	GO:0000228	2.86E-02	5.14E-01

Table 2.3. Gene IDs and Log_2 fold change (Log_2 FC) expression values of a selected annotated genes on the downregulated (A) and the upregulated (B) coexpression network from N- *cht7*/ N- PL comparison (Figure 2.2E and F).
Log_2 FC values of these genes from N+ *cht7*/ N+ PL and N- PL/ N+ PL comparisons are also included as references.

A	Gene ID	Annotation	N+ *cht7*/ N+ PL	N- PL/ N+ PL	N- *cht7*/ N- PL
1	Cre04.g223300	Low-CO2-inducible chloroplast envelope protein: *CCP1*	-7.78	NA	-7.88
2	Cre12.g555700	DnaJ-like protein; *DNJ15*	-4.21	1.45	-6.08
3	Cre08.g360200	Urea active transporter; *DUR3*	-1.57	6.05	-5.82
4	Cre12.g530400	Sulfate ABC-transporter; *ABCG2*	-2.26	5.15	-5.12
5	Cre14.g631145	Papain family cysteine protease (Peptidase C1); glycosyltransferase	NA	NA	-4.85
6	Cre05.g248450	Mitochondrial carbonic anhydrase; *CAH5*	-6.16	-2.17	-4.8
7	Cre06.g281600	Low-CO2 inducible protein, septin-like; *LCI23*	-6.45	0.84	-4.74
8	Cre02.g141600	Mannan endo-1,4-beta-mannosidase 2-related; *EBM3*	NA	7.3	-4.61
9	Cre05.g248400	Mitochondrial carbonic anhydrase, beta type; *CAH4*	-5.7	-1.89	-4.53
10	Cre05.g236650	Guanylate cyclase / Guanylyl cyclase; *CYG63*	-5.51	NA	-4.33
11	Cre06.g309000	Formate transporter-related anion transporter; *LCIA*; *NAR1.2*	-6.27	1.21	-4.19
12	Cre03.g176833	Actin; *ACT2*	-0.45	3.43	-4.02
13	Cre06.g284600	Mitochondrial rubredoxin; *RBD2*	-0.92	-2.9	-3.74
14	Cre07.g327800	Sulfate ABC-transporter; *ABCG2*	1.18	8.99	-3.48
15	Cre06.g291950	Magnesium transporter; *CorA-Like*	-0.52	3.79	-2.5

Table 2.3 (cont'd)

16	Cre09.g410800	Nitrate transporter; *NRT2.2*	NA	7.43	-2.1
17	Cre13.g562550	NADP adrenodoxin-like ferredoxin reductase	-0.32	3.05	-1.9
18	Cre04.g214050	Molybdate transporter; *SUL4*	NA	4.63	-1.71
19	Cre09.g396000	Nitrate transporter; *NRT2.3*	NA	6.97	-1.66
20	Cre02.g145700	Transmembrane amino acid transporter family protein	-1.02	0.85	-1.51
21	Cre03.g159254	Ammonium transporter; *AMT*	NA	8.91	-1.51
22	Cre17.g714150	Potassium transporter; *KUP1*	-1.25	4.01	-1.34
23	Cre09.g410850	Nitrate/nitrite transporter; *NRT2.1*	NA	8.59	-1.19

B	**Gene ID**	**Annotation**	**N+ *cht7*/ N+ PL**	**N- PL/ N+ PL**	**N- *cht7*/ N- PL**
1	Cre06.g254100	Non-specific serine/threonine protein kinase	1.4	-8.05	9.18
2	Cre01.g035250	Coiled-coil domain-containing protein 112	0.39	-7.86	9.12
3	Cre12.g549000	Cell wall protein pherophorin-C4; *PHC4*	1.22	-7.62	8.35
4	Cre11.g481600	Hydroxyproline-rich glycoprotein; pherophorin; *GAS28*	1.69	-7.1	8.33
5	Cre09.g388351	Pherophorin; *DUF3707*	3.95	-4.81	8.28
6	Cre17.g696500	Cell wall protein pherophorin-C19; *PHC19*	1.29	-7.09	8.18
7	Cre09.g388353	Pherophorin; *DUF3707*	4.17	-4.03	8.1
8	Cre13.g575200	Serine/threonine specific protein phosphatase PP1, catalytic subunit; *PPP42*	1.49	-6.17	7.82

Table 2.3 (cont'd)

9	Cre17.g710300	Pherophorin; *DUF3707*	0.83	-7.75	7.74
10	Cre10.g421350	Gametolysin/Lysin; *MMP25*	1.89	-6.26	7.58
11	Cre09.g388355	Pherophorin; *PHC20*	4.5	-2.96	7.52
12	Cre08.g374750	Nonspecific serine/threonine protein kinase	0.97	-6.43	7.5
13	Cre14.g614050	Microtubule-associated protein 65; *MAP65*; protein regulator of cytokinesis 1 (*PRC1*)	0.52	-6.59	7.48
14	Cre09.g396100	Cell wall protein pherophorin-C15; *PHC15*	0.78	-7.23	7.18
15	Cre08.g376950	Matrix metalloproteinase; Gametolyn; *MPP14*	0.65	-6.3	7.13
16	Cre01.g020550	Small Heat-Shock Protein HSP20 Family; *HSP22D*	1.4	-4.01	6.98
17	Cre17.g699800	Pherophorin; *DUF3707*	1.11	-6.65	6.73
18	Cre02.g117150	Pachytene Checkpoint Protein 2 Homolog	2.1	-2.93	6.66
19	Cre02.g077000	Expansin A1-related	4.43	-2.02	6.65
20	Cre17.g717900	Cell wall protein pherophorin-C1; *PHC1*	0.92	-8.83	6.62
21	Cre12.g489850	Serine/threonine protein kinase; MEKK-related	4.66	-1.75	6.57
22	Cre11.g483351	Pherophorin (*DUF3707*)	0.48	-5.61	6.53
23	Cre07.g328500	Arylsulfatase; *ARS17*	0.46	-4.94	6.03
24	Cre04.g226650	MYND finger (*zf-MYND*)	5.38	NA	5.72
25	Cre13.g580250	Inner centromere protein	NA	-5.06	5.62

Table 2.4. Primers used for cloning and genotyping PCR.

Primer	Sequence 5'--3'	Published
*pSL18 Hind*III-F	CCAAGGCGCGTGTAAAGGGTTCGAAAG GTC	
*pSL18 Hind*III-R	CCGCCGGCCGGCTTGCGG	
APH7-F	CTCAAGTGCTGAAGCGGTAG	(Tsai et al., 2014)
APH7-R	TGGTGGTCGACAAACTCTTG	(Tsai et al., 2014)
CHT7-F	TTCTCGGGTCAGATATTGGG	(Tsai et al., 2014)
CHT7-R	TTGAGGCAGAACGACTTCTTG	(Tsai et al., 2014)

Table 2.5. Primers used for RT-qPCR.

Primer	Gene ID	Sequence 5'—3’	Published
Cre12.CXC-F	Cre12.g550250	AGGACAAAGGACGAGGACTATGAC	
Cre12.CXC-R	Cre12.g550250	AGCAAAGCACACGCAGTAAAGC	
Cre08.CXC-F	Cre08.g361400	GTACTGCGAGTGCTTCCAGG	
Cre08.CXC-R	Cre08.g361400	GCGTCGTCATCCATGTTCTC	
CHT7-F	Cre11.g481800	CTGCAAGAAGTCGTTCTGCC	
CHT7-R	Cre11.g481800	TCAAAATTGCGGCACTCCAC	
CDKA1-F	Cre10.g465900	TTAGGCTGGAGCAGGAGGAT	
CDKA1-R	Cre10.g465900	GTAGAGCACGTCGTAGAGCC	
CDKB1-F	Cre08.g372550	GACAACGCTGCGTGAGATTTC	Fang et al., (2006)
CDKB1-R	Cre08.g372550	ACCAGGTAAAGGCATGGCTTG	Fang et al., (2006)
CYCA1-F	Cre03.g207900	CTGGGTGACCTGACAAACAA	
CYCA1-R	Cre03.g207900	GAATGGAAGGCTGGTGGAA	
CYCB1-F	Cre08.g370400	AGCGACTACATGACCAAGCAGACC	
CYCB1-R	Cre08.g370400	TTCAGGAAGCGGTCGATGAGGTTC	
CYCAB1-F	Cre10.g466200	AGCAGGAGACATGGAATGAC	
CYCAB1-R	Cre10.g466200	CATGGAGGCGCTGATCTC	
Wee 1-F	Cre07.g355250	GACGGCCCAGTTCTTTCTCA	
Wee 1-R	Cre07.g355250	GGCTCATACTCCATGCGGAA	
FTSZ1-F	Cre02.g118600	CTGCTATGGAGAGCGAGGAG	
FTSZ1-R	Cre02.g118600	ACAGTCAGGATGCCCAACTC	
MIND1-F	Cre12.g522950	AAGACCACCTCGTCTGCTAACC	

Table 2.5 (cont'd)

MIND1-R	Cre12.g522950	TCAGCATCAATCAGGCACACCTTG	
MINE1-F	Cre17.g720350	ATGAGCCCCAACTCTCTTGG	
MINE1-R	Cre17.g720350	TGTTGACCTCAATCGCGTCC	
ARC6-F	Cre03.g184500	GTACGGGATGTGAACGACATGG	
ARC6-R	Cre03.g184500	GTTAGCTCACACTGACCAACCTC	
ORC1-F	Cre10.g455600	GCACAGGGCAAGATTACAGA	
ORC1-R	Cre10.g455600	ATTCCTGGTGCCGATTAAGG	
MCM2-F	Cre07.g338000	TTCTTTGATGCGTTCAAGGC	Fang et al., (2006)
MCM2-R	Cre07.g338000	GAGGCAGTTGAGGTGGTAGTTG	Fang et al., (2006)
MCM10-F	Cre07.g351400	GAACGGTGTATTTTACCTCG	
MCM10-R	Cre07.g351400	GTGCGATCCAGGTAGCCATC	
GINS3-F	Cre06.g251750	TGCCGCTGAAGTTCAAGTAT	
GINS3-R	Cre06.g251750	GTCCACCTTTGTCCCAGAAT	
RPA-F	Cre16.g651000	ACGACAAGGCCATCTTCCAG	
RPA-R	Cre16.g651000	TCGGGGTTAGCGAGGTAGAA	
CDC45-F	Cre06.g270250	CTACGGGAAACCGTCCTCAC	
CDC45-R	Cre06.g270250	GATGGCACACCAGAGGTGAA	
CDT-like-F	Cre03.g163300	CGCCAATTCAGGAGACTGTTA	
CDT-like-R	Cre03.g163300	TGCTTCACGCTGTTGTAGG	
PRI2-F	Cre06.g293000	TCGGACCTGAGCATGTATAGC	
PRI2-R	Cre06.g293000	GCCTCCATTTCCTTCAGCAC	
TOPO II-F	Cre01.g009250	ATCGTCAACCAGGTGGTCAAGC	

Table 2.5 (cont'd)

TOPO II-R	Cre01.g009250	CGTCTTGGTGGTCTTCTTGCTCAG	
RIR2-F	Cre12.g491050	AAGTGGATCGGCAGTGACTC	
RIR2-R	Cre12.g491050	GCTCGTTGGAGAAGGTGAGG	
MAD3-BUB1-F	Cre07.g351450	CCCGGTACAACAACGACATA	
MAD3-BUB1-R	Cre07.g351450	TGTCTTTCTCCCGAAGGTAAAG	
RIR1-F	Cre12.g492950	TTGACAAGATTACAGCGCGC	Fang et al., (2006)
RIR1-R	Cre12.g492950	GACACCCTTGTAGACACCACCA	Fang et al., (2006)
HFO-F	Cre06.g268000	AGCGTATCAGCGGCCTCATCTA	Fang et al., (2006)
HFO-R	Cre06.g268000	GGATGACGTTCTCCAGGAAGGT	Fang et al., (2006)
POLA4-F	Cre07.g312350	AGGCACAGATGGACCGAGAAT	Fang et al., (2006)
POLA4-R	Cre07.g312350	TTCCGTAGGACAGCCACTTCAC	Fang et al., (2006)
PCN1-F	Cre12.g515850	GCCTTCCACGTCTCACAATCAT	Fang et al., (2006)
PCN1-R	Cre12.g515850	GCTGACATCGAAATTGCCCTC	Fang et al., (2006)
CBLP-F	Cre06.g278222	GCCACACCGAGTGGGTGTCGTGCG	Tsai et al., (2014)
CBLP-R	Cre06.g278222	CCTTGCCGCCCGAGGCGCACAGCG	Tsai et al., (2014)

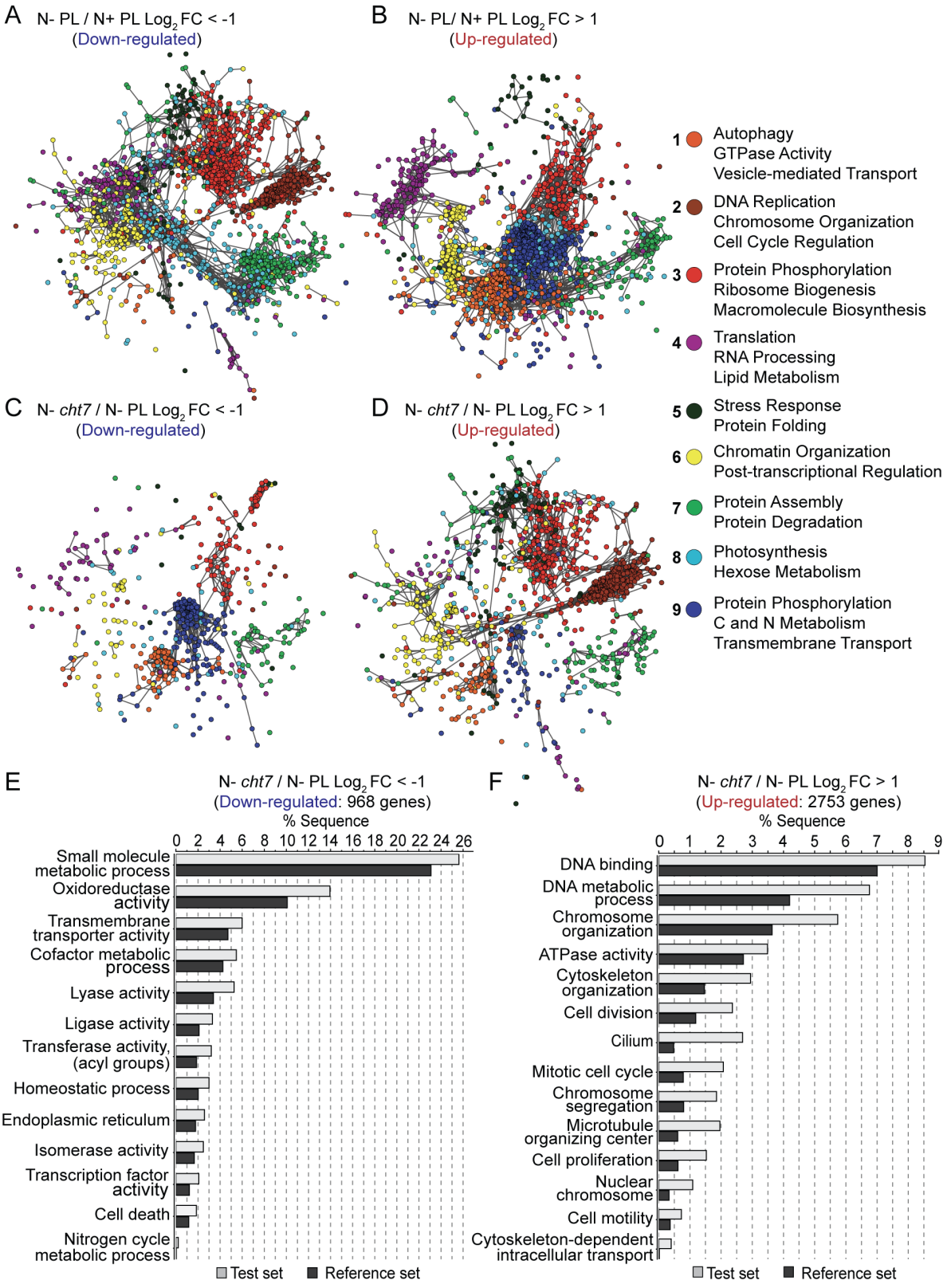

Figure 2.1. Transcriptomes of parental line (PL) and the *cht7* mutant following N deprivation.

Figure 2.1 (cont'd)

Coexpression networks of significantly down- or upregulated genes in N- PL/ N+ PL (**A**, **B**) and N- *cht7*/ N- PL comparisons (**C**, **D**) using a two-fold expression change cut-off and an adjusted p-value of < 0.05 (N+: N-replete; N-: N-deprived). Each node represents a gene, and two nodes are connected by an edge if the corresponding genes show significant coexpression (defined by the absolute Pearsons correlation coefficient (PCC) > 0.90) across different physiological conditions integrated into ChlamyNET. Nodes are colored according to the cluster to which they belong, and the GO-terms enriched within each cluster as described in Romero-Campero et al. (2016) are listed to the right.
(**E-F**) GO-slim terms enriched among the down- (968) and upregulated (2753) genes in N- *cht7*/ N- PL comparison using the Fisher's Exact Test and p < 0.05. The whole Chlamydomonas genome was used as a reference set, and the same criteria as above were used to define significant differential expression in the test set.
GO IDs, p- and q-values for the GO-slim terms shown are provided in Table 2.2A and B.

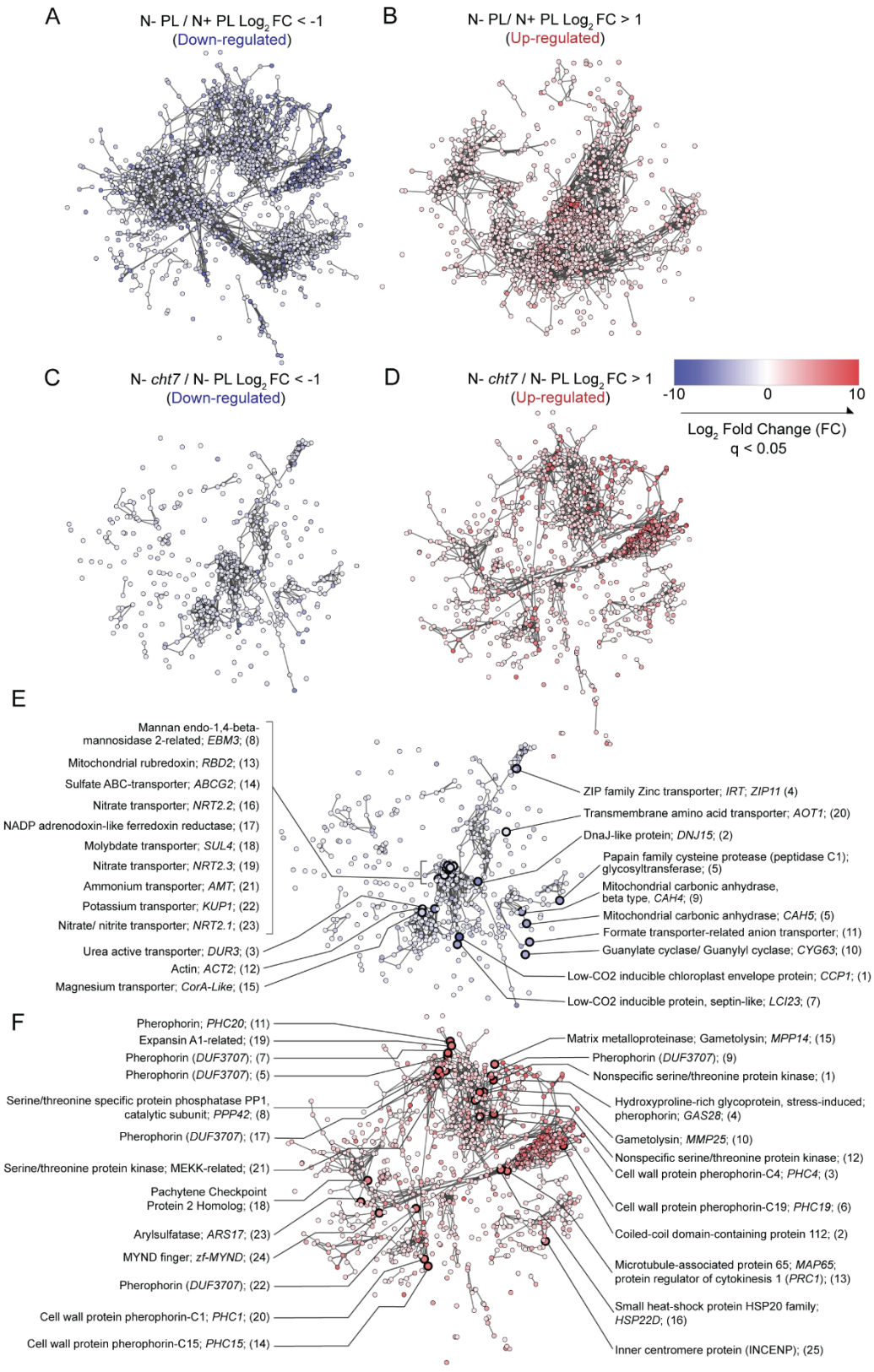

Figure 2.2. Log_2 fold change (Log_2 FC) expression values for nodes on networks shown in Figure 2.1.

Figure 2.2 (cont'd)

Coexpression networks of significantly down- or upregulated genes in N- PL/ N+ PL (**A**, **B**) and N- *cht7*/ N- PL comparisons (**C**, **D**) using a two-fold expression exchange cut-off and an adjusted p-value of < 0.05, as in Figure 2.1, but the nodes are colored according to their Log_2 fold expression change values: parental line, PL.
(**E**) Downregulated and (**F**) upregulated coexpression networks from N- *cht7*/ N- PL comparison, where some of the most misregulated genes or nodes are labeled with annotations when available. They are numbered from the most to least misregulated, and gene model IDs and expression values of these genes are provided in Table 2.3.
Nodes within the brown cluster (2; Figure 2.1) are analyzed further in Figure 2.5.
Edges represent significant coexpression relationships (the absolute PCC > 0.90) (Romero-Campero et al., 2016).

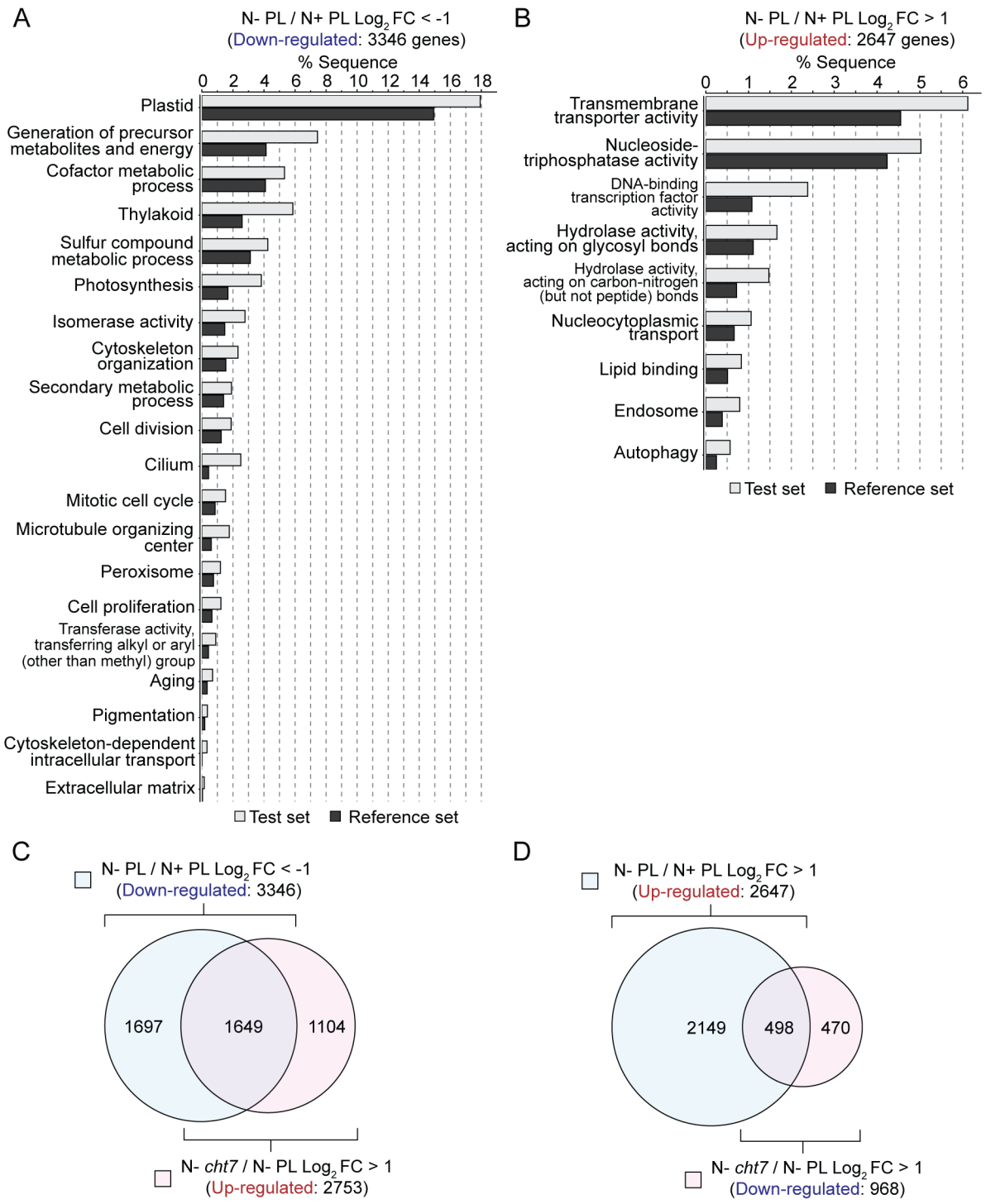

Figure 2.3. GO Enrichment analyses and abnormal expression of genes in *cht7* following N deprivation.

GO-slim terms significantly enriched among the down- (3346) (**A**) and upregulated (2647) (**B**) genes in N- PL/ N+ PL comparison using the Fisher's Exact Test and $p < 0.05$; (N+: N-replete; N-: N-deprived). The whole Chlamydomonas genome was used as a reference set, and the GO IDs, p- and q-values for the GO-slim terms shown are provided in Table 2.2C and D.

Figure 2.3 (cont'd)

(**C-D**) Venn Diagrams showing the number and proportion of genes that show the opposite expression patterns between the N- PL/ N+ PL and N- *cht7*/ N- PL datasets (purple overlaps). For all analyses, a two-fold expression change cut-off and an adjusted p-value of < 0.05 were used to define significant differential expression.

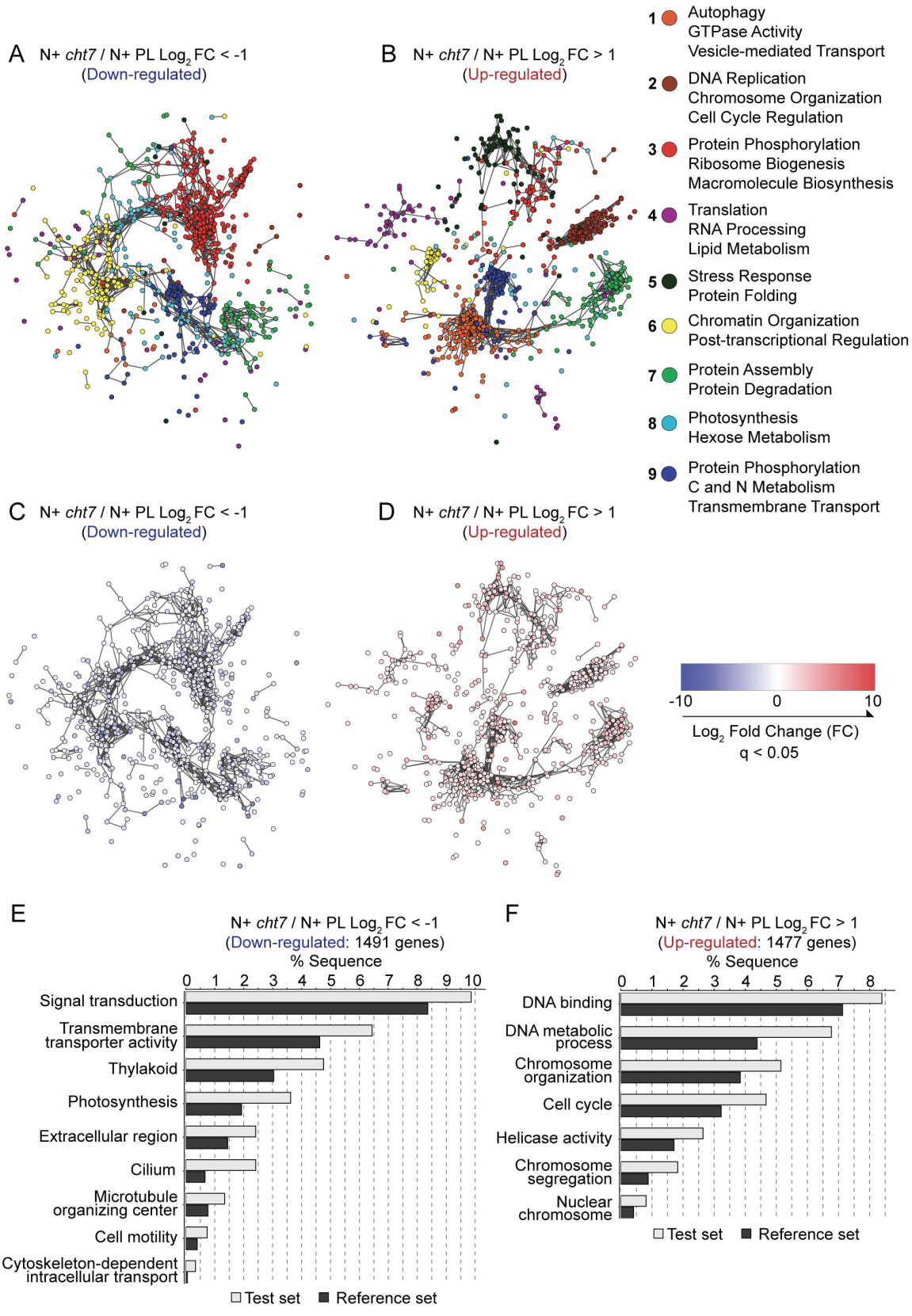

Figure 2.4. Transcriptome of the *cht7* mutant during N-replete conditions.

Figure 2.4 (cont'd)

Coexpression networks of significantly down- (left) or upregulated (right) genes in N+ *cht7*/ N+ PL comparison, where the nodes are colored according to the functionally-annotated cluster to which they belong (**A-B**), or their expression values in Log_2 FC (**C-D**); (N+: N-replete). Edges represent significant coexpression relationships (the absolute PCC > 0.9) (Romero-Campero et al., 2016).
GO-slim terms significantly enriched among the down- (1491) (**E**) and upregulated (1477) (**F**) genes in N+ *cht7*/ N+ PL comparison using the Fisher's Exact Test and $p < 0.05$. The whole Chlamydomonas genome was used as a reference set, and the GO IDs, p- and q-values for the GO-slim terms shown are provided in Table 2.2E and F.
For all analyses, a two-fold expression change cut-off and an adjusted p-value of < 0.05 were used to define significant differential expression.

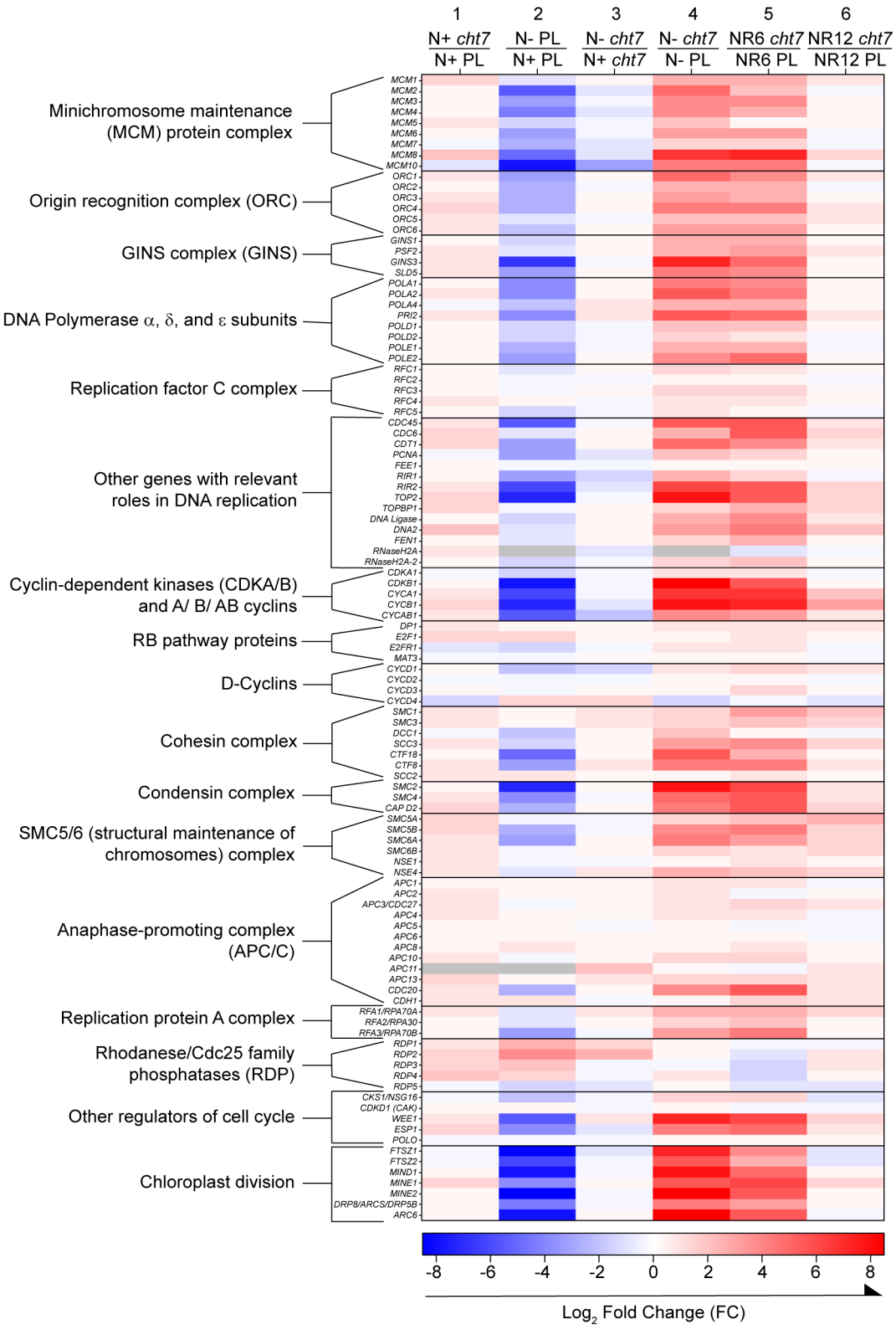

Figure 2.5. Derepression of S/M phase genes in *cht7* mutant becomes more apparent during N deprivation.

Figure 2.5 (cont'd)

Log_2 FC values of 108 curated genes involved in the synthesis, licensing, initiation and replication of DNA, chromosome organization and segregation, cell cycle progression and chloroplast division are shown for different comparisons across varying N conditions; (N+: N-replete; N-: N-deprived; NR: N resupply). Columns 1, 4, 5 and 6 show relative differences in gene expression under the same growth conditions when the *cht7* mutant is compared to the PL line during N-replete growth (1) and following N deprivation for 48 h (4) and N resupply for 6 h (5) or 12 h (6). In column 2, PL following N deprivation is compared to PL during N-replete growth, and in column 3, *cht7* following N deprivation is compared to *cht7* during N-replete growth. Boxes are greyed out when log_2 FC values were absent from the RNA-Seq datasets. Gene model IDs for the genes shown are available from Zones et al. (2015).

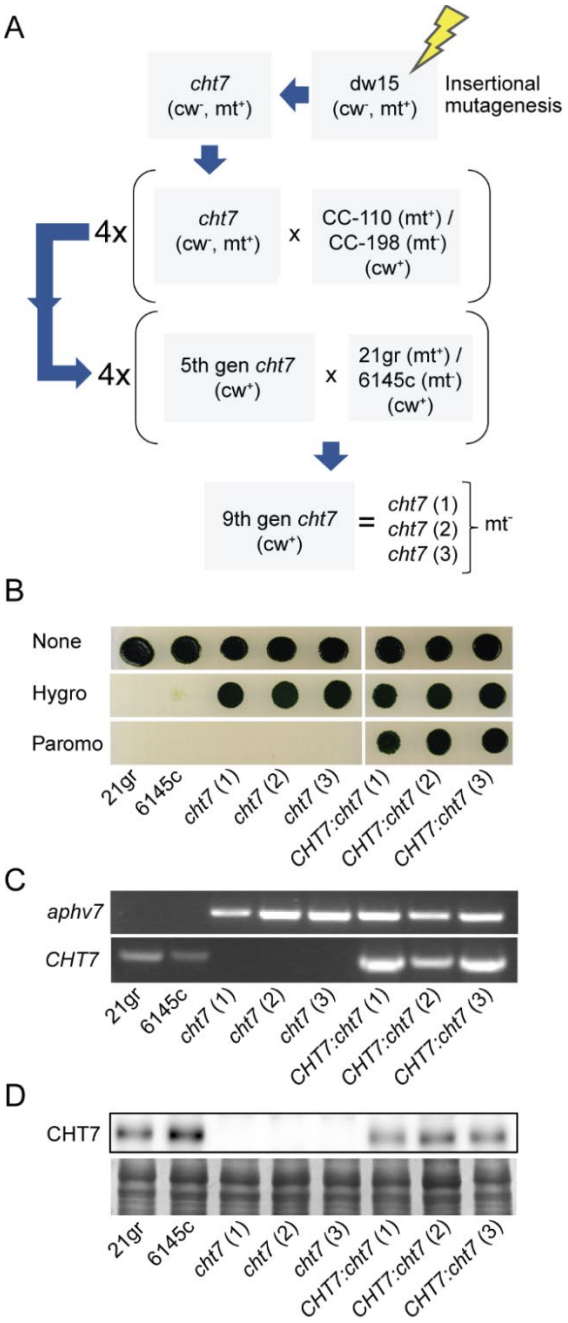

Figure 2.6. Generation of 9th generation cell-walled *cht7* lines and the complementation lines.

(**A**) Overview of the crossing scheme that produced the cw^{+} *cht7* (1-3) lines descended from the original cw^{-} *cht7* line.

(**B**) Growth of wild types (21gr and 6145c), *cht7* (1-3) and *CHT7:cht7* (1-3) complemented lines on TAP (top), TAP + 10 µg Hygromycin B (Hygro) and TAP + 10 µg Paromomycin (Paromo) plates. The *cht7* mutation is linked to a Hygromycin B resistance marker *aphv7*, while the *CHT7* complementation construct is linked to a Paromomycin resistance marker *aphv8*.

(**C**) Genotyping PCR for the presence of *aphv7* insertion and the *CHT7* gene.

(**D**) Immunoblot of CHT7 probed with CHT7-antibody.

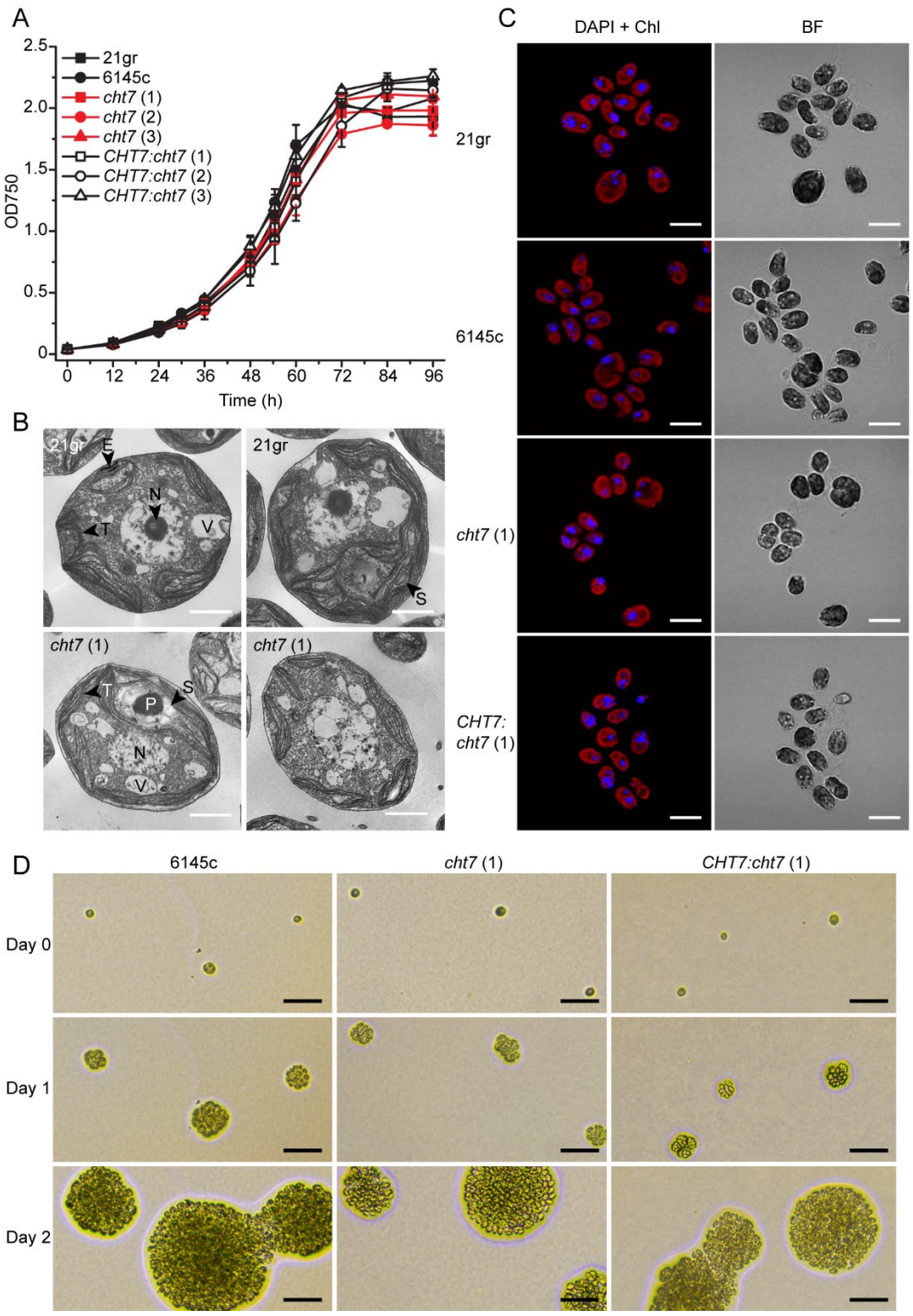

Figure 2.7. Growth and cytology of cell-walled *cht7* during N-replete growth.
(**A**) Growth of wild types (21gr and 6145c), *cht7* (1-3) and *CHT7:cht7* (1-3) complementation lines under N-replete conditions. Values represent the averages and the standard deviations of two biological replicates, where they refer to respective lines in separate flasks.

Figure 2.7 (cont'd)

(**B**) TEM images of 21gr and *cht7* (1) cells cultured in N-replete medium (TAP). Black arrows indicate subcellular structures, which are abbreviated and shown as follows: eyespots, E; pyrenoid, P; nucleus, N; thylakoid membrane, T; starch, S; vacuole, V. Bars represent 2 μm.
(**C**) Confocal microscopy images of wild types (21gr and 6145c), *cht7* (1) and *CHT7:cht7* (1) complementation lines during N-replete growth. DAPI signals indicating nuclei are shown in blue, whereas chlorophyll autofluorescence (Chl) is shown in red; bright field, BF. Bars represent 10 μm.
(**D**) Growth of 6145c wild type, *cht7* (1) and *CHT7:cht7* (1) on N-replete agar plates. Mid-log phase cultures grown in N-replete medium were plated onto N-replete agar plates. Bars represent 50 μm.

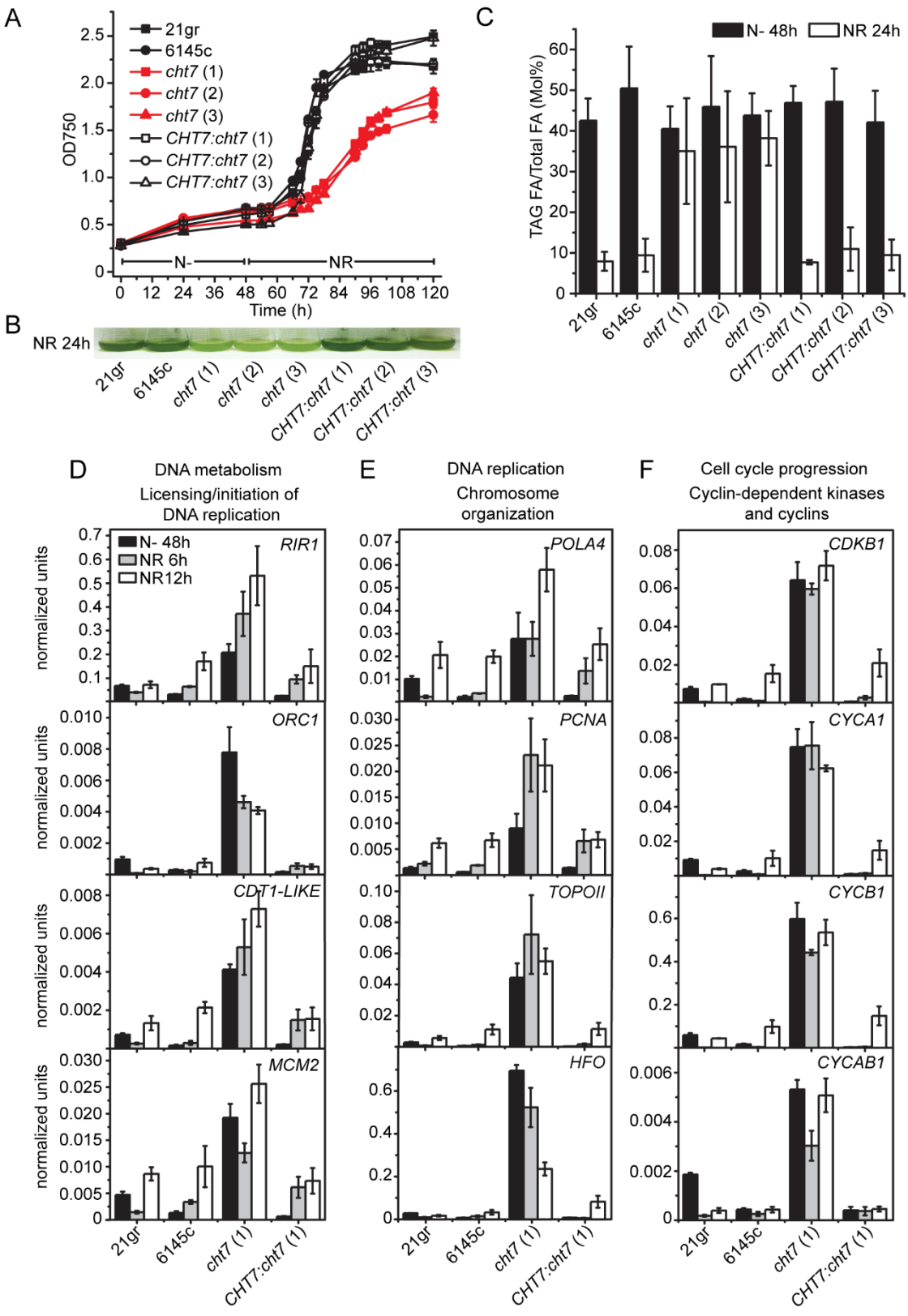

Figure 2.8. Phenotypes of *cht7* and RT-qPCR analyses of genes involved in DNA replication and cell cycle-related processes following N deprivation and N resupply.

Figure 2.8 (cont'd)

(**A**) Growth of wild types (21gr and 6145c), cell-walled *cht7* (1-3) and their *CHT7:cht7* (1-3) complemented lines during N deprivation followed by N resupply. Values represent the averages and the standard deviations of two biological replicates.
(**B**) Photo of these cultures after 24 h of N resupply following 48 h of N deprivation.
(**C**) Degradation of TAG after 24 h of N resupply following 48 h of N deprivation. Values represent the averages and standard deviations of three biological replicates.
(**D-F**) Expression levels of representative genes were assessed by RT-qPCR in wild types, *cht7* (1) and *CHT7:cht7* (1) after 48 h of N deprivation and following N resupply for 6 h and 12 h. These include genes involved in deoxyribonucleotide synthesis and licensing/initiation of DNA replication (**D**), DNA replication and chromosome organization (**E**) and the regulation of cell cycle progression (**F**). Values represent the averages and the standard errors of three biological replicates. Target gene expression was normalized to the *CBLP* gene. In (**A**, **C**, **D-F**), biological replicates refer to respective lines in separate flasks.

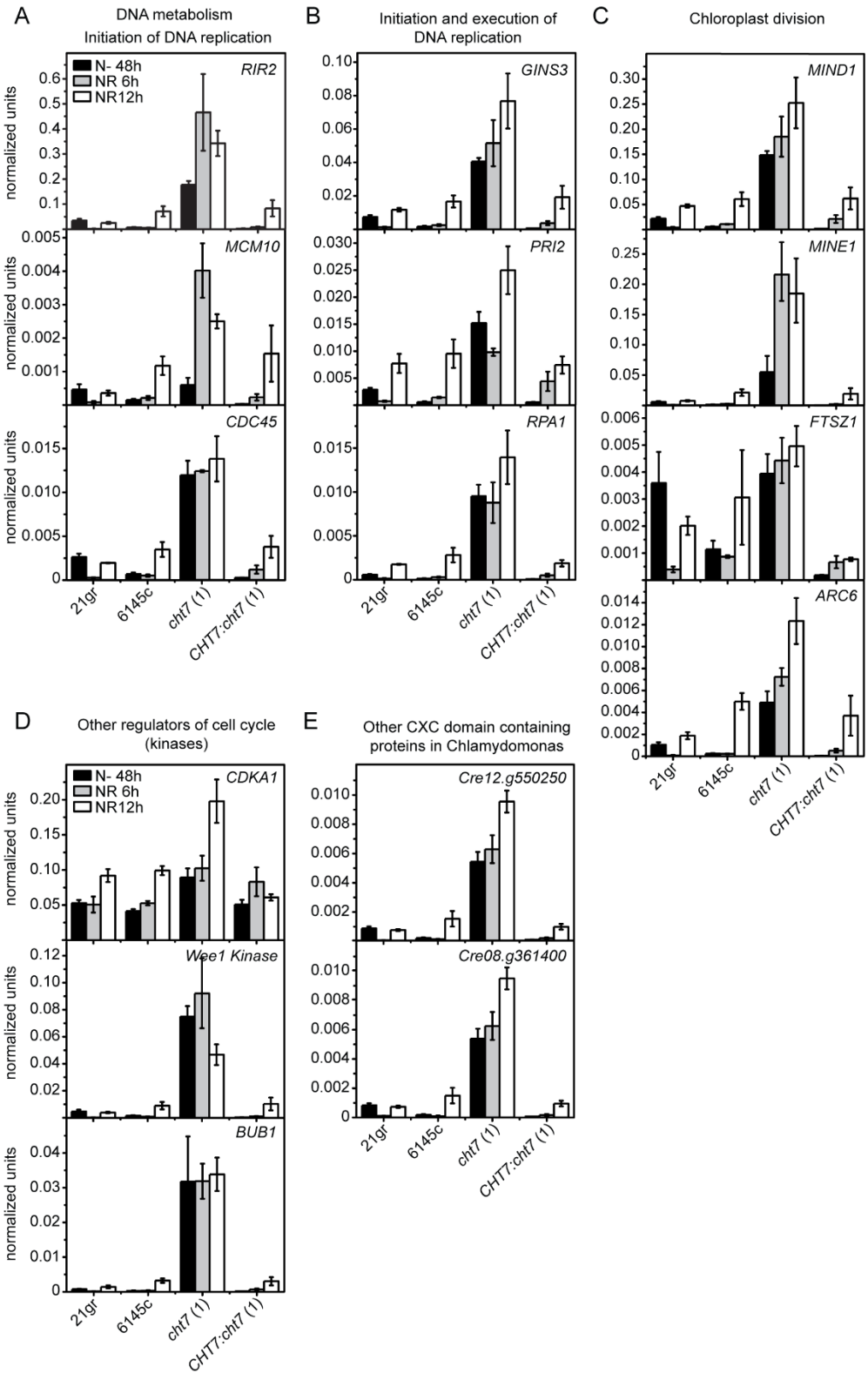

Figure 2.9. Expression levels of additional genes that were assessed in wild types, *cht7* (1) and *CHT7:cht7* (1) after 48 h of N deprivation and following N resupply for 6 h and 12 h by RT-qPCR.

Figure 2.9 (cont'd)

These include genes that have roles in deoxyribonucleotide synthesis and DNA replication (**A-B**), chloroplast division (**C**), and cell cycle regulation (**D**). Transcript levels of two other CXC domain containing proteins in Chlamydomonas were also determined in (**E**).
Values represent the averages and the standard errors of three biological replicates, where they refer to respective lines in separate flasks.
The target gene expression was normalized to the *CBLP* gene.

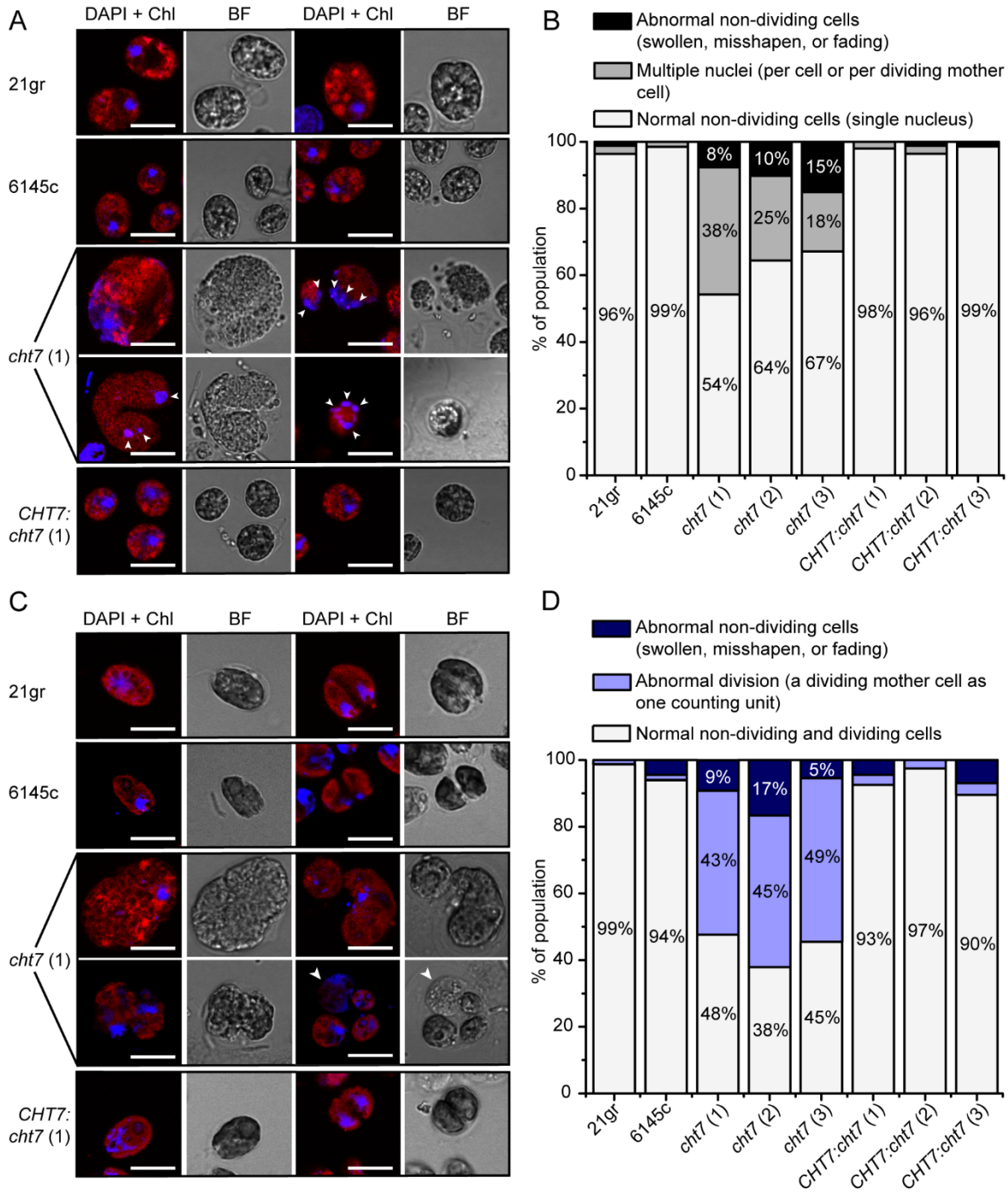

Figure 2.10. Abnormal cytology of *cht7* following N deprivation and upon N resupply. (**A, C**) Confocal microscopy images of wild types (21gr and 6145c), *cht7* (1) and *CHT7:cht7* (1) complemented line after 48 h of N deprivation (**A**) or after 24 h of N resupply following 48 h of N deprivation (**C**). The white arrowheads point to the presence of multiple nuclei (**A**) or a terminated daughter cell enclosed within the mother cell wall (**C**) in *cht7* (1). DAPI signals indicating nuclei are shown in blue, whereas chlorophyll autofluorescence (Chl) is shown in red; bright field, BF. Bars represent 10 μm.

Figure 2.10 (cont'd)

(**B, D**) Quantification of the observed phenotypes in the confocal images of wild-type (21gr and 6145c), *cht7* (1-3), and *CHT7:cht7* (1-3) cells following 48 h of N deprivation (**B**) or after 24 h of N refeeding following 48 h of N deprivation (**D**).
Whereas the percentages of population with multiple nuclei (per cell or per dividing mother cell) were assessed in (**B**), the percentages of population that underwent abnormal division (defined as the presence of one or more terminated daughter cell(s) enclosed within the mother cell wall) were quantified in (**C**).
For each independent line, ~50-150 cells were assessed.

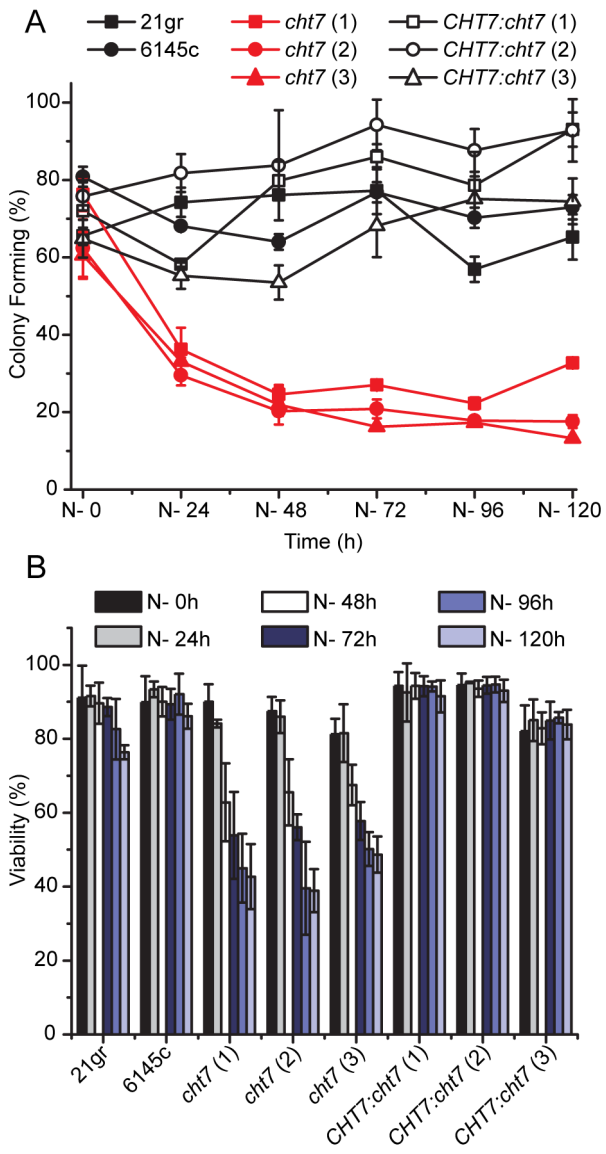

Figure 2.11. Viability assessments of *cht7* (1-3) mutants following N deprivation.
(**A**) Percent colony formation assessed for wild types (21gr and 6145c), *cht7* (1-3) and *CHT7:cht7* (1-3) complemented lines after growth for 7 days on N-replete TAP plates. Prior to plating, the cultures were N-deprived for the times indicated on the X-axis. Values represent the averages and the standard deviations of two biological replicates.
(**B**) Viability assessment of the same set of lines by SYTOX Green stain during N deprivation. Values represent the averages and the standard deviations of two to four biological replicates. In both (**A**) and (**B**), biological replicates refer to respective lines cultured in separate flasks across two to four independent experiments.

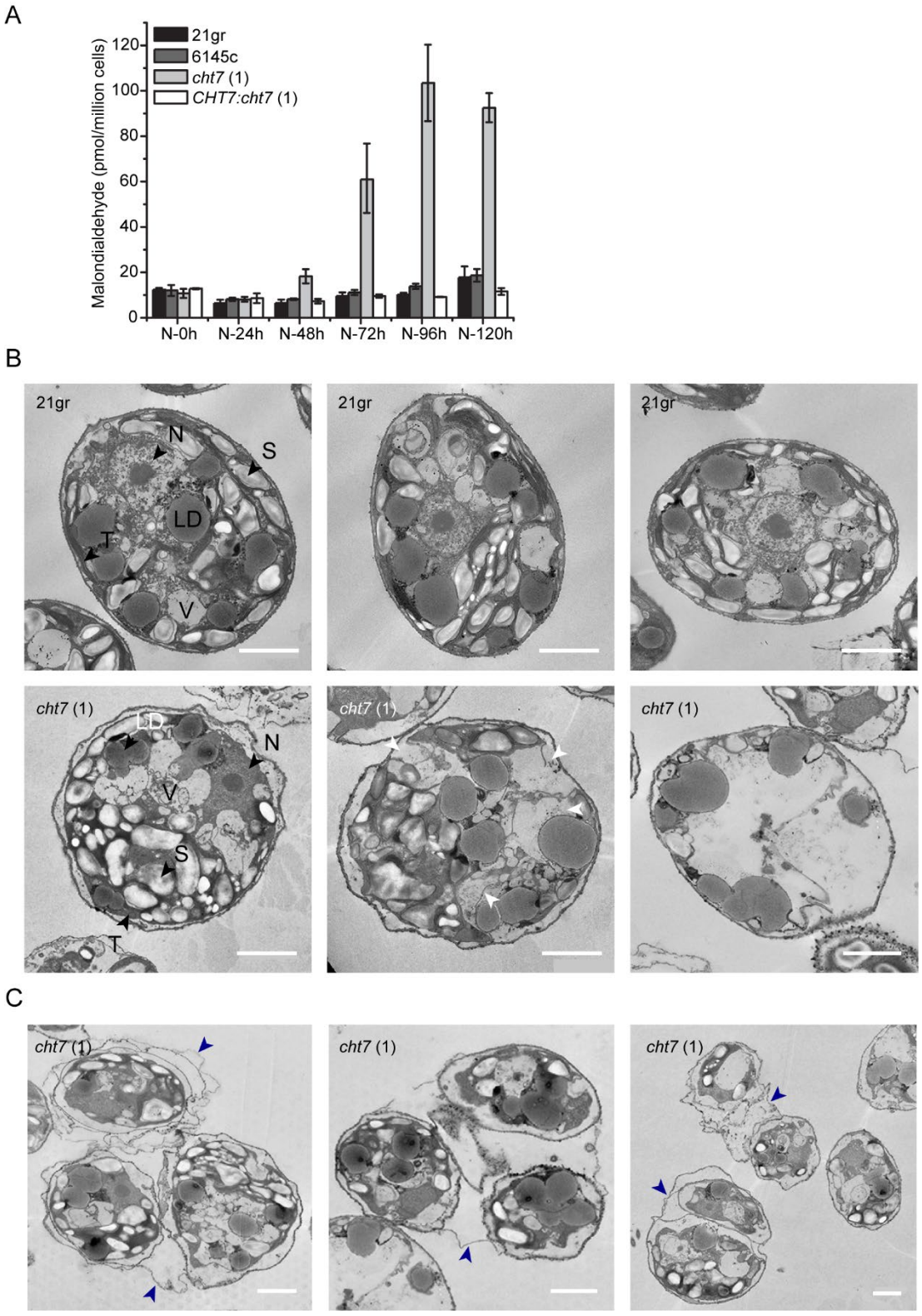

Figure 2.12. Altered physiological processes of *cht7* (1) following N deprivation.
(**A**) Quantification of thiobarbituric acid reactive substances (TBARS) in wild types (21gr and 6145c), *cht7* (1), and *CHT7:cht7* (1) during the 5 days of N deprivation.

Figure 2.12 (cont'd)

(**B**) TEM images of wild type 21gr and *cht7* (1) cells following 48 h of N deprivation. Three representative *cht7* (1) cells with increasingly severe defects are shown from left to right, where the right cell represents a dead ghost cell. Structures are abbreviated as follows: nucleus, N; thylakoid membrane, T; starch, S; lipid droplet, LD; vacuole, V. Black arrowheads indicate common subcellular structures in both 21gr and *cht7* (1), while white arrowheads indicate the degradation of thylakoids.
(**C**) TEM images of *cht7* (1) cells with accumulated lipids and starch that appear to be going through cell division even following 48 h of N deprivation. The presence of mother cell wall is indicated by the blue arrowheads.
In both (**B**) and (**C**), bars represent 2 μm.

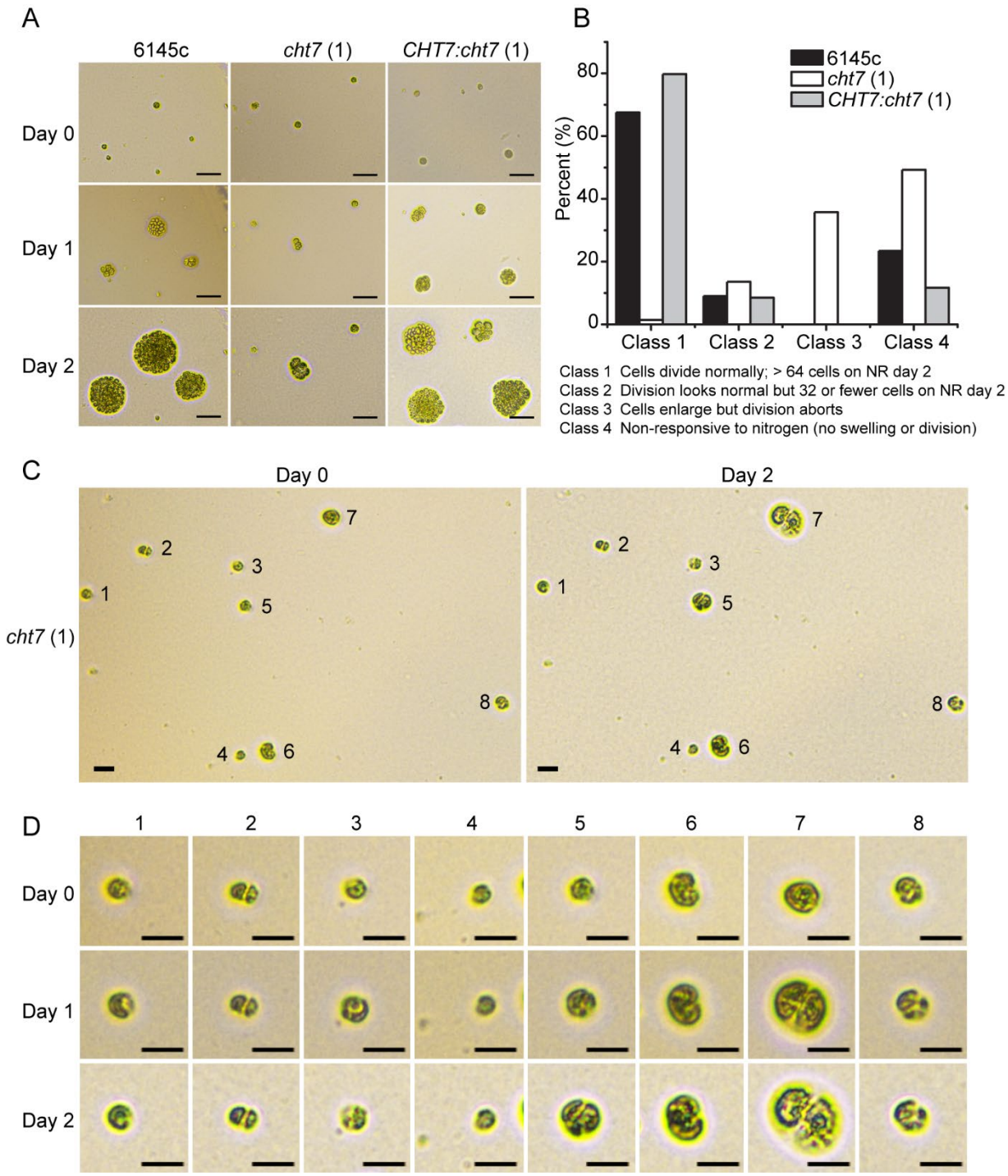

Figure 2.13. Single cell tracking of the *cht7* mutant during N resupply following 48 h of N deprivation.

Cells were N-deprived in liquid culture for 48 h and then grown for the times indicated on N-replete TAP agar plates.

(**A**) Colony size differences between wild type 6145c, *cht7* (1) and *CHT7:cht7* (1) complemented line during growth on N-replete TAP agar plates following 48 h of N deprivation. Bars represent 50 μm.

Figure 2.13 (cont'd)

(**B**) Percentage of 6145c, *cht7* (1) and *CHT7:cht7* (1) cells during growth on N-replete TAP agar plates following 48 h of N deprivation that: divide normally (class 1; > 64 cells on day 2), divide slowly (class 2; divide normally but contain 32 or fewer cells on day 2), enlarge but division aborts (class 3) or are non-responsive to nitrogen (class 4; no swelling or division). ~100-150 cells of each line were assessed in total.
(**C**) Overview of *cht7* (1) cells at 0 h (day 0) and 48 h (day 2) of growth on N-replete TAP agar plates following 48 h of N deprivation.
(**D**) Detailed view of individual *cht7* (1) cells shown in (**C**). *cht7* (1) cells labeled 1-4 were scored as class 4, while cells labeled 5-8 were scored as class 3.
In (**C-D**), bars represent 20 μm.

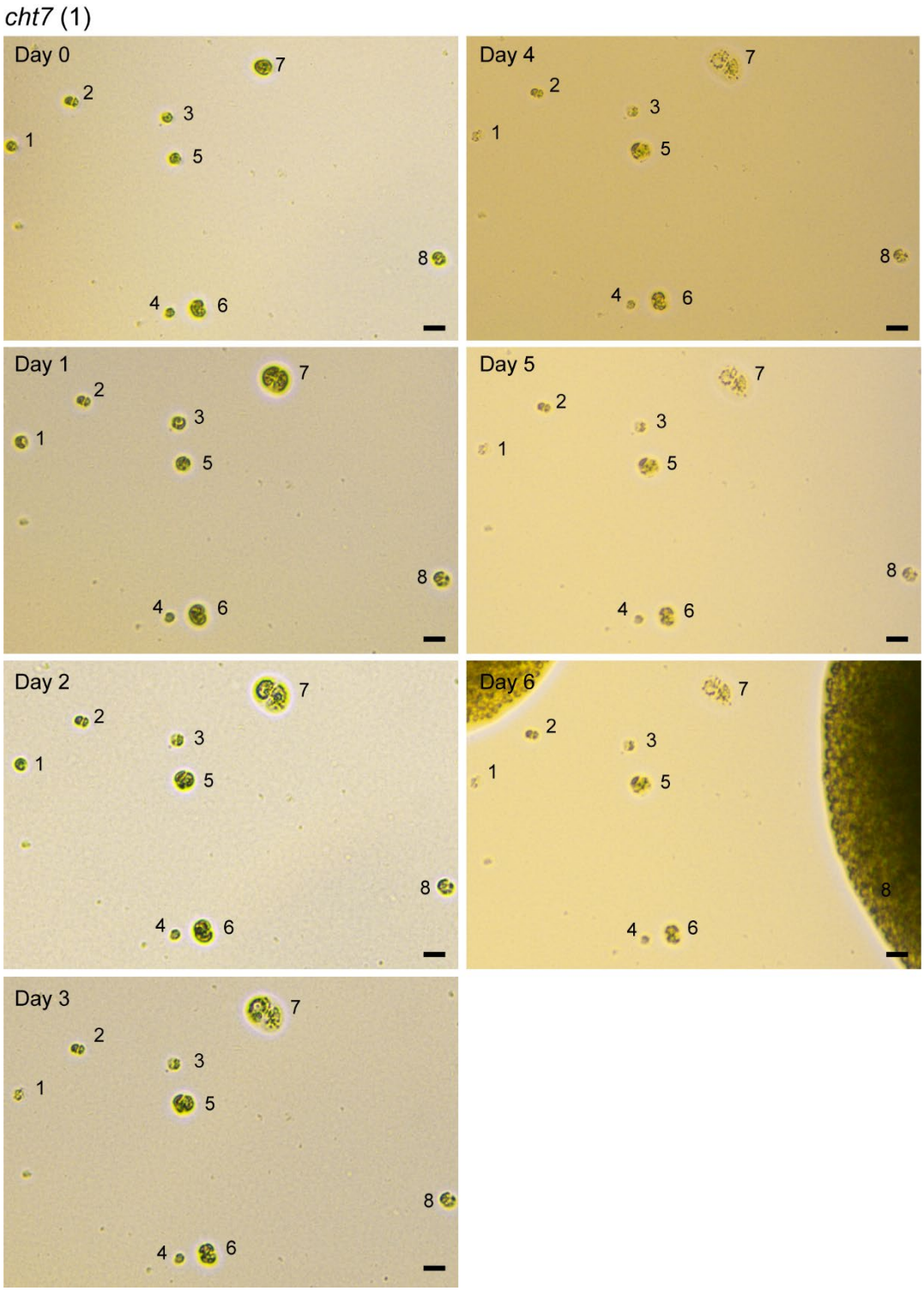

Figure 2.14. Overview of *cht7* (1) cells during N resupply on plate following 48 h of N deprivation.
Cells were N-deprived in liquid culture for 48 h and N resupplied on N-replete TAP agar plate. Overview of eight example *cht7* (1) cells imaged at N- 48 h (day 0) and on days 1-6 following N resupply are shown. Bars represent 20 μm.

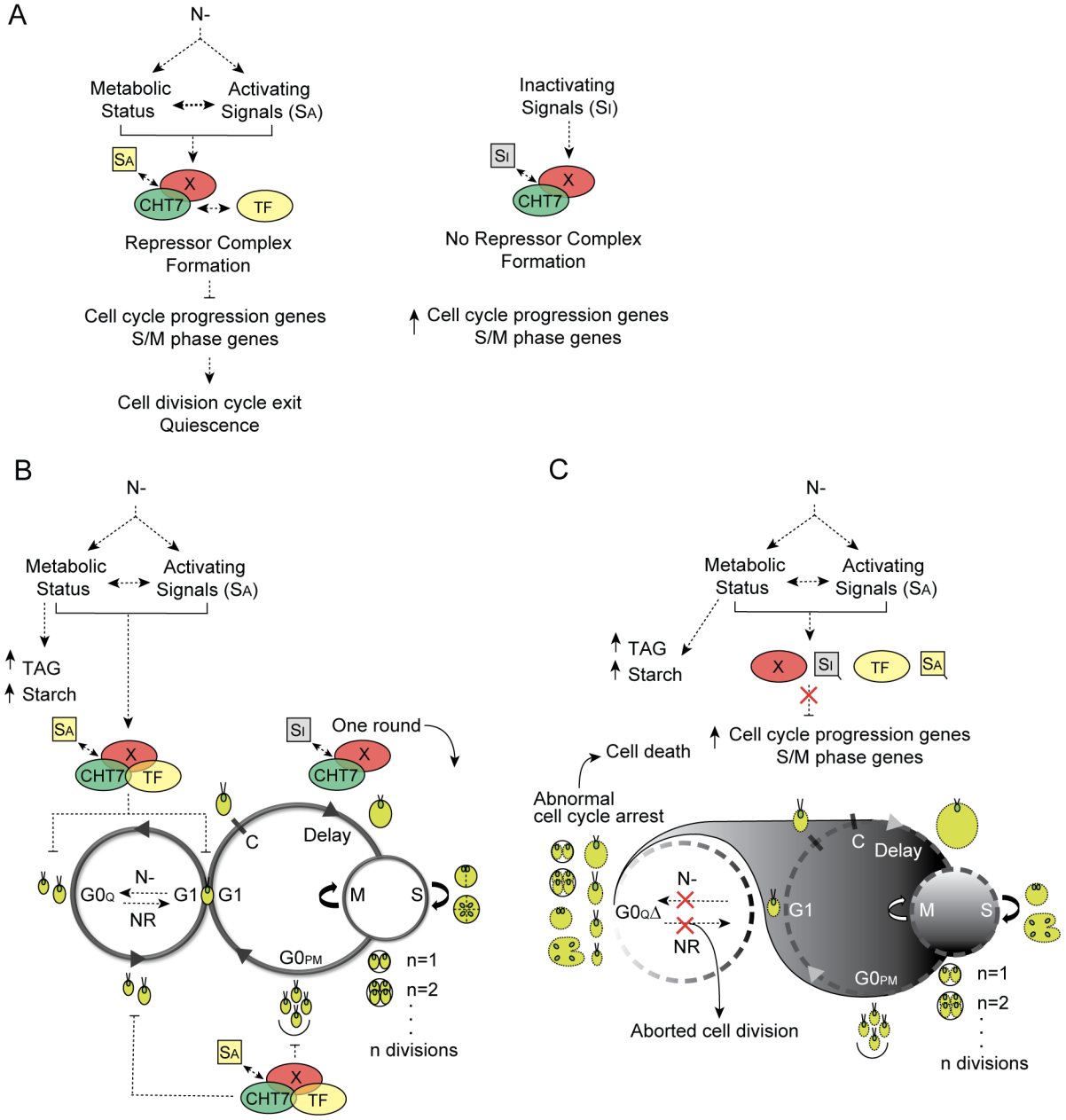

Figure 2.15. Model of CHT7 function in response to N availability.
(**A**) Hypothesized role of CHT7 in mediating repression of the S/M phase related genes in response to N starvation. CHT7 and unknown component(s) X represent the most abundant CHT7 complex (CHT7-C) that is observed by BN-PAGE during N-replete growth and following N deprivation that do not change in size (Tsai et al., 2014); transcription factor(s), TF. In response to signals that promote quiescence (left diagram), some fraction of CHT7-C is postulated to form a repressor complex with transcription factor(s) to repress S/M phase gene expression. The dotted double-sided arrows indicate signals that are hypothesized to either directly or indirectly affect CHT7. When the conditions for mitotic entry are met (right diagram), the repression of S/M phase genes is lifted. This is depicted by the changes in CHT7-C status and the absence of transcription factor(s) for simplicity.

Figure 2.15 (cont'd)

(**B**) Wild type (WT) CHT7-containing repressor complex coordinates an appropriate entry into and exit from the quiescent state in response to changing N availability by repressing S/M phase genes until cells reach an appropriate stage of the cell division cycle. Entry into and exit out of quiescence cycle is depicted by the left circle, and one round of division that the post-commitment WT cells go through after N starvation before exiting the cell division cycle is represented by the right circle: N deprivation-induced quiescence, $G0_Q$; post-mitotic resting state, $G0_{PM}$; commitment point, C.
(**C**) In the absence of CHT7, the formation of repressor complex does not take place, and the *cht7* mutant cells therefore lose their ability to mediate the orderly and cell cycle-stage appropriate repression of S/M phase genes when presented with cues to cease growth and cell division. This compromised state of quiescence in the mutant is represented by $G0_Q\Delta$, where the constitutive expression of S/M phase genes that occurs despite the absence of external N likely leads to the abnormal cell division cycle exit or arrest and contributes to the reduced viability of *cht7* cells both during N deprivation and N refeeding.

REFERENCES

REFERENCES

Aoki, K., Ogata, Y., and Shibata, D. (2007). Approaches for extracting practical information from gene co-expression networks in plant biology. Plant Cell Physiol 48: 381-390.

Aoki, Y., Okamura, Y., Ohta, H., Kinoshita, K., and Obayashi, T. (2016). ALCOdb: Gene Coexpression Database for Microalgae. Plant Cell Physiol 57: e3.

Atkins, K.C., and Cross, F.R. (2018). Interregulation of CDKA/CDK1 and the Plant-Specific Cyclin-Dependent Kinase CDKB in Control of the Chlamydomonas Cell Cycle. Plant Cell 30: 429-446.

Bassel, G., Lan, H., Glaab, E., Gibbs, D., Gerjets, T., Krasnogor, N., Bonner, A., Holdsworth, M., and Provart, N. (2011). Genome-wide network model capturing seed germination reveals coordinated regulation of plant cellular phase transitions. Proc Natl Acad Sci 108.

Bernard, P., Hardwick, K., and Javerzat, J.P. (1998). Fission yeast bub1 is a mitotic centromere protein essential for the spindle checkpoint and the preservation of correct ploidy through mitosis. J Cell Biol 143: 1775-1787.

Bisova, K., Krylov, D.M., and Umen, J.G. (2005). Genome-wide annotation and expression profiling of cell cycle regulatory genes in *Chlamydomonas reinhardtii*. Plant Physiol 137: 475-491.

Blaby, I.K., Glaesener, A.G., Mettler, T., Fitz-Gibbon, S.T., Gallaher, S.D., Liu, B., Boyle, N.R., Kropat, J., Stitt, M., Johnson, S., et al. (2013). Systems-level analysis of nitrogen starvation-induced modifications of carbon metabolism in a *Chlamydomonas reinhardtii* starchless mutant. Plant Cell 25: 4305-4323.

Cai, B., Li, C.H., and Huang, J. (2014). Systematic identification of cell-wall related genes in Populus based on analysis of functional modules in co-expression network. PLoS One 9: e95176.

Colina, F., Amaral, J., Carbo, M., Pinto, G., Soares, A., Canal, M.J., and Valledor, L. (2019). Genome-wide identification and characterization of CKIN/SnRK gene family in *Chlamydomonas reinhardtii*. Sci Rep 9: 350.

Donnan, L., and John, P.C.L. (1983). Cell cycle control by timer and sizer in Chlamydomonas. Nature 304: 630-633.

Eriksson, M., Karlsson, J., Ramazanov, Z., Gardestrom, P., and Samuelsson, G. (1996). Discovery of an algal mitochondrial carbonic anhydrase: molecular cloning and characterization of a low-CO_2-induced polypeptide in *Chlamydomonas reinhardtii*. Proc Natl Acad Sci 93: 12031-12034.

Fan, J., Zheng, L., Bai, Y., Saroussi, S., and Grossman, A.R. (2017). Flocculation of *Chlamydomonas reinhardtii* with different phenotypic traits by metal cations and high pH. Front Plant Sci 8: 1997-1997.

Featherstone, C., and Russell, P. (1991). Fission yeast p107 wee1 mitotic inhibitor is a tyrosine/serine kinase. Nature 349: 808-811.

Fernandez, E., and Cardenas, J. (1982). Regulation of the nitrate-reducing system enzymes in wild and mutant strains fom *Chlamydomonas reinhardttii*. Mol Gen Genet 186: 164-169.

Giordano, M., Norici, A., Forssen, M., Eriksson, M., and Raven, J.A. (2003). An anaplerotic role for mitochondrial carbonic anhydrase in *Chlamydomonas reinhardtii*. Plant Physiol 132: 2126-2134.

GO-Consortium. (2004). The Gene Ontology (GO) database and informatics resource. Nucleic Acids Res 32: D258-261.

Godl, K., Hallmann, A., Rappel, A., and Sumper, M. (1995). Pherophorins: a family of extracellular matrix glycoproteins from Volvox structurally related to the sex-inducing pheromone. Planta 196: 781-787.

Harris, E.H. (1989). Chlamydomonas Sourcebook. (New York: Academic Press).

Hodges, D.M., DeLong, J.M., Forney, C.F., and Prange, R.K. (1999). Improving the thiobarbituric acid-reactive-substances assay for estimating lipid peroxidation in plant tissues containing anthocyanin and other interfering compounds. Planta 207: 604-611.

Hoffmann, X.K., and Beck, C.F. (2005). Mating-induced shedding of cell walls, removal of walls from vegetative cells, and osmotic stress induce presumed cell wall genes in Chlamydomonas. Plant Physiol 139: 999-1014.

Hughes, T.R., Marton, M.J., Jones, A.R., Roberts, C.J., Stoughton, R., Armour, C.D., Bennett, H.A., Coffey, E., Dai, H., He, Y.D., et al. (2000). Functional discovery via a compendium of expression profiles. Cell 102: 109-126.

Lauersen, K.J., Willamme, R., Coosemans, N., Joris, M., Kruse, O., and Remacle, C. (2016). Peroxisomal microbodies are at the crossroads of acetate assimilation in the green microalga *Chlamydomonas reinhardtii*. Algal Res 16: 266-274.

Li, X., Moellering, E.R., Liu, B., Johnny, C., Fedewa, M., Sears, B.B., Kuo, M.H., and Benning, C. (2012). A galactoglycerolipid lipase is required for triacylglycerol accumulation and survival following nitrogen deprivation in *Chlamydomonas reinhardtii*. Plant Cell 24: 4670-4686.

Martin, N.C., and Goodenough, U.W. (1975). Gametic differentiation in *Chlamydomonas reinhardtii*. I. Production of gametes and their fine structure. J Cell Biol 67: 587-605.

Miles, S., Li, L., Davison, J., and Breeden, L.L. (2013). Xbp1 directs global repression of budding yeast transcription during the transition to quiescence and is important for the longevity and reversibility of the quiescent state. PLoS Genet 9: e1003854.

Miller, R., Wu, G., Deshpande, R.R., Vieler, A., Gartner, K., Li, X., Moellering, E.R., Zauner, S., Cornish, A.J., Liu, B., et al. (2010). Changes in transcript abundance in *Chlamydomonas reinhardtii* following nitrogen deprivation predict diversion of metabolism. Plant Physiol 154: 1737-1752.

Msanne, J., Xu, D., Konda, A.R., Casas-Mollano, J.A., Awada, T., Cahoon, E.B., and Cerutti, H. (2012). Metabolic and gene expression changes triggered by nitrogen deprivation in the photoautotrophically grown microalgae *Chlamydomonas reinhardtii* and *Coccomyxa sp. C-169*. Phytochemistry 75: 50-59.

Panchy, N., Wu, G., Newton, L., Tsai, C.H., Chen, J., Benning, C., Farre, E.M., and Shiu, S.H. (2014). Prevalence, evolution, and cis-regulation of diel transcription in *Chlamydomonas reinhardtii*. G3 4: 2461-2471.

Park, J.J., Wang, H., Gargouri, M., Deshpande, R.R., Skepper, J.N., Holguin, F.O., Juergens, M.T., Shachar-Hill, Y., Hicks, L.M., and Gang, D.R. (2015). The response of *Chlamydomonas reinhardtii* to nitrogen deprivation: a systems biology analysis. Plant J 81: 611-624.

Rittershaus, E.S., Baek, S.H., and Sassetti, C.M. (2013). The normalcy of dormancy: Common themes in microbial quiescence. Cell Host Microbe 13: 643-651.

Rodriguez, H., Haring, M.A., and Beck, C.F. (1999). Molecular characterization of two light-induced, gamete-specific genes from *Chlamydomonas reinhardtii* that encode hydroxyproline-rich proteins. Mol Gen Genet 261: 267-274.

Romero-Campero, F.J., Perez-Hurtado, I., Lucas-Reina, E., Romero, J.M., and Valverde, F. (2016). ChlamyNET: a Chlamydomonas gene co-expression network reveals global properties of the transcriptome and the early setup of key co-expression patterns in the green lineage. BMC Genomics 17: 227.

Sager, R. (1955). Inheritance in the green alga *Chlamydomonas Reinhardtii*. Genetics 40: 476-489.

Schloss, J.A. (1990). A Chlamydomonas gene encodes a G protein β subunit-like polypeptide. Molecular and General Genetics MGG 221: 443-452.

Schmollinger, S., Muhlhaus, T., Boyle, N.R., Blaby, I.K., Casero, D., Mettler, T., Moseley, J.L., Kropat, J., Sommer, F., Strenkert, D., et al. (2014). Nitrogen-sparing mechanisms in Chlamydomonas affect the transcriptome, the proteome, and photosynthetic metabolism. Plant Cell 26: 1410-1435.

Shimogawara, K., Fujiwara, S., Grossman, A.R., and Usuda, H. (1998). High-efficiency transformation of *Chlamydomonas reinhardtii* by electroporation. Genetics 148: 1821-1828.

Spudich, J.L., and Sager, R. (1980). Regulation of the Chlamydomonas cell cycle by light and dark. J Cell Biol 85: 136-145.

Tang, Z., Shu, H., Oncel, D., Chen, S., and Yu, H. (2004). Phosphorylation of Cdc20 by Bub1 provides a catalytic mechanism for APC/C inhibition by the spindle checkpoint. Mol Cell 16: 387-397.

Tsai, C.H., Uygun, S., Roston, R., Shiu, S.H., and Benning, C. (2018). Recovery from N deprivation is a transcriptionally and functionally distinct state in Chlamydomonas. Plant Physiol 176: 2007-2023.

Tsai, C.H., Warakanont, J., Takeuchi, T., Sears, B.B., Moellering, E.R., and Benning, C. (2014). The protein Compromised Hydrolysis of Triacylglycerols 7 (CHT7) acts as a repressor of cellular quiescence in Chlamydomonas. Proc Natl Acad Sci U S A 111: 15833-15838.

Tulin, F., and Cross, F.R. (2015). Cyclin-dependent kinase regulation of diurnal transcription in Chlamydomonas. Plant Cell 27: 2727-2742.

Usadel, B., Obayashi, T., Mutwil, M., Giorgi, F.M., Bassel, G.W., Tanimoto, M., Chow, A., Steinhauser, D., Persson, S., and Provart, N.J. (2009). Co-expression tools for plant biology: opportunities for hypothesis generation and caveats. Plant Cell Environ 32: 1633-1651.

Valcourt, J.R., Lemons, J.M., Haley, E.M., Kojima, M., Demuren, O.O., and Coller, H.A. (2012). Staying alive: metabolic adaptations to quiescence. Cell Cycle 11: 1680-1696.

Valledor, L., Furuhashi, T., Recuenco-Munoz, L., Wienkoop, S., and Weckwerth, W. (2014). System-level network analysis of nitrogen starvation and recovery in *Chlamydomonas reinhardtii* reveals potential new targets for increased lipid accumulation. Biotechnol Biofuels 7: 171.

Wang, X.F., and Chen, G. (2003). Complex networks: small-world, scale-free and beyond. IEEE Circuits and Systems Magazine 3: 6-20.

Warakanont, J., Tsai, C.H., Michel, E.J., Murphy, G.R., 3rd, Hsueh, P.Y., Roston, R.L., Sears, B.B., and Benning, C. (2015). Chloroplast lipid transfer processes in *Chlamydomonas reinhardtii* involving a Trigalactosyldiacylglycerol 2 (TGD2) orthologue. Plant J 84: 1005-1020.

Yao, N.Y., and O'Donnell, M. (2010). SnapShot: The replisome. Cell 141: 1088, 1088.e1081.

Zauner, S., Jochum, W., Bigorowski, T., and Benning, C. (2012). A cytochrome b5-containing plastid-located fatty acid desaturase from *Chlamydomonas reinhardtii*. Eukaryot Cell 11: 856-863.

Zhang, Y.-H., and Robinson, D.G. (1990). Cell-wall synthesis in *Chlamydomonas reinhardtii:* an immunological study on the wild type and wall-less mutants cw2 and cw15. Planta 180: 229-236.

Zones, J.M., Blaby, I.K., Merchant, S.S., and Umen, J.G. (2015). High-resolution profiling of a synchronized diurnal transcriptome from *Chlamydomonas reinhardtii* reveals continuous cell and metabolic differentiation. Plant Cell 27: 2743-2769.

CHAPTER 3

The protein-interaction domains, and not its CXC domain, are critical for CHT7 function[1,2]

[1]The work presented in this chapter has been reviewed, and the revised manuscript has been resubmitted to the Plant Cell journal.

Takeuchi T., Sears B.B., Lindeboom C., Lin YT., Fekaris N., Zienkiewicz K., Zienkiewicz, A., Poliner E., Benning C. (2019). Chlamydomonas CHT7 is required for an effective quiescent state by regulating nutrient-responsive cell cycle gene expression. Plant Cell. Revision submitted.

[2]A section of the work presented in this chapter was published in: Tsai C.H., Warakanont J., Takeuchi T., Sears B.B., Moellering E.R., and Benning C. (2014). The protein COMPROMISED HYDROLYSIS OF TRIACYLGLYCEROLS 7 (CHT7) acts as a repressor of cellular quiescence in Chlamydomonas. Proc Natl Acad Sci U S A 111(44):15833-8. I contributed the data on CHT7 complex formation by performing the blue native-PAGE and 2D SDS-PAGE.

ABSTRACT

In animals, CXC domains are known for their ability to bind DNA through consensus sequences termed cell cycle genes homology region (CHR). However, the role of these domains in CXC domain-containing proteins of photosynthetic organisms are not well-characterized. Here, extensive negative results from both targeted and non-targeted ChIP-approaches have prompted us to examine the precise functional contributions of CXC domain to CHT7 activity. Surprisingly, the largely unstructured C-terminal half of CHT7 with predicted protein-binding domains, but not the canonical CXC DNA-binding domain, is essential for the ability of CHT7 to form stable complexes and reverse the cellular phenotypes and transcription levels in the *cht7* mutant. Hence, although lacking the presumed DNA-binding domain, CHT7 modulates the expression of cell cycle genes in response to N availability, which is essential for establishing an effective quiescent state and the coordinated resumption of growth following N refeeding.

INTRODUCTION

CHT7 contains two cysteine-rich motifs or domains that are often collectively referred to as the CXC domain. CXC domain-containing proteins are ubiquitous among eukaryotes with the exception of yeast, and many are extensively studied for their roles in differentiation and proliferation of cells, organismal and sexual organ development, and in disease states such as cancer (Sadasivam and DeCaprio, 2013; Fischer and Muller, 2017). For example, CXC domain proteins such as the mammalian LIN54 (Litovchick et al., 2007; Schmit et al., 2007), fruit fly (*Drosophila melanogaster*) Mip120 (Beall et al., 2002; Korenjak et al., 2004), and worm (*Caenorhabditis elegans*) Lin-54 (Harrison et al., 2006) are members of multi-subunit transcriptional regulatory complexes called DREAM (DP, RB, E2F, and Myb-MuvB) complexes,

along with their respective orthologous retinoblastoma tumor suppressor (RB) pathway proteins. These CXC domain-containing proteins within the DREAM complexes (Beall et al., 2002; Schmit et al., 2009; Tabuchi et al., 2011; Marceau et al., 2016) and other CXC proteins from animal lineages (Fauth et al., 2010; Zheng et al., 2014) have been shown to bind DNA in a sequence-specific manner.

In contrast to the CXC domain-containing proteins of metazoans, the modes of actions for those of plant lineages are comparatively less characterized. Despite the numerous CXC domain proteins in plants, only the CXC domains of soybean (*Glycine max*) CPP1 (Cvitanich et al., 2000) and maize (*Zea mays*) CBBP (Brzeska et al., 2010) have been shown as important for DNA-binding, thus far. In Arabidopsis (*Arabidopsis thaliana*), DREAM-like complexes containing RB pathway proteins, ALY2/3, MYB3R proteins and a CXC domain protein, TCX5, also exist and seem to play a functionally similar role to those of animals (Kobayashi et al., 2015). In addition, another CXC domain protein, TSO1 has been shown to mediate the proper development of Arabidopsis meristems, shoots, and roots (Liu et al., 1997; Hauser et al., 1998; Hauser et al., 2000; Song et al., 2000; Sijacic et al., 2011; Wang et al., 2018). The closest paralogues of *TSO1*, *SOL1* and *2* have recently been shown as necessary for the cell fate transitions and divisions in the Arabidopsis cells of stomatal-origin (Simmons et al., 2019). However, the precise functional contributions of the CXC domains to the activities of these Arabidopsis proteins are not yet known. To understand the mechanism of CHT7-mediated gene regulation, the sizes of CHT7 complex were assessed both during N-replete growth and following N deprivation by blue native PAGE (BN-PAGE). We then performed a structure-function characterization of the CHT7 protein, and importantly, the results suggest that the mechanism of CHT7 action differs from those of canonical CXC domain-containing proteins.

RESULTS

The majority of CHT7 proteins exist in a complex of constant size during N-replete growth and following N deprivation

The abundance of CHT7 proteins on total protein-basis during N-replete growth, following N deprivation and subsequent N resupply was previously reported to be similar across different N conditions (Tsai et al., 2014). To test whether CHT7 proteins form a complex in vivo, BN-PAGE was initially performed using non-denatured total protein extracts from parental line (PL; dw15, cw^-) cells during N-replete growth and following 48 h of N starvation (Figure 3.1A and B). The immunoblotting was later performed with CHT7-antibody. Whereas the monomeric CHT7 has a predicted molecular weight of ~75 kDa, the bulk of CHT7 existed as a complex of approximately ~242 kDa, whose apparent size and abundance were constant regardless of the availability of N (Figure 3.1A and B) (Tsai et al., 2014). The presence of CHT7 within this native complex was confirmed 1D BN-PAGE followed by 2D SDS-PAGE (Figure 3.1C) (Tsai et al., 2014).

The CXC domain of CHT7 is dispensable for its function

To begin to understand how CHT7 represses cell cycle-related genes during N deprivation, we focused on the CXC domain defining the presumed orthologous proteins, since the CXC domains had been widely implicated in the sequence-specific binding of DNA (Cvitanich et al., 2000; Beall et al., 2002; Schmit et al., 2009; Brzeska et al., 2010; Fauth et al., 2010; Tabuchi et al., 2011; Zheng et al., 2014; Marceau et al., 2016). The amino acid (AA) sequence alignment of the CXC domain containing proteins from representative species revealed a high similarity within their CXC domains, and the tyrosine residues identified as critical for the CXC domain-mediated binding of specific DNA sequences in LIN54 by a crystal structure (Marceau et al., 2016) were

conserved across species, including in CHT7 (Figure 3.2A and B). However, these proteins did not appear to share extensive similarity throughout the full AA sequences (Figure 3.2C). Nevertheless, given the high percent identity of the CXC domains of LIN54 and CHT7 (56.1%) and the presence of critical tyrosines, we hypothesized that CHT7 might also bind to similar target sequences as LIN54 through its CXC domain. Therefore, we conducted a targeted chromatin immunoprecipitation (ChIP)-qPCR experiment to test whether CHT7 would associate with the identified DNA binding elements of LIN54 in DNA sequences up to 2500 bp upstream of the respective 5' untranslated region of derepressed cell cycle-related genes in *cht7* (1). A C-terminally 3xHA-tagged CHT7 complemented line (*CHT7-HA:cht7*) was used for the ChIP experiments after determining that it fully complemented the *cht7* mutation since HA antibodies were more sensitive and specific than the CHT7 antibodies (Figure 3.4A). The putative binding sites in the presumed promoters of the cell cycle genes (Figure 3.3) were identified based on the consensus target sequences for the LIN54 CXC domain known as cell cycle genes homology region (CHR) elements, defined as TTYRAA, where Y is a pyrimidine base and R is a purine base. All sequence variants of CHR elements that the LIN54 CXC domain was able to bind in an isothermal titration calorimetry assay were considered (Marceau et al., 2016).

Of the 34 putative CXC domain binding sites for seven genes tested, none of the target fragments were enriched in the ChIP of *CHT7-HA:cht7* performed with HA-antibody after qPCR (Figure 3.4D), suggesting that CHT7-HA does not directly associate with promoters of these target genes through the CHR consensus sequences. It should be noted that the efficiency of chromatin shearing and immunoprecipitation were always tested prior to each ChIP-qPCR experiment (Figure 3.4B and C), and the control immunoblots consistently showed that CHT7-HA was specifically immunoprecipitated and enriched in the appropriate IP sample (Figure 3.4C).

Furthermore, the positive ChIP-qPCR control performed against histone H3 using the same *CHT7-HA:cht7* line showed an enrichment of test-target promoters, *HSP70A*, *RBSC2*, and *CYC6* (Strenkert et al., 2011) in the ChIP performed with H3-antibody but not with uncoupled beads. Since CHR consensus sequences are AT-rich in contrast to the GC-rich genome of Chlamydomonas (Merchant et al., 2007), we also made extensive attempts to identify the binding sites of CHT7-HA through an untargeted ChIP-Seq approach. However, the DNA concentrations of the amplified library remained too low for sequencing even after combining purified DNA from multiple scaled-up ChIP reactions, and no putative DNA fragments directly interacting with CHT7 were identified.

These negative results prompted us to test directly whether the CXC domain of CHT7 was required for CHT7 function. Towards this end, we generated three deletion constructs of *CHT7-HA* near its N-terminus. As depicted in Figure 3.5A, the first construct (*N1 C-HA*) removed the protein-interacting sequence, P1, predicted by the DisoRDPbind program (Peng and Kurgan, 2015), the second removed the P1 and the CXC domain (*N2 C-HA*), and the third only removed the CXC domain (Δ*CXC C-HA*). When these deletion constructs were introduced into the *cht7* (1) mutant, the corresponding mutant proteins of expected molecular sizes were produced (Figure 3.5B). We found that the three altered proteins were able to complement the *cht7* mutation by restoring the growth of *cht7* (1) as well as the full length CHT7-HA (Figure 3.5C), which was also readily apparent from the color of these cultures after 24 h of N refeeding (Figure 3.5D). The CHT7-HA proteins having deletions of the N-terminus or CXC domain also completely rescued the delayed TAG degradation phenotype of *cht7* (1) (Figure 3.5E). The empty *pSL18* vector introduced into *cht7* (1) served as a negative control in the above experiments (Figure 3.5C and E). Based on these results we conclude that the CXC domain is dispensable for the activity of

CHT7 and that CHT7 likely exerts its function in different ways than previously characterized CXC domain proteins.

Predicted protein-binding amino acid residues in the CHT7 C-terminal region, especially within P3, are necessary for its function

Outside of the CXC domain, CHT7 does not contain any known structurally ordered domains. In particular, the C-terminal region of CHT7 was found to contain intermittent clusters of AA residues that were highly disordered, suggesting that the C-terminus of CHT7 largely lacks a stable structure under native conditions (Figure 3.6A). When the AA sequence of CHT7 (AA1-770) was analyzed by DisoRDPbind (Peng and Kurgan, 2015), an AA functional binding prediction algorithm for disordered proteins, the AA residues within the C-terminal half of CHT7 (AA450-770) were found to have consistently high probabilities of being involved in protein-binding (Figure 3.6A). Three AA clusters, named P2, P3, and P4, which contain AA residues predicted as protein-binding with probabilities of greater than 0.8, were identified within this region of CHT7 (Figure 3.6B). To identify regions of CHT7 that are essential for function, we generated four C-terminal deletion constructs of *HA-CHT7* with progressively larger deletions by the insertion of stop-codons. As depicted in Figure 3.7A, the first construct removed the region containing P3 and P4 (*HA-C STOP1*), the second removed all three predicted protein-interacting AA clusters (P2-P4) (*HA-C STOP2*), and the third and fourth constructs only left the N terminus and the CXC domain, entirely removing the sequence past the CXC domain (*HA-C STOP3* and *HA-C STOP4*) (Figure 3.7A). When these deletion constructs were introduced into the *cht7* (1) mutant, progressively smaller HA-CHT7 mutant proteins of expected molecular sizes were produced (Figure 3.7B). All four mutated HA-CHT7 proteins were unable to reverse the delayed growth (Figure 3.7C) and

TAG degradation (Figure 3.7D) phenotypes of *cht7* (1) during N resupply following 48 h of N deprivation, although a slight improvement of growth was observed for lines producing HA-C STOP1 and HA-C STOP2 proteins, which retained the AA residues between the CXC domain and P2. The loss of HA-CHT7 functions in these four mutant proteins was also apparent from the pale color of these cultures following 24 h of N resupply, while parallel cultures of the wild type, the respective HA-tagged full-length *CHT7*-complemented lines, and the N-terminal and CXC domain deletion lines of *CHT7-HA* readily regained chlorophyll and biomass (Figure 3.7E). The box plot distributions of percent colony formation of the above lines during N-replete growth or following 48 h of N deprivation showed the N starvation-specific decline in the ability of *cht7* (1) to form colonies, and a similar N deprivation-induced reduction in colony formation was observed for all four C-terminally mutated *HA-CHT7* lines (*HA-C STOP1*, *2*, *3* and *4*) but not for any of the N-terminal or CXC domain deletion *CHT7-HA* lines (*N1*, *N2*, and Δ*CXC C-HA*) (Figure 3.7F). These results indicated that the largely disordered C-terminal region (AA450-750) of CHT7, which corresponds to AA residues predicted to mediate protein-protein interaction, was essential for the ability of CHT7 to complement the *cht7* mutation.

To determine which of the predicted protein-binding AA clusters (P2, P3, or P4) are important for CHT7 functionality, we generated three additional *HA-CHT7* constructs that specifically removed the AA residues within P2, P3, or P4 regions (Figure 3.8A). The expression of corresponding mutated HA-CHT7 proteins with deletions in P2, P3, or P4 in the *cht7* (1) mutant background was confirmed by the immunoblot of their respective transformants (Figure 3.8B). The removal of the P2, P3, or P4 region resulted in 47, 62, and 83 AA deletions, respectively; however, HA-CHT7 ΔP2, ΔP3, and ΔP4 proteins did not migrate based on the expected molecular weight (Figure 3.8B). While the full-length CHT7 has a predicted isoelectric point of 7.43, the

removal of the P2, P3, or P4 region from CHT7 changes their isoelectric points to 8.42, 7.05 and 8.42, respectively. Thus, the net charge of native HA-C ΔP3 proteins became more negative, and the net charges of the native HA-C ΔP2 and ΔP4 proteins became more positive relative to the full-length HA-CHT7 at a given pH, likely affecting the proportional binding of anionic amphiphilic SDS detergents and consequently the migration, as previously noted (Nelson, 1971). Regardless, the presence of the correct mutated *HA-CHT7* construct in the *cht7* (1) transformants was confirmed by PCR amplification of the mutated region followed by sequencing.

While the mutated HA-CHT7 proteins without the P2 or P4 AA clusters were able to completely restore the growth and division of *cht7* (1) during N resupply following 48 h of N deprivation, the HA-CHT7 proteins without the P3 region were not, suggesting that the AA residues within P3 are essential for CHT7 functionality (Figure 3.8C). Following N resupply of 24 h, the *HA-C* Δ*P3* deletion line lagged in the remobilization of TAG (Figure 3.8D) and remained pale-green in color (Figure 3.8E), in much of the same manner as the *cht7* (1) mutant. At the same time point, the *HA-C ΔP2* and *ΔP4* deletion lines also showed a noticeable delay in TAG degradation but to a lesser extent than the *HA-C ΔP3* deletion line, and the colorations of these cultures were more similar to those of the wild type and the full-length *HA-CHT7* line than the *cht7* (1) mutant (Figure 3.8E). The colony formation following N deprivation of 48 h was observed to be similarly impacted in all three *HA-C ΔP2*, *ΔP3* and *ΔP4* deletion lines (Figure 3.8F). These results suggested that AA residues within the P2, P3 and P4 regions may all contribute to the functional stability of CHT7, although not to the same degree. The deletion of P3 clearly affected the ability of the mutated HA-CHT7 protein to complement *cht7* (1) phenotypes more than the deletion of P2 or P4, suggesting that the AA residues within P3 are crucial for CHT7 function.

Compromised CHT7 protein function correlates with derepression of cell cycle-marker genes during N deprivation

To examine whether the results of structure-function analyses of CHT7 were also reflected in gene expression, we tested the ability of respectively HA-tagged and mutated CHT7 to repress a representative set of cell cycle-related genes that were found to be derepressed in *cht7* (1). The expression levels of six genes, *CDKB1*, *CYCA1*, *CYCB1*, *CYCAB1*, *ORC1*, and *CDC45* were assessed in the three sets of CHT7 deletion lines described in the study following 48 h of N deprivation by qPCR (Figure 3.9A and B). The ability of CHT7 variants to repress the tested genes largely corresponded to how well they reversed the *cht7* (1) mutant phenotypes in the previous experiments (Figures 3.5, 3.7 and 3.8). Specifically, HA-CHT7 proteins with deletions in the C-terminal end (HA-C STOP1, 2, 3, 4) and P3 (HA-C ΔP3) that failed to restore the *cht7* (1) phenotypes were also unable to repress the six representative cell cycle genes tested following N deprivation. On the other hand, CHT7-HA proteins with deletions in the N-terminal end or the CXC domain that fully complemented the *cht7* (1) phenotypes were able to repress these genes following N deprivation, except in the case of *CDC45*, where *N2 C-HA* and *ΔCXC C-HA* lines showed a moderate derepression. However, it should be noted that the relative expression of genes shown in Figure 3.9B (*CYCAB1*, *ORC1*, and *CDC45*) was at least an order of magnitude lower than that shown in Figure 3.9A (*CDKB1*, *CYCA1*, and *CYCB1*), and the differences in gene expression observed in Figure 3.9B are likely more sensitive to perturbation (i.e., less robust) than those observed in Figure 3.9A. HA-CHT7 proteins without the P2 or P4 region (HA-C ΔP2 and ΔP4) that showed partial complementation of *cht7* (1) phenotypes also showed a tight repression of these genes following N deprivation. The deletions of these regions alone did not negatively impact the ability of CHT7 to repress the genes tested following N deprivation, supporting the

notion that P2 and P4 regions likely play a less substantial role in the overall function of CHT7. Taken together, these results showed that the regions identified as most important for the ability of CHT7 to rescue *cht7* (1) in the structure-function studies were also necessary for CHT7 to properly repress a representative set of derepressed genes in *cht7* (1) following N deprivation, further suggesting that the altered gene expression is causal for the observed *cht7* (1) phenotypes.

Large deletions to the CHT7 C-terminus negatively affect complex formation

Most of the CHT7 protein has been found in a complex with an observed molecular weight of approximately 242 kDa as determined by blue native (BN)-PAGE during N-replete growth and following N deprivation (Figure 3.1A and B) (Tsai et al., 2014). Since many of the AA residues with predicted functions in protein-binding are located in the C-terminal half of the CHT7 protein (Figure 3.6A), we tested the ability of the mutated HA-tagged CHT7 variants to form the CHT7 complex observed by BN-PAGE. We only tested cells that were grown in the presence of N, because the wild-type complex size observed by BN-PAGE was the same regardless of N availability. Total protein extracts were prepared under non-denaturing native conditions, and equal amounts of total protein were separated on a native BN-PAGE gel or a denaturing SDS-PAGE gel to concurrently probe for the abundance of the CHT7 complex and total CHT7 protein in the same sample (Figure 3.10). In both cases, the immunoblotting was subsequently performed using the HA-antibody. As expected, the N1, N2 or CXC domain deletions of CHT7-HA proteins did not affect their ability to form the complex observed by BN-PAGE (Figure 3.10A). Within the same set of experiments, the levels of respective CHT7-HA variants were assessed by SDS-PAGE (Figure 3.10B) and were observed to approximately reflect the levels of corresponding CHT7-HA complex variants (Figure 3.10A). Indeed, when the levels of total CHT7-HA variants from SDS-

PAGE and those of the corresponding CHT7-HA complexes from BN-PAGE were quantified from independent experimental repeats, the relative abundance of the total mutated CHT7-HA proteins and their corresponding complexes was similar, suggesting that most of the mutated CHT7-HA proteins exist as components of the observed complex (Figure 3.10C).

The mutated HA-CHT7 proteins without the P2, P3, or P4 region retained their ability to form the complex observed by BN-PAGE, although the levels of the HA-C ΔP2 or ΔP3 complexes were reduced to about half of that observed for the full length HA-CHT7 (Figure 3.10D and F). The levels of total HA-C ΔP3 proteins observed by SDS-PAGE followed by immunoblotting were consistently lower than those observed for the full length HA-CHT7 when the initial samples were prepared under native conditions (Figure 3.10E and F). However, when the whole cell lysates were prepared under denaturing conditions using cells from *HA-CHT7* or *HA-C ΔP3* lines, no such reduction in HA-C ΔP3 proteins relative to the full-length HA-CHT7 were observed by immunoblotting (Figure 3.8B), suggesting that the HA-C ΔP3 proteins may have a reduced stability under native conditions. However, the compromised ability of the mutated HA-CHT7 proteins to form a complex was more obvious for those that lacked the larger portions of the C-terminal end (Figure 3.10D). The complex abundance of HA-C STOP1, which is missing the region including and past P3, was markedly reduced compared to that of the full-length HA-CHT7 Figure 3.10D and F) or the abundance of total HA-C STOP1 proteins prepared from the same sample (Figure 3.10E and F). Although the apparent complex abundance of the HA-C STOP2 protein, which is missing the region including and past P2, was similar to that of the full-length HA-CHT7 (Figure 3.10D and F), only about 50% of the total HA-C STOP2 protein was found in the observed complex (Figure 3.10E and F). The complex formation was almost completely abolished for HA-C STOP3 and 4 (Figure 3.10D), which retain only the N-terminus and the CXC

domain of CHT7, and the quantified levels of respective complexes were essentially the same as the background levels observed for *cht7* (1) (Figure 3.10F), although varying reductions in total HA-C STOP3 and STOP4 protein were observed as was the case for HA-C ΔP3 proteins. Taken together, we conclude that AA residues within the C-terminal half of the CHT7 protein are required for the formation of stable CHT7 complexes and, hence, function.

DISCUSSION

Our initial mechanistic studies of CHT7 as a genuine member of the family of CXC domain proteins were built on the premise that the functional significance of CXC domains had been widely demonstrated in a number of animal orthologs (Beall et al., 2002; Schmit et al., 2009; Fauth et al., 2010; Tabuchi et al., 2011; Zheng et al., 2014; Marceau et al., 2016) and in some plant orthologs (Cvitanich et al., 2000; Brzeska et al., 2010). Importantly, the crystal structures of the CXC domains have been solved for some CXC domain proteins of animal origin, giving insights into how they bind DNA and provide target specificity at the AA level (Zheng et al., 2012; Zheng et al., 2014; Marceau et al., 2016). However, the functional contributions of the CXC domains in proteins of plant lineages remain comparatively less known. Among the compared AA sequences, the CXC domain of CHT7 showed the highest similarity (61.5%) to that of Arabidopsis TCX5 (Figure 3.2A and B), which is one of the core components of the plant DREAM-like complexes (Kobayashi et al., 2015). In contrast to humans (Muller et al., 2012; Muller et al., 2014), fly (Korenjak et al., 2012) and worm (Tabuchi et al., 2011), the CHR consensus sequences have yet to be identified in the promoters of G2/M phase-specific genes that the Arabidopsis DREAM-like complexes target (Fischer and DeCaprio, 2015; Kobayashi et al., 2015; Fischer and Muller, 2017). The CXC domains of two paralogous proteins in Chlamydomonas, encoded by genes

Cre08.g361400 and *Cre12.g550250*, shared the highest similarities (51.3% and 52.3%) to that of Arabidopsis TSO1 (Figure 3.2 A and B). These genes were also derepressed in *cht7* following N deprivation and refeeding (Figure 2.9). TSO1 coordinates the cell division cycle in the meristem, shoot, and root during the plant development (Liu et al., 1997; Hauser et al., 1998; Hauser et al., 2000; Song et al., 2000; Sijacic et al., 2011; Wang et al., 2018). In genetic interaction experiments, *TSO1* was found to repress the transcription of *MYB3R1*, which encodes a protein thought to be an activator in the shoot and a repressor in the root, and TSO1 and MYB3R1 were found to co-immunoprecipitate together (Wang et al., 2018). Whether TCX5 and TSO1 exert their function by directly binding DNA as in animals is not yet known.

A series of negative results from both targeted and non-targeted ChIP experiments in an attempt to identify DNA fragments that could be directly bound by CHT7 led us to question the functional significance of its putative CXC DNA-binding domain and prompted us to pursue a structure-function characterization of CHT7. In fact, mutated versions of CHT7-HA proteins with N-terminal and CXC domain deletions remained fully functional as indicated by their ability to form complexes (Figure 3.10A-C), repress a representative set of cell cycle-related genes (Figure 3.9A and B), and fully reverse the observed *cht7* phenotypes (Figures 3.5 and 3.7E-F). On the other hand, the HA-CHT7 STOP3 and 4 proteins, which contain only the N-terminus and the CXC domain, completely lost their ability to form stable complexes (Figure 3.10D-F), exert repression of cell cycle-marker genes (Figure 3.9), and complement the *cht7* phenotypes (Figure 3.7). Thus, the disordered C-terminal region of CHT7 (AA450-770), which contains a high number of predicted protein-binding AA residues (Figure 3.6), was necessary for the functionality of CHT7. The HA-CHT7 STOP1 and 2 proteins, where the former lacks the region containing P3 and P4 and the latter lacks all three predicted protein-interacting AA clusters (P2-4) in the C-terminus of

CHT7, were largely compromised in their ability to form stable complexes (Figure 3.10D-F), repress genes (Figure 3.9), and rescue the *cht7* phenotypes (Figure 3.7). In particular, the deletion of AA residues within the P3 region had the most impact on CHT7 function (Figures 3.8 and 3.9). The predictions of CHT7 secondary structures showed that the removal of AA residues within the P3 region results in a disruption of predicted helix-coil-helix like secondary structures (Figure 3.11). Indeed, the propensities of the C-termini of animal CXC domain proteins to form helices have been observed (Jiang et al., 2007; Schmit et al., 2009; Marceau et al., 2016), and such helix-coil-helix motifs identified by secondary structure predictions have been implicated in mediating protein-protein interactions, such as in the binding of LIN54 to p130 and B-Myb (Schmit et al., 2009). Thus, the current data suggest that CHT7 might serve a role as a protein-scaffold, with which potential DNA-binding proteins interact to mediate transcriptional regulation, as the predicted protein-binding AA residues, not the proposed CXC domain, are important for CHT7 functionality. In this context, it is note-worthy that Arabidopsis TCX5 is a core component that is present in both the repressor and activator DREAM complexes, where the associations of other transcription factors such as MYB3Rs and E2Fs determine the direction of the transcriptional regulation (Kobayashi et al., 2015). Based on the deletion analysis of CHT7 described here, a possible function of the CXC domain in CHT7 and its orthologs should be revisited.

MATERIALS AND METHODS

Generation and Validation of Lines

The generation of *pMN24 CHT7* and *pSL18 (-Asc*I*) CHT7* was described in Tsai et al. (2014), and Chapter 2, respectively. To tag the C-terminus of *CHT7* with 3x HA, the C-terminus of *CHT7* flanked by two *Avr*II cut-sites was digested from *pMN24 CHT7*, subcloned into the *pBR322* vector

using *Sty*I, which generates *Avr*II-compatible ends, and the site-direct mutageneses (SDM) PCRs were carried out using *C-term 3xHA*-F and -R primers (Table 3.1). To tag the N-terminus of *CHT7* with 1x HA, the N-terminus of *CHT7* was cleaved from *pSL18 (-Asc*I*) CHT7* using *Not*I and *Sal*I, blunted with Klenow, ligated into the *EcoR*V site of *Zero Blunt* (ZB) vector, and the SDM PCR was carried out using *N-term 1xHA*-F and -R primers (Table 3.1). To make *pSL18 (-Asc*I*) CHT7-3xHA*, the C-terminal *CHT7* fragment fused to 3x HA was obtained from digesting *pBR332 CHT7-3xHA Avr*II-*Avr*II with *Avr*II, ligated into *pSL18 (-Asc*I*) CHT7* digested with *Avr*II, and the clones with correctly oriented inserts were identified by restriction digests and sequencing. For the generation of *pSL18 (-Asc*I*) 1xHA-CHT7*, the 1x HA fused to the N-terminus of the *CHT7* fragment was obtained from digesting *ZB 1xHA-CHT7 Not*I-*Sal*I with *Asc*I and *Bsu36*I and ligated into *pSL18 (-Asc*I*) CHT7* digested with the same enzyme.

To generate *pGEM CHT7*, which served as a template for most *CHT7* SDM PCRs, a fragment containing the *CHT7* sequence was obtained by digesting *pMN24 CHT7* with *Sal*I and was ligated into the *Sal*I site of the *pGEM* vector. SDM PCRs were carried out using the SDM primer pairs detailed in Table 3.1. To make *pSL18 (-Asc*I*) CHT7-3xHA N1*, *N2*, and *ΔCXC* constructs, SDM PCRs were carried out using *pGEM CHT7* as a template. *pGEM CHT7* constructs containing the respective deletions were then digested with *Asc*I and *BsrG*I-HF and ligated into *pSL18 (-Asc*I*) CHT7-3xHA* digested with the same enzymes. For the generation of *pSL18 (-AscI) HA-CHT7 STOP1* and *2*, *pBR332 CHT7* was used as a template for SDM PCRs. The mutated *pBR322 CHT7* constructs with correctly inserted stop-codons were digested with *Srf*I and *BsrG*I-HF, and the inserts were ligated into *pSL18 (-Asc*I*) 1xHA-CHT7* digested with the same enzymes. To generate *pSL18 (-AscI) HA-CHT7 STOP3*, *STOP4*, *ΔP2*, *ΔP3*, and *ΔP4*, SDM PCRs were carried out using *pGEM CHT7* as a template. The mutated *pGEM CHT7* constructs containing

stop-codons at *STOP3* and *4* sites were cleaved using *Bsu36*I and *BsrG*I-HF and ligated into *pSL18 (-Asc*I*) 1xHA-CHT7* digested with the same enzymes. The mutated *pGEM CHT7* constructs containing deletions in *ΔP2* or *ΔP3* were digested with *Bsu36*I and *BsrGI*-HF while that containing the *ΔP4* deletion was digested with *Mlu*I-HF and *BsrG*I-HF. The obtained inserts were then ligated into *pSL18 (-Asc*I*) 1xHA-CHT7* digested with respective sets of enzymes. For all cloning PCR steps, the correctness of the amplified regions were verified by sequencing. For the transformation of cell-walled *cht7* mutant lines, all constructs were linearized first with *Ahd*I and introduced into the cells by electroporation as previously described (Shimogawara et al., 1998) and in Chapter 2. The presence of respectively HA-tagged CHT7 proteins and their mutated variants was verified by SDS-PAGE followed by immunoblotting using 1:1000 dilution of HA-HRP antibody (Sigma, catalog #: 12013819001) against the fused HA-epitope(s).

Growth Conditions

Cells were cultured in Tris acetate phosphate (TAP) medium (Harris, 1989) as described in Chapter 2. For growth curves during N refeeding, the cells were N-deprived for 48 h as described in Chapter 2, and the cell densities of cultures were adjusted to $2x10^6$ cells/mL prior to resupplying the N from a 100 x NH_4Cl solution. For all time points, the cell density was assessed using a Beckman Coulter Counter Z2.

Protein Sequence Alignment and Predictions of Disorder, AA Function, and Secondary Structure

Protein sequences were aligned and compared using Clustal O (1.2.4) (Larkin et al., 2007). Disorder and AA functional predictions of CHT7 were performed using IUPred2A (Mészáros et

al., 2018) and DisoRDPbind (Peng and Kurgan, 2015), respectively. The prediction of CHT7 secondary structures was performed using PSIPRED 4.0 (McGuffin et al., 2000; Buchan and Jones, 2019).

Lipid Analysis

The quantification of TAG was performed as described in Chapter 2.

Assessment of Cell Viability by Percent Colony Formation

The assessment of cell viability by colony formation was performed as described in Chapter 2.

Chromatin Immunoprecipitation

Chromatin immunoprecipitation (ChIP) was carried out by a modified protocol based on the method described by Strenkert et al. (2011). For the preparation of input chromatin, mid-log phase cultures of *cht7* (1) and *CHT7-HA::cht7* were grown in N-replete TAP medium, and the cells were adjusted to an OD_{750} of 0.5 in a volume of 400 mL TAP N^- as described above. After 48 h of N deprivation, the cultures were centrifuged at 3,000 x g at 4 ºC in the presence of 1:4000 20% tween-20, and the resulting cell pellets were fixed with 10 mL of 0.35% formaldehyde crosslinking solution (0.35% formaldehyde, 20 mM Hepes, 80 mM KCl) at room temperature for 10 minutes with gentle rotation. Upon the addition of 1.25 mL 1 M glycine, cells were further rotated at room temperature for 5 min and centrifuged at 3,000 x g for 5 minutes at 4 ºC. Cells were then resuspended in 5 mL of KH buffer (20 mM Hepes KOH pH7.6, 80 mM KCl), centrifuged again as above, and resuspended in 5 mL of lysis buffer (Strenkert et al., 2011) in the presence of 1:100 plant protease inhibitor cocktail (Sigma-Aldrich), 1x Roche cOmplete protease inhibitor (Sigma-

Aldrich), 5 mM benzamidine and 50 μM Mg-132. Cells were then sonicated using Misonix Inc S-3000 sonicator (Cole-Parmer) with a 1/8th inch probe in the cold room in a 40% ethanol ice bath as follows: total process time of 2 minutes and 30 seconds with a pulse on-time of 0.6 seconds and off-time of 0.5 seconds, and the power output set at 4.0. Sonication was repeated for a total of eight times with 20 second rest intervals. Following sonication, cells were centrifuged at 4,500 x g for 10 min at 4 ºC, the supernatant was filtered through a 0.45 μm filter, and the chromatin volume was adjusted to 5 mL. Chromatin was aliquoted, snap frozen in liquid N and stored in -80 ºC until ChIP was performed. For ChIP, Protein G Dynabeads (Invitrogen) were conjugated with H3-antibody (abcam, catalog #: ab1791), HA-antibody (BioLegend, 16B12, catalog #: 901503) or mouse IgG (BioLegend, mock control, catalog #: 400102). Chromatin extracts were diluted 1:10 with ChIP buffer (Strenkert et al., 2011) in the presence of 1:100 plant protease inhibitor cocktail (Sigma-Aldrich) and 1x Roche cOmplete protease inhibitor (Sigma-Aldrich). 2 mL of diluted chromatin solution was immunoprecipitated with beads conjugated with the respective antibodies for 3.5 h at 4 ºC with gentle rotation. 200 μL of the chromatin was used as the input control. Washing buffers 1, 2, 3, and TE were prepared as detailed in (Strenkert et al., 2011). Beads were washed with 1 mL washing buffer 1 (low salt) once, 1 mL washing buffer 2 (high salt) once, 1 mL washing buffer 3 (LiCl) once, and 1 mL TE twice. After the wash, the chromatin was eluted off the beads twice with 100 μL elution buffer (50 mM Tris-HCl, pH 8.0, 10 mM EDTA, 1% SDS) separated by a 15 min incubation at 65 ºC. After incubation at 65 ºC overnight to reverse the cross link, the DNA was treated with 100 μg RNaseA for 2 h at 37 ºC and 2 μL Proteinase K (0.2mg/mL) for 2 hours at 65°C. The DNA was purified using the QIAquick PCR Purification kit (Qiagen) and eluted in 50 μL of the Qiagen Elution Buffer. 1 μL of 10x diluted input and 1 μL of the

immunoprecipitate (IP) were used for the qPCR as detailed above using the primers listed in Table 3.2.

Real-Time Quantitative PCR (RT-qPCR)

RT-qPCR analyses were performed as described in Chapter 2. The qPCR primers of genes tested are provided in Table 3.3.

BN-PAGE and SDS-PAGE Followed by Immunoblotting

For the preparation of native protein extracts for BN-PAGE, cells from 50 mL cultures during mid-log growth were resuspended in 0.5 mL of PBS with 1x Roche cOmplete protease inhibitor (Sigma-Aldrich), and 1:100 dilutions of plant protease inhibitor cocktail (Sigma-Aldrich), phosphatase inhibitor cocktail (Halt^{TM}, Thermo Scientific), and PMSF (Sigma-Aldrich, 93482). Samples were sonicated on watery ice using Misonix Inc S-3000 sonicator (Cole-Parmer) with a 1/16th inch micro-tip probe at 4 ºC. While cw^{-} strains were sonicated with 0.6 sec on- and 0.5 sec off-pulses for a total process time of 20 sec repeated 20 times at the power output setting of 2.0, cw^{+} strains were sonicated for a total process time of 2 min with 10 sec on- and 2.5 sec off-pulses repeated six times at the same power output. The protein extracts were obtained by centrifuging at 20,000 × g for 30 min at 4 °C to remove insoluble materials. Protein concentration was determined using the Bradford protein assay (Bio-Rad). Supernatants containing 25 µg of proteins were loaded onto each lane of Novex 4–16% (wt/vol) Bis-Tris gels (Life Technologies), and BN electrophoresis was performed as described (Wittig et al., 2006). After denaturation, gels were either blotted directly or run in a second dimension by SDS-PAGE. For experiments where the denatured proteins for SDS-PAGE were prepared using the native protein extracts from above,

protein extracts were mixed with an equal volume of 2x Laemmli sample buffer (4% SDS, 20% glycerol, 125 mM Tris-HCl, pH 6.8, 0.004% bromophenol blue) containing 1x Roche cOmplete protease inhibitor (Sigma-Aldrich), 1:100 dilutions of plant protease inhibitor cocktail (Sigma-Aldrich), phosphatase inhibitor cocktail (Halt^{TM}, Thermo Scientific) and PMSF (Sigma-Aldrich, 93482), and 5% v/v of β-mercaptoethanol. Samples were incubated at 95^{o}C for 5 min, and 25 μg of protein were loaded for SDS-PAGE. To analyze and verify the expression of HA-tagged full-length or mutated CHT7 in the *cht7* (1) background, the denatured total cell lysates were prepared and quantified as described in Chapter 2. In all instances, SDS-PAGE and immunoblotting were performed as previously described using CHT7 antibody (Tsai et al., 2014), or 1:1000 dilution of HA-HRP antibody (Sigma, catalog #: 12013819001). Signal quantifications of the blots were performed by Bio-Rad Image Lab software (https://www.bio-rad.com).

APPENDIX

Table 3.1. Primers used for site directed mutagenesis (SDM) PCR.

Primer	Sequence 5'—3'	Purpose
C-term 3xHA-F	CCAGATTACGCTTATCCATATGAC GTTCCAGATTACGCTTGAGGAACG AGAGGACAGGGG	Forward primer used for inserting 3x HA tag at the C-terminus end of CHT7
C-term 3xHA-R	AACGTCATATGGATAAGCGTAATC TGGAACGTCATATGGATACGTGAG CGCGCCTTCAAG	Reverse primer used for inserting 3x HA tag at the C-terminus end of CHT7
N1-F	AAGGTGCCCTCGGCGTCG	Forward primer used for *N1 CHT7-HA* cloning
N2-F	AAGCGCGTGCGCTACAGC	Forward primer used for *N2 CHT7-HA* cloning
N1/N2-R	CGCGTCAACAAGCGGTGG	Reverse primer used for *N1* and *N2 CHT7-HA* cloning
ΔCXC-F	GGCACTGGCGGCAAGCGCG	Forward primer used for *ΔCXC CHT7-HA* cloning
ΔCXC-R	CTGCTTTCTCCCGGCCCCGCTG	Reverse primer used for *ΔCXC CHT7-HA* cloning
N-term 1xHA-F	GATTATGCAGACGCTGACCAAAAT GGA	Forward primer used for inserting 1x HA tag at the N-terminus end of CHT7
N-term 1xHA-R	CGGAACGTCGTAAGGATACATGAT TTCGCCCTCCAG	Reverse primer used for inserting 1x HA tag at the N-terminus end of CHT7
Stop1-F	TAAAACAAGCTGGGGGAGACT	Forward primer used for inserting stop-codons for *HA-CHT7 STOP1* cloning
Stop1-R	TCAGACAATGGACAGAAACTC	Reverse primer used for inserting stop-codons for *HA-CHT7 STOP1* cloning
Stop2-F	TAAATCAACGAGCTGTGCCAG	Forward primer used for inserting stop-codons for *HA-CHT7 STOP2* cloning

Table 3.1 (cont'd)

Stop2-R	TCAGACGGACAGCTTCACCAT	Reverse primer used for inserting stop-codons for *HA-CHT7 STOP2* cloning
Stop3-F	TAATGCAAGAAGTCGTTCTGC	Forward primer used for inserting stop-codons for *HA-CHT7 STOP3* cloning
Stop3-R	TCAGTTGCACCCCTTGAGG	Reverse primer used for inserting stop-codons for *HA-CHT7 STOP3* cloning
Stop4-F	TAATGCAAGTGTGTGGAGTGC	Forward primer used for inserting stop-codons for *HA-CHT7 STOP4* cloning
Stop4-R	TCAGTTGTCGGAGCAGTGGAT	Reverse primer used for inserting stop-codons for *HA-CHT7 STOP4* cloning
ΔP2-F	CTGTATGTGCGGCAGGAGCG	Forward primer used for *HA-CHT7 ΔP2* cloning
ΔP2-R	GTCCGTGGCGGCTCCGTT	Reverse primer used for *HA-CHT7 ΔP2* cloning
ΔP3-F	CTGCAGTATGTGGTGCCG	Forward primer used for *HA-CHT7 ΔP3* cloning
ΔP3-R	GGACAGAAACTCCTCCAGCA	Reverse primer used for *HA-CHT7 ΔP3* cloning
ΔP4-F	TAAGTCATTCTGGCGCCCTCG	Forward primer used for *HA-CHT7 ΔP4* cloning
ΔP4-R	TCAAGGTACGCCCGAATGCAG	Reverse primer used for *HA-CHT7 ΔP4* cloning

Table 3.2. Primers used for ChIP-qPCR.
Untranslated region, UTR; upstream; US.

Primer	Gene ID	Sequence 5'—3'	Location	Published
*CYCB1*_ChIP1-F	Cre08.g370400	ACAGCTATGAGCA ACCTGGG	5' UTR	
*CYCB1*_ChIP1-R	Cre08.g370401	GTTCCCCCGAAAT TGAAGCG	5' UTR	
*CYCB1*_ChIP2-F	Cre08.g370402	TGGTGTTGGTGCC CTTCAAT	1000 bp US	
*CYCB1*_ChIP2-R	Cre08.g370403	ATATAGAGCTGGG TTGCGGG	1000 bp US	
*CYCB1*_ChIP3-F	Cre08.g370404	GCTGAGCCTGGGC AATTCTA	1000 bp US	
*CYCB1*_ChIP3-R	Cre08.g370405	GCGCTCAGCACAT TTTCGAC	1000 bp US	
*CYCB1*_ChIP4-F	Cre08.g370406	CCAATCAACGGTG AGGTCCC	2500 bp US	
*CYCB1*_ChIP4-R	Cre08.g370407	GTGGGGTCAAGAA GCCATGA	2500 bp US	
*CYCA1*_ChIP1-F	Cre03.g207900	ACCCACTTGAAAG GGCACAA	1000 bp US	
*CYCA1*_ChIP1-R	Cre03.g207901	ACTGAAGCAGGGA AGACAGC	1000 bp US	
*CYCA1*_ChIP2-F	Cre03.g207902	CGGAGGGGTTCAA GGAAAGC	1000 bp US	
*CYCA1*_ChIP2-R	Cre03.g207903	GGCAGAGCAAGGC ACTGTAA	1000 bp US	
*CYCA1*_ChIP3-F	Cre03.g207904	CACCAGACAAAAG ACAACCCC	2500 bp US	
*CYCA1*_ChIP3-R	Cre03.g207905	AGGTTCTTACCCC ATGCTCAG	2500 bp US	

Table 3.2 (cont'd)

*CYCA1*_ChIP4-F	Cre03.g207906	TGCTCGCATCCTG AATCCAA	2500 bp US
*CYCA1*_ChIP4-R	Cre03.g207907	AAATGGCCTGGCC TTCAAGT	2500 bp US
*CYCA1*_ChIP5-F	Cre03.g207908	CGAAACCTTTGGC CTCGGA	2500 bp US
*CYCA1*_ChIP5-R	Cre03.g207909	ACCAGCCCAAACT AAACCCC	2500 bp US
*CYCAB1*_ChIP1-F	Cre10.g466200	GCCGCCCCTGCAA TTTTATG	1000 bp US
*CYCAB1*_ChIP1-R	Cre10.g466201	GAATATGGGGGCA ACCGTCA	1000 bp US
*CYCAB1*_ChIP2-F	Cre10.g466202	CGTACCATGCCCA TCCTTGA	2500 bp US
*CYCAB1*_ChIP2-R	Cre10.g466203	GGCCACGGATTTC ACCAAAG	2500 bp US
*CDKB1*_ChIP1-Fr	Cre08.g372550	TCGTGCTTCCCCA ACCATAG	1000 bp US
*CDKB1*_ChIP1-R	Cre08.g372551	TCCCATGCATCAC CCTTGAC	1000 bp US
*CDKB1*_ChIP2-F	Cre08.g372552	GCTATCCCCCTTTC CTCGTG	2500 bp US
*CDKB1*_ChIP2-R	Cre08.g372553	GAACCAGGTGGGT TTCAAGC	2500 bp US
*CDKB1*_ChIP3-F	Cre08.g372554	GGCAGCAGGCAGT CGAAA	2500 bp US
*CDKB1*_ChIP3-R	Cre08.g372555	CCATGTACGGATC TGGGATCG	2500 bp US
*CDKB1*_ChIP4-F	Cre08.g372556	TCTGAGTCACAGC TCCATGC	2500 bp US

Table 3.2 (cont'd)

*CDKB1*_ChIP4-R	Cre08.g372557	TACCATTTGCAAC CGCACAC	2500 bp US
*Wee1*_ChIP1-F	Cre07.g355250	CTTGCATACATCG AAACCGCA	5'UTR and 1000 bp US
*Wee1*_ChIP1-R	Cre07.g355251	GGGTGAAATTGAC AGTGGCG	5'UTR and 1000 bp US
*Wee1*_ChIP2-F	Cre07.g355252	CTGTAGAAGGCAT CCCGTGG	2500 bp US
*Wee1*_ChIP2-R	Cre07.g355253	CGGTTTAAAAAGG TGGGGCG	2500 bp US
*Wee1*_ChIP3-F	Cre07.g355254	GCAAAGGTGGTCA GGTTGAAG	2500 bp US
*Wee1*_ChIP3-R	Cre07.g355255	CGGTATTCGTGCT TCATGTGC	2500 bp US
*Wee1*_ChIP4-F	Cre07.g355256	GAAATGTGCCGAC AGCCAC	2500 bp US
*Wee1*_ChIP4-R	Cre07.g355257	GCTCGCGCAGATT TAGACAC	2500 bp US
*Cre12CXC*_ChIP1-F	Cre12.g550250	AACAGCTTTACGA CGGCTCA	1000 bp US
*Cre12CXC*_ChIP1-R	Cre12.g550251	CTACTGTAACACA GCGGCCA	1000 bp US
*Cre12CXC*_ChIP2-F	Cre12.g550252	GGGACAAAAGTTG TGCGGTC	1000 bp US
*Cre12CXC*_ChIP2-R	Cre12.g550253	AGCCGTCGTAAAG CTGTTGA	1000 bp US
*Cre12CXC*_ChIP3-F	Cre12.g550254	TGCCTTTCCATGG GGTGGT	2500 bp US
*Cre12CXC*_ChIP3-R	Cre12.g550255	CGCTCCAACTCCT CAATCTCC	2500 bp US

Table 3.2 (cont'd)

*ORC1*_ChIP1-F	Cre10.g455600	TCAGTGTGTAGGT TGCCGAG	1000 bp US
*ORC1*_ChIP1-R	Cre10.g455601	AGGCCAGTTTGAG CAGTGAA	1000 bp US
*ORC1*_ChIP2-F	Cre10.g455602	CCATGTGTGTTGC GGACTTG	2500 bp US
*ORC1*_ChIP2-R	Cre10.g455603	CTGGATGGCGAAA ACACAGC	2500 bp US
*CDC45*_ChIP1-F	Cre06.g270250	CTGTCCTCAAAGC CCACGAA	5' UTR
*CDC45*_ChIP1-R	Cre06.g270251	CCAGTCGCTAGCA AAATGCC	5' UTR
*CDC45*_ChIP2-F	Cre06.g270252	TGTGAAGCATGGG AGTTGCC	1000 bp US
*CDC45*_ChIP2-R	Cre06.g270253	TAACTCTGGGTTG CCTGCAC	1000 bp US
*CDC45*_ChIP3-F	Cre06.g270254	TGGCACTTGCGTA CACGATA	1000 bp US
*CDC45*_ChIP3-R	Cre06.g270255	AGAGGTGGTCCAG TCCAGTT	1000 bp US
*CDC45*_ChIP4-F	Cre06.g270256	CGCCATTTTTGTTG CGGTTG	2500 bp US
*CDC45*_ChIP4-R	Cre06.g270257	ATGTCTGCACCCG ACACATC	2500 bp US
*CDC45*_ChIP5-F	Cre06.g270258	CGAGAGTGATGGG GGCAAAT	2500 bp US
*CDC45*_ChIP5-R	Cre06.g270259	AACCGCAACAAAA ATGGCGT	2500 bp US
*CDC45*_ChIP6-F	Cre06.g270260	CGGCTGATCGCAG ACAAAAG	2500 bp US

Table 3.2 (cont'd)

*CDC45*_ChIP6-R	Cre06.g270261	CCATCACTCTCGAGCATCCTT	2500 bp US	
*CDC45*_ChIP7-F	Cre06.g270262	ACGGAGCACTTGCTTATCGG	2500 bp US	
*CDC45*_ChIP7-R	Cre06.g270263	TCAACGCAGCCCTTCGAATTA	2500 bp US	
*CDC45*_ChIP8-F	Cre06.g270264	CCTGGGTCAAGGTCAGCTTC	2500 bp US	
*CDC45*_ChIP8-R	Cre06.g270265	GATAAGCAAGTGCTCCGTGC	2500 bp US	
*CDC45*_ChIP9-F	Cre06.g270266	CGTGCGCGTATCCATGTATTTT	2500 bp US	
*CDC45*_ChIP9-R	Cre06.g270267	GGCAGCATTACCAGGGATGA	2500 bp US	
*CDC45*_ChIP10-F	Cre06.g270268	CGTGTCCGTGTTCAAGGATG	2500 bp US	
*CDC45*_ChIP10-R	Cre06.g270269	CTTTGCCCAGGTGGCTATGT	2500 bp US	
*CBLP*_ChIP1-F	Cre06.g278222	AGCGCATGATGTGGATGTCA	1000 bp US	
*CBLP*_ChIP1-R	Cre06.g278223	TATACTTCGTGACCGCGTCG	1000 bp US	
*CBLP*_ChIP2-F	Cre06.g278224	GTCTCGCTCCCTTGTCCAAA	2500 bp US	
*CBLP*_ChIP2-R	Cre06.g278225	GCGTGAGTGGGTGTGGTAAA	2500 bp US	
HSP70A-F	Cre08.g372100	CGGTATAAAAGCCCGCGAC		(Strenkert et al., 2011)
HSP70A-R	Cre08.g372100	GTGCCCAGGTCAATACCGATAG		(Strenkert et al., 2011)

Table 3.2 (cont'd)

RBCS2-F	Cre02.g120150	CAATGCAAGCAGT TCGCATG	(Strenkert et al., 2011)
RBCS2-R	Cre02.g120150	ACGGAGGACTTGG CAATGAC	(Strenkert et al., 2011)
CYC6-F	Cre16.g651050	ACACGCCCCTCAT TCACAGA	(Strenkert et al., 2011)
CYC6-R	Cre16.g651050	GCACACGAGACAC TCCGAGC	(Strenkert et al., 2011)

Table 3.3. Primers used for RT-qPCR.

Description	Gene ID	RT qPCR Primer Sequence (5' --> 3')	Published
CDKB1-F	Cre08.g372550	GACAACGCTGCGTGAGATTTC	Fang et al., (2006)
CDKB1-R	Cre08.g372550	ACCAGGTAAAGGCATGGCTTG	Fang et al., (2006)
CYCA1-F	Cre03.g207900	CTGGGTGACCTGACAAACAA	
CYCA1-R	Cre03.g207900	GAATGGAAGGCTGGTGGAA	
CYCB1-F	Cre08.g370400	AGCGACTACATGACCAAGCAGACC	
CYCB1-R	Cre08.g370400	TTCAGGAAGCGGTCGATGAGGTTC	
CYCAB1-F	Cre10.g466200	AGCAGGAGACATGGAATGAC	
CYCAB1-R	Cre10.g466200	CATGGAGGCGCTGATCTC	
ORC1-F	Cre10.g455600	GCACAGGGCAAGATTACAGA	
ORC1-R	Cre10.g455600	ATTCCTGGTGCCGATTAAGG	
CDC45-F	Cre06.g270250	CTACGGGAAACCGTCCTCAC	
CDC45-R	Cre06.g270250	GATGGCACACCAGAGGTGAA	
CBLP-F	Cre06.g278222	GCCACACCGAGTGGGTGTCGTGCG	Tsai et al., (2014)
CBLP-R	Cre06.g278222	CCTTGCCGCCCGAGGCGCACAGCG	Tsai et al., (2014)

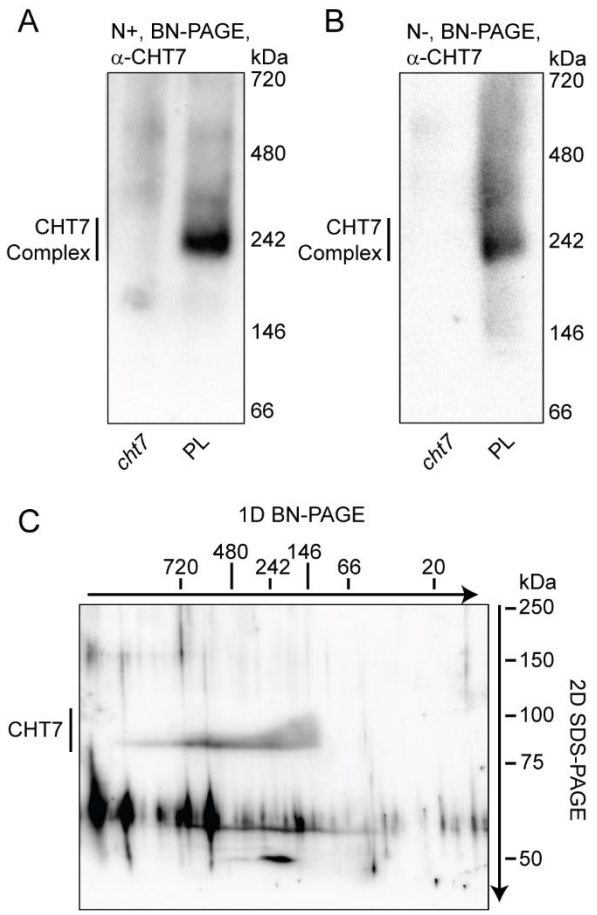

Figure 3.1. BN-PAGE assessment of CHT7 complex during N-replete growth and following N deprivation.

The molecular weight and abundance of CHT7 complex in parental line (PL) dw15 analyzed by BN-PAGE during N-replete growth (**A**) and following 48 h of N deprivation (**B**).
(**C**) The cell lysates of PL dw15 separated in the first dimension by BN-PAGE, denatured and analyzed in the second dimension by SDS-PAGE. In all cases, equal amounts of total protein (25 μg) prepared under native non-denaturing conditions were separated as described and subjected to immunoblotting. The blots were probed with CHT7-antibody.

A

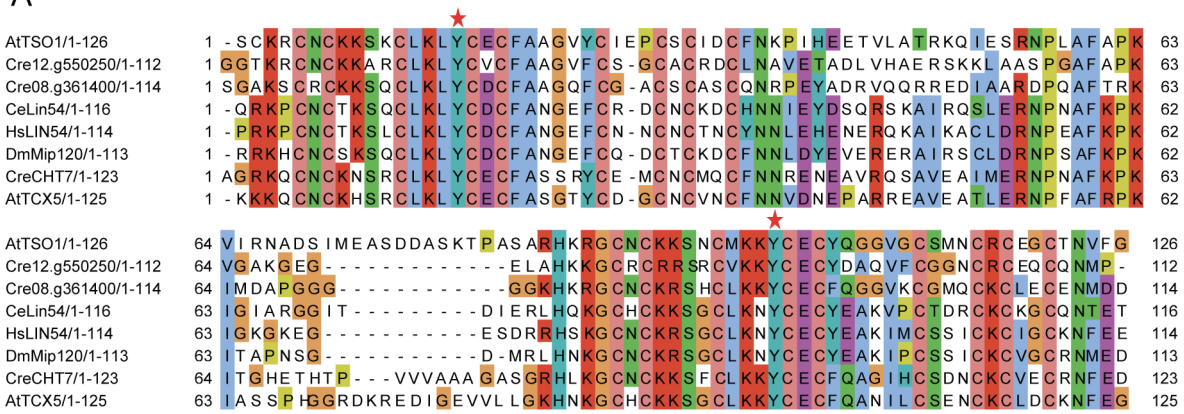

B

	1	2	3	4	5	6	7	8
1: AtTSO1	100.0	52.3	51.3	44.8	46.5	46.0	48.4	44.8
2: Cre12.g550250	52.3	100.0	50.0	47.8	46.0	46.0	42.0	45.1
3: Cre08.g361400	51.3	50.0	100.0	47.8	46.4	48.2	50.0	48.7
4: CeLin54	44.8	47.8	47.8	100.0	66.7	69.9	51.7	51.7
5: HsLIN54	46.5	46.0	46.4	66.7	100.0	71.7	56.1	56.1
6: DmMip120	46.0	46.0	48.2	69.9	71.7	100.0	55.8	54.9
7: CreCHT7	48.4	42.0	50.0	51.7	56.1	55.8	100.0	61.5
8: AtTCX5	44.8	45.1	48.7	51.7	56.1	54.9	61.5	100.0

C

	1	2	3	4	5	6	7	8
1: Cre12.g550250	100.0	24.4	30.3	29.6	29.8	26.2	31.1	28.0
2: AtTCX5	24.4	100.0	30.9	27.3	26.5	30.3	35.2	31.5
3: CreCHT7	30.3	30.9	100.0	30.8	30.2	37.3	38.2	33.9
4: Cre08.g361400	29.6	27.3	30.8	100.0	23.4	22.8	18.9	22.7
5: AtTSO1	29.8	26.5	30.2	23.4	100.0	22.5	24.5	21.8
6: DmMip120	26.2	30.3	37.3	22.8	22.5	100.0	29.5	36.1
7: HsLIN54	31.1	35.2	38.2	18.9	24.5	29.5	100.0	37.1
8: CeLin54	28.0	31.5	33.9	22.7	21.8	36.1	37.1	100.0

Figure 3.2. Alignment of CXC domain-containing proteins.
(**A**) Protein sequence alignment of CXC domains from representative species generated by Clustal O (1.2.4) (Larkin et al., 2007); *Arabidopsis thaliana*, At; *Chlamydomonas reinhardtii*, Cre; *Caenorhabditis elegans*, Ce; *Homo sapiens*, Hs; *Drosophilla melanogaster*, Dm. The conserved tyrosine (Y) residues identified in Marceau et al. (2016) that confer specificity of DNA binding to the CXC domain of LIN54 are marked with red stars. Amino acids are color coded by Clustal O default color scheme: hydrophobic, blue; positive charge, red; negative charge, magenta; polar, green; cysteines, pink; glycines, orange; prolines, yellow; aromatic, cyan and unconserved/gap, white.
(**B**) Percent identity matrix of CXC domains from representative species generated by Clustal 2.1 (Larkin et al., 2007).
(**C**) Percent identity matrix of the entire protein sequence of representative CXC domain containing proteins generated by Clustal 2.1 (Larkin et al., 2007). Gene IDs, unless mentioned in the figure, are as follows: AtTSO1, *AT3G22780*; CreCHT7, *Cre11.g481800*; CeLin54, *WBGene00003037*; HsLIN54, *HGNC25397*; DmMip120, *FBgn0033846*; and AtTCX5, *AT4G29000*.

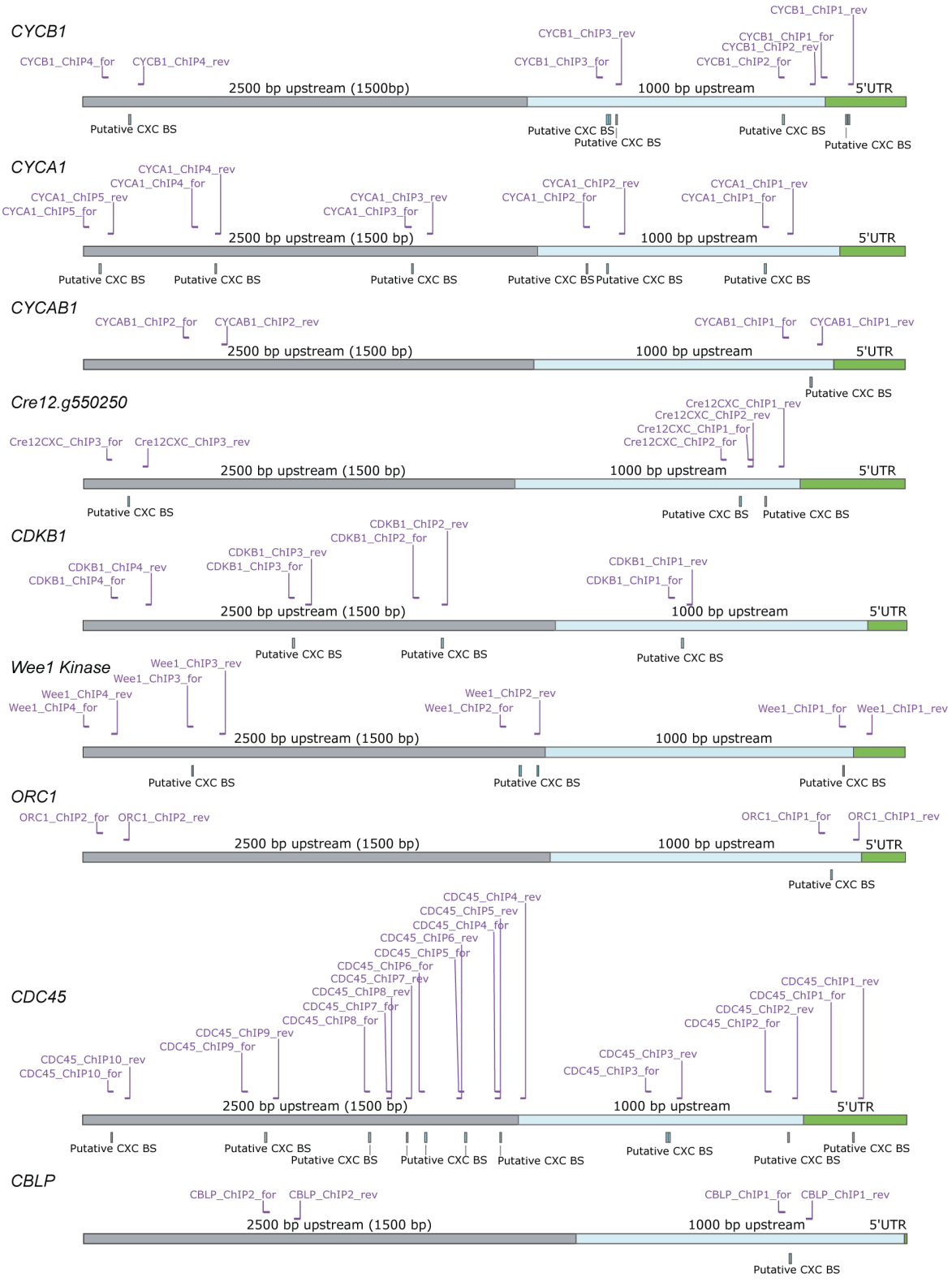

Figure 3.3. LIN54 CXC domain target sequences identified in the promoter regions of CHT7-regulated DNA metabolism and cell cycle-related genes.

Figure 3.3 (cont'd)

The presumed promoter regions of eight genes are schematically depicted: 5' UTR, green; 1000 bp 5' of the UTR, blue; and an additional 1500 bp 5' of that region, grey. Cell cycle genes homology region (CHR) elements identified for the LIN54 CXC domain located within the presumed promoter regions shown are indicated as putative CXC binding site(s) (CXC BS). The qPCR primer placements used in the ChIP-qPCR experiments are indicated above each diagram. The primer sequences can be found in Table 3.2.

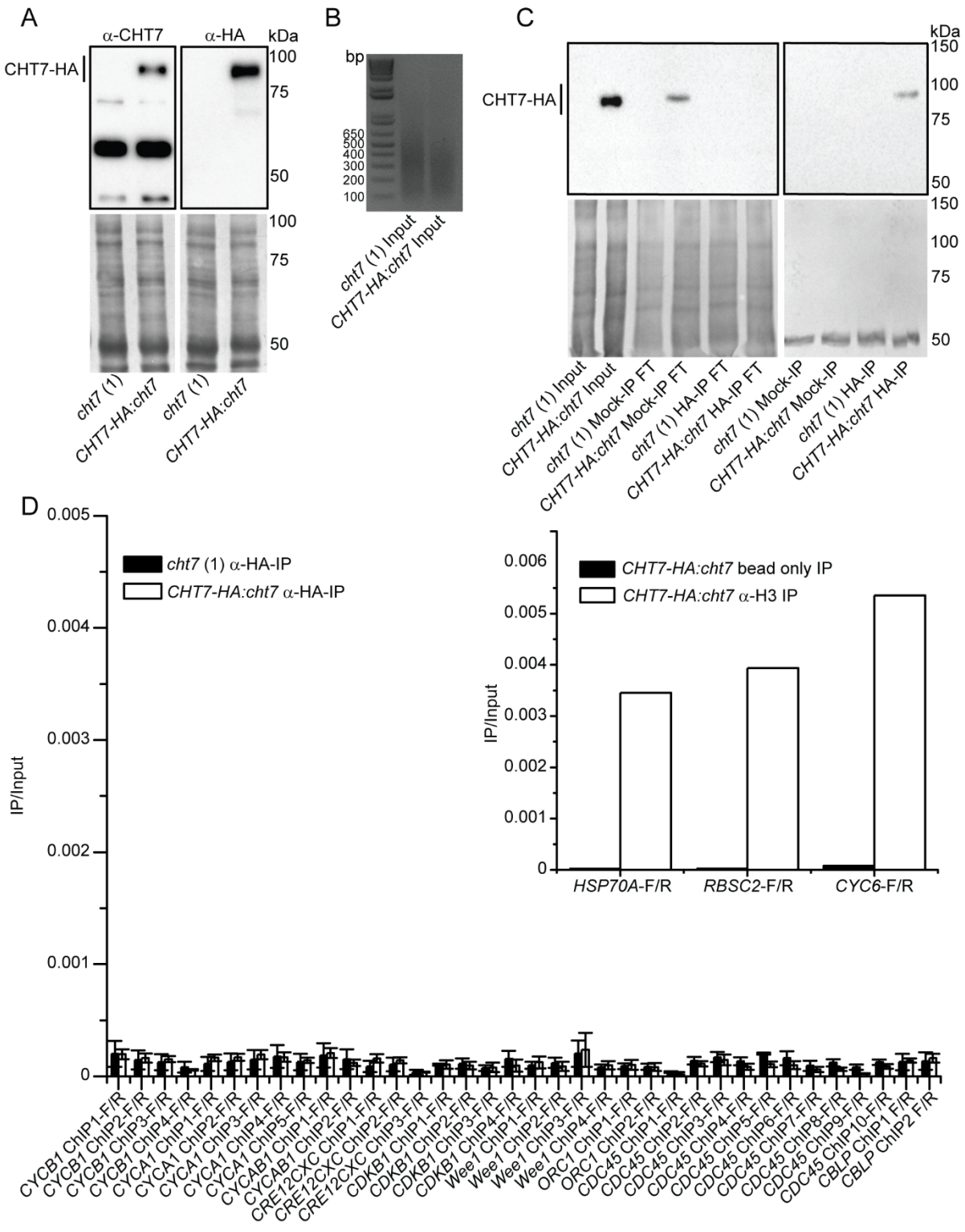

Figure 3.4. ChIP-qPCR-based probing of potential CHT7 binding sites in presumed promoters of cell cycle-related genes.

(**A**) Immunoblots of *cht7* (1) and *CHT7-HA:cht7* detected with CHT7-antibody (left) or HA-antibody (right).

Figure 3.4 (cont'd)

(**B**) Quality control DNA of sheared chromatin input used for ChIP studies. 10 μg of DNA was separated on a 1.5% agarose gel.
(**C**) Quality control immunoblots of *cht7* (1) and *CHT7-HA:cht7* α-HA and α-mock-ChIP; flow through, FT. 25 μg of total protein was loaded for input and FT; 5% volume of IP was taken out and loaded to check for the enrichment of CHT7-HA in the IP fraction.
(**D**) ChIP assays using N-deprived *cht7* (1) and *CHT7-HA:cht7* showing the enrichment of promoter fragments co-immunoprecipitated with HA-antibody relative to the input DNA. The enrichment of immunoprecipitated promoter regions was analyzed by qPCR. Values represent the averages and standard errors of three independent experiments. The inset shows the results of control ChIP-qPCR experiment, where the ChIP was performed using non-coupled beads or beads coupled with Histone 3 (H3)-antibody. The sheared *CHT7-HA:cht7* chromatin was used as inputs, and the enrichment of three respective promoter regions (*HSP70A*, *RBSC2* and *CYC6*) were tested with qPCR using published ChIP-qPCR primers from (Strenkert et al., 2011).

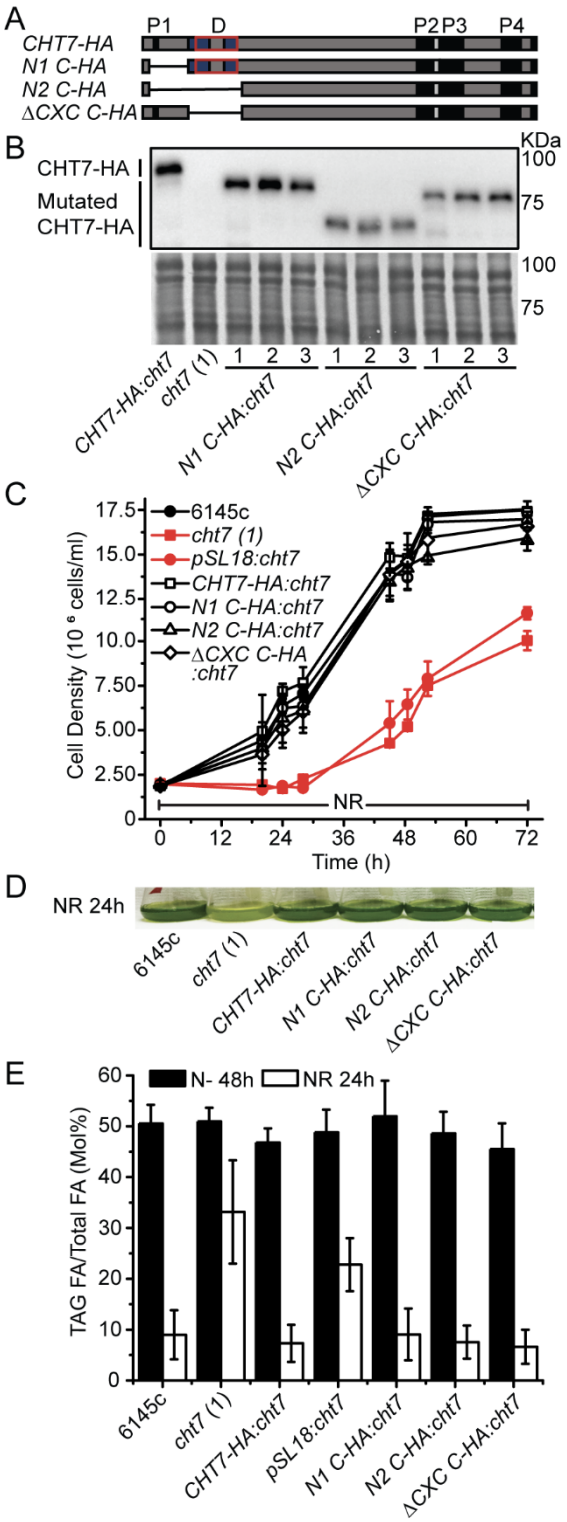

Figure 3.5. Deletion of the CHT7 CXC domain does not disrupt CHT7 function.
(**A**) Schematic representation of the full-length and deletion clones (*N1*, *N2*, *ΔCXC*) of *CHT7-HA*; predicted DNA binding site, D; predicted protein interacting regions, P1-P4; CXC domain, red box. Deletions are indicated by a thin solid line.

Figure 3.5 (cont'd)

(**B**) Immunoblot of independent *cht7* (1) transformants expressing the *CHT7-HA* deletion constructs shown in (**A**) probed with HA-antibody and later stained with Coomassie.
(**C**) Growth of wild type 6145c, *cht7* (1), empty vector control (*pSL18*), *CHT7-HA* complemented line and N-terminal and CXC domain deletion mutants in *cht7* (1) background during N refeeding following 48 h of N deprivation.
Photo (**D**) and TAG degradation of the respective lines after 24 h of N resupply following 48 h of N deprivation (**E**).
For (**C**) and (**E**), values represent the averages and the standard deviations of 3-7 biological replicates, where they refer to respective lines or independent isolates shown in (**B**) cultured in separate flasks.

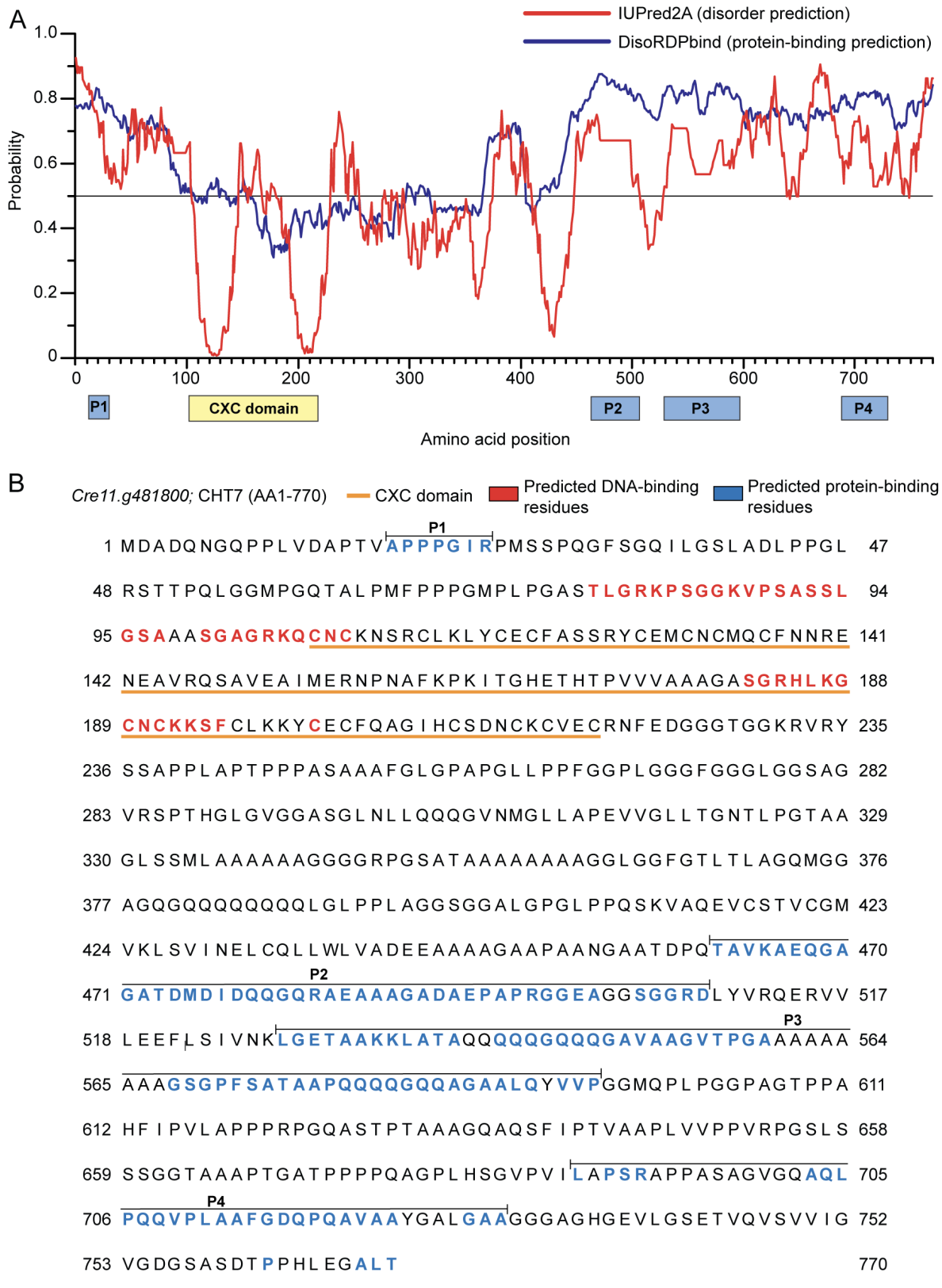

Figure 3.6. Prediction of disordered regions and DNA- and protein-binding amino acid (AA) residues within CHT7.

Figure 3.6 (cont'd)

(**A**) Probability (from 0 to 1) that the given AA residue within CHT7 (AA1-770) is part of a disordered region as predicted by IUPred2A (Mészáros et al., 2018) (red) or is involved in protein-binding as predicted by DisoRDPbind (Peng and Kurgan, 2015) (blue).
(**B**) Amino acid sequence of CHT7. AA residues that were annotated by DisoRDPbind to participate in DNA-binding (residues with probabilities greater than 0.24) or protein-binding (residues with probabilities greater than 0.80) are colored in red and blue, respectively. CXC domain is underlined in orange while the clusters of AA residues within regions termed P1-P4 are denoted by the bracket above the AA sequence.

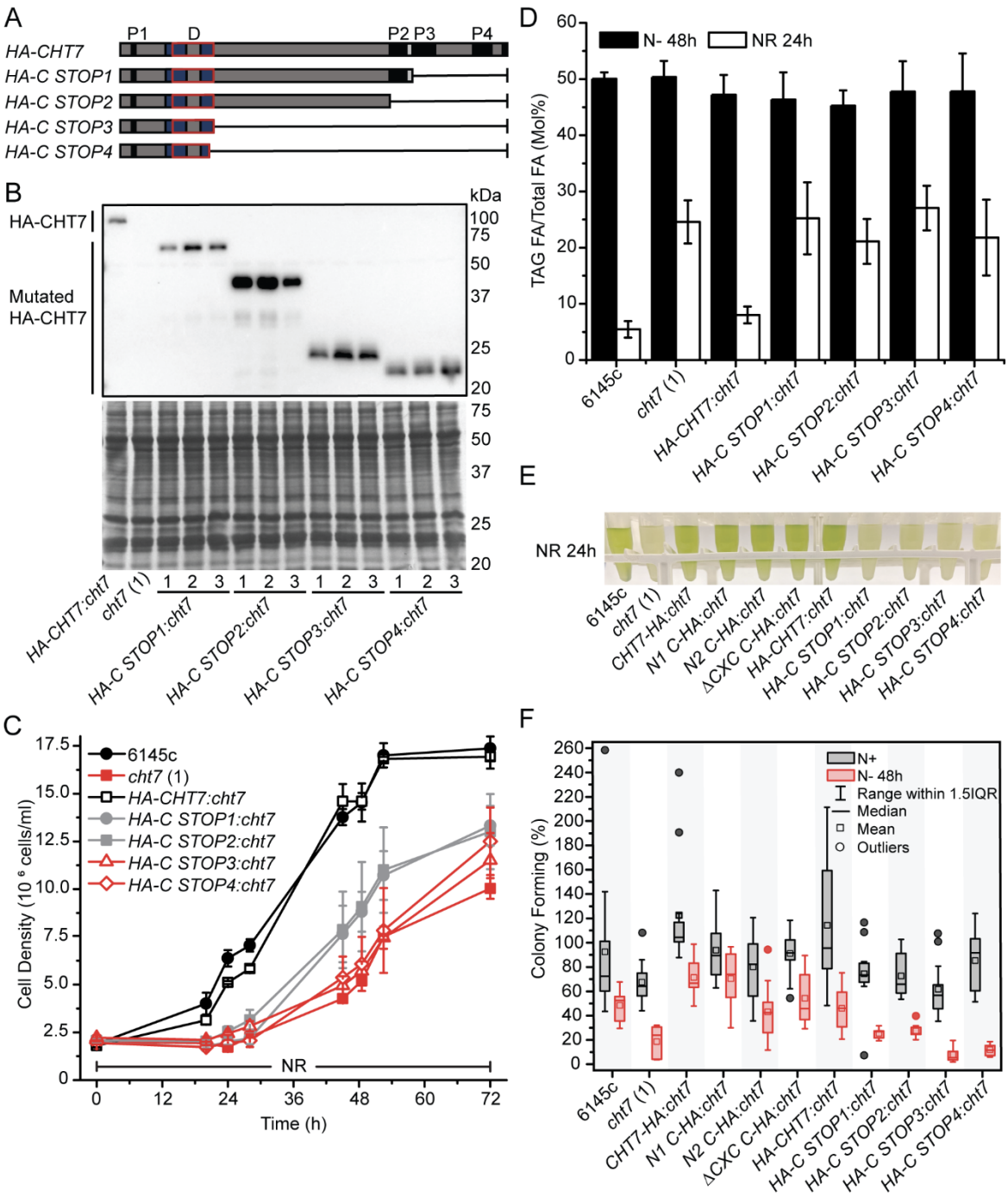

Figure 3.7. Step-wise C-terminal deletions of CHT7 result in a progressive decline of its functionality.

(**A**) Schematic representation of the full-length and stop-codon insertion mutants (*STOP1*, *2*, *3*, *4*) of *HA-CHT7*; predicted DNA binding site, D; predicted protein interacting regions, P1-P4; CXC domain, red box. Deletions are indicated by a thin solid line.

(**B**) Immunoblot of independent *cht7* (1) transformants expressing the *HA-CHT7* constructs with prematurely inserted stop-codon(s) shown in (**A**) probed with HA-antibody and later stained with Coomassie.

Figure 3.7 (cont'd)

(**C**) Growth of wild type 6145c, *cht7* (1), *HA-CHT7* complemented line and *HA-CHT7 STOP* mutant lines in the *cht7* (1) background during N refeeding following 48 h of N deprivation.
(**D**) TAG content of the respective lines after 24 h of N resupply following 48 h of N deprivation.
(**E**) Visual comparison of *CHT7-HA* N-terminal/CXC domain deletion lines (*N1*, *N2*, *ΔCXC*) and *HA-CHT7* C-terminal stop-codon insertion lines (*STOP1*, *2*, *3*, *4*) with their respective wild type, mutant and complemented controls after 24 h of N resupply following 48 h of N deprivation.
(**F**) Box plot distributions of percent colony formation assessed for *CHT7-HA* N-terminal/CXC domain deletion (*N1*, *N2*, *ΔCXC*) lines and HA-CHT7 C-terminal stop-codon insertion (*STOP1*, *2*, *3*, *4*) lines with their respective controls during N-replete growth (grey boxes) or following 48 h of N deprivation (red boxes) after 7 days of growth on N-replete TAP plates.
For (**C-D**), values represent the averages and the standard deviations of 3-7 biological replicates, where they refer to respective lines or independent isolates shown in (**B**) cultured in separate flasks.
For (**F**), box plot distributions represent percent colony formation calculated from 9-12 platings of respective lines or isolates performed across three to four independent experiments.

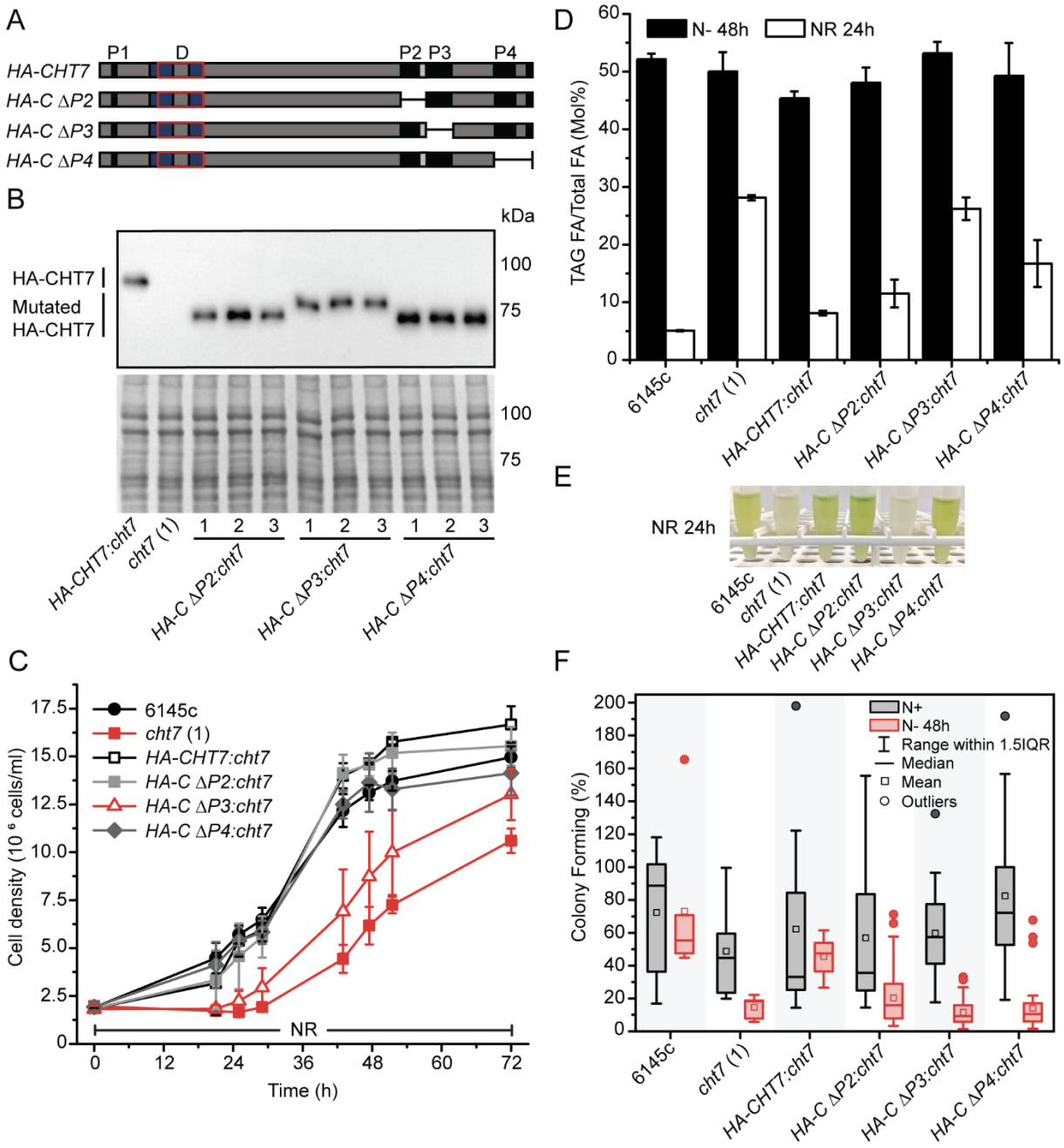

Figure 3.8. The deletion of amino acid residues within the P3 region alone leads to a near complete loss of CHT7 function.

(**A**) Schematic representation of the full-length and *ΔP2*, *P3*, and *P4* deletion mutants of *HA-CHT7*; predicted DNA binding site, D; predicted protein interacting regions, P1-P4; CXC domain, red box. Deletions are indicated by a thin solid line.

(**B**) Immunoblot of independent *cht7* (1) transformants expressing the *HA-CHT7 ΔP2*, *P3* or *P4* deletion constructs shown in (**A**) probed with HA-antibody and later stained with Coomassie.

(**C**) Growth of wild type 6145c, *cht7* (1), *HA-CHT7* complemented line and *HA-CHT7 ΔP2*, *P3* and *P4* deletion lines in *cht7* (1) background during N refeeding following 48 h of N deprivation.

(**D**) TAG content of the same lines after 24 h of N resupply following 48 h of N deprivation.

Figure 3.8 (cont'd)

(**E**) Visual comparison of wild type, *cht7* (1), *HA-CHT7* complemented line and *HA-CHT7 ΔP2*, *P3* and *P4* deletion lines after 24 h of N resupply following 48 h of N deprivation.
(**F**) Box plot distributions of percent colony formation assessed for *HA-CHT7 ΔP2*, *P3* and *P4* deletion lines and their respective controls during N-replete growth (grey boxes) or following 48 h of N deprivation (red boxes) after 7 days of growth on N-replete TAP plates.
For (**C-D**), values represent the averages and the standard deviations of 3-7 biological replicates, where they refer to respective lines or independent isolates shown in (**B**) cultured in separate flasks.
For (**F**), box plot distributions represent percent colony formation calculated from 9-45 platings of respective lines or isolates performed across three independent experiments.

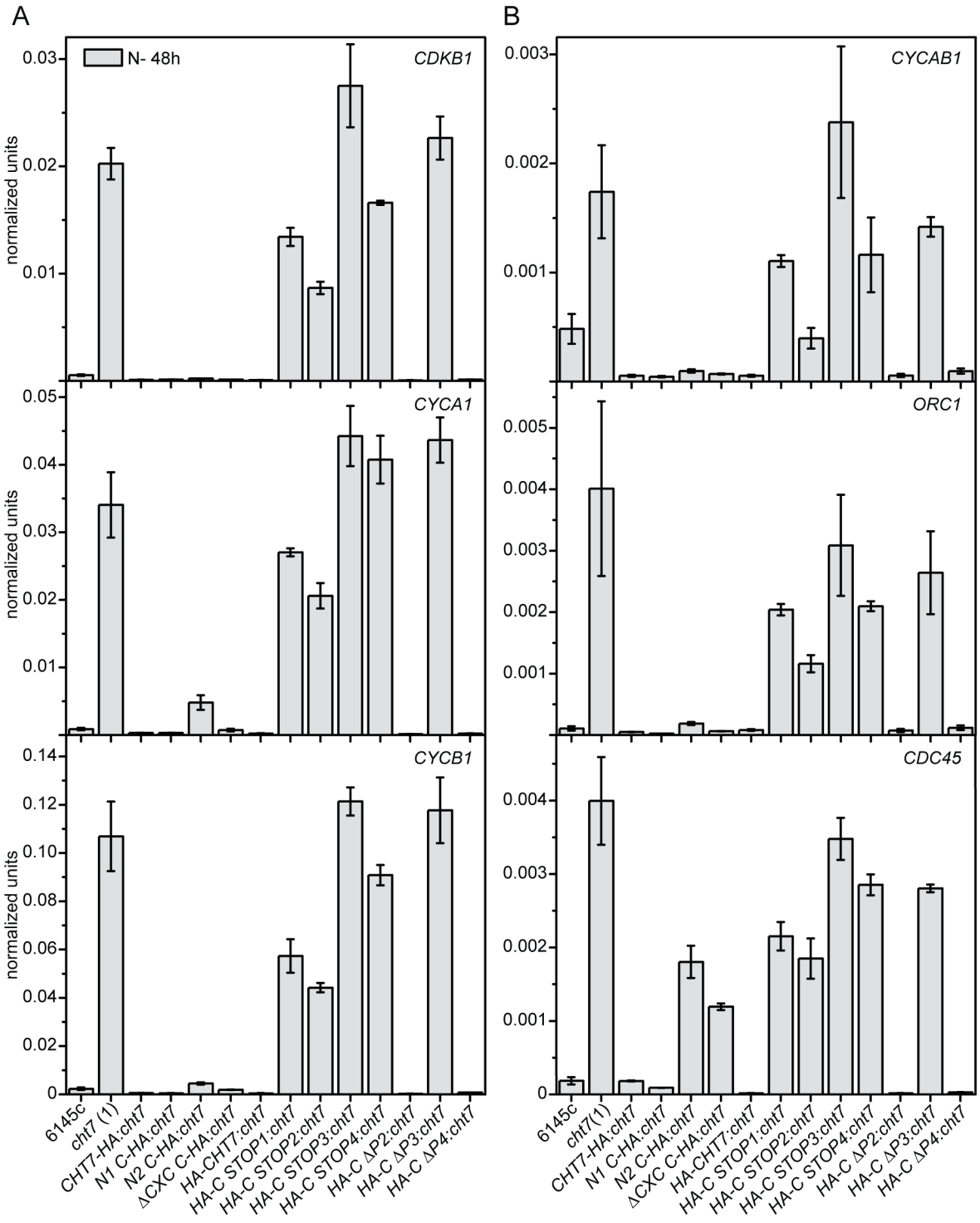

Figure 3.9. RT-qPCR analyses of representative cell cycle-marker genes in *cht7* (1) transformants producing various mutated HA-tagged versions of CHT7.
(**A**) Expression levels of *Cyclin-Dependent Kinase B1* (*CDKB1*), *Cyclin A1* (*CYCA1*) and *B1* (*CYCB1*), and (**B**) *Cyclin AB1* (*CYCAB1*), *Origin Recognition Complex 1* (*ORC1*) and *Cell Division Cycle 45* (*CDC45*) genes in wild type 6145c, *cht7* (1), *CHT7-HA* N-terminus and CXC-

Figure 3.9 (cont'd)

domain deletion lines (*N1*, *N2*, *ΔCXC*), *HA-CHT7* C-terminus truncation lines (via stop-codon insertions; *STOP1*, *2*, *3*, *4*), P2-P4 deletion lines (*ΔP2*, *P3*, *P4*), and the respective full-length complemented HA-tagged *CHT7* lines in the *cht7* (1) background following 48 h of N deprivation. Values represent the averages and the standard errors of three to five biological replicates, where they refer to representative isolates cultured in separate flasks sampled across two independent experiments. Target gene expression was normalized to the *CBLP* gene.

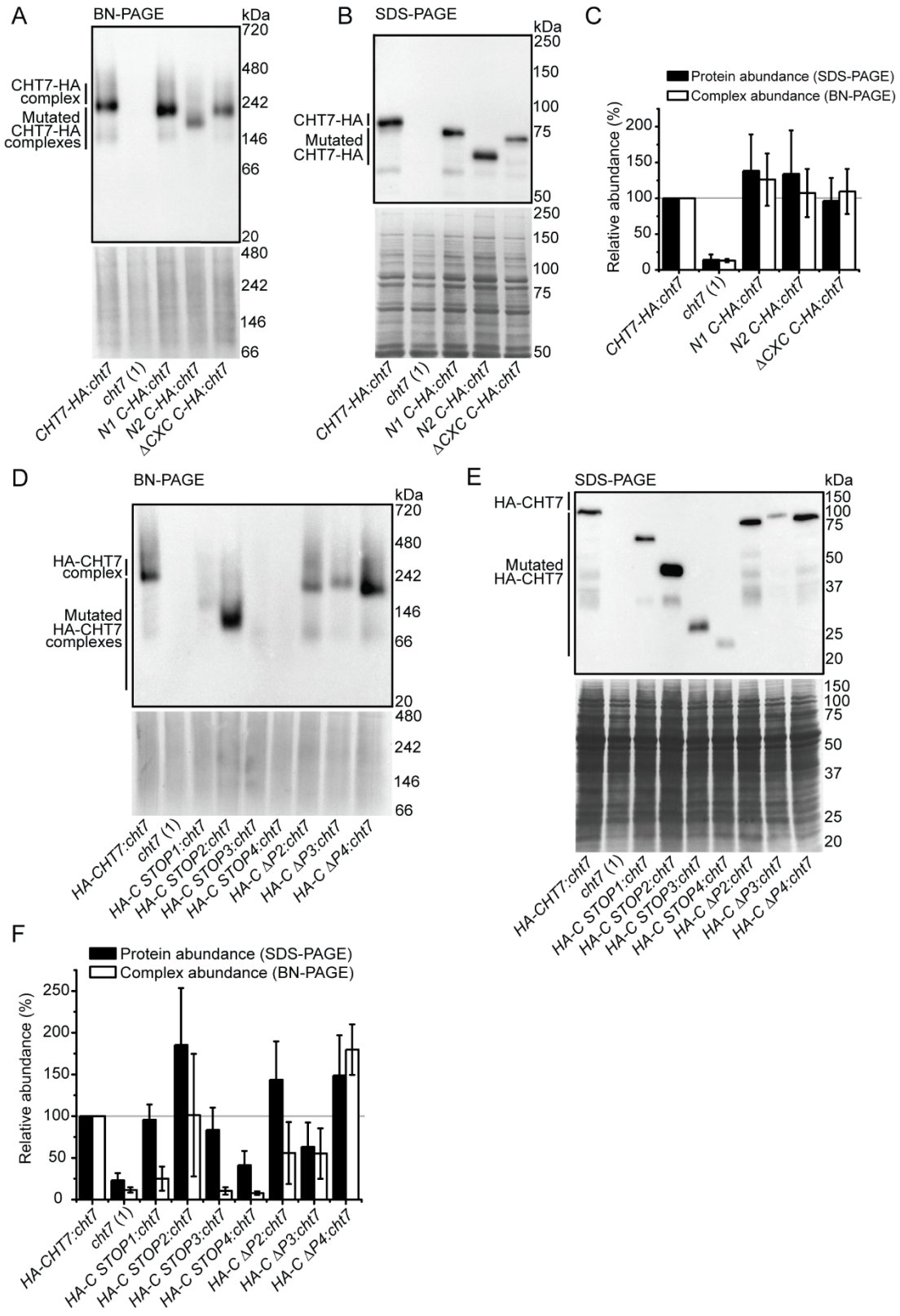

Figure 3.10. Assessment of protein complex formation and abundance in various HA-tagged mutated *CHT7:cht7* lines.

Figure 3.10 (cont'd)

Total protein extracts of N-replete *CHT7-HA:cht7*, *cht7* (1), and respective N-terminal and CXC deletion *CHT7-HA* cells prepared under native conditions were separated on blue native (BN)-PAGE (**A**) or denatured then separated on SDS-PAGE (**B**) and subjected to immunoblotting. 25 μg of total protein were loaded per lane, and blots were probed with HA-antibody.
(**C**) Quantification of CHT7 protein and complex abundance in the respective lines. Signals from the BN-PAGE and SDS-PAGE immunoblots were first normalized against loading (i.e., intensity from a lane or band from the Coomassie stained membrane) and then normalized to the respective HA-tagged *CHT7:cht7* complemented lines.
Similar BN-PAGE (**D**), SDS-PAGE (**E**) and quantification (**F**) analyses were carried out using *HA-CHT7:cht7*, *cht7* (1), *HA-CHT7* C-terminal truncation lines (*STOP1*, *2*, *3*, *4*) and *P2*, *P3*, and *P4* deletion lines.
For (**C**) and (**F**), values represent the averages and standard deviations of 3-4 independent experiments.
For (**A-B**) and (**D-E**), representative blots from one experimental set are shown.

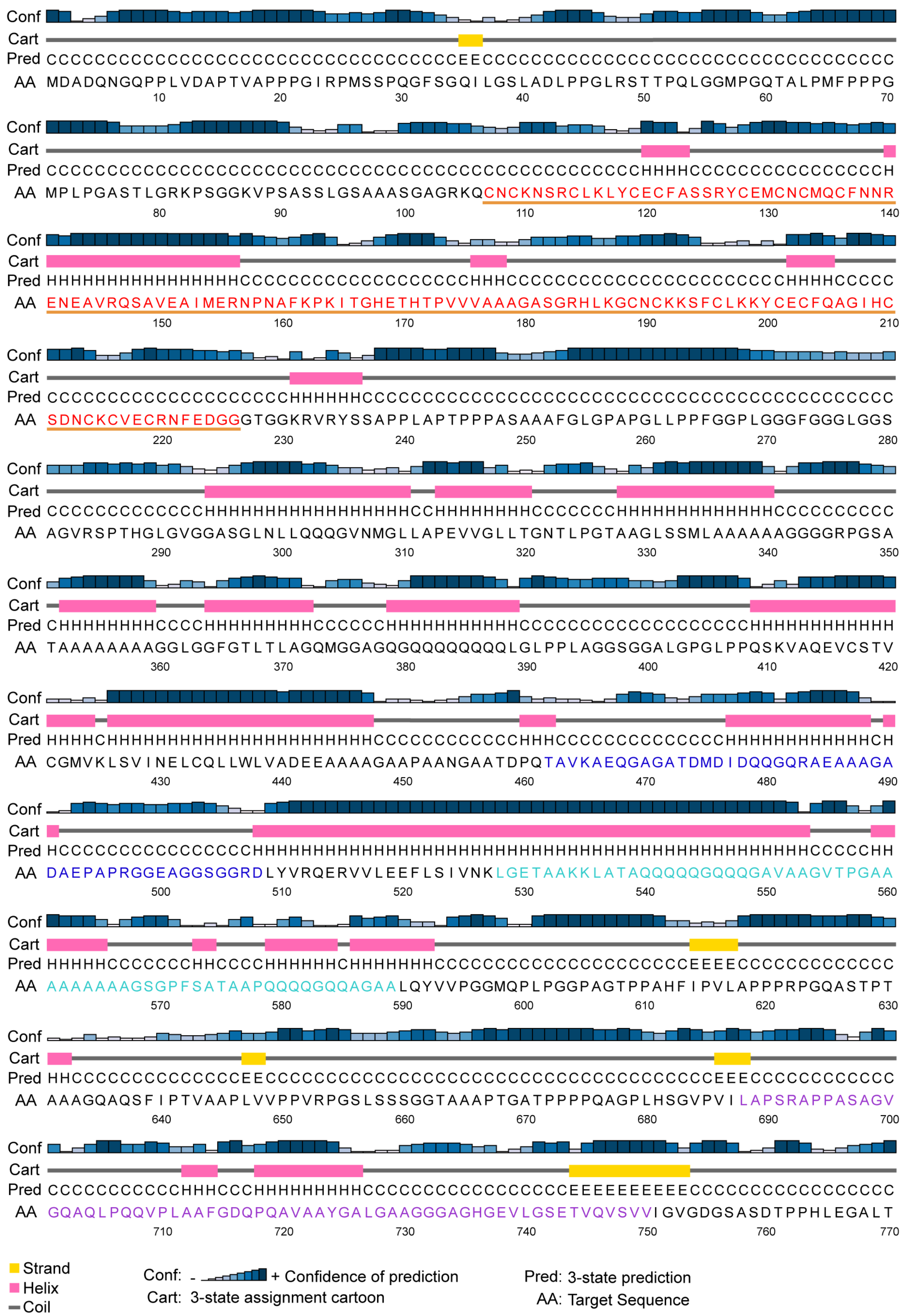

Figure 3.11. Predictions of CHT7 secondary structures by PSIPRED 4.0 (McGuffin et al., 2000; Buchan and Jones, 2019).

Figure 3.11 (cont'd)

Colored AA residues indicate deleted AAs in ΔCXC CHT7-HA (red), and HA-CHT7 ΔP2 (blue), ΔP3 (turquoise), and ΔP4 (purple) proteins. The deletion of P3 results in a disruption of helix-coil-helix like motifs located between AA498-592 of CHT7. The AA residues underlined in orange represent the presumed CXC domain of CHT7.

REFERENCES

REFERENCES

Beall, E.L., Manak, J.R., Zhou, S., Bell, M., Lipsick, J.S., and Botchan, M.R. (2002). Role for a Drosophila Myb-containing protein complex in site-specific DNA replication. Nature 420: 833-837.

Brzeska, K., Brzeski, J., Smith, J., and Chandler, V.L. (2010). Transgenic expression of CBBP, a CXC domain protein, establishes paramutation in maize. Proc Natl Acad Sci U S A 107: 5516-5521.

Buchan, D.W.A., and Jones, D.T. (2019). The PSIPRED protein analysis workbench: 20 years on. Nucleic Acids Res 47: W402-W407.

Cvitanich, C., Pallisgaard, N., Nielsen, K.A., Hansen, A.C., Larsen, K., Pihakaski-Maunsbach, K., Marcker, K.A., and Jensen, E.O. (2000). CPP1, a DNA-binding protein involved in the expression of a soybean leghemoglobin c3 gene. Proc Natl Acad Sci 97: 8163-8168.

Fauth, T., Muller-Planitz, F., Konig, C., Straub, T., and Becker, P.B. (2010). The DNA binding CXC domain of MSL2 is required for faithful targeting the Dosage Compensation Complex to the X chromosome. Nucleic Acids Res 38: 3209-3221.

Fischer, M., and DeCaprio, J.A. (2015). Does *Arabidopsis thaliana* DREAM of cell cycle control? EMBO J 34: 1987-1989.

Fischer, M., and Muller, G.A. (2017). Cell cycle transcription control: DREAM/MuvB and RB-E2F complexes. Crit Rev Biochem Mol Biol 52: 638-662.

Harris, E.H. (1989). Chlamydomonas Sourcebook. (New York: Academic Press).

Harrison, M.M., Ceol, C.J., Lu, X., and Horvitz, H.R. (2006). Some *C. elegans* class B synthetic multivulva proteins encode a conserved LIN-35 Rb-containing complex distinct from a NuRD-like complex. Proc Natl Acad Sci 103: 16782-16787.

Hauser, B.A., Villanueva, J.M., and Gasser, C.S. (1998). Arabidopsis *TSO1* regulates directional processes in cells during floral organogenesis. Genetics 150: 411-423.

Hauser, B.A., He, J.Q., Park, S.O., and Gasser, C.S. (2000). TSO1 is a novel protein that modulates cytokinesis and cell expansion in Arabidopsis. Development 127: 2219-2226.

Jiang, J., Benson, E., Bausek, N., Doggett, K., and White-Cooper, H. (2007). Tombola, a tesmin/TSO1-family protein, regulates transcriptional activation in the Drosophila male germline and physically interacts with always early. Development 134: 1549-1559.

Kobayashi, K., Suzuki, T., Iwata, E., Nakamichi, N., Chen, P., Ohtani, M., Ishida, T., Hosoya, H., Muller, S., Leviczky, T., et al. (2015). Transcriptional repression by MYB3R proteins regulates plant organ growth. EMBO J 34: 1992-2007.

Korenjak, M., Anderssen, E., Ramaswamy, S., Whetstine, J.R., and Dyson, N.J. (2012). RBF binding to both canonical E2F targets and noncanonical targets depends on functional dE2F/dDP complexes. Mol Cell Biol 32: 4375-4387.

Korenjak, M., Taylor-Harding, B., Binne, U.K., Satterlee, J.S., Stevaux, O., Aasland, R., White-Cooper, H., Dyson, N., and Brehm, A. (2004). Native E2F/RBF complexes contain Myb-interacting proteins and repress transcription of developmentally controlled E2F target genes. Cell 119: 181-193.

Larkin, M.A., Blackshields, G., Brown, N.P., Chenna, R., McGettigan, P.A., McWilliam, H., Valentin, F., Wallace, I.M., Wilm, A., Lopez, R., et al. (2007). Clustal W and Clustal X version 2.0. Bioinformatics 23: 2947-2948.

Litovchick, L., Sadasivam, S., Florens, L., Zhu, X., Swanson, S.K., Velmurugan, S., Chen, R., Washburn, M.P., Liu, X.S., and DeCaprio, J.A. (2007). Evolutionarily conserved multisubunit RBL2/p130 and E2F4 protein complex represses human cell cycle-dependent genes in quiescence. Mol Cell 26: 539-551.

Liu, Z., Running, M.P., and Meyerowitz, E.M. (1997). TSO1 functions in cell division during Arabidopsis flower development. Development 124: 665-672.

Marceau, A.H., Felthousen, J.G., Goetsch, P.D., Iness, A.N., Lee, H.W., Tripathi, S.M., Strome, S., Litovchick, L., and Rubin, S.M. (2016). Structural basis for LIN54 recognition of CHR elements in cell cycle-regulated promoters. Nat Commun 7: 12301.

McGuffin, L.J., Bryson, K., and Jones, D.T. (2000). The PSIPRED protein structure prediction server. Bioinformatics 16: 404-405.

Merchant, S.S., Prochnik, S.E., Vallon, O., Harris, E.H., Karpowicz, S.J., Witman, G.B., Terry, A., Salamov, A., Fritz-Laylin, L.K., Maréchal-Drouard, L., et al. (2007). The Chlamydomonas genome reveals the evolution of key animal and plant functions. Science 318: 245-250.

Mészáros, B., Erdős, G., and Dosztányi, Z. (2018). IUPred2A: context-dependent prediction of protein disorder as a function of redox state and protein binding. Nucleic Acids Res 46: W329-W337.

Muller, G.A., Wintsche, A., Stangner, K., Prohaska, S.J., Stadler, P.F., and Engeland, K. (2014). The CHR site: definition and genome-wide identification of a cell cycle transcriptional element. Nucleic Acids Res 42: 10331-10350.

Muller, G.A., Quaas, M., Schumann, M., Krause, E., Padi, M., Fischer, M., Litovchick, L., DeCaprio, J.A., and Engeland, K. (2012). The CHR promoter element controls cell cycle-dependent gene transcription and binds the DREAM and MMB complexes. Nucleic Acids Res 40: 1561-1578.

Nelson, C.A. (1971). The binding of detergents to proteins. I. The maximum amount of dodecyl sulfate bound to proteins and the resistance to binding of several proteins. J Biol Chem 246: 3895-3901.

Peng, Z., and Kurgan, L. (2015). High-throughput prediction of RNA, DNA and protein binding regions mediated by intrinsic disorder. Nucleic Acids Res 43: e121.

Sadasivam, S., and DeCaprio, J.A. (2013). The DREAM complex: master coordinator of cell cycle-dependent gene expression. Nat Rev Cancer 13: 585-595.

Schmit, F., Cremer, S., and Gaubatz, S. (2009). LIN54 is an essential core subunit of the DREAM/LINC complex that binds to the cdc2 promoter in a sequence-specific manner. FEBS J 276: 5703-5716.

Schmit, F., Korenjak, M., Mannefeld, M., Schmitt, K., Franke, C., von Eyss, B., Gagrica, S., Hanel, F., Brehm, A., and Gaubatz, S. (2007). LINC, a human complex that is related to pRB-containing complexes in invertebrates regulates the expression of G2/M genes. Cell Cycle 6: 1903-1913.

Shimogawara, K., Fujiwara, S., Grossman, A.R., and Usuda, H. (1998). High-efficiency transformation of *Chlamydomonas reinhardtii* by electroporation. Genetics 148: 1821-1828.

Sijacic, P., Wang, W., and Liu, Z. (2011). Recessive antimorphic alleles overcome functionally redundant loci to reveal TSO1 function in Arabidopsis flowers and meristems. PLoS Genet 7: e1002352.

Simmons, A.R., Davies, K.A., Wang, W., Liu, Z., and Bergmann, D.C. (2019). SOL1 and SOL2 regulate fate transition and cell divisions in the Arabidopsis stomatal lineage. Development 146: dev171066.

Song, J.Y., Leung, T., Ehler, L.K., Wang, C., and Liu, Z. (2000). Regulation of meristem organization and cell division by TSO1, an Arabidopsis gene with cysteine-rich repeats. Development 127: 2207-2217.

Strenkert, D., Schmollinger, S., and Schroda, M. (2011). Protocol: methodology for chromatin immunoprecipitation (ChIP) in *Chlamydomonas reinhardtii*. Plant Methods 7: 1746-4811.

Tabuchi, T.M., Deplancke, B., Osato, N., Zhu, L.J., Barrasa, M.I., Harrison, M.M., Horvitz, H.R., Walhout, A.J., and Hagstrom, K.A. (2011). Chromosome-biased binding and gene regulation by the *Caenorhabditis elegans* DRM complex. PLoS Genet 7: e1002074.

Tsai, C.H., Warakanont, J., Takeuchi, T., Sears, B.B., Moellering, E.R., and Benning, C. (2014). The protein Compromised Hydrolysis of Triacylglycerols 7 (CHT7) acts as a repressor of cellular quiescence in Chlamydomonas. Proc Natl Acad Sci U S A 111: 15833-15838.

Wang, W., Sijacic, P., Xu, P., Lian, H., and Liu, Z. (2018). Arabidopsis TSO1 and MYB3R1 form a regulatory module to coordinate cell proliferation with differentiation in shoot and root. Proc Natl Acad Sci U S A 115: E3045-E3054.

Wittig, I., Braun, H.P., and Schagger, H. (2006). Blue native PAGE. Nat Protoc 1: 418-428.

Zheng, S., Wang, J., Feng, Y., Wang, J., and Ye, K. (2012). Solution structure of MSL2 CXC domain reveals an unusual Zn3Cys9 cluster and similarity to pre-SET domains of histone lysine methyltransferases. PLOS ONE 7: e45437.

Zheng, S., Villa, R., Wang, J., Feng, Y., Wang, J., Becker, P.B., and Ye, K. (2014). Structural basis of X chromosome DNA recognition by the MSL2 CXC domain during Drosophila dosage compensation. Genes Dev 28: 2652-2662.

CHAPTER 4

Modulation of CHT7 complex activities during life-cycle transitions[1, 2]

[1]The introduction to this Chapter was derived from the section of the manuscript submitted to the Biotechnology for Biofuels journal as a review article. I conceptualized the manuscript and prepared the first draft of all sections and figures. Christoph Benning provided the critical review and contributed to the writing and editing of all sections.

Takeuchi T. and Benning C. (2019). Nitrogen-dependent coordination of cell cycle, quiescence and TAG accumulation in Chlamydomonas. Biotechnol Biofuels. Accepted for publication.

[2]Harvesting of samples during N-replete synchronized growth and RT-qPCR analyses of N-replete synchronized cells were performed in collaborations with a fellow graduate student in the Benning lab, Yang-Tsung Lin. I contributed to these experiments and produced the rest of data presented in this Chapter.

ABSTRACT

Chapters 2 and 3 focused on the role of the CHT7 complex in the nutrient-responsive regulation of DNA metabolism and cell cycle-related gene expression and its functional significance during N deprivation and refeeding. In Chapter 4, the impacts of the *cht7* mutation during the cell division cycle under nutrient-sufficient conditions are examined in light-dark synchronized cultures of Chlamydomonas cells. Furthermore, potential mechanisms regulating CHT7 complex activities are explored. In particular, whether the interaction between CHT7 and MAT3, an ortholog of RB protein, and the phosphorylation status of CHT7 are regulated in a cell cycle- or nutrient-dependent manner was tested. Although the findings presented here suggest the presence of a sub-complex that contains both CHT7 and MAT3, and the potential role of phosphorylation in the regulation of CHT7 structure and function, further studies are necessary to gain a deeper mechanistic insights by which the CHT7 complex conducts its transcriptional regulatory activities. A series of lines producing mutated CHT7 versions described in Chapter 3 should serve as a solid foundation upon which the future efforts investigating the CHT7 composition and its phosphorylation sites during proliferation as well as quiescence can take place.

INTRODUCTION

As a photosynthetic organism, much of the life-cycle decisions of Chlamydomonas cells are dictated by the diurnal signals present in the environment, such as the daily cycles of alternating light and dark periods. The cell cycle of photoautotrophically grown Chlamydomonas cells synchronizes under diel conditions such that cellular growth, flagella-dependent phototaxis and light-dependent reactions of photosynthesis are maximized during the day. Processes such as the replication of DNA and cell division (i.e., S/M phase), which may benefit from the absence of

potentially damaging photons and require the resorption of flagella for the basal body-mediated coordination of mitosis and cytokinesis, are timed to occur during the night (Spudich and Sager, 1980; Bisova and Zachleder, 2014; Cross and Umen, 2015; Zones et al., 2015). Thus, prior to the start of the light period, the newly hatched Chlamydomonas daughter cells are in a stage called pre-commitment, where the cells have not yet reached the critical size necessary to achieve competency for division. When these pre-commitment cells reach a critical volume during the light period, they pass a size-regulated checkpoint termed ”Commitment”, which is a point of no return similar to “Start” in yeast and “Restriction Point” in mammalian cell cycles (Spudich and Sager, 1980; Craigie and Cavalier-Smith, 1982; Donnan and John, 1983; Umen and Goodenough, 2001). After the passage of the commitment point, the Chlamydomonas cells will complete at least one round of division even when the light or nutrients are removed. Since growing Chlamydomonas cells may reach more than ten times their initial volume before the start of the S/M phase after a prolonged G1 phase, multiple rounds (n) of S/M cycles are necessary to produce 2^n daughters of equal size (Umen and Goodenough, 2001). Thus, the number of S/M cycles that each mother cell undergoes is determined by its cell size such that daughters of uniform size distributions are always achieved (Craigie and Cavalier-Smith, 1982; Donnan and John, 1983) (Figure 1.1).

In Chapter 2, the misregulation of transcriptome and its physiological consequences that occur in the absence of CHT7 following the removal of N was explored. Notably, the *cht7* mutant was clearly unable to repress genes involved in DNA metabolic and cell cycle-related processes following N deprivation. Furthermore, the C-terminal disordered region with protein interaction domains, and not the presumed CXC domain implicated in DNA-binding, was essential for the function of CHT7, as detailed in Chapter 3. In a broad range of model organisms (Korenjak et al., 2004; Lewis et al., 2004; Harrison et al., 2006; Georlette et al., 2007; Harrison et al., 2007;

Litovchick et al., 2007; Pilkinton et al., 2007; Schmit et al., 2007; Tabuchi et al., 2011; Kobayashi et al., 2015), a conserved transcriptional regulatory module, termed DREAM (DP, RB, E2F, and Myb-MuvB), whose activities are determined by the combinatorial presence of distinct components, is responsible for mediating the context-dependent transcriptional regulation of cell cycle genes. Chlamydomonas also utilizes a homolog of the mammalian RB protein, MAT3, in coordination with the E2F1 transcriptional activator and its dimerization partner, DP1, to regulate cell size and cell cycle progression (Umen and Goodenough, 2001; Fang et al., 2006; Olson et al., 2010). Unlike its metazoan counterpart, the Chlamydomonas MAT3/RB complex is stably associated with chromatin, and the progression through the cell division cycle is thought to involve differential phosphorylation of the RB protein or the participation of additional activator or repressor proteins (Olson et al., 2010). Due to the misregulation of cell size homeostasis, the *mat3-4* mutant cells are smaller in size than wild-type cells. The *mat3-4* mutant cells pass the commitment point at a smaller volume and also undergo more rounds of the S/M cycle than the wild type (Umen and Goodenough, 2001; Fang et al., 2006). A novel class of cyclin dependent kinase, CDKG1, is one of the regulators responsible for coupling the mother cell size to the number of subsequent divisions, by phosphorylating MAT3 in a cyclin D-dependent manner (Li et al., 2016b). Although a CHT7 complex of unchanging molecular weight is observed both during N-replete growth and following N-deprivation by BN-PAGE (Figure 3.1) and both CHT7 and MAT3 are observed in the nucleus (Olson et al., 2010; Tsai et al., 2014), how CHT7 function is mediated at the molecular level is still largely unknown.

In this chapter, the impact of the *cht7* mutation on the cell division cycle is assessed using N-replete synchronized *cht7* cells cultured under 12 h light: 12 h dark diel cycles. In addition, the potential mechanisms by which the transcriptional or gene regulatory activity of CHT7 is

controlled at the levels of the protein are explored, both during N-replete light-dark synchronized growth and following N deprivation. In particular, the interactions between CHT7 and MAT3 complexes and the physiological functions of CHT7 phosphorylation are investigated. Although the results here suggest the potential existence of DREAM-like complexes in Chlamydomonas and their function in the regulation of cell cycle, further studies are needed to elucidate the exact compositions of CHT7 complexes, in addition to the phosphorylation sites within CHT7 and their physiological significance during the distinct life cycle stages of this alga.

RESULTS

Synchronization of the *cht7* (1) mutant and its complemented line under N-replete alternating light-dark cycles

To test whether the absence of CHT7 affects the degree of synchrony observed in the *cht7* (1) mutant, cells from the wild-type 6145c, *cht7* (1) and C-terminally HA-tagged *CHT7-HA:cht7* (1) complemented lines were grown photoautotrophically under alternating 12 h light: 12 h dark cycles in environmental photobioreactors (ePBRs) (Lucker et al., 2014). All cultures were maintained in a steady-state logarithmic growth using a turbidostat prior to the start of the experiment, and the extent of synchrony for each line was assessed qualitatively by microscopy (Figure 4.1A) and quantitatively by measuring the cell size distribution (Figure 4.1B) at different times during the diel cycle. Beginning at the start of light period (ZT 0; Zeitgeber), cells from all three lines, including the *cht7* (1) mutant, increased visibly in volume (ZT 6); by the start of dark period (ZT 12), these cells showed clear signs of cell division, as indicated by the increased number of dividing mother cells (Figure 4.1A). By the end of the dark period (ZT 24), nearly all of the divided daughter cells were observed as hatched single cells outside of the mother cell wall (Figure 4.1A). These

observations were also supported by the measured cell size distributions, although the subpopulation of *cht7* (1) cells was observed to be larger than the wild-type or complemented cells at both ZT 0 and 6, as indicated by the wider cell size distributions of *cht7* (1) cells (Figure 4.1B). While such a subpopulation may represent a partial asynchrony of the mutant cultures or the innate differences in cell size, the vast majority of *cht7* (1) cells grew and divided synchronously just as observed for the wild-type and the complemented cells (Figure 4.1A and B). These results indicate that the loss of CHT7 does not have a major impact on the cell cycle progression during N-replete photoautotrophic diel growth.

Levels of *CHT7* transcripts and CHT7 proteins in wild type during the N-replete diel cycle

When the coexpression analysis of the *CHT7* gene was performed using the coexpression database for microalgae, ALCOdb (Aoki et al., 2016), the most enriched GO-term among the top 100 genes that are coexpressed with *CHT7* was cell cycle (GO:0007049) with a p-value of $2.357e10^{-3}$. To assess whether the transcripts of *CHT7* oscillate according to the distinct phase of the cell division cycle or the time of day, the expression levels of *CHT7* in addition to the *RB* pathway genes (*MAT3*, *E2F1* and *DP1*) were obtained from the high-resolution transcriptomic data of synchronized wild-type Chlamydomonas cells (CC-5152, cw^+, mt^-; a progeny from a cross between 21gr and 6145c) during 12 h light: 12 h dark cycle (Zones et al., 2015) (Figure 4.2A). The transcript levels of all four genes examined showed a strong diurnal regulation, and their peak expression occurred between 10 and 12 h after the start of a light period, around the time the cells are entering the S/M phase of the cell division cycle. When the protein levels of CHT7 were assessed by immunoblotting using the CHT7-antibody in two wild-type strains (21gr and 6145c) and the *CHT7-HA:cht7* complemented lines, they were also found to oscillate under the diel cycle (Figure

4.2B-D). However, the increase in CHT7 protein amounts lagged noticeably behind compare to that of its transcript, such that the abundance of CHT7 was at its lowest when its transcript levels were at its highest (Figure 4.2). Therefore, the CHT7 protein was at its peak abundance outside the window of times when wild-type Chlamydomonas cells are undergoing S/M phase and division, suggesting that CHT7 may also act to repress mitotic gene expression during N-replete diel-synchronized growth.

RT-qPCR analyses of cell cycle-marker genes in *cht7* (1) during N-replete synchronized growth

In Chapter 2, the elevated transcript levels of a group of S/M phase-specific genes were also observed in the transcriptomic datasets of the cell-wall deficient *cht7* mutant as compared to PL during N-replete mixotrophic growth, although the number of genes and degree of their derepression were less extensive when compared to their expression in N-deprived cells (Figures 2.4B, D, F and 2.5). However, since the transcriptomic studies were conducted using non-synchronized cultures with cells at different cell cycle stages, it was unclear whether the observed increase in transcripts was indeed caused by the loss of CHT7, as these genes are highly induced in cells that are undergoing division (Bisova et al., 2005; Tulin and Cross, 2015; Zones et al., 2015). Thus, the expression levels of a representative set of cell cycle genes (Figure 4.3C; cyclin-dependent kinase B1, *CDKB1* and mitotic cyclins) were analyzed in wild type 6145c, *cht7* (1) and the *CHT7-HA:cht7* complemented line synchronized in N-replete medium under 12 h light: 12 h dark cycles by RT-qPCR. The transcripts of *CHT7* (Figure 4.3A) and two representative genes involved in photosynthesis (Figure 4.3B; light-harvesting protein of photosystem I, *LHCA8* and cytochrome b6f complex subunit V, *PETO*) were also quantified in the respective lines under the

same growth conditions. Although the peak transcript levels of *CHT7*, *LHCA8*, and *PETO*, in addition to *CYCB1* were observed to be higher in the *CHT7-HA:cht7* complemented line (Figure 4.3A, B, and *CYCB1* in C), the diurnal expression patterns of the genes tested were similar across different lines, such that the RNA levels of both photosynthetic genes peaked between ZT4 and 6 (Figure 4.3B), while those of *CHT7* and the representative cell cycle genes peaked between ZT10 and 12 (Figure 4.3A and C). However, the expression levels of *CDKB1*, *CYCB1*, and *CYCAB1* tended to be slightly higher in the *cht7* (1) mutant outside of their mitotic peak compared to the wild type and the complemented line, and those of *CYCA1* were clearly and consistently more elevated in *cht7* (1) throughout the light-dark cycle. The fact that these cell cycle genes oscillate in the *cht7* (1) mutant may suggest that the transcriptional regulation of the cell division cycle during nutrient-sufficient diel growth is controlled by additional activators and repressors that constitute the self-regulating feedback loops, which enable the progression of the cell cycle. However, the elevated transcripts of some cell cycle genes are indeed present in the *cht7* (1) mutant, giving further insights into the effect of the *cht7* mutation on cell cycle transcript levels during N-replete light-dark synchronized growth.

The majority of CHT7 and RB proteins exist in different complexes

To test whether CHT7 complex components change with N availability, the size of the CHT7 complex was assessed during N-replete growth and following 48 h of N deprivation using BN-PAGE. However, the most abundant CHT7 complex observed in dw15 parental line (PL) cells during mixotrophic N-replete growth and following N deprivation by BN-PAGE did not change in size under either conditions tested (Figure 3.1) (Tsai et al., 2014). Similar results were obtained when the same experiment was performed using N-replete synchronized wild-type 21gr cells

harvested at indicated times during the 12 h light: 12 h dark cycle (Figure 4.4). Since a number of CXC domain-containing proteins are known to exist in a conserved multi-subunit protein complex with their respective orthologous RB protein (Korenjak et al., 2004; Lewis et al., 2004; Harrison et al., 2006; Litovchick et al., 2007; Pilkinton et al., 2007; Schmit et al., 2007; Tabuchi et al., 2011; Kobayashi et al., 2015), the molecular size of the Chlamydomonas HA-MAT3 complex was also assessed by BN-PAGE using total protein extracts from the *HA-MAT3:mat3-4* complemented cells during N-replete growth (Figure 4.5A) and following 48 h of N deprivation (Figure 4.5B). HA-MAT3 proteins were found to exist in a complex with a molecular weight slightly less than 480 kDa regardless of the presence of N (Figure 4.5A and B), although the abundance of HA-MAT3 appeared to be reduced following N deprivation. These results indicated that the majority of CHT7 and HA-MAT3 proteins exist in complexes of different sizes during normal growth and following N deprivation.

To test whether MAT3 is a component of the CHT7 complex, the size of CHT7 complex was determined in the *mat3-4* mutant and wild type 21gr by BN-PAGE followed by immunoblotting with the CHT7-antibody. All experiments were performed using N-replete cells during mixotrophic growth for simplicity. The CHT7 complex detected in the *mat3-4* mutant was similar in size to that of wild type, and no downward shift in their apparent molecular weight was observed in *mat3-4* (Figure 4.5C), indicating that MAT3 is not a part of the major CHT7 complex visualized by BN-PAGE. These findings were further corroborated by an antibody super-shift assay followed by BN-PAGE and immunoblotting using HA- and then the CHT7-antibody (Figure 4.5D). Total protein extract from the *HA-MAT3*:*mat3-4* line was incubated with HA-antibody to allow for the formation of an antibody bound HA-MAT3 complex, and the native proteins were separated using BN-PAGE. As expected, the antibody coupled HA-MAT3 complex showed an

increase in its apparent molecular weight when compared to the HA-MAT3 complex without the antibody coupling (Figure 4.5D, left). However, when the same blot was stripped and probed with the CHT7-antibody, the apparent size of the CHT7 complex in the HA-antibody coupled sample remained similar to that without the antibody coupling (Figure 4.5D, right), leading to a definitive conclusion that HA-MAT3 is indeed not a component of the major CHT7 complex that is detected by BN-PAGE. Whether or not these two complexes share other overlapping protein components, and if other less abundant forms of MAT3 and CHT7 complexes that are below the detection limit of BN-PAGE exist in the cell, remains to be determined.

Interaction between CHT7 and MAT3 assessed by co-immunoprecipitation (co-IP) assays during N-replete synchronized growth and following N deprivation

In previous native gel experiments, microgram amounts of non-denatured total cell lysates were separated to estimate the molecular masses of respective complexes. Therefore, less abundant or short-lived forms of CHT7 and MAT3 complexes may not be detectable by BN-PAGE, since the protocol is performed without the prior enrichment for CHT7 or MAT3 proteins and without the use of crosslinkers. Thus, to test the hypothesis that CHT7 and MAT3 interact in a cell cycle- or nutrient-dependent manner, in-vivo co-immunoprecipitation (co-IP) experiments were conducted using the *mat3-4 cht7* double mutant cells producing HA-MAT3 and CHT7-GFP proteins during N-replete light-dark synchronized photoautotrophic growth (Figure 4.6B) and following 48 h of N deprivation under mixotrophic growth (Figure 4.6C), with the *HA-MAT3:mat3-4* complemented line as a control. Microscopy images of *HA-MAT3 CHT7-GFP:mat3-4 cht7* cells at indicated times during the diel cycle, corresponding to cells in pre- (ZT 5) and post-commitment (ZT 10) phases, in addition to those undergoing S/M phase (ZT 13) are shown in Figure 4.6A, and the co-IP assays

were performed using these cells in Figure 4.6B. Prior to immunoprecipitation (IP), cells were cross-linked with DSP (dithiobis-succinimidyl propionate) and treated with ethidium bromide to eliminate DNA-dependent interaction (Lai and Herr, 1992). GFP-tagged CHT7 was pulled down with a GFP-antibody, and different fractions were subjected to immunoblotting, then probed with the CHT7-antibody to check for the efficiency of IP (Figure 4.6B, left blots) or HA-antibody to check for the coimmunoprecipitation of HA-MAT3 with CHT7-GFP (Figure 4.6B, right blots). While HA-MAT3 coimmunoprecipitated with CHT7-GFP regardless of the cell cycle stages, the signals for HA-MAT3 pulled down with CHT7-GFP were the strongest in cells undergoing S/M phase (ZT13) (Figure 4.6B). HA-MAT3 was also observed in the IP fraction when the protein inputs were prepared using N-deprived cells, and GFP-tagged CHT7 proteins were pulled down using the GFP-antibody (Figure 4.6C). Furthermore, this interaction was also detectable when the reverse co-IP experiments were performed by immunoprecipitating HA-MAT3 proteins with HA-antibody, and the blots were probed with HA- or CHT7 antibody, even though the observed bands for GFP-tagged CHT7 were harder to distinguish due to the background signals (Figure 4.7). These results suggest the presence of complex(es) that contain both MAT3 and CHT7. However, the exact compositions of these CHT7/MAT3 complexes during the cell division cycle or following N deprivation, and how they may affect the transcriptional regulatory activity of CHT7 under these conditions are yet to be elucidated.

Phosphorylation status of CHT7 during life-cycle transitions

Post-translational modifications play a key role in the regulation proteins with intrinsically disordered regions, which may need post-translational modifications for structure and function (Oldfield and Dunker, 2014). While a variety of post-translational modifications may play a role,

CHT7 was reported to be phosphorylated at S84 and S90 during N-replete mixotrophic growth in a Chlamydomonas phosphoproteomic study by Wang et al. (2014). Thus, the phosphorylation status of CHT7 was initially assessed in the *CHT7-HA:cht7* complemented line during N-replete mixotrophic growth and following 48 h of N deprivation by phos-tag SDS-PAGE followed by immunoblotting with HA-antibody. Phos-tag molecules contain divalent cations which bind specifically to phosphorylated proteins and retard their migration within the acrylamide gel (Kinoshita et al., 2006; Kinoshita and Kinoshita-Kikuta, 2011). In all cases, control samples were treated with calf intestinal phosphatase (CIP) to remove phosphorylation. Non-phosphorylated CHT7-HA as well as two phosphorylated isoforms of CHT7-HA were observed both during N-replete growth (Figure 4.8A) and following N deprivation (Figure 4.8B). To determine whether CHT7 is phosphorylated in a cell cycle stage-dependent manner, the phos-tag experiments were also carried out using the *CHT7-HA:cht7* complemented line enriched in pre- (ZT 4) or post-commitment (ZT9) cells, in addition to the S/M phase (ZT 12 and 13) during N-replete light-dark synchronized growth (Figure 4.8C and D). The immunoblots probed by HA-antibody revealed the presence of non-phosphorylated CHT7-HA as well as phosphorylated isoforms of CHT7-HA that increase in abundance as the cell cycle progresses, with its peak level during S/M phase (ZT 12 and 13). The percentages of phosphorylated CHT7-HA at indicated times were quantified from immunoblots across three independent experiments and are shown in Figure 4.8E in support of this observation.

The impact of CHT7 phospho-mimic and -silent S84 and S90 mutations on its activity

While the presence of different CHT7 phosphorylated isoforms suggests CHT7 as a potential target of a yet unspecified protein kinase-based signaling pathway, the exact phosphorylation sites and

their functional significance remain unknown. Given the knowledge of putative CHT7 phosphorylation sites (Wang et al., 2014), whether or not the sites of CHT7 phosphorylation correspond to S84 and S90, and their potential contributions to CHT7 were assessed in *cht7* (1) cells producing CHT7-HA proteins carrying the phospho-mimic (D84/D90) or -silent (A84/A90) mutations of the two serine residues (Figure 4.9A). Phos-tag gels of the phospho-silent *CHT7-HA A84/A90:cht7* line showed that the non-, mono- and di-phosphorylated isoforms of CHT7-HA persist despite the amino acid (AA) substitutions, although the observed signals for CHT7-HA A84/A90 proteins were always weaker than those observed for non-mutated CHT7-HA proteins (Figure 4.9B). No differences in abundance between the two CHT7-HA versions were observed when the denatured proteins were separated by SDS-PAGE and subjected to immunoblotting using HA-antibody (Figure 4.9C). Moreover, the growth and TAG degradation defects observed in the *cht7* mutant during N refeeding were fully complemented in *cht7* cells producing CHT7-HA with phospho-mimic (D84/D90) or -silent (A84/A90) mutations (Figure 4.9C and D, respectively). These results suggest that while these two serine residues of CHT7 may still be phosphorylated, they do not significantly contribute to the physiological function of CHT7 under the conditions tested.

DISCUSSION

Because CHT7 acts to repress a number of S/M phase-specific genes following a period of N starvation, its contributions to the regulation of the cell division cycle were assessed in the *cht7* mutant during N-replete light-dark synchronized growth under photoautotrophic conditions. The *CHT7* transcripts and CHT7 proteins both appear to show patterns of diurnal expression similar to those involved in S/M phase of the cell cycle, and some of these genes were also misregulated in

the *cht7* mutant during synchronized growth. However, representative cell cycle genes tested also showed a properly phased expression in the *cht7* (1) mutant, and no readily obvious defects in the kinetics of cell cycle progression were observed in *cht7* (1) cells during the diel cycle, indicating that the physiological impact of the loss of CHT7 is more profound when N availability is limiting.

Nevertheless, potential mechanisms governing CHT7 complex activity were explored both during synchronized growth and following N deprivation. In particular, the cell cycle- or nutrient-dependent regulation of CHT7 and MAT3 interaction and the differential phosphorylation of CHT7 were tested. Our data obtained, thus far, point to the presence of a sub-complex, in which both CHT7 and MAT3 coexist, and several phosphorylated isoforms of CHT7. In Arabidopsis DREAM-like complexes, CXC domain protein, TCX5 and its RB ortholog, RBR1, represent the two core components present in both the repressor and activator forms of DREAM-complexes (Kobayashi et al., 2015). However, the transcriptional regulatory activities of these complexes have not been attributed directly to TCX5 (Fischer and DeCaprio, 2015; Kobayashi et al., 2015; Fischer and Muller, 2017). In light of finding that the highly disordered C-terminus end of CHT7 with predicted protein-interaction domains is essential for the function of CHT7, the identification of CHT7 complex components during the cell division cycle and N deprivation-induced quiescence is now critical in gaining deeper mechanistic insights into how the CHT7 protein exert its activity. Furthermore, although the presence of different phosphorylated CHT7 isoforms (i.e., CHT7 proteins with one or two phosphate groups) were observed regardless of the cell cycle- or nutrient-context by phos-tag SDS-PAGE, the potential role of phosphorylation in regulating CHT7 activity should be further explored, as the method does not provide information regarding the sites or combinations of such phosphorylation. Indeed, the mutation of S84 and S90 does not abolish the phosphorylated CHT7 isoforms observed by phos-tag SDS-PAGE, and the N-terminus of

CHT7, including these serines and the proposed CXC domain, is inessential for its function. Whether or not phosphorylation plays a role in the regulation of the largely unstructured C-terminus of CHT7 remains to be tested. Various mutated versions of CHT7 generated herein should serve as useful tools in future mass spectrometry endeavors to determine CHT7 complex members and the sites of CHT7 phosphorylation, in addition to gaining further mechanistic insights into CHT7 function during N-replete synchronized growth and especially N deprivation-induced quiescence.

MATERIALS AND METHODS

Generation and Validation of Lines

The cell wall-less *Chlamydomonas reinhardtii* parental line, dw15 (cw15, *nit1*, mt^+) was obtained from A. Grossman, Department of Plant Biology, Carnegie Institution for Science, Stanford, CA. Generation of the original cell wall-less *cht7* mutant in the dw15 background and the *cht7* cells (cw^-, mt^+) transformed with a complementation construct, *pMN24 CHT7-GFP*, which carries the Chlamydomonas nitrate reductase *NIT1* gene as a selectable marker and the *CHT7* genomic fragment fused to a GFP tag in addition to 1 kb upstream and downstream of *CHT7*, were previously described (Tsai et al., 2014). To produce the *HA-MAT3 CHT7-GFP:mat3-4 cht7* (cw^+, mt^+) line used in this study, *CHT7-GFP:cht7* (cw^-, mt^+) was first crossed to cw^+ CC198 (*er-u-37*, *str-u-2-60*, cw^+, mt^-), and the cw^+ *cht7* progeny producing CHT7-GFP was further crossed to the *HA-MAT3:mat3-4* complemented line (cw^+, mt^+). The resulting meiotic progenies were initially screened based on their resistance to Hygromycin B (*aphv7*, linked to the *cht7* mutation) and Paromomycin (*aphv8*, linked to the *pSL18 HA-MAT3* complementation construct), in addition to their ability to grow using nitrate (*NIT1*, linked to the *pMN24 CHT7-GFP* complementation

construct). Since the *mat3-4* mutation is known to be linked to the mt^+ locus (Armbrust et al., 1995), mt^+ lines were selected by mating type PCR using the published primers (Zamora et al., 2004) (Table 4.1). Primers published in Tsai et al. (2014), *APH7*-F and *APH7*-R, in addition to *CHT7*-F and *CHT7*-R, were used for genotyping PCR to validate the presence of the *aphv7* insert, the *CHT7* gene respectively (Table 4.1). The presence of CHT7-GFP and HA-MAT3 proteins was verified by SDS-PAGE followed by immunoblotting, using 1:1000 dilution of GFP antibody (abcam, ab6673) and 1:10,000 donkey α-goat-HRP secondary antibody (Santa Cruz Biotechnolgy, sc2020), or using 1:1000 dilution of HA-HRP antibody (Sigma, catalog #: 12013819001), respectively. CC-198 and the *mat3-4* mutant (cw^+, mt^+, CC3994) were obtained from the Chlamydomonas Resource Center (http://www.chlamycollection.org). Wild type 21gr and the *HA-MAT3:mat3-4* complemented line (Olson et al., 2010) were obtained from J. Umen, Donald Danforth Plant Science Center, St. Louis, MO.

The generation of *pSL18* (-*Asc*I) *CHT7-3xHA* and *pGEM CHT7* constructs, which served as final destination vector and template for *CHT7* phospho-mimic (D84/D90) and -silent (A84/A90) site directed mutagenesis (SDM) PCRs, respectively is described in Chapter 3. SDM PCRs were carried out using *pGEM CHT7* as a template, with SDM primer pairs provided in Table 4.1. The presence of the desired mutations and the correctness of the PCR amplified sequences were confirmed by sequencing. To make *pSL18 (-Asc*I*) CHT7-3xHA D84/D90* and *A84/A90* constructs, *pGEM CHT7* constructs containing the respective mutations were digested with *Asc*I and *BsrG*I-HF and ligated into *pSL18 (-Asc*I*) CHT7-3xHA* digested with the same enzymes. Transformation of the 9th generation cw^+ *cht7* (1) mutant was performed as described in Chapter 2, using *pSL18 (-Asc*I*) CHT7-3xHA D84/D90* and *A84/A90* constructs linearized with *Nco*I and *Ahd*I, respectively. The production the CHT7-3xHA proteins (with or without the respective

mutations) in *cht7* (1) was verified by SDS-PAGE followed by immunoblotting, using 1:1000 dilution of HA-HRP antibody (Sigma, catalog #: 12013819001). Denatured total cell lysates were prepared as described in Chapter 2.

Growth Conditions

For synchronization, the cells from respective lines were inoculated into high salt (HS) medium (Sueoka, 1960) in 125 mL Erlenmeyer flasks, and the cultures were bubbled with an equal volume of mixed gas (95% air and 5% CO_2) every hour, with constant stirring using a magnetic bar at 200 rpm. The cultures were kept under a 12 h light: 12 h dark cycle and 250 µmol $m^{-2}s^{-1}$ of light (5600K; YUJILEDS® VTC Series High CRI LED 2835) at ambient room temperature (~24 ºC) until reaching the log phase growth. The ePBRs (Phenometrics, PBR102-F model) were inoculated to a final cell density of approximately $1x10^5$ cells/mL in 330-350 mL of HS media, and the cultures were grown under a 12 h light: 12 h dark cycle with 2,000 µmol $m^{-2}s^{-1}$ of light (FSL200 Full Spectrum Light, https://www.phenometricsinc.com). The reactors were kept at a constant temperature of 28 ºC with stirring at 200 rpm. The ePBR cultures were injected with air mixed with 5% CO_2 for 30 seconds every 15 min at a flow rate of 0.36 L/min. Each ePBR was normalized to approximately 3 µg/mL of total chlorophyll by measuring the chlorophyll levels at ZT 6 and setting the automated-dilution using a turbidostat. The cultures were maintained under a steady-state logarithmic growth for at least two days prior to the start of the experiment. More information on the ePBR designs and parts can be found in Lucker et al. (2014) and the manufacturer's website (https://www.phenometricsinc.com).

To obtain N-deprived cultures, cells were grown mixotrophically in Tris acetate phosphate (TAP) medium (Harris, 1989) to a mid-log phase under 100-120 mmol $m^{-2}s^{-1}$ of constant light

(4200K; SYLVANIA F24T12, CW/HO – 35W) at 22 ºC and were N-deprived as described in Chapter 2. For growth curves during N refeeding, N was resupplied from a 100 x NH_4Cl solution after 48 h of N deprivation and by assessing OD750 of cultures at indicated times.

Assessment of Total Chlorophyll Content

For normalization of each ePBR culture based on chlorophyll content, cells collected from 1 mL of culture at ZT 6 were resuspended in 1 mL of 80% acetone, centrifuged at 15,000 x g, and absorbance of the supernatant was assessed at 646 and 663 nm. Total chlorophyll per mL was calculated according to Porra (2002).

Microscopy and Cell Size Analysis

At indicated times during the 12 h light: 12 h dark cycle, cells were fixed in 0.2 % glutaraldehyde in PBS for 1 h at room temperature or overnight at 4 ºC. The fixed cells were centrifuged at 3,000 x g, washed once and resuspended in PBS. All microscopy was performed using the Leica DMi 800 inverted microscope (Leica Microsystems Inc, IL, USA) and a 63x oil immersion objective (HC PL APO 63x/1.40 Oil CS2), and the images were collected using Leica Application Software (LAS) (https://www.leica-microsystems.com). The cell size distributions were analyzed by a Beckman Coulter Counter Z2 and AccuComp Z2 software (https://www.beckman.com).

Real-Time Quantitative PCR (RT-PCR)

RT-qPCR analyses were performed as described in Chapter 2. The qPCR primers of genes tested are provided in Table 4.2.

Immunoblotting

SDS-PAGE and immunoblotting were performed as previously described in Tsai et al. (2014) using respective antibodies. The probing of CHT7 using CHT7-antibody was described in Tsai et al. (2014). The fused epitopes (HA and GFP tags) were probed by 1:1000 dilution of HA-HRP antibody (Sigma, catalog #: 12013819001), or 1:1000 dilution of GFP antibody (abcam, ab6673) followed by 1:10,000 donkey α-goat-HRP secondary antibody (Santa Cruz Biotechnolgy, sc2020).

BN-PAGE

BN-PAGE was performed as described in Chapter 3. For antibody-supershift assay followed by BN-PAGE, the native protein extracts of *HA-MAT3:mat3-4* cells were prepared, and approximately 100 μg of total protein was incubated with 10 μg of HA-antibody (BioLegend, 16B12, catalog #: 901503) for 1 h on ice. Equal protein amounts (25 μg, prior to the antibody addition) were loaded. The preparation of native lysate and the rest of BN-PAGE protocol was carried out as described in Chapter 3.

Coimmunoprecipitation (Co-IP) Assays

For the preparation of input proteins, 200-250 mL of cultures grown under respective conditions were centrifuged at 3,000 x g for 5 min at 4 ºC in the presence of 1:4000 dilution of 20% tween-20 and resuspended in 1 mL of Resuspension Buffer (PBS, 1:100 plant protease inhibitor cocktail (Sigma-Aldrich), 1:100 phosphatase inhibitor cocktail (Halt^{TM}, Thermo Scientific), and 1:100 PMSF (Sigma-Aldrich, 93482)). Cells were crosslinked by the addition of freshly prepared DSP-crosslinker (Thermo Scientific) to a final concentration of 1 mM and incubation on ice for 30 min. The crosslinking reaction was quenched by the addition of Tris-HCl, pH 7.5, to a final

concentration of approximately 100 mM and incubation on ice for 15 min. When the lysate preparation was not performed on the same day, cells were centrifuged at 3,000 x g for 5 min at 4 ºC, resuspended in 1 mL of Storage Buffer (Resuspension Buffer containing 20% v/v of glycerol), and kept at -80 ºC upon freezing in liquid N. Prior to sonication, samples were thawed on ice, and the Storage Buffer was again replaced by 1 mL of Resuspension Buffer. The sonication was performed using Misonix Inc S-3000 sonicator (Cole-Parmer) with a $1/16^{th}$ inch micro-tip probe at 4 ºC. Samples were kept on watery ice, and the sonication program (total process time of 2 min with 0.5 sec on- and off-pulses at the power output setting of 2.0) was repeated six times with inversion of tubes after the end of each cycle. To eliminate DNA-dependent interactions, the lysate was incubated with 50 µg/mL of ethidium bromide on ice for 30 min, and the supernatant was obtained by centrifuging for 30 min at 20,000 x g and 4 ºC. The protein concentration was assessed using Bradford reagent (Bio-Rad), and 3-5 mg of total protein extracts in 1 mL volume (adjusted with Resuspension Buffer) were used for immunoprecipitation after pre-clearing the lysate with 20 µL of pre-washed uncoupled Protein G Dynabeads (Thermo Scientific) for 45 min at 4 ºC with rotation. For IP, Protein G Dynabeads (Thermo Scientific) were coupled to either HA- (BioLegend, 16B12, catalog #: 901503) or GFP-antibody (abcam, catalog #: ab1791), and the IP was performed by rotating 50 µL of antibody-coupled beads and the aforementioned pre-cleared lysate at 4 ºC overnight (~14 h). The antigen-bound beads were washed five times with 1 mL of cold Washing Buffer 1 (PBS,150 mM NaCl, 0.05% tween-20 and 1:100 PMSF (Sigma-Aldrich, 93482)) and once with 1 mL of Washing Buffer 2 (PBS, 1:00 PMSF (Sigma-Aldrich, 93482)). The bound-proteins were eluted from beads in 50 µL of 2x Laemmli sample buffer (4% SDS, 20% glycerol, 125 mM Tris-HCl, pH 6.8, 0.004% bromophenol blue) with β-mercaptoethanol (5%, v/v)

and DTT (to a final concentration of 100 mM) added immediately before use and by incubating the samples for 10 min at 95 ºC prior to SDS-PAGE and immunoblotting.

Phos-tag SDS-PAGE

For sample preparation, 10-15 mL of cultures grown under respective conditions were centrifuged at 3,000 x g for 5 min at 4 ºC in the presence of 1:4000 dilution of 20% tween-20, and the cells were resuspended to a final volume of 250 µL with 1x NEB Buffer 3 (New England BioLabs, NEBuffer^{TM} 3) containing 1:100 dilutions of plant protease inhibitor cocktail (Sigma-Aldrich) and PMSF (Sigma-Aldrich, 93482). For the CIP treatment, the cells were sonicated using Misonix Inc S-3000 sonicator (Cole-Parmer) with a 1/16th inch micro-tip probe at 4 ºC. Samples were kept on watery ice and were sonicated for a total process time of 2 min, with 10 sec on- and off-pulses at the power output setting of 1.0. Calf intestinal alkaline phosphatase (CIP, New England BioLabs) was added to a final concentration of 0.8 U per µL of sample, and the tubes were incubated on ice for 15 min and at 37 ºC for 15 min. Reactions were stopped by the addition of an equal volume (250 µL) of 2x Laemmli sample buffer (4% SDS, 20% glycerol, 125 mM Tris-HCl, pH 6.8, 0.004% bromophenol blue, 10% β-mercaptoethanol, 200 mM DTT) and by incubating the samples for 5 min at 95 ºC. For non-CIP treatment samples, the cells were resuspended to a final volume of 250 µL in 1x NEB Buffer 3 mixture described above and an equal volume of 2x Laemmli sample buffer, followed by heating for 5 min at 95 ºC. The protein concentration was assessed using RC DC protein assay (Bio-Rad), and equal amounts of proteins were separated in Bis-Tris (pH 6.8, final concentration of 357 mM) acrylamide gels containing 75 µM of phos-tag (NARD Institute, LTD, AAL-107) and 150 µM of Zinc nitrate. Phos-tag SDS-PAGE was performed as described in Kinoshita and Kinoshita-Kikuta (2011) and followed by immunoblotting using 1:1000 dilution of

HA-HRP antibody (Sigma, catalog #: 12013819001). Signal quantification of the blots were performed by Bio-Rad Image Lab software (https://www.bio-rad.com).

Lipid Analysis

The quantification of TAG was performed as described in Chapter 2.

APPENDIX

Table 4.1. Primers used for site directed mutagenesis (SDM) and genotyping PCR.

Primer	Sequence 5'--3'	Published
CHT7-HA D84/D90-F	CAAGGTGCCCGACGCGTCGTCG	
CHT7-HA D84/D90-R	CCGCCGTCCGGCTTGCGG	
CHT7-HA A84/A90-F	CAAGGTGCCCGCGGCGTCGTCG	
CHT7-HA A84/A90-R	CCGCCGGCCGGCTTGCGG	
APH7-F	CTCAAGTGCTGAAGCGGTAG	(Tsai et al., 2014)
APH7-R	TGGTGGTCGACAAACTCTTG	(Tsai et al., 2014)
CHT7-F	TTCTCGGGTCAGATATTGGG	(Tsai et al., 2014)
CHT7-R	TTGAGGCAGAACGACTTCTTG	(Tsai et al., 2014)
MTP(+)-F	GCTGGCATTCCTGTATCCTTGACGC	(Zamora et al., 2004)
MTP(+)-R	GCGGCGTAACATAAAGGAGGGTCG	(Zamora et al., 2004)
MTM(-)-F	CGACGACTTGGCATCGACAGGTG	(Zamora et al., 2004)
MTM(-)-R	CTCGGCCAGAACCTTTCATAGGGTGG	(Zamora et al., 2004)

Table 4.2. Primers used for RT-qPCR.

Primer	Gene ID	Sequence 5'—3'	Published
CHT7-F	Cre11.g481800	TGCAACTGCAAGAAGTCGTT	
CHT7-R	Cre11.g481800	CGGCACTCCACACACTTG	
LHC8A-F	Cre06.g272650	GCTTCGTTGCCCAGAAGTA	
LHC8A-R	Cre06.g272650	TTACAGGAAGGGCAGGGA	
PETO-F	Cre12.g558900	TCCGGGACTCCAACAACTA	
PETO-R	Cre12.g558900	GCGGCCTTCACCTTCTT	
CDKB1-F	Cre08.g372550	GACAACGCTGCGTGAGATTTC	(Fang et al., 2006)
CDKB1-R	Cre08.g372550	ACCAGGTAAAGGCATGGCTTG	(Fang et al., 2006)
CYCA1-F	Cre03.g207900	CTGGGTGACCTGACAAACAA	
CYCA1-R	Cre03.g207900	GAATGGAAGGCTGGTGGAA	
CYCB1-F	Cre08.g370400	AGCGACTACATGACCAAGCAGACC	
CYCB1-R	Cre08.g370400	TTCAGGAAGCGGTCGATGAGGTTC	
CYCAB1-F	Cre10.g466200	AGCAGGAGACATGGAATGAC	
CYCAB1-R	Cre10.g466200	CATGGAGGCGCTGATCTC	

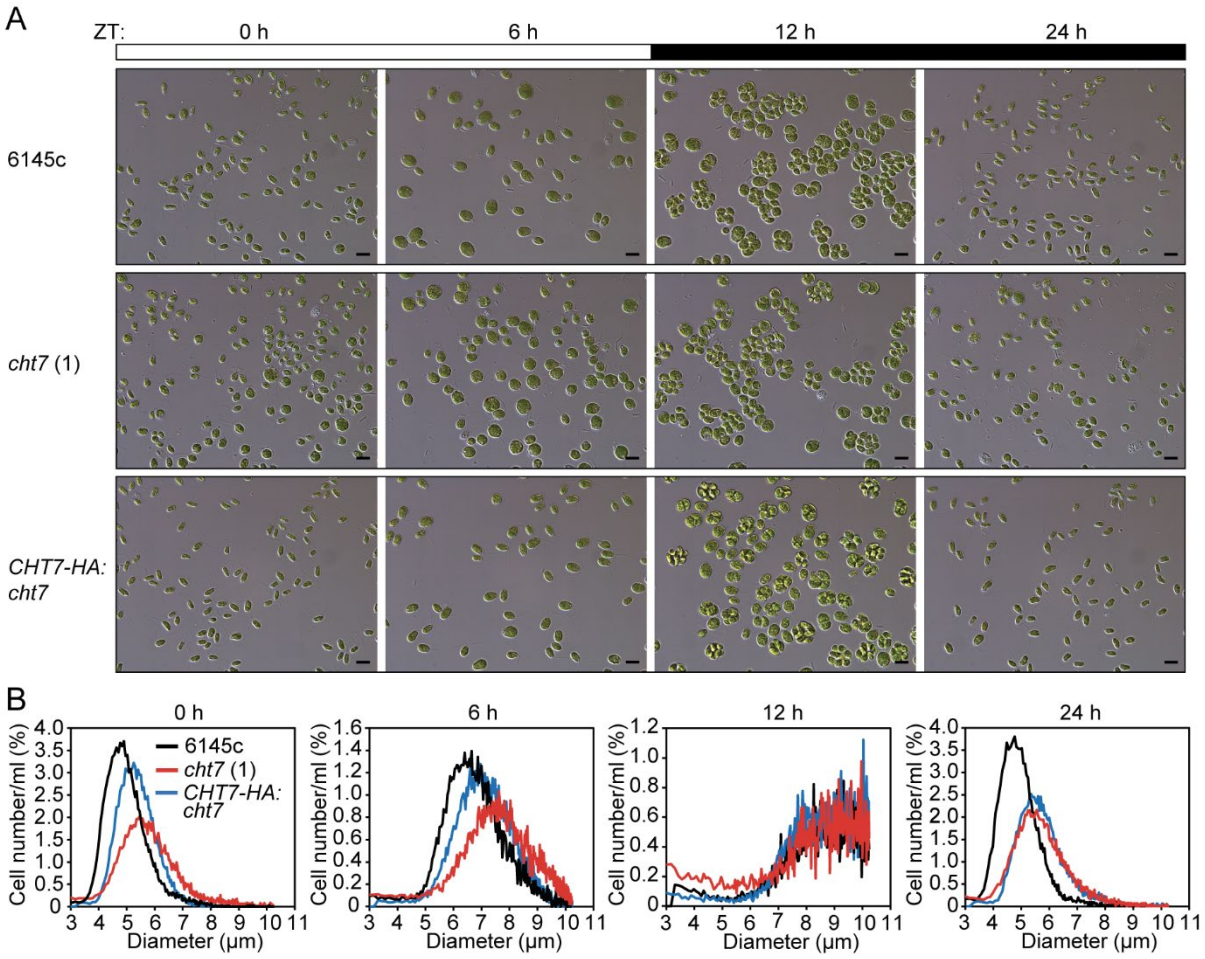

Figure 4.1. N-replete synchronized growth of the *cht7* mutant during 12 h light: 12 h dark cycle under photoautotrophic conditions.

(**A**) Microscopy images of wild-type 6145c, *cht7* (1) and *CHT7-HA:cht7* cells at 0, 6, 12, and 24 h into the diel cycle; Zeitgeber, ZT. The light and dark periods are represented by white and black boxes respectively. Scale bars represent 10 μm.

(**B**) The cell size distributions of wild-type 6145c, *cht7* (1) and *CHT7-HA:cht7* cultures at 0, 6, 12, and 24 h into the diel cycle.

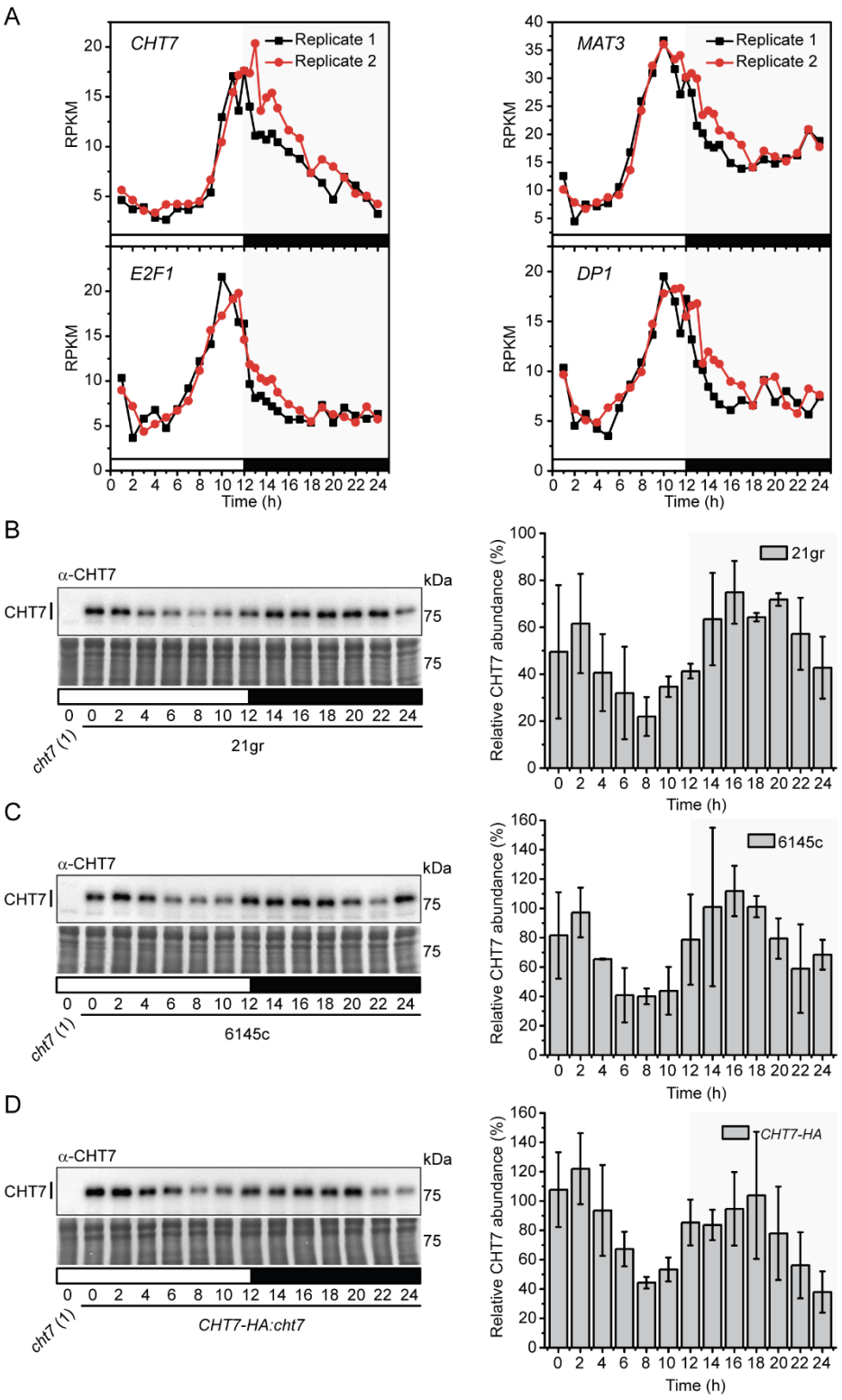

Figure 4.2. Levels of *CHT7* transcripts and CHT7 proteins during N-replete synchronized growth.

Figure 4.2 (cont'd)

(**A**) High-resolution expression profiles of *CHT7* and RB pathway genes (*MAT3*, Cre06.g255450; *E2F1,* Cre01.g052300; *DP1*, Cre07.g323000) of wild type 21gr cultured under 12 h light: 12 h dark cycles obtained from the RNA-Seq datasets generated by Zones et al. (2015); reads per kilobase of transcript per million mapped reads, RPKM.
(**B-D**) CHT7 protein levels and their quantification in wild types, 21gr (**B**) and 6145c (**C**), in addition to the *CHT7-HA:cht7* complemented line (**D**) during the diel cycle. Equal amounts of total protein (25 μg) were separated by SDS-PAGE and followed by immunoblotting. The blots were probed with CHT7-antibody and later stained with Coomassie. For the quantification, values represent the averages and the standard deviations of two to three replicates harvested at respective time points.

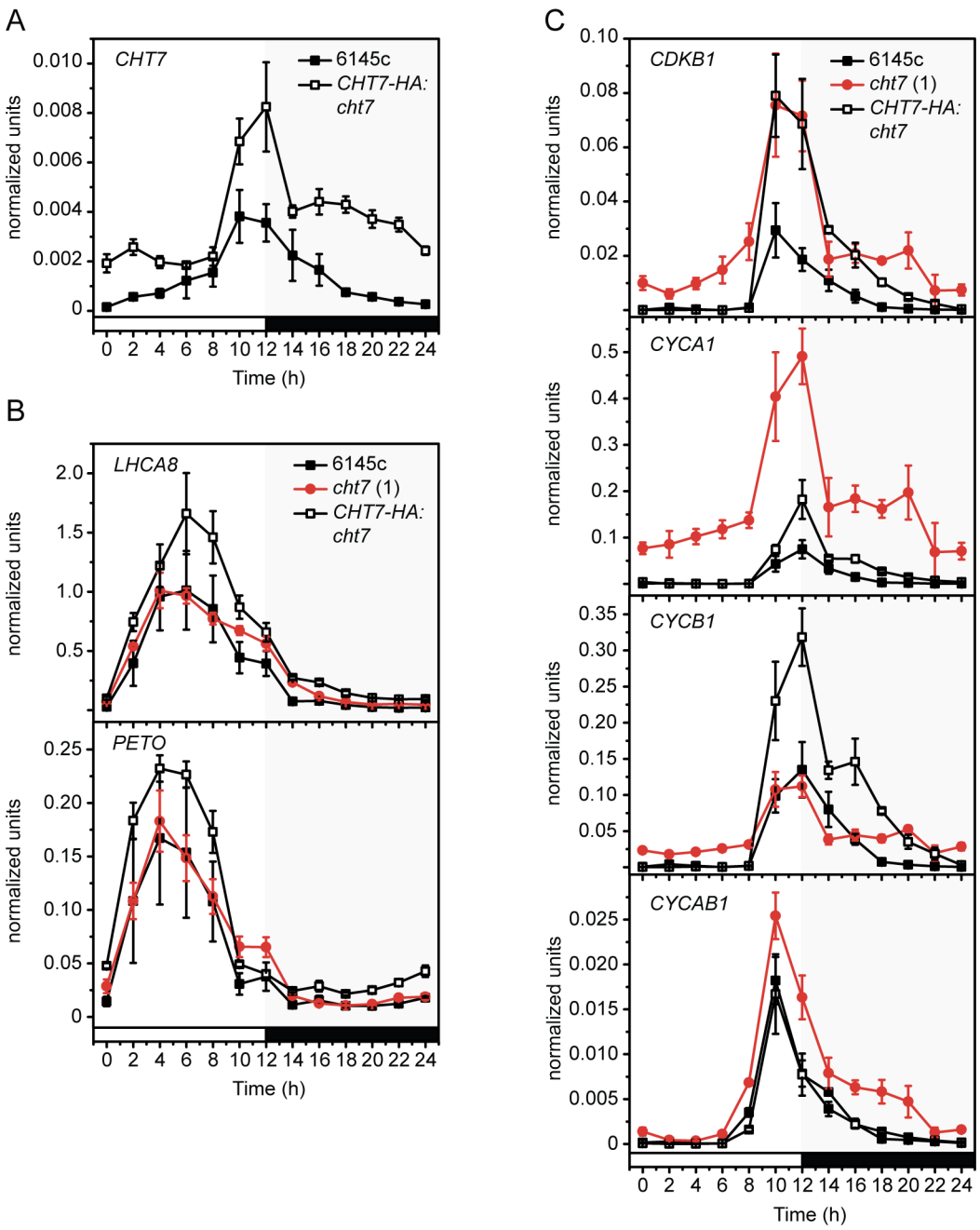

Figure 4.3. RT-qPCR analyses of representative cell cycle-marker genes in *cht7* (1) during N-replete synchronized growth.

(**A**) *CHT7* expression patterns in wild type 6145c and the *CHT7-HA:cht7* complemented line during 12 h light: 12 h dark cycle assessed by RT-qPCR.

Expression profiles of representative photosynthesis- (**B**) and cell cycle- (**C**) marker genes in wild type 6145c, *cht7* (1) and its complemented line, *CHT7-HA:cht7*, under the same conditions. Values represent the averages and the standard errors of three replicates harvested at respective time points. Target gene expression was normalized to the *CBLP* gene.

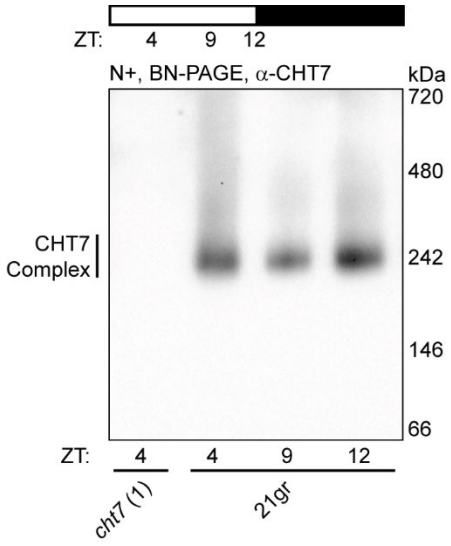

Figure 4.4. BN-PAGE assessment of CHT7 complex during N-replete synchronized growth. The molecular weight and abundance of CHT7 complex in wild type 21gr analyzed by BN-PAGE at indicated times during 12 h light: 12 h dark cycle Equal amounts of total protein (25 μg) prepared under native non-denaturing conditions were subjected to BN-PAGE and immunoblotting. The blots were probed with CHT7-antibody.

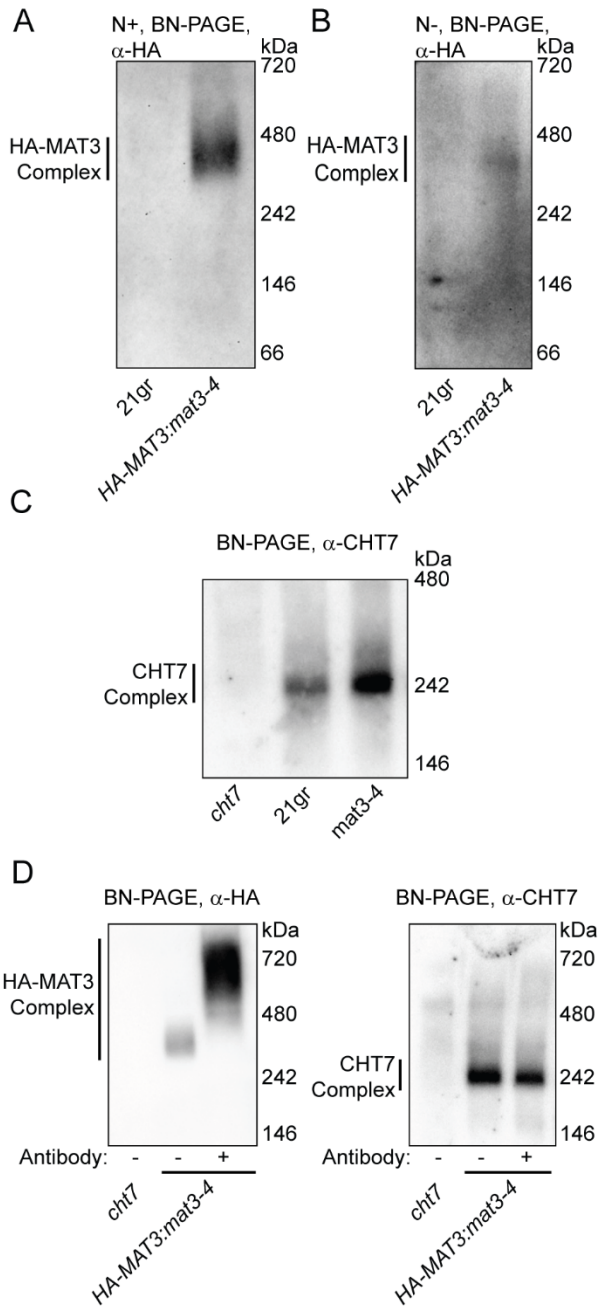

Figure 4.5. The bulk of CHT7 and MAT3 proteins as observed by BN-PAGE exist in complexes of different sizes.

HA-MAT3 complex sizes in wild type 21gr and *HA-MAT3:mat3-4* complemented line during N-replete mixotrophic growth (**A**) and following 48 h of N deprivation (**B**) as observed by BN-PAGE and subsequent immunoblotting. Immunoblots were probed with HA-antibody.

(**C**) Comparison of CHT7 complex sizes in wild type 21gr and the *mat3-4* mutant by BN-PAGE. Immunoblotting was performed using CHT7-antibody.

(**D**) Antibody supershift assay followed by BN-PAGE and immunoblotting. The native protein extract from *HA-MAT3:mat3-4* complemented line was incubated with 10 μg of HA-antibody,

Figure 4.5 (cont'd)

separated on a native gel and subjected to immunoblotting. The blots were probed by HA-antibody (left blot) or by CHT7-antibody (right). In all cases, equal amounts of total non-denatured protein (25 μg) were used for gel electrophoresis. In (**C-D**), protein extracts were prepared from cells cultured under N-replete mixotrophic conditions.

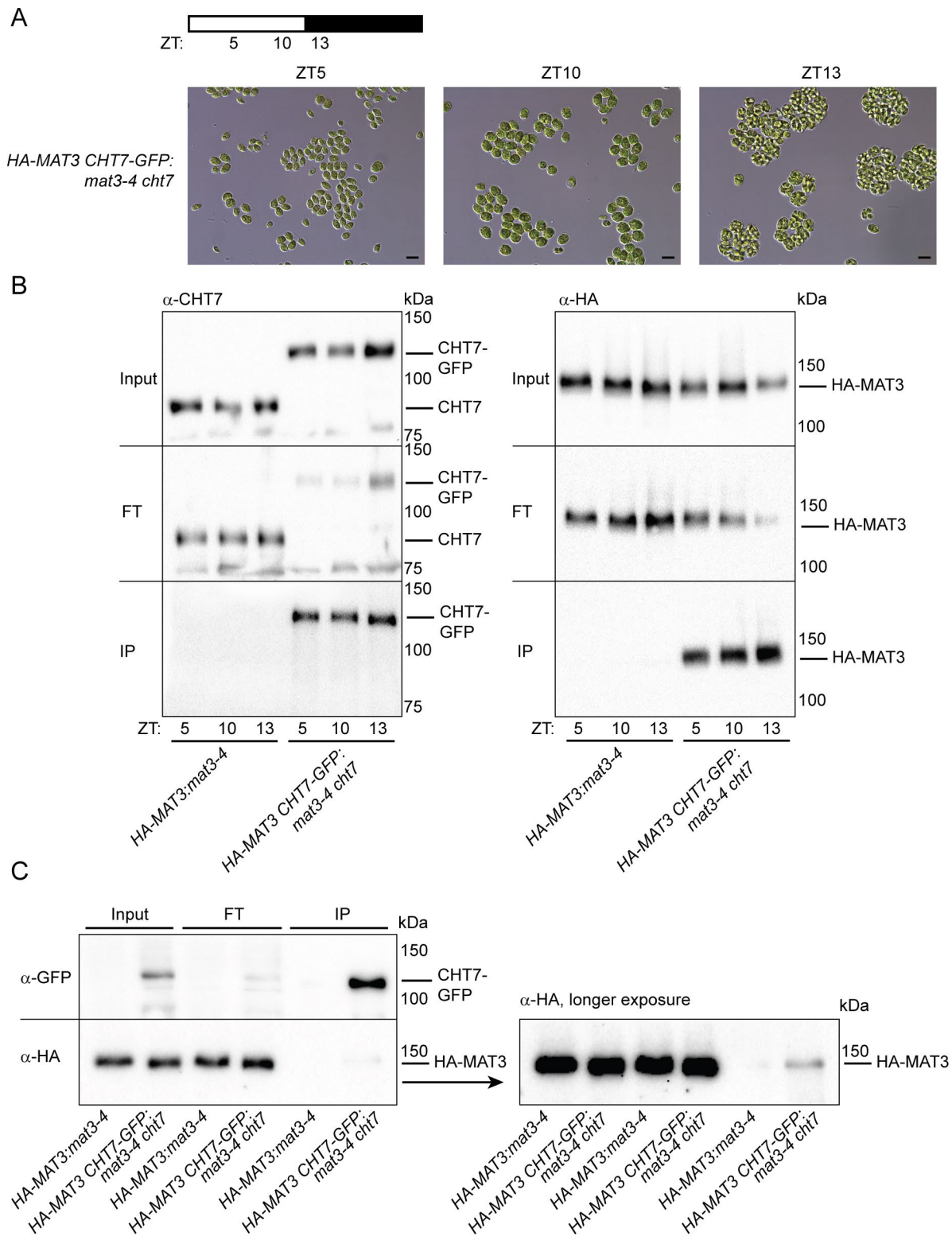

Figure 4.6. Co-immunoprecipitation (Co-IP) of HA-MAT3 with CHT7-GFP during N-replete synchronized growth and following N deprivation.

Figure 4.6 (cont'd)

(**A**) Microscopy images of the *mat3-4 cht7* double mutant cells producing HA-MAT3 and CHT7-GFP proteins during 12 h light: 12 h dark N-replete synchronized growth at indicated times; Zeitgeber, ZT. Scale bars represent 10 μm.
Co-IP of HA-MAT3 with CHT7-GFP assessed at indicated times during the N-replete diel cycle (**B**) or after 48 h of N deprivation (**C**).
For both (**B**) and (**C**), the immunoprecipitation was performed using the GFP-antibody against the GFP tag fused to CHT7. 25 μg of total protein was loaded for input and flow through (FT). 10% volume of immunoprecipitated (IP) sample was used to check for the enrichment of CHT7-GFP in the IP fraction, and the rest was used to check whether HA-MAT3 coimmunoprecipitates with CHT7-GFP.
In (**B**), the blots to the left were probed with the CHT7-antibody, while those shown to the right were probed with the HA-antibody.
In (**C**), the blots were probed with GFP-antibody or HA-antibody as indicated. A longer exposure of the immunoblot performed against the HA-epitopes of MAT3 is shown to the right to clearly show the presence of HA-MAT3 in the IP fraction.

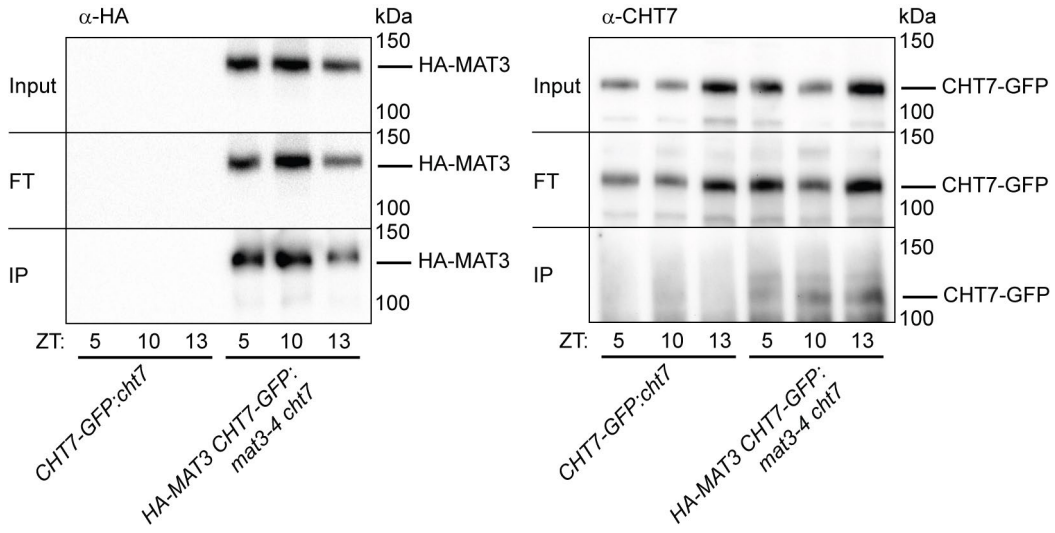

Figure 4.7. Co-IP of CHT7-GFP with HA-MAT3 during N-replete synchronized growth. Co-IP of CHT7-GFP with HA-MAT3 assessed at indicated times during 12 h light: 12 h dark N-replete synchronized growth. The immunoprecipitation was performed using the HA-antibody against the HA epitopes fused to HA-MAT3. 25 μg of total protein was loaded for input and flow through (FT). 10% volume of immunoprecipitated (IP) sample was used to check for the enrichment of HA-MAT3 in the IP fraction, and the rest was used to check for the coimmunoprecipitation of CHT7-GFP with HA-MAT3. The blots to the left were probed with HA-antibody, while those shown to the right were probed with CHT7-antibody.

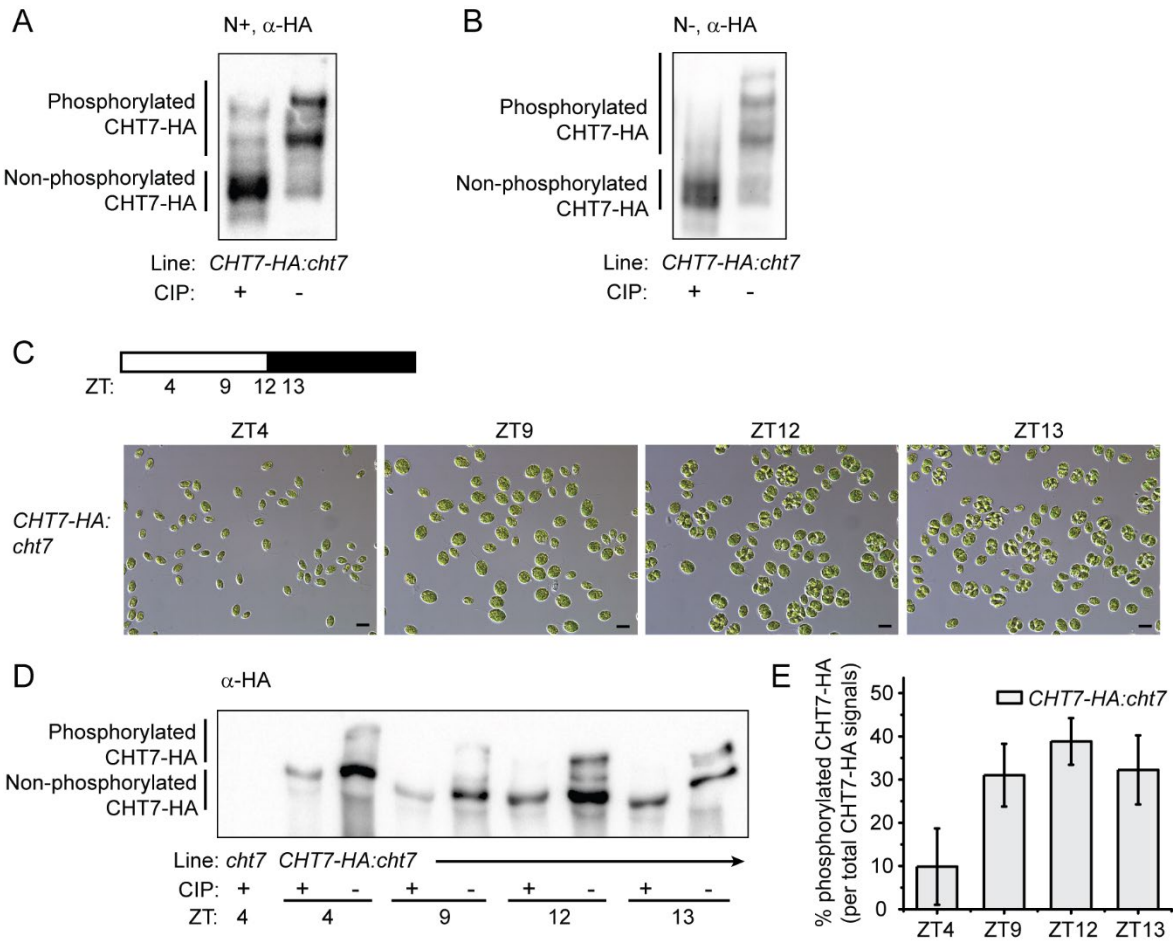

Figure 4.8. Phosphorylation status of CHT7-HA during N-replete synchronized growth and following N deprivation.

Detection of phosphorylated CHT7-HA isoforms during N-replete mixotrophic growth (**A**) or following 48 h of N deprivation (**B**) by phos-tag SDS-PAGE followed by immunoblotting with HA-antibody. One sample under each condition was treated with calf intestinal phosphatase (CIP; plus signs) to indicate the non-phosphorylated isoform of CHT7-HA.

(**C**) Microscopy images of *CHT7-HA:cht7* complemented cells during 12 h light: 12 h dark N-replete synchronized growth at indicated times; Zeitgeber, ZT. Scale bars represent 10 μm.

(**D**) Detection of phosphorylated CHT7-HA isoforms at indicated times during N-replete synchronized growth by phos-tag SDS-PAGE followed by immunoblotting with HA-antibody. CIP treated samples are indicated with plus signs as above. Equal amounts of total protein were loaded.

(**E**) Quantification of phosphorylated CHT7-HA signals (per total CHT7-HA signals detected) at indicated times during synchronized growth by phos-tag acrylamide gels followed by immunoblotting with HA-antibody. The values represent averages and standard deviations of three independent experiments.

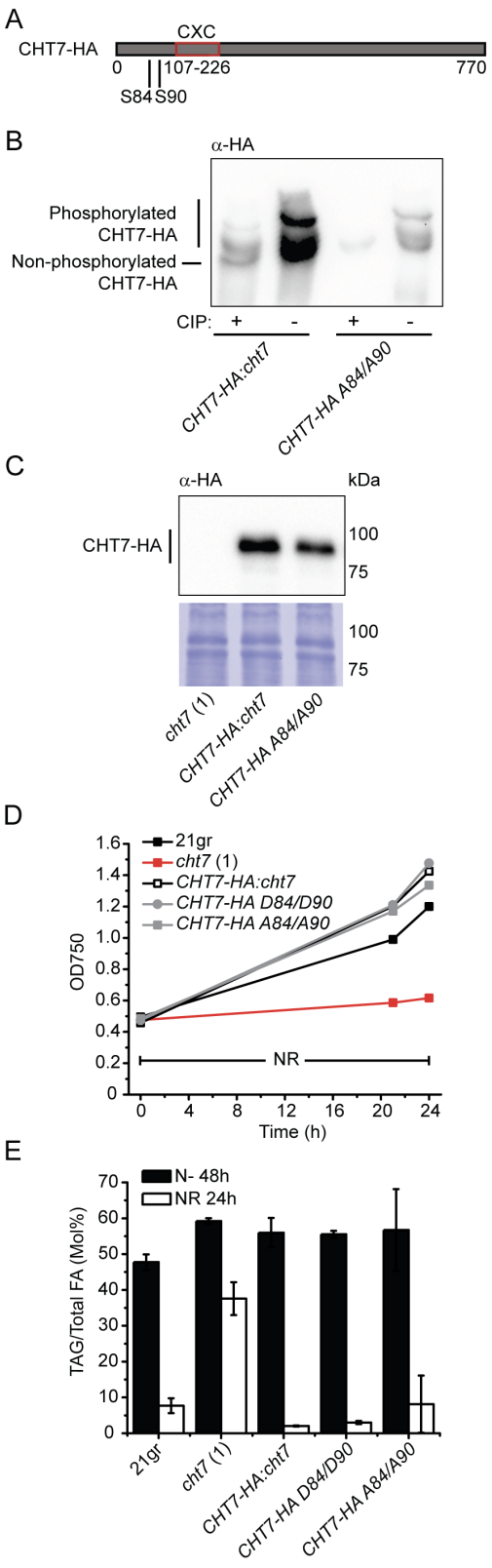

Figure 4.9. Characterization of putative CHT7-HA phosphorylation sites using phospho-mimic and -silent *CHT7-HA* mutants.

Figure 4.9 (cont'd)

(**A**) Schematic representation of the full-length CHT7-HA protein sequence showing the putative CHT7 phosphorylation sites, S84 and S90, identified in the Chlamydomonas phosphoproteomic studies by Wang et al. (2014). The CXC domain (AA107-226) is also indicated by the red box outline.
(**B**) Detection of phosphorylated CHT7-HA isoforms during N-replete mixotrophic growth in *CHT7-HA:cht7* complemented and phospho-silent *CHT7-HA A84/A90:cht7* lines by phos-tag acrylamide gels followed by immunoblotting with HA-antibody. Samples treated by calf intestinal phosphatase (CIP) are indicated by the plus signs. Equal amounts of total protein were used.
(**C**) An immunoblot of denatured *CHT7-HA:cht7* complemented and phospho-silent *CHT7-HA A84/A90:cht7* proteins probed by HA antibody. The blot was subsequently stained by Coomassie. Equal protein amounts of lines shown were loaded and separated by SDS-PAGE.
(**D**) Growth curve of wild type 21gr, *cht7* (1), in addition to the full length *CHT7-HA* and its clones with either phospho-mimic (D84/D90) or -silent (A84/A90) mutations in the background of *cht7* (1) during N refeeding after 48 h of N deprivation.
(**E**) TAG content of the same set of lines after 48 h of N deprivation and following 24 h of N resupply.

REFERENCES

REFERENCES

Aoki, Y., Okamura, Y., Ohta, H., Kinoshita, K., and Obayashi, T. (2016). ALCOdb: Gene Coexpression Database for Microalgae. Plant Cell Physiol 57: e3.

Armbrust, E., Ibrahim, A., and Goodenough, U.W. (1995). A mating type-linked mutation that disrupts the uniparental inheritance of chloroplast DNA also disrupts cell-size control in Chlamdomonas. Mol Biol Cell 6: 1807-1818.

Bisova, K., and Zachleder, V. (2014). Cell-cycle regulation in green algae dividing by multiple fission. J Exp Bot 65: 2585-2602.

Bisova, K., Krylov, D.M., and Umen, J.G. (2005). Genome-wide annotation and expression profiling of cell cycle regulatory genes in *Chlamydomonas reinhardtii*. Plant Physiol 137: 475-491.

Craigie, R.A., and Cavalier-Smith, T. (1982). Cell volume and the control of the Chlamydomonas cell cycle. J Cell Sci 54: 173-191.

Cross, F.R., and Umen, J.G. (2015). The Chlamydomonas cell cycle. Plant J 82: 370-392.

Donnan, L., and John, P.C.L. (1983). Cell cycle control by timer and sizer in Chlamydomonas. Nature 304: 630-633.

Fang, S.C., de los Reyes, C., and Umen, J.G. (2006). Cell size checkpoint control by the retinoblastoma tumor suppressor pathway. PLoS Genet 2: e167.

Fischer, M., and DeCaprio, J.A. (2015). Does *Arabidopsis thaliana* DREAM of cell cycle control? EMBO J 34: 1987-1989.

Fischer, M., and Muller, G.A. (2017). Cell cycle transcription control: DREAM/MuvB and RB-E2F complexes. Crit Rev Biochem Mol Biol 52: 638-662.

Georlette, D., Ahn, S., MacAlpine, D.M., Cheung, E., Lewis, P.W., Beall, E.L., Bell, S.P., Speed, T., Manak, J.R., and Botchan, M.R. (2007). Genomic profiling and expression studies reveal both positive and negative activities for the Drosophila Myb MuvB/dREAM complex in proliferating cells. Gene Dev 21: 2880-2896.

Harris, E.H. (1989). Chlamydomonas Sourcebook. (New York: Academic Press).

Harrison, M.M., Lu, X., and Horvitz, H.R. (2007). LIN-61, one of two *Caenorhabditis elegans* malignant-brain-tumor-repeat-containing proteins, acts with the DRM and NuRD-like protein complexes in vulval development but not in certain other biological processes. Genetics 176: 255-271.

Harrison, M.M., Ceol, C.J., Lu, X., and Horvitz, H.R. (2006). Some *C. elegans* class B synthetic multivulva proteins encode a conserved LIN-35 Rb-containing complex distinct from a NuRD-like complex. Proc Natl Acad Sci 103: 16782-16787.

Kinoshita, E., and Kinoshita-Kikuta, E. (2011). Improved Phos-tag SDS-PAGE under neutral pH conditions for advanced protein phosphorylation profiling. Proteomics 11: 319-323.

Kinoshita, E., Kinoshita-Kikuta, E., Takiyama, K., and Koike, T. (2006). Phosphate-binding tag, a new tool to visualize phosphorylated proteins. Mol Cell Proteomics 5: 749-757.

Kobayashi, K., Suzuki, T., Iwata, E., Nakamichi, N., Chen, P., Ohtani, M., Ishida, T., Hosoya, H., Muller, S., Leviczky, T., et al. (2015). Transcriptional repression by MYB3R proteins regulates plant organ growth. EMBO J 34: 1992-2007.

Korenjak, M., Taylor-Harding, B., Binne, U.K., Satterlee, J.S., Stevaux, O., Aasland, R., White-Cooper, H., Dyson, N., and Brehm, A. (2004). Native E2F/RBF complexes contain Myb-interacting proteins and repress transcription of developmentally controlled E2F target genes. Cell 119: 181-193.

Lai, J.S., and Herr, W. (1992). Ethidium bromide provides a simple tool for identifying genuine DNA-independent protein associations. Proc Natl Acad Sci U S A 89: 6958-6962.

Lewis, P.W., Beall, E.L., Fleischer, T.C., Georlette, D., Link, A.J., and Botchan, M.R. (2004). Identification of a Drosophila Myb-E2F2/RBF transcriptional repressor complex. Genes Dev 18: 2929-2940.

Li, Y., Liu, D., Lopez-Paz, C., Olson, B.J., and Umen, J.G. (2016). A new class of cyclin dependent kinase in Chlamydomonas is required for coupling cell size to cell division. Elife 5: e10767.

Litovchick, L., Sadasivam, S., Florens, L., Zhu, X., Swanson, S.K., Velmurugan, S., Chen, R., Washburn, M.P., Liu, X.S., and DeCaprio, J.A. (2007). Evolutionarily conserved multisubunit RBL2/p130 and E2F4 protein complex represses human cell cycle-dependent genes in quiescence. Mol Cell 26: 539-551.

Lucker, B.F., Hall, C.C., Zegarac, R., and Kramer, D.M. (2014). The environmental photobioreactor (ePBR): an algal culturing platform for simulating dynamic natural environments. Algal Res 6: 242-249.

Oldfield, C.J., and Dunker, A.K. (2014). Intrinsically disordered proteins and intrinsically disordered protein regions. Annu Rev Biochem 83: 553-584.

Olson, B.J., Oberholzer, M., Li, Y., Zones, J.M., Kohli, H.S., Bisova, K., Fang, S.C., Meisenhelder, J., Hunter, T., and Umen, J.G. (2010). Regulation of the Chlamydomonas cell cycle by a stable, chromatin-associated retinoblastoma tumor suppressor complex. Plant Cell 22: 3331-3347.

Pilkinton, M., Sandoval, R., and Colamonici, O.R. (2007). Mammalian Mip/LIN-9 interacts with either the p107, p130/E2F4 repressor complex or B-Myb in a cell cycle-phase-dependent context distinct from the Drosophila dREAM complex. Oncogene 26: 7535-7543.

Porra, R.J. (2002). The chequered history of the development and use of simultaneous equations for the accurate determination of chlorophylls a and b. Photosyn Res 73: 149-156.

Schmit, F., Korenjak, M., Mannefeld, M., Schmitt, K., Franke, C., von Eyss, B., Gagrica, S., Hanel, F., Brehm, A., and Gaubatz, S. (2007). LINC, a human complex that is related to pRB-containing complexes in invertebrates regulates the expression of G2/M genes. Cell Cycle 6: 1903-1913.

Spudich, J.L., and Sager, R. (1980). Regulation of the Chlamydomonas cell cycle by light and dark. J Cell Biol 85: 136-145.

Sueoka, N. (1960). Mitotic replication of deoxyribonucleic acid in *Chlamydomonas reinhardtii*. Proc Natl Acad Sci U S A 46: 83-91.

Tabuchi, T.M., Deplancke, B., Osato, N., Zhu, L.J., Barrasa, M.I., Harrison, M.M., Horvitz, H.R., Walhout, A.J., and Hagstrom, K.A. (2011). Chromosome-biased binding and gene regulation by the *Caenorhabditis elegans* DRM complex. PLoS Genet 7: e1002074.

Tsai, C.H., Warakanont, J., Takeuchi, T., Sears, B.B., Moellering, E.R., and Benning, C. (2014). The protein Compromised Hydrolysis of Triacylglycerols 7 (CHT7) acts as a repressor of cellular quiescence in Chlamydomonas. Proc Natl Acad Sci U S A 111: 15833-15838.

Tulin, F., and Cross, F.R. (2015). Cyclin-dependent kinase regulation of diurnal transcription in Chlamydomonas. Plant Cell 27: 2727-2742.

Umen, J.G., and Goodenough, U.W. (2001). Control of cell division by a retinoblastoma protein homolog in Chlamydomonas. Genes Dev 15: 1652-1661.

Wang, H., Gau, B., Slade, W.O., Juergens, M., Li, P., and Hicks, L.M. (2014). The global phosphoproteome of *Chlamydomonas reinhardtii* reveals complex organellar phosphorylation in the flagella and thylakoid membrane. Mol Cell Proteomics 13: 2337-2353.

Zamora, I., Feldman, J.L., and Marshall, W.F. (2004). PCR-based assay for mating type and diploidy in Chlamydomonas. BioTechniques 37: 534-536.

Zones, J.M., Blaby, I.K., Merchant, S.S., and Umen, J.G. (2015). High-resolution profiling of a synchronized diurnal transcriptome from *Chlamydomonas reinhardtii* reveals continuous cell and metabolic differentiation. Plant Cell 27: 2743-2769.

CHAPTER 5

Concluding remarks and future perspectives[1]

[1]A part of the writing presented in this chapter has been modified and expanded from the concluding remarks of the revised manuscript submitted to the Plant Cell journal.

Takeuchi T., Sears B.B., Lindeboom C., Lin YT., Fekaris N., Zienkiewicz K., Zienkiewicz, A., Poliner E., Benning C. (2019). Chlamydomonas CHT7 is required for an effective quiescent state by regulating nutrient-responsive cell cycle gene expression. Plant Cell. Revision submitted.

Regardless of cellular origin, the ability of an organism to coordinate metabolic, developmental and contextual cues to the cell division cycle is essential for its continual survival. Indeed, understanding the mechanisms by which cells transit between proliferation and quiescence is of fundamental importance to many areas of biology, including human health, as the loss of control governing these processes is often associated with pathological states, such as those observed for cancer or degenerative diseases (Valcourt et al., 2012; Sadasivam and DeCaprio, 2013; Dhawan and Laxman, 2015). In photosynthetic microalgae, further knowledge of how metabolism is coupled to cell division is essential for future metabolic engineering efforts to achieve an optimal balance between the production of economically valuable products, such as triacylglycerols (TAG) and carotenoids, and the accumulation of biomass. The work presented here explores the role of CHT7 protein in mediating the nutrient- or cell cycle-dependent transitions between two distinct life cycle stages of Chlamydomonas—proliferation and quiescence—and paves the way towards a better understanding of how these processes are regulated at molecular levels.

As detailed in Chapter 2, the failure to curtail energy-consuming metabolism characteristic of the cell division cycle and, thus, establish an effective quiescent state in the face of nutrient scarcity have grave consequences for the survival of microalgal cells. The misregulation of genes following N deprivation that results from the loss of CHT7 is likely causal for the observed phenotypes of the *cht7* mutant. The repression of genes involved in DNA metabolism and cell cycle progression mediated by CHT7 in the wild type following N deprivation is not only necessary for the cells to cease growth and division at an appropriate stage of the cell cycle, but also for promoting cellular survival (Figure 2.15A and B). As the reduced viability of the *cht7* mutant cell population suggests (Figure 2.11), the derepression of these genes likely presents a high metabolic burden on the N-deprived *cht7* cells. The acclimation to nutrient-stress may be

further hindered in *cht7* cells by their inability to transcriptionally adjust the expression of genes involved in nutrient transport or oxidoreductase-mediated electron transfer processes (Figure 2.1C and E). An ineffectiveness of the latter process could result in the generation of ROS or compromised ROS scavenging, which is highly damaging to the cells. The transcriptional establishment of an effective quiescent state by CHT7 in the wild type following N deprivation is also crucial for the coordinated reentry into the cell division cycle upon N resupply (Figure 2.13). In the absence of CHT7, the pre-existing derepression of DNA metabolism and cell cycle-related genes as observed in the *cht7* mutant following N deprivation likely prevents the orderly transcription of these genes following N refeeding (Figure 2.15C). In two previous studies, the delayed remobilization of TAG and resumption of growth as well as the reduction in colony formation during N resupply were attributed to the inability of *cht7* cells to metabolically reverse quiescence-associated programs following refeeding, since no phenotypic defects were observed in the cw^- *cht7* mutant during N deprivation (Tsai et al., 2014; Tsai et al., 2018). However, through the re-examination of the transcriptome during N deprivation and the detailed phenotypic characterization of the newly generated cw^+ *cht7* mutants, we now clearly see the defects that already exist during N deprivation, before N is resupplied. These findings advance our understanding of CHT7 function and elucidate the way in which it promotes quiescence entry as well as its exit.

Despite extensive attempts to identify DNA-binding targets of CHT7, the results of both targeted and non-targeted ChIP were negative or unfruitful (Figure 3.4), giving rise to the notion that CHT7 may not directly bind DNA to carry out its function. In support of these results, the subsequent structure-function analyses of the CHT7 protein detailed in Chapter 3 revealed that the predicted protein-binding AA residues, not the proposed CXC domain, are important for CHT7

functionality (Figures 3.5, 3.7 and 3.8). Indeed, unlike the canonical CXC domains found in animals, CXC domain-deletion of CHT7 had no impact on its ability to restore the mutant phenotypes to wild type, repress cell cycle-marker genes, or form complexes (Figures 3.5, 3.9 and 3.10). Thus, the current data suggest that CHT7 might serve a role as a protein-scaffold, with which potential DNA-binding proteins interact to mediate transcriptional regulation. These findings considerably widen the mechanistic and functional view of CXC domain proteins in general. In this context, it is note-worthy that Arabidopsis TCX5 is a core component that is present in both the repressor and activator DREAM complexes, where the associations of other transcription factors such as MYB3Rs and E2Fs determine the direction of the transcriptional regulation (Kobayashi et al., 2015). Furthermore, while the promoters of genes targeted by the metazoan DREAM complexes are enriched in consensus sequences known as cell cycle genes homology region (CHR) (Tabuchi et al., 2011; Korenjak et al., 2012; Muller et al., 2012; Muller et al., 2014), such cis-regulatory elements are yet to be identified in plants (Fischer and Muller, 2017). The target promoter regions of Arabidopsis DREAM-like complexes are, instead, enriched in MSA and E2F elements (Fischer and DeCaprio, 2015; Kobayashi et al., 2015). Therefore, based on the deletion analysis of CHT7 described here, a possible function of the CXC domain in CHT7 and its orthologs, particularly for those of plant-lineages, should be revisited.

Finally in Chapter 4, the potential role of CHT7 in the regulation of cell division during N-replete light-dark synchronized growth, and the molecular mechanisms by which CHT7 proteins mediate nutrient-dependent transitions into and out of quiescence are examined. Furthermore, because a large portion of the CHT7 protein was found to lack an apparent stable tertiary structure (Figures 3.6 and 3.11), the potential role of phosphorylation in the regulation or stabilization of the CHT7 structure and thus activity was also explored. Because no major defects in the

progression of cell cycle were observed during N-replete synchronized growth by microscopy and the assessment of cell size distributions (Figure 4.1), the impact of the *cht7* mutation appears to be more severe following N deprivation when the transcriptional repression of cell cycle progression genes is crucial for energy-conservation and survival. Despite the finding that the majority of MAT3 and CHT7 as observed by native gels exist in separate complexes of different molecular sizes (Figure 4.5), the coimmunoprecipitation (co-IP) of CHT7 and MAT3 suggested the potential presence of DREAM-like complexes also in this alga (Figures 4.6 and 4.7). Several phosphorylated isoforms of CHT7 were also identified (Figure 4.8), suggesting that CHT7 is a potential target of a yet unidentified protein-kinase pathway, and that phosphorylation may play a role in the regulation of its activity. However, the physiological significance of these observations is yet to be determined, as no differences in interaction or phosphorylation status were observed in a nutrient- or cell cycle-dependent manner, thus far. In mammals, the transcriptional regulatory activities of DREAM complexes are regulated by the phosphorylation-mediated changes in their protein constituents, with a MuvB complex containing LIN54 as a core (Litovchick et al., 2011; Sadasivam et al., 2012; Sadasivam and DeCaprio, 2013; Fischer and Muller, 2017). In contrast, the Arabidopsis RB ortholog, RBR1, and TCX5 are observed in both the activator and repressor forms of DREAM-like complexes (Kobayashi et al., 2015), which may potentially support the finding that MAT3 coimmunoprecipitates with CHT7 also in Chlamydomonas regardless of cell cycle stages or nutrient status (Figures 4.6 and 4.7).

Although, it is clear that the understanding of the CHT7 mechanism and the regulatory modules governing life cycle decisions in Chlamydomonas is far from complete, the functional significance of CHT7 in coordinating the cellular growth and division in response to the changes in nutrient availability is now firmly established. Therefore, future mass spectrometry-based

studies are now crucial in order to determine the compositions of the CHT7 complexes under various conditions, whether the predicted functional domains of CHT7 are indeed necessary for interaction with other DNA-binding proteins, and to identify the physiologically relevant phosphorylation sites within CHT7. Various epitope-tagged versions of CHT7 as well as its deletion mutants generated in the present work will be useful in gaining deeper mechanistic insights into CHT7-mediated life cycle transitions of this alga and may also prove beneficial for our understanding the modes of action of orthologous proteins in other photosynthetic organisms.

REFERENCES

REFERENCES

Dhawan, J., and Laxman, S. (2015). Decoding the stem cell quiescence cycle – lessons from yeast for regenerative biology. J Cell Sci 128: 4467-4474.

Fischer, M., and DeCaprio, J.A. (2015). Does *Arabidopsis thaliana* DREAM of cell cycle control? EMBO J 34: 1987-1989.

Fischer, M., and Muller, G.A. (2017). Cell cycle transcription control: DREAM/MuvB and RB-E2F complexes. Crit Rev Biochem Mol Biol 52: 638-662.

Kobayashi, K., Suzuki, T., Iwata, E., Nakamichi, N., Chen, P., Ohtani, M., Ishida, T., Hosoya, H., Muller, S., Leviczky, T., et al. (2015). Transcriptional repression by MYB3R proteins regulates plant organ growth. EMBO J 34: 1992-2007.

Korenjak, M., Anderssen, E., Ramaswamy, S., Whetstine, J.R., and Dyson, N.J. (2012). RBF binding to both canonical E2F targets and noncanonical targets depends on functional dE2F/dDP complexes. Mol Cell Biol 32: 4375-4387.

Litovchick, L., Florens, L.A., Swanson, S.K., Washburn, M.P., and DeCaprio, J.A. (2011). DYRK1A protein kinase promotes quiescence and senescence through DREAM complex assembly. Genes Dev 25: 801-813.

Muller, G.A., Wintsche, A., Stangner, K., Prohaska, S.J., Stadler, P.F., and Engeland, K. (2014). The CHR site: definition and genome-wide identification of a cell cycle transcriptional element. Nucleic Acids Res 42: 10331-10350.

Muller, G.A., Quaas, M., Schumann, M., Krause, E., Padi, M., Fischer, M., Litovchick, L., DeCaprio, J.A., and Engeland, K. (2012). The CHR promoter element controls cell cycle-dependent gene transcription and binds the DREAM and MMB complexes. Nucleic Acids Res 40: 1561-1578.

Sadasivam, S., and DeCaprio, J.A. (2013). The DREAM complex: master coordinator of cell cycle-dependent gene expression. Nat Rev Cancer 13: 585-595.

Sadasivam, S., Duan, S., and DeCaprio, J.A. (2012). The MuvB complex sequentially recruits B-Myb and FoxM1 to promote mitotic gene expression. Genes Dev 26: 474-489.

Tabuchi, T.M., Deplancke, B., Osato, N., Zhu, L.J., Barrasa, M.I., Harrison, M.M., Horvitz, H.R., Walhout, A.J., and Hagstrom, K.A. (2011). Chromosome-biased binding and gene regulation by the *Caenorhabditis elegans* DRM complex. PLoS Genet 7: e1002074.

Tsai, C.H., Uygun, S., Roston, R., Shiu, S.H., and Benning, C. (2018). Recovery from N deprivation is a transcriptionally and functionally distinct state in Chlamydomonas. Plant Physiol 176: 2007-2023.

Tsai, C.H., Warakanont, J., Takeuchi, T., Sears, B.B., Moellering, E.R., and Benning, C. (2014). The protein Compromised Hydrolysis of Triacylglycerols 7 (CHT7) acts as a repressor of cellular quiescence in Chlamydomonas. Proc Natl Acad Sci U S A 111: 15833-15838.

Valcourt, J.R., Lemons, J.M., Haley, E.M., Kojima, M., Demuren, O.O., and Coller, H.A. (2012). Staying alive: metabolic adaptations to quiescence. Cell Cycle 11: 1680-1696.